Doctoral Dissertation
Doctoral Program in Material Science and Technology (34th Cycle)

Exploring proteins in Roughland: on the adsorption of proteins on biomaterials for osseointegration

Jacopo Barberi
* * * * * *

Supervisors
Prof. S. Spriano
Prof. E. Vernè, Co-Supervisor
Dr, S. Ferraris, Co-Supervisor

Politecnico di Torino
2022

I hereby declare that, the contents and organisation of this dissertation constitute my own original work and does not compromise in any way the rights of third parties, including those relating to the security of personal data.

Jacopo Barberi
Turin, 2022

Acknowledgments

The end of this three-year long journey must start thanking all the people who shared them with me and provided me their support and help in good and bad times, even trough the pandemic.

First of all, I would like to thank with gratitude my tutors Prof. Silvia Spriano, Prof Enrica Vernè and Dr. Sara Ferraris, who guided me through my PhD, sharing with me their knowledge and their experience. I am grateful that I could have them as a model in the research world.

All the work in this thesis would have not be possible without the contribution of the people that I had the fortune to encounter along the way. I would like to acknowledge with sincere gratitude Prof. Seiji Yamaguchi, from Department of Biomedical Sciences, College of Life and Health Sciences, Chubu University; Dr. Luisa Mandrile, Dr. Andrea Mario Giovannozzi and Dr. Andrea Mario Rossi, from Chemical physics and nanotechnology department, National Institute of Metrological Research; Prof. Alessandra Vitale, Prof. Renato Gonnelli, Dr. Erik Piatti, Dr. Lucia Napione, Dr Francesca Frascella and Dr. Desirèe Baruffaldi, from Department of Applied Science and Technologies, Politecnico di Torino.

Thanks to my officemates, Fabi and Zeta, and the open-space crew, Ale, Ange, Fra, Cami, Andre, Dani, Ste, Carla, Mari, Sofia, Eli, who filled the long working hour with laughter and joy. My gratitude goes also to all the Glance groups, for the help, the knowledge and the possibility to work with them.

I would also to Matte, Pollo, Lu, Andy, Cami, Marina and Franz, for sharing with me my voyage in the amazing world of materials since the first university exams. Thanks to all the friends outside Politecnico, sharing moments, baseball fields and rocks.

At last, but obviously not the least, thanks to Irene, for being at my side, bothering and encouraging me, and to Umbi and my parents, for all they’ve done and will do for me.

Summary

The interactions between implantable medical devices and human tissues depend upon a large number of factors, which determine their successful integration or failure. One of the main players is the serum protein layer, which forms on the surface of every biomaterials in few minutes after the contact with biological fluids. Hydrophobic and electrostatic interactions are the main driving forces of protein adsorption, heavily depending on surface properties surfaces. Topography, chemistry, surface free energy, wettability, and functional groups determine which proteins are adsorbed, how many of them and their conformation in the transient matrix: all fundamental factors for the host response to the implant. The possibility of controlling the formation of the protein layer will open new horizons for the design and development of new biomaterials. A lot of work has been done to unveil this matter, in particular by investigating simple systems, involving single protein adsorption on model cases, such as flat surfaces with a well-known chemistry. Unfortunately, adsorption mechanisms are still quite mysterious, due to the extreme complexity of protein-surface interactions, which relate not only on the properties of the single protein or the particular surface, but also on the surrounding environment (composition of the solution, pH, temperature). In addition, the surface of biomaterials is far from ideality, being rough, with complex chemistry and properties. All of these not being enough, there is a lack of suitable techniques to characterize events at the nanoscale that take place on surfaces with micro or even millimetric features.

The main idea of this PhD thesis is to investigate protein adsorption on biomaterials of clinical interest, in particular for orthopedic and dental applications, in conditions as close as possible to the physiological environment. Therefore, the focus was put on seven different substrates for bone contact, which include: pure titanium and Ti6Al4V alloy, polished and with three different chemical treatments; a silica-based bioactive glass with and without silver doping; polystyrene, as a model hydrophobic surface.

At first, the samples were thoroughly characterized, with particular attention on the topography, surface chemistry, exposed OH groups, surface energy, wettability, and ζ potential. Then, adsorption of albumin and fibronectin at near physiological

concentration was investigated. The first goal was to find a set of techniques suitable for such a task. Conventional analysis, such as XPS or micro ATR-FTIR, were coupled with innovative approaches, such as solid surface ζ potential and Kelvin probe force microscopy. In the end, seven techniques have been merged to obtain novel and interesting insight on protein-material interactions. Noticeably, surface topography has a central role in determining the amount of proteins adsorbed, both albumin and fibronectin, while protein denaturation is more related to acidic hydroxyl groups on titanium substrates and to silver on bioactive glasses. On them, the adsorption mechanism is further complicated by the glass reactivity, involving the incorporation of proteins inside the silica gel layer. Then, the competition for the surface was evaluated, exploiting sequential adsorptions and co-adsorption. Effect of proteins on titanium bioactivity was also assessed.

The second focus of this work was about the osteoimmunomodulation effect of different surface treatments on Ti6Al4V alloy. Osteogenic cells are intimately related to immune cells, and implant osseointegration cannot succeed without a proper inflammatory response. The foreign body reaction was evaluated by culturing macrophages on the titanium surfaces, measuring their viability and quantifying 27 different factors and chemokines released.

Contents

List of Tables

List of Figures

Introduction

An enormous number of biomedical devices are implanted in patients on a daily basis, in all shapes, materials, and for different purposes. The positive outcome of an implant is determined by the complex cascade of events that takes place as soon as the biomaterial gets in contact with biological fluids, such as blood, saliva or serum. In the context of orthopedic and dental implants, the osseointegration depends as first upon the formation of a transient matrix (serum proteins, activated complement and platelets), secondary by the material-mediated osteoimmune response. These events can lead to the formation of a fibrous capsule and implant failure or to a successful activation of osteoprogenitor cells and the formation of new healthy bone around the implant.

The adsorbed protein layer, which forms long before the attachment of cells on the implant surface, is the actual interface between the biomaterial and the human body. Thus, its properties mediate the cellular response, depending on the type and amount of proteins adherent to the material, and whether or not they maintain their native structure and biological activity upon adsorption. Those factors certainly depend on the physical-chemical properties of the biomaterials, such as wettability, surface energy and charge, functional groups and topography.

In the past decades lots of efforts have been spent by researchers trying to unveil the correlation between the properties of many different materials (metals, ceramics and polymers) and the final protein layer. Unfortunately, due to the extreme complexity of the systems involved and the incredible numbers of influent factors, the mechanisms driving protein adsorption from physiological fluids on implant surfaces are still quite a mystery. The possibility to control protein adsorption will open new horizon in biomaterial design.

Furthermore, protein adsorption takes place at the nanoscale, while biosurfaces of clinical interest have features ranging from the nano- to the microscale and even to the milliscale. As consequence, it is also hard to find characterization techniques that are suitable to investigate phenomena happening on substrates with such different dimensional scale. In fact, the majority of the studies have been conducted on flat model surfaces, in what can be called the world of *flatland*, borrowing and daring to expand the concept invented by Norde in 2008.

This PhD thesis aims to understand the adsorption of proteins in *roughland*, on biomaterials relevant for osseointegration, which are usually rough and far from model surfaces, searching for correlation between surface properties and the features of the adsorbed protein layer, and to develop new characterization techniques suitable to investigate adsorption on actual biomaterial surfaces. This was done by focusing on the adsorption of two proteins abundant in blood serum and with paramount biological roles, albumin and fibronectin, on common implantable materials. In particular, titanium and titanium Ti6Al4V alloy were chosen since they are the gold standard for metallic implant in clinical use. Three different surface treatments were employed to enhance and promote osseointegration, which can be interesting for future clinical application. A bioactive glass composition was also used, since such class of materials is also promising as bone substitutes. Polystyrene was included as reference for non-polar, hydrophobic material.

After a preliminary and thorough characterization of the selected biosurfaces, protein adsorption was investigated at first from single protein solution, in order to obtain a set of experimental techniques suitable for being applied on rough and complex surfaces. Then the competition between albumin and fibronectin was studied by sequential adsorption and adsorption from protein binary solutions. The effect of proteins in *in vitro* bioactivity of modified Ti6Al4V alloy was also assessed. In the end, it was evaluated the first step of the osteoimmunomodulation process of titanium alloys, by macrophages cultures.

In order to describe the work performed, this thesis has been organized with the following structure.

Chapter 1: a brief description of proteins, their composition, structure and properties, with a focus on albumin and fibronectin.

Chapter 2: the matter of protein adsorption on surfaces is introduced, discussing the physical principles that governs protein-material interactions and the factors influencing the adsorption process, in terms of surface properties, protein solution characteristic and environmental effect. The literature regarding adsorption on titanium based materials and bioactive glasses has also been reported, with a deepening on the characterization techniques employed.

Chapter 3: the concept of osteoimmunomodulation is here presented, illustrating the interplay between immune and osteoprogenitor cells and how the inflammatory reaction to the implant must be tuned and controlled in order to achieve a proper integration of the implant.

Chapter 4: the experimental methodology is detailed, starting from the depiction of the sample preparation with the several surface treatment and protein solution used. The characterization techniques used for characterizing both the substrate surface and protein adsorption are summarized, along with the cellular culture methodology and biological assay.

Chapter 5: the results obtained are reported and discussed in this chapter. Substrate surface physiochemical properties are deeply described, as the adsorption results, in terms of protein amount on the surface, their distribution, conformation and orientation. Correlation between surface properties and protein-material

interactions have been observed. Also, the results of competitive adsorption and cellular culture are reported and discussed.

Chapter 6: the final conclusions are drawn in this chapter, and some suggestion for future research are also proposed.

Chapter 1

Proteins

What do rhinoceros' horn, spider web and our hair have in common? They are all made of the same kind of biological structure: proteins.

Proteins are the most common macromolecule that can be found in all living being. They constitute the most part of cells, accounting for about 50% of vertebrate tissue dry weight[1]. Proteins are biological macromolecules that have an enormous variety of structures, dimensions and functions. They range from very small molecules up to structures weighting some hundreds of kDa and can exploit an incredible range of different functions, from structural support (keratin) to immunes response (antibody) to in-cell reactions catalysis (enzymes). Regardless of their incredible diversity, all proteins are made of few different atoms, in particular C (50-55%), O (20-23%), H (6-7%), N (12-19%) and a bit of S (0.2-0.3%) (w/w)[2]. These elements combine in just 20 protein precursors called amino acids. They covalently bond one another forming chains of specific sequences. Those chains will form the building block for proteins by folding and arranging into three dimensional hierarchical structures.

1.1. Amino Acids: monomers of proteins

Amino acids are small molecules that bond one another, via peptide bonds, to form polymeric chains of different length. If the sequence contains less than 50 residues (as are called amino acid after bonding), it is called a polypeptide; if the molecule is larger, it is a protein[1]. The discovery and classification of the amino acids lasts over a century, starting by the finding of asparagine (1806) till the identification of threonine (1938)[3].

All of amino acids have a similar structure, with a common primary chain, differing from each other by the side group. They are α-amino acids, which means that they present an amino and a carboxyl group bonded to an α-C. To the same atom is also bonded a side group, called R group, which is typical for each amino acid. The amino acid general structure is shown in Figure 1.1.

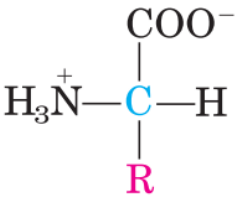

Figure 1.1 Structural scheme of common amino acid. The α-C is in blue, with attached the carboxyl and amino groups, in black. The side group R is represented in red [3]

Amino acids, both in their crystalline form or dissolute in water, are in their ionized form, as shown in Figure 1.1. Both the carboxyl group and the amine group are ionized as follows:

$$-COOH \rightarrow -COO^- + H^+$$

$$-NH_2 + H^+ \rightarrow NH_3^+$$

Thus, every amino acid presents contemporary a negative and a positive charge, at least. For their dipolar nature, amino acids are referred as *zwitterion*.

It is interesting to notice that the αC is bound to four different groups. Therefore, the α-carbon is chiral and all the amino acid are optically active. This is true for all amino acids, but not for glycine, since its R-group is just a hydrogen atom. According to the spatial arrangement of the chemical groups around the αC (stereoisomery), amino acids can present different optical effect, exploiting the ability of change light polarization. The different stereoisomers are called enantiomers. If the light is rotated clockwise, so to the right, the molecule is referred as dextrorotatory and the isomer is in the D-form. On the other side, a molecule that rotates a polarized photon beam counter-clockwise, or to the left, it is referred as levorotatory and it is the L-isomer. Cells are sensible to stereoisomers and proteins present only L-amino acids.

The R group is typical for each of the 20 basic amino acid and it presents different complexity levels, from being a simple -H atom for glycine, to more complex indol for tryptophan (Figure 1.2). The most common amino acids are known as follows, with their abbreviated notation: glycine (Gly), alanine (Ala), proline (Pro), valine (Val), leucine (Leu), isoleucine (Ile), methionine (Met), phenylalanine (Phe), tyrosine (Tyr), tryptophan (Trp), serine (Ser), threonine (Thr), cysteine (Cys), asparagine (Asn), glutamine (Gln), lysine (Lys), arginine (Arg), histidine (His), aspartatic acid (aspartate in its deprotonated form)(Asp), glutamatic acid (glutamate in its deprotonated form)(Glu)

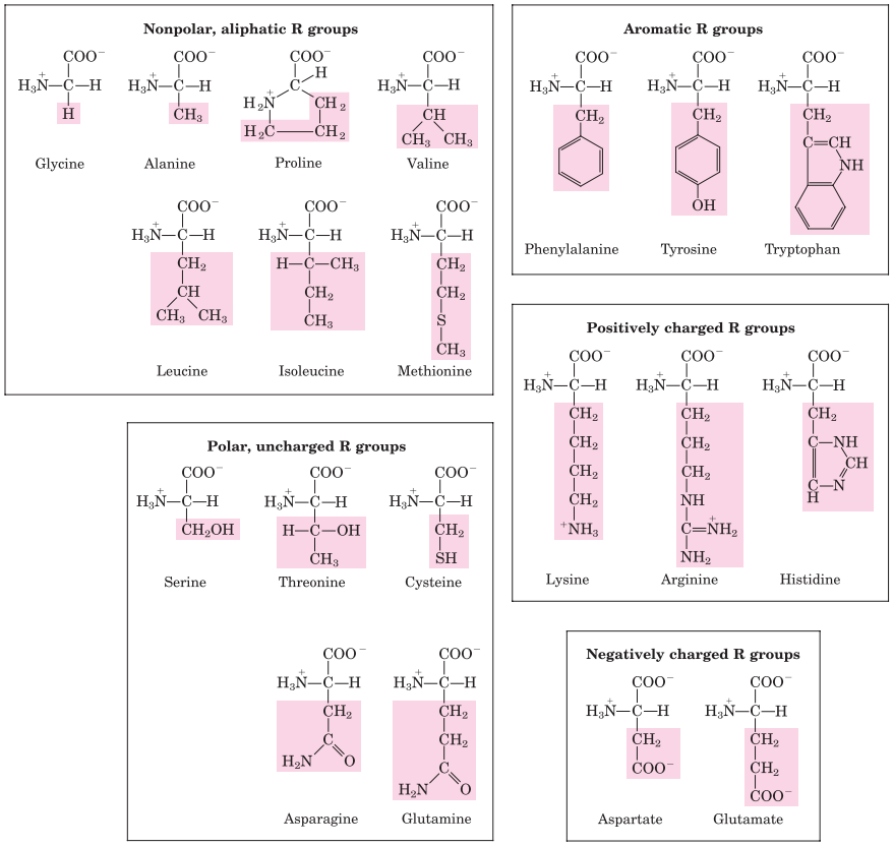

Figure 1.2 Classification and structure of the 20 most common amino acids. The R groups are highlighted in pink [3]

Based on the properties of the R group, amino acids present different properties and can be divided into different classes. One of the first differences is the type of R groups, aliphatic or aromatic. Other classification can be made on the polarizability or net charge of side groups:

- Nonpolar: this group contains hydrophobic and nonpolar amino acids. Some of them, such as valine, alanine, leucine and isoleucine, tend to stabilize protein structures through hydrophobic interactions. Proline reduces the flexibility of the peptide chain due to its cyclic side chains.
- Aromatic: R groups containing aromatic rings are usually non polar and hydrophobic, such as phenylalanine and tryptophan. Tyrosine, instead, presents a polar OH groups, that can deprotonate at high pH (>10). This amino acids represents the fluorophore residues in proteins, and can be analyzed during characterization studies [4,5].
- Polar: these amino acids present an uncharged R group, but with polar moieties. They are hydrophilic. The polarity is conferred by different groups: hydroxyl in serine and threonine; in cysteine there are sulfhydryls groups, responsible for di-sulfide bonds, which are very important in protein three-dimensional structure (as it will be discussed later in this chapter); and asparagine and glutamine have amide groups.
- Basic: in this group are present those amino acid that are positively charged at neutral pH, thanks to their N-containing R groups: lysine contains a second amino group; histidine an imidazole group and arginine presents a guanidino one.

- Acid: in the opposite way with respect to basic amino acids, R groups of aspartate and glutamate presents a carboxyl group which is negatively charged at physiological pH. Basic and acid amino acid are the most hydrophilic.

In addition to the basic set of 20 amino acids, many more have been found in proteins. Those are the product of modifications of residues already incorporated into polypeptides[1].

A consequence of acid/basic behavior of R groups, amino acid electric properties may change. If amino acids are dissolved in a medium, the pH of the solution can influence the net charge of the molecules, since in acid or alkaline condition amino or carboxyl groups can become neutral by protonation or deprotonation. The charge of amino acids is also influenced by means of secondary carboxyl or amino groups that might be present in the R group. Those groups exploit an acid or basic behavior, acting as proton donor or acceptor in dependence of solution pH. Acid-basic properties of amino acid can be studied by titration curves and pK_a values for different groups can be defined (Figure 1.3). At a certain pH, there is an equilibrium between positive and negative charge. This point is called the isoelectric point (IEP) and it is represented by the point of inflection between the acid and basic part of the curve. Titration curves are also useful to predict net charges of amino acids.

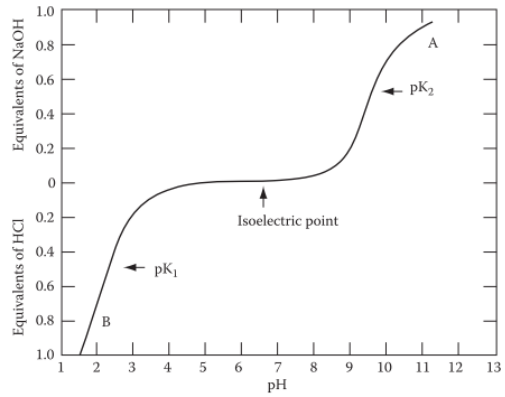

Figure 1.3 Typical titration curve of an amino acid [2]

1.2. Peptides and peptide bond

Amino acids can act as monomers to form chains of residues in a theoretically infinite number of combinations, by sequences and length. A chain formed by two residues is called dipeptide, if three residues are linked then it is a tripeptide and so on. If the overall weight is below 6000 Da, the molecule is called peptide, larger macromolecules are considered proteins[1].

The typical bond that connects two amino acid in a protein chain is the so-called peptide bond. It is a covalent bond formed between the carboxyl end of one amino acid and the amino end of another one. A water molecule is removed during the bond formation. Due to this process, each peptide present an amino groups, called N-terminus, at one end, and a carboxyl group, called C-terminus, at the other one [6,7]. The atoms involved in the peptide bond can be schematized as follow: -αC-

CO-NH-αC-. The peptide bonds are planar and rigid, in fact the N-C bond presents a partial double-bond nature avoiding twisting. This is due to amido-imido tautomerization and resonance of electrons between the C-O and N-C bonds[8]. This fact has several implications. First of all, all the six atoms involved in the peptide bond lie in the same plane, while R groups and amine H reach out of it. A polypeptide chain can be represented by a series of planes connected through a single point, which is the αC (Figure 1.4-a). This provide a certain rigidity to the chain. As second, binding-electron resonance generates a dipole in the bond, by providing a partial positive charge to the amino group and a partial negative charge to the O of the carboxyl one. As consequences, dipole-dipole interactions may occur. Furthermore, cis and trans configurations of the bond are possible, but usually only trans geometry is present in proteins (Figure 1.4-b)[2].

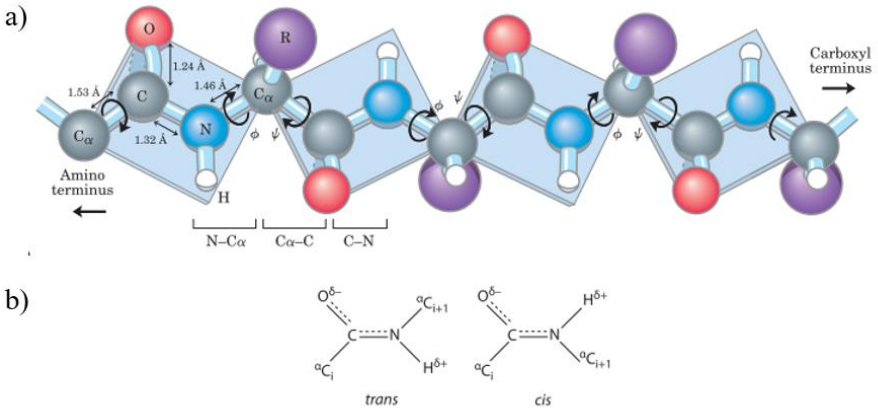

Figure 1.4 a) peptide chain, the planar nature of the peptide bond is shown [3] b) scheme of dipoles generated by electron delocalization and representation of *cis* and *trans* form [2]

Regardless the rigid planar structure of the peptide bond, peptide chains still present a certain degree of flexibility, thanks to rotation around the axes of N-αC and αC-C pure single bonds. These bond angles, referred as φ for the former and ψ for the latter bond, can theoretically assume any value between -180° and 180°. However, steric interferences limit those ranges and possible configurations can be displayed in the so called Ramachandran plot, which provides insight on protein structures [9].

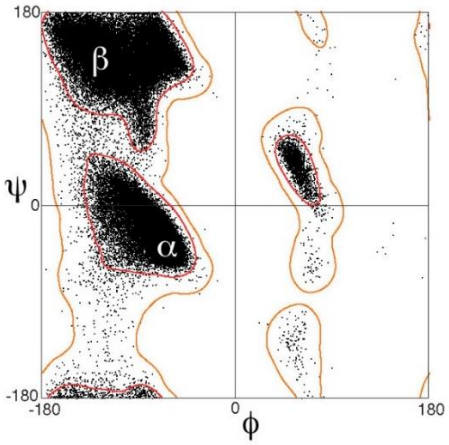

Figure 1.5 Example of Ramachandran plot. α and β region defined the possible combination of ψ and φ values that can be find in those secondary structures. Modified from [10]

1.3. Proteins Structure

All proteins present a three-level hierarchical structure. The first level is known as primary structure and it is represented by the amino acid sequence that constitutes the polypeptide chain. It is responsible for protein functions and spatial architectures. Folding of separate chain segments into several 3D structure, the most common ones are helical (α-helix) or in a more planar conformation (β-sheet), constitutes protein secondary structure. The last architectural levels of protein structure, the tertiary structure, is the configuration in space of different chain domains. Most of proteins are constituted by only one peptide chain, but some others can be formed by more than one component. These particular proteins present also a quaternary structures, which is the arrangement of various parts [1]. Protein conformation in physiological condition is called native configuration. It can be modified and destroyed at several different degrees, in a process called denaturation, if proteins are subjected to environmental stimuli such as temperature, pH and ionic strength of liquid medium variation and mechanical stresses [2].

1.3.1. Primary structure

The first level of proteins structure refers to the amino acid sequences in the protein chain. Each protein has a very well-defined residues composition arranged in a specific manner. Amino acid sequence determines protein conformation, properties and functions. In order to exploit their biological role in an appropriate manner, proteins must fulfill very stringent requirements. The exact residues compositions and their precise position in the chain are fundamental, since every alteration can lead to functionality loss. The instructions for protein synthesis are recorded within the genetic code, in the DNA.

A strict correlation between structure and protein function is confirmed by the fact that within individuals of the same species, proteins with specific roles are identical. While they differs from same kind of protein among different species[1].

1.3.2. Secondary structure

Polypeptide chains can fold into ordered structures, due to different kind of weak bonds. Among them, the most influent are hydrogen bonds. Those structure are referred as secondary structure of proteins. There are three common ordinate secondary structure that can be present within proteins: α-helix, β-sheets and β-turns. Chain portions without a specific pattern can be also found, they are referred as random coil. Protein can show different secondary structures at the same time, even though usually there is a predominance of one of them, as listed in Table 1.1.

Table 1.1 Secondary structure composition of different proteins. Percentages are referred to the portion of chains involved in the structures with respect to the total number of residues. Adapted from ref. [2,11]

Protein	% α-helix	% β-sheet	% β-turns	% random coil
Deoxyhemoglobin	85.7	0	8.8	5.5
Bovine Serum Albumin	67.0	0	0	33.0
α_{s1}-Casein	15.0	12.0	19.0	54.0
β-Casein	12.0	14.0	17.0	57.0
Chymotrypsinogen	11.0	49.4	21.2	18.4
Immuboglobulin G	2.5	67.2	17.8	12.5
Insulin (dimer)	60.8	14.7	10.8	15.7
Ribonuclease A	22.6	46.0	18.5	12.9
Egg lysozyme	45.7	19.4	22.5	12.4
Ovalbumin	49.0	13.0	14.0	24.0
Papain	27.8	29.2	24.5	18.5
α-Lactalbumin	26.0	14.0	0	60.0
B-Lactoglobulin	6.8	51.2	10.5	31.5
Soy 11S	8.5	64.5	0	27.0
Soy 7S	6.0	62.5	2.0	29.5
Phaseolin	10.5	50.5	11.5	27.5
Myoglobin	79.0	0	5.0	16.0
Fibronectin	0	35.0	0	65.0

α-helix

During late 40s, Pauling and Corey confirmed the planar geometry and rigid structure of the peptide bonds by means of X-ray diffraction (XRD). Furthermore, they proposed a simple structure for polypeptide chain folding, based on H-bonds: the α-helix [12]. According to their studies, this was the only model, among the ones previously proposed, to well represent the structure of some fibrous proteins. In α-helix, polypeptide chain is wrapped around a central axis (Figure 1.7). Protein coiling is possible thanks to H-bonds between the hydrogen of the amino group of the first residue with the carbonyl oxygen of the fourth one. In this manner, each residue of the chain participates to one bond, providing stability to the structure. This is possible only in case of great amount of H-bonds. In fact, short peptides show no similar structure to the α-helix [9]. Each turn of the helix is composed by 3.6 amino acid, with an height of 0.15 nm and a length of 0.54 [13]. Both right-handed and left-handed α-helix conformation are possible, according to the coiling direction of the chain, but the latter is less stable as result of steric interaction between R groups. This kind of secondary structure is the most common to be found in proteins, nevertheless not all the amino acid sequences allow this folding. For instance, α-helix formation is prevented by electrostatic repulsion between side groups or presence of proline, in which the α-carbon is not able to rotate since it is included in the pyrrolidine ring.

Figure 1.7 Representation of a right-handed α-helix. H-bonds are represented by red dotted lines [1]

β-sheet

Peptide chains can arrange also in a more extended configuration than in α-helix. Each amino acid residue has a length of 0.35 nm, while in helical structure it was of 0.15 nm. Astbury proposed this conformation in 1933, but the correct description was made only about 20 year later by Pauling and Corey [14]. In β-sheet, protein backbone is in the extended conformation and paired. This allows the formation of inter-chain H-bonds, involving amino groups of one chain and carboxyl groups of the other one. β-sheet presents a so-called pleated structure, meaning that α-carbons do not lie all in the same plane, but they are little above or below it, alternately. This fact confers them a zig-zag fashion folding. As consequence of the direction of the chains involved, β-sheet can be parallel (both chains go from N-terminal to C-terminal) or antiparallel. Protein chains direction affects the angle and the distances between hydrogen bonds of β-sheets. A scheme of parallel and antiparallel β-sheet is represented in Figure 1.8.

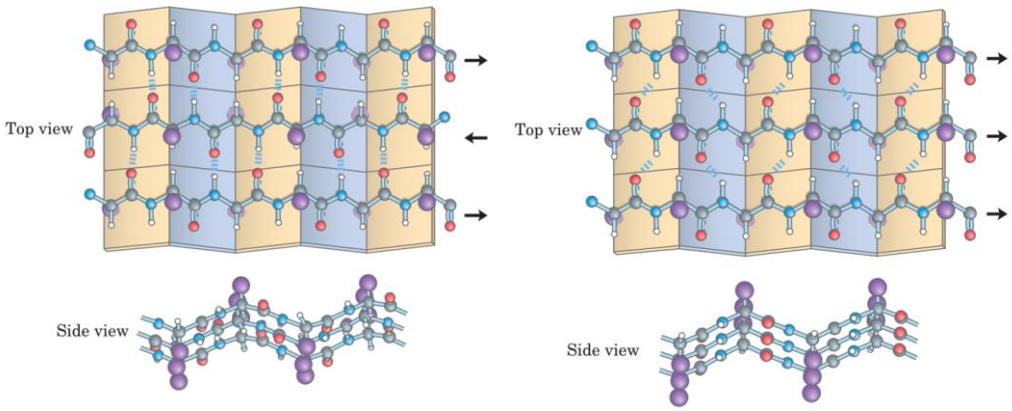

Figure 1.8 Sphere and rods scheme (top and side view) of antiparallel (left) and parallel (right) pleated β-sheet. Color legend: C green; N blue; O red; H white; R groups purple. Inter-chain H-bonds are represented as blue dotted lines. Arrows refer to N-terminal to C-terminal direction. Modified from ref [3]

β-turns

A third type of common structure in proteins is β-turn. Differently from helices and sheets, β-turns are non-repetitive [14]. They are usually connecting segments

between ordered chain parts, such as two adjacent segments of antiparallel β-sheets. β-turn are formed by four amino acid residues, linked by a hydrogen bond between the first and the fourth. Glycine and proline are common residues to be found in β-turn. Some different types of β-turn have been reported, but the most common ones are Type I and Type II (Figure 1.8)[3,14].

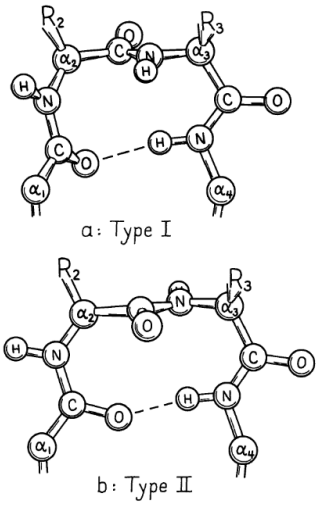

Figure 1.9 Type I and II β-turn [14]

Random coil

Protein regions without any repeated pattern are defined as random coil. This arrangement is a consequence of energy minimization resulting from protein primary structure. Random coils are often the connecting segments between ordered parts in globular proteins, due to the absence of a predominant axis [3].

1.3.3. Tertiary structure

Various segments, ordered or random, of the protein chain are spatially arranged in a precise architecture. This overall 3D conformation is referred as tertiary structure, as shown in Figure 1.10 [15].

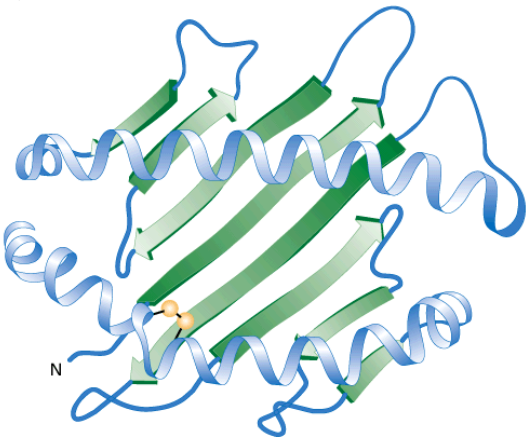

Figure 1.10 Representation of a protein tertiary structure containing different secondary structures (α-helix light blue; β-sheet green; random coils and β-turn blue)[16]

Proteins can be classified according to their shape. Based on their tertiary structure, they are globular or fibrous proteins [1,17]:

- Globular: proteins in this class present all types of secondary structure, forming compact spheroid or ovoid, with similar length of the three axes. Usually they possess a hydrophobic core and hydrophilic groups lie on the surface, thus proteins in this group are water soluble. Functional proteins, such as enzymes, antibodies, hormones and hemoglobin, belong to this class;
- Fibrous or fibrillary: this type of proteins present parallel peptide chains, forming extended fibers or sheets. Inter-chain disulfide bonds confer stability and strength and proteins in this group are insoluble. Fibrillary proteins exploit structural functions. Keratin and collagen present fibrous conformation, for instance.

The spatial configuration of a protein is due to interaction between R groups of amino acid residues. They can bind one another via strong or weak interactions both[1,18,19]:

- Electrostatic interaction: attractive or repulsive forces affect the position of charged side groups that may present ionic parts, such as $-NH_3^+$ or $-COO^-$;
- Hydrogen bonds: some residues, for instance aspartate or histidine, can attract some others, like threonine or serine. However, these bonds are different from ones responsible of secondary structure formation;
- Disulfide bridges: free sulfhydryl groups (-SH) of cysteine can covalently bind forming a bridge (-S-S-), connecting two distant regions of a proteins. This kind of interaction is very common, for instance albumin presents several disulfide bridges [20];
- Hydrophobic and hydrophilic interactions: if proteins are dissolved within a solvent, polar and nonpolar R groups of amino acid residues play a fundamental role in defining protein structure. For instance, in polar solvent such as water, hydrophobic groups cluster together to avoid contact with liquid medium, while hydrophilic residues will be exposed on the surface of the protein. This hydrophobic effect is the main driving forces in protein folding [18] In nonpolar solvents the revers happens.
- Van der Waals interactions: electronic clouds of very close atom can interact when temporary dipoles are formed. If a large number of atoms are involved, this kind of weak interaction might become significant.

1.3.4. Quaternary structure

Even though some proteins are composed by just one polypeptide chains, others are constituted by two or more of them, called subunits. Those can be identical or different. Hemoglobin, as an example, is composed by four subunits (Figure 1.11). The quaternary structure describes how subunits arrange in the space, held together

by noncovalent force [21]. Proteins composed by one single peptide chain cannot exhibit a quaternary structure.

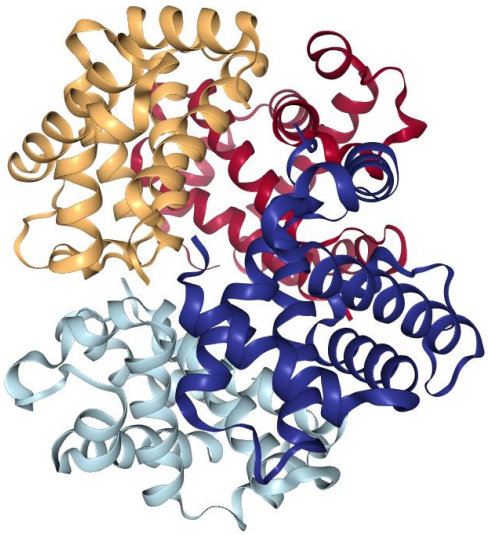

Figure 1.11 Hemoglobine quaternay structure. Different subuinits are shown in different colors [22]

1.4. Protein denaturation

In order to fully exploit their biological functions, proteins conformation need to be strictly defined. In other words, they must be in their native state. In non-physiological environment, some of the forces that held protein conformation may change, leading to denaturation. This is a process where there some portions of the peptide chain loss their spatial arrangements. Nevertheless, covalent bonds are not cleaved. Usually denaturation is not complete, proteins are not in a fully random conformation, retaining some ordered portions.

Denaturation process can be described from a thermodynamic point of view. The stability of a protein is proportional to the difference between native and denatured states free energy. Therefore, the activation energy for the process, denaturation free energy ΔG_d, can be express as follows:

$$\Delta G_d = \Delta G_{H\text{-}bond} + \Delta G_{ele} + \Delta G_{Hy} + \Delta G_{vdW} - T\,\Delta S_{conf}$$

Where:

- $\Delta G_{H\text{-}bond}$: free energy changes for hydrogen bonding
- ΔG_{ele}: free energy changes for electrostatic interactions
- ΔG_{Hy}: free energy changes for hydrophobic interactions
- ΔG_{vdW}: free energy changes for van der Waals interactions
- ΔS_{conf}: changes in conformational entropy

The overall changes in free energy presents contributions by all the forces involved in maintaining protein secondary and tertiary structures. Even though the number of weak interactions within protein are very large, ΔG_d is usually a low value, corresponding to a couple of H-bonds. Rupture of just few noncovalent bonds can destabilize the whole protein native conformation[2]. This fact reflects in the cooperative nature of the denaturation process, which is carried on in a two-step manner. The transition between native and denature state is abrurtp and sudden

with the increase of denaturing agent impact, without a transition state between folded and unfolded conformations[23].

Different environmental parameters may affect the natural conformation of proteins, both physical and chemical. It is interesting to notice how, to some extent, when the external stimuli are removed protein chains are able to refold themselves, regaining their native structure. Renaturation is a clear proof of how secondary and tertiary structures are defined by the amino acid sequence, as found by Anfinsen studies about the refolding of ribonuclease [24].

The principal causes of denaturation in proteins are [3,19,25]:

- Temperature: both high and low temperature can affect protein structural configuration. High temperature can disrupt atomic patterns by increasing the kinetic energy of the system, breaking noncovalent bonds and increasing the entropy contribution to free energy. Cold temperature can also weaken hydrophobic interaction, therefore proteins that are mainly stabilized by them can loss their stability due to conformational entropy predominance. Disulfide bonds, on the other way, help stabilize native conformation at high and low temperature both;
- High pressure and mechanical stresses: more physical parameters other than temperature can provoke denaturation of proteins. Even though proteins are compact, some voids are still present in their structure and they are flexible. When pressure is applied, those voids are compressed, causing a small volume reduction (some tens of ml/mol). Another mechanism is the hydration of nonpolar reissued, that became exposed to water molecules because of hydrostatic pressure. This result in a loss of volume to. Mechanical shear can also lead to protein unfolding and precipitation. Vigorous shaking generates air bubbles in the solution and, at the air-liquid interface, proteins denature due to excess in free energy;
- pH: values that differs from physiological pH (about 7.4) may cause denaturation. Many proteins are stable in a range from pH value of 4-5 up to 9-10. When pH changes, protonation or deprotonation of charged and uncharged groups may occur, affecting electrostatic interactions within proteins. These changes are usually abrupt at pH variations, since many buried groups can be unmasked simultaneously and interact with liquid medium at once;
- Solvents, detergents and additives: the composition of the liquid medium where proteins are dissolved plays a fundamental role in their configuration, a part from pH variations. Organic and nonpolar solvents change the stability of H-bonds, hydrophobic and electrostatic interactions. Certain detergents denature proteins to a large extent since they bind preferentially to denature protein, affecting the native-unfolded state equilibrium. This kind of denaturation is irreversible due to the strength of bonds. Sodium dodecyl sulfate (SDS) is one of the

most common detergent. Small molecules or organic additives affect protein stability in both ways, by decreasing or increasing it. Addition of polyols and sugar tend to stabilize native protein conformations, while others, in particular urea and guanidinium hydrochloride, act as denaturants. Some of these compounds can act both ways, in dependence of their concentration within the solutions.

One more aspect of protein denaturation exists, which is of great interest within the frame of this work. Loss of native configuration can occur also after adsorption on solid surfaces. Proteins can change their conformation upon interaction, of different kinds (covalent, electrostatic, hydrophilic, hydrophobic) with materials interfaces and also by interaction with neighbor proteins. These aspects will be further discussed later on, in Chapter 2.

1.5. Albumin, fibronectin and fetal bovine serum

1.5.1. Albumin

Albumin is among the first proteins ever studies. Early observation of albumin effects on human body were reported to happen in antique Greek, by Hippocrates of Cos, who connected foamy urines to chronic kidney disease, in the fifth century [26]. Since then, human serum albumin (HSA) and its homologous from other animal species have been largely investigated, due to albumin extensive use in therapeutic applications and as protein model for researchers [27–30].

Along with globulins, albumin is the most abundant protein that can be found in blood plasma, with a typical concentration of about 3.5-5 g/dl (≈60% of total proteins)[31]. Albumin is a globular protein synthesized in the liver then released into the portal circulation, and it covers a wide range of biological functions: it is responsible for 80% of plasma osmotic pressure, it regulates blood pH and it is a transporter of several compounds, such as metals, fatty acids, amino acids and drugs [28].

As protein, HSA is relatively small, with a weight of 69 kDa. It is composed by a single peptide chain, containing 585 residues. HAS contains almost all the 20 common amino acids: Lys (10.1%), His (2.7%), Arg (4.1%), Asp (9.0%), Thr (4.7%), Ser (4.1%), Glu (14.0%), Pro (4.1%), Gly (2.0%), Ala (10.0%), Cys (6.0%), Val (7.0%), Ile (1.4%), Leu (10.4%), Try (3.1%), Phe (5.3%), Trp (one residue)(percentages are referred to the number of each residues with respect to the total number within the protein)[32]. Noticeably, it has 17 pairs of disulfide bridges and one free cysteine residue (Cys-34), exhibiting a free sulfhydryl group. Even though some differences in amino acid sequences exist between albumin of different species, mammalian albumins share a similar structure. Disulfide bridges form nine double loops, repeated as triplets. This looped structure can be divided into three homologous domains (I, II, III), each containing three loops. Each albumin domain is further subdivided in subdomains A and B, where the former contains the first two loops of each domains, of equal length, and the latter the last one, the sorter. Albumins are mainly composed by α-helix (67%), without β-sheets).

Remaining portions of peptide chain are in random coil or turn conformations. Each subdomains A presents six helices, divided into one cluster of four (a-h1 to a-h4) and two more (a-h5 and a-h6), antiparallel and connected by a pair of disulfide bridges. Subdomains B are constituted by a single cluster of four helices (b-H1 to b-h4). Connection between each domain is achieved through fusion of helices b-h10 C-terminal and a-h1 N-terminal of domains I-II and II-III respectively [33]. Domain I differs from the others due to lack of disulfide bridges connecting helices a-h1 and a-h3[26,29,30,32,34,35]. HSA secondary structure is displayed in Figure 1.10.

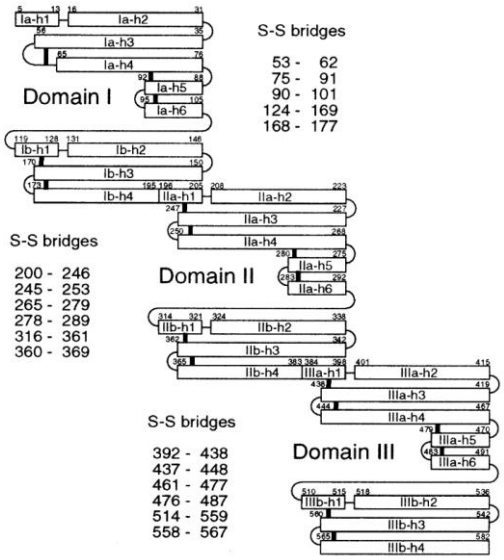

Figure 1.12 Scheme and features of HSA secondary structures. α-helices are drawn as rectangle, peptide chains an loops as thin lines and disulfide bridges as thick ones. Position of S-S bridges is also listed [34]

Native configuration of albumin, the so-called N-form, has a peculiar heart-shape conformation. Domain I and II dispose almost perpendicularly one with respect to the other, in a T-shaped assembly. Domain III interacts only with domain II, and forms an angle about 45° with its B subdomain[34].

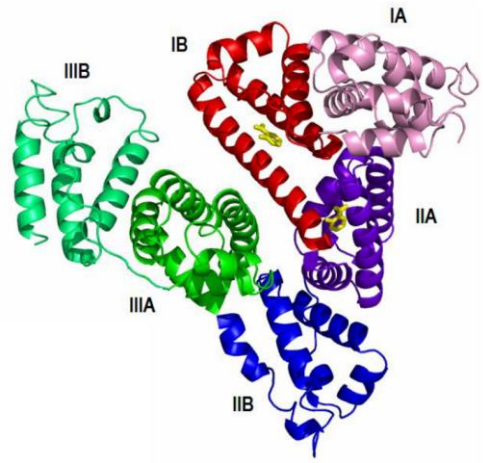

Figure 1.13 HSA N-form. Subdomains are colored as follow: pink, IA; red, IB; purple, IIA; blue, IIB; green, IIIA; cyan, IIIB. Modified from ref [36].

Serum albumin has appeared long time ago, in early vertebrate, so all mammals blood plasma is rich with this protein. Evolution stages carried along with them also

modification to albumin structures and sequences, so albumin of different species differs in some manner. Beside HAS, also bovine serum albumin (BSA) is of great interest for researches, mainly due to its wide availability and low cost. Overall conformation of HSA and BSA are similar, but they share just the 75.8% of the amino acid residues sequence [27]. Still, BSA is widely used as protein model for adsorption studies on biomaterials.

Albumin peptide chain has residues with acid/basic and polar or non-polar properties both. This confers to different regions of albumin hydrophilicity or hydrophobicity, according to the position in the peptide chain. It has been shown that most of HSA surface in physiological condition is hydrophilic, with some hydrophobic regions [37]. This fact, coupled with albumin easiness to undergo conformational changes, allows albumin to interact with hydrophobic and hydrophilic surfaces both. According to surface polarity, albumin will expose to them proper residues groups [38]. Due to acid/basic behavior of different amino acids residues, pH value of the solution has a strong influence on albumin net surface charge. BSA IEP is at pH equal to 4.7. Below this value, in more acidic medium, albumin surface potential is positive, while BSA is negatively charged at pH above the IEP [39].

BSA, as well as HSA, undergoes conformational modification in dependence of the pH of the solution. Several studies have investigated the possible isomers that albumin can form at different pH. In dependence of pH values, BSA and HSA exhibit four different isomers (Figure 1.12) [4,26,40]:

- N-form: it is the native state of albumin and it is present at pH between 4 and 8;
- Basic conformation: it is stable at pH > 8. Its conformation has not been well characterized yet;
- F-form: this conformation is known as the fast form, which is stable in a pH range between 3.5 and 4. It is a transition conformation, between the N-form and the expanded configuration, stable at lower pH:
- E-form: it is the conformation stable at lower pH. Albumin loses part of its helical structure and disulfide bridges.

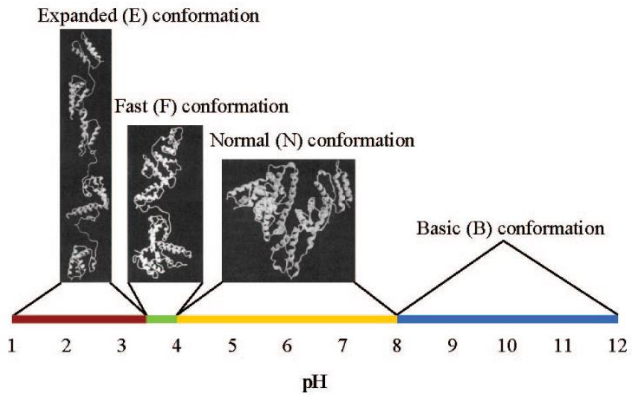

Figure 1.14 Albumin conformation and their stability according to pH values [40]

Heating also causes albumin denaturation, which can be reversible or irreversible, depending on temperatures reached and heating time. With rising temperature, first changes in structure are detected above 30 °C. There, helical

content decreases, while β-structures and random coils increase. At 65 °C, α-helix percentage drop from 67 to 44, while β-structures increases greatly from 3 to 13 %. It has been shown that BSA structure can be recovered upon cooling. Changes became irreversible when a critical temperature region is reached, which is around 55 °C Protein unfolding in solution provokes also aggregation and precipitation [41–43].

1.5.2. Fibronectin

Fibronectin (FN) is a single-gene protein (meaning that its sequence is encoded in a single gene in the DNA), expressed by several cell types, and it takes part in cell-extracellular matrix (ECM) interactions and it affects cells adhesion, growth, migration and differentiation. It acts as ligand for important biomolecules such as integrins, fibrin, heparin and collagen [44]. Also, it plays a fundamental role in vertebrate fetal development. FN is quite a large fibrous protein and exists in several different conformation due to pre-mRNA splicing. Changes in protein sequence results into generation of 20 different polypeptides [45]. FN can be found in blood plasma and within ECM both, in two different form referred as plasma or cellular FN respectively. The main difference is the solubility: the former is highly soluble in plasma, where it is one of the most abundant protein showing a concentration of 300 μg/ml in human plasma; the latter is almost insoluble. Plasma FN is shorter than cellular FN due to splicing [46].

FN is usually present as its dimer conformation, with two homologous parts connected by a pair of disulfide bridges thanks to cysteine residues in the C-terminal region of each monomer. Each subunit weights approximately 250 kDa and in primary sequences there are most of basic amino acids. Skorstengaard et al.[47] proposed the following composition for bovine FN subunits: Cys (0.1%), half-Cys (2.6%), Asp (4.7%), Asn (4.4%), Thr (10.7%), Ser (7.9%), Glu (6.0%), Gln (5.5%), Pro (7.8%), Gly (8.2%), Ala (4.2%), Val (8.1%), Met (1.1%), Ile (4.8%), Leu (5.4%), Tyr (4.2%), Phe (2.0%), Lys (3.4%), His (2.0%), Arg (5.3%), Try (1.7%)(percentages are referred to the number of each residues with respect to the total number within one subunit).

Human and bovine FN share 93% of their structure [47]. For research purposes the latter is used.

FN molecule is a repetition of three structural units, referred as repeats or modules:

- Type I repeat/F1 module: it contains 40-45 residues, along with two disulfide bonds. Four cysteine residues are present and generate disulfide bridges. It is secondary structure consists into a double-stranded anti-parallel β-sheet folded over a longer β-sheet segments, triple-stranded and anti-parallel as well;
- Type II repeat/F2 module: its length covers about 60 amino acids and it exhibits two intrachain disulfide bonds, due to cysteine residues as happens in type I repeats. It presents two short β-sheets, oriented

perpendicularly one with respect to the other, and two disordered loops;

- Type III repeat/F3 module: it is the longer repeats, with a chain of about 90 amino acids. Typically, seven β-strands are overlapped to form a sandwich of anti-parallel β-sheet, composed of three or four β-strands. In fibronectin F3 module, there are no disulfide bonds and it presents a compact hydrophobic core. F3 main role is to mediate protein-protein interactions and ensures correct positioning of functional sites.

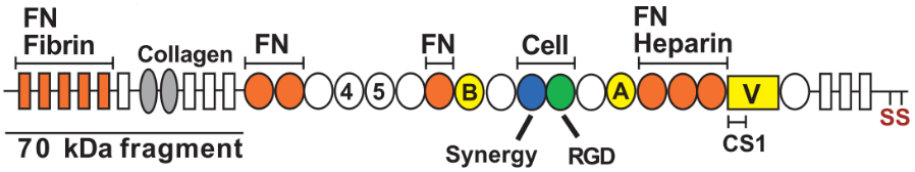

Figure 1.15 Structure of FN monomer. Different features are represented: repeats (type I rectangles, type II ovals and type III circles); binding sites for different molecules; splicing sites EDA, EDB and V region; terminal cysteine residues acting as dimerization binding site [48].

FN includes 12 type I, two type II and 15 to 17 type III repeats. They form globular domains, each with specific affinities for biomolecules or cell surfaces. These repeats have been found also in several different other proteins. 10% of amino acid in the protein sequence is out of repeats [46,49]. FN monomer is schematized in Figure 1.13. Fibronectin is classified as a β-protein, since its secondary structures shows no α-helix content. β-sheets and β-turns account for the 79 and 21 percent of FN structure respectively [45].

The large variability of FN forms is due to several type of splicing. One type of splicing involves the inclusion or exclusion of two type III repeats: extra domain A (EDA) and extra domain B (EDB). Another splicing can occur in connecting segments of type III repeats (IIICS or V region), which can present variation among different FN types or even not being present at all. It happens in case of plasma FN [46].

One of FN functions is to act as ligand of integrins, which are cell-surface receptors that bind intracellular cytoskeleton with ECM. FN-integrins interactions is important in multimeric fibronectin fibrils assembly, which is a cell-mediated process [48]. In order carry on the process, FN needs to be activated: plasma FN are usually in a non-active form. In solutions, it exhibits a compact disc-like shape (axes length is 13.8, 13.8, and 1.4 nm)[45]. Activation of FN dimers is possible thanks to α5β1 integrin receptor, which recognizes RGD-synergy repeats sequence. RGD, a trypeptide Arg-Gly-Asp, is the main binding sites for integrins, in the repeat III_{10} of FN. After activation, FN clusters are formed through four FN-binding sites within FN itself [48]. Dimeric conformation is crucial for the fibril assembly process. For active FN-domains to be exposed, fibronectin has to assume an expanded configuration. This is achieved upon integrins interactions. Also, as it happens for albumins, structure expansion is also provoked by variations in solution pH or ionic strength. High pH turns FN conformation from compact to extended.

FN surface charged is influenced by the strength of different acid/basic residues. It has an IEP between pH 5.6 and 6, while it is negatively charged at higher

pH and positively charged at lower [50]. Hydrophobic and hydrophilic regions can be found within FN as well. This allows the protein to bind to hydrophobic and hydrophilic surfaces both, through conformational changes and re-orientation on the surface [51].

FN can undergo denaturation if subjected to high temperature or acidic pH. Calorimetric studies demonstrated that each module presents its characteristic melting temperature and temperatures above 60 °C result in a loss of β-sheet content. At acidic pH, below 5.2, α-helix structures appear, substituting some β-sheet domains [45].

1.5.3. Fetal Bovine Serum

Fetal bovine serum (FBS) has been employed as cell and tissue culture substrate since late ‘50s, and nowadays it is still the most widely applied serum type [52,53]. It is used also for research purposes, and drugs and vaccines manufacturing, due to its low content of antibody[54]. FBS is derived from fetal calf blood and it is obtained by removing coagulation proteins, such as fibrin, clotting factors and cells. Practically, it is the liquid fraction of clotted blood. It is rich in serum proteins, cell nutritional elements and growth factors (Table 1.2)

Human serum is composed for its 99% of 22 different proteins, such as albumin, which alone accounts for about half of total proteins content, fibrinogen and globulins. The remaining 1% includes hundreds of different other proteins[54].

Despites FBS use is largely widespread, several issues connected with its employment have been discussed. Lot-to-lot variability, undesired side reactions with biological molecules and ethical concerns about the harvesting method from claves led to extensive researches through the employment of serum-free method [52].

As it concerns the present work, FBS can be employed for protein adsorption studies as standard for complex protein mixture.

Table 1.2 Fetal bovine serum composition [55]

Component	Averge	Range
Endotoxins (ng/ml)	0.35	0.01 - 10.0
Glucose (mg/ml)	1.25	0.85 - 1.81
Protein (mg/ml)	38	32 - 70
Albumin (mg/ml)	23	20 - 36
Hemoglobin (µg/ml)	113	24 - 181
Bilirubin, total (µg/ml)	4	3 - 11
Bilirubin, direct (µg/ml)	2	0 - 5
Urea (µg/ml)	160	140 - 200
Urate (µg/ml)	29	13 - 41
Creatinine (µg/ml)	31	16 - 43
Insulin (µU/ml)	10	6 - 14
Cortisol (ng/ml)	0.5	0.1 - 23
Growth hormone (ng/ml)	39.0	18.7 - 51.6
Parathormone (ng/ml)	1.72	0.085 - 6.18
Triiodothyronine (ng/ml)	1.2	0.56 - 2.23
Thyroxine (ng/ml)	0.12	0.08 - 0.16
Thyroid-stimulating hormone (ng/ml)	1.22	0.2 - 4.5
Follicle-stimulating hormone, (pg/ml)	95	20 - 338
Testosterone (pg/ml)	400	210 - 990
Progesterone, P4 (pg/ml)	80	3 - 360
Prolactin = Luteotropic hormone (pg/ml)	176	20 - 500
Luteinizing hormone (pg/ml)	8	1,2 - 18
Prostaglandin E (ng/ml)	5.9	0.5 - 30.5
Prostaglandin F (ng/ml)	12.3	3.8 - 42.0
Vitamin A (ng/ml)	90	10 - 350
Vitamin E (ng/ml)	1.1	1 - 4.2
Cholesterol (µg/ml)	310	120 - 630
Lactate-dehydrogenase (mU/ml)	864	260 - 1,215
Alkaline Phosphatase (mU/ml)	255	110 - 352
Aspartate-Aminotransferase (mU/ml)	130	20 - 200
Sodium, Na^+ (µeq/ml)	137	125 - 143
Potassium, K^+ (µeq/ml)	11.2	10.0 - 14.0
Calcium, Ca^{2+} (µeq/ml)	6.75	6.30 - 7.15
Chloride, Cl^- (µeq/ml)	103	98 - 108
Phosphate, P_i (µg/ml)	98	43 - 114
Selen (µg/ml)	0.026	0.014 - 0.038
pH	7.40	7.20 - 7.60

1.6. Bibliography

[1] A. Blanco, G. Blanco, Proteins, in: Med. Biochem., Elsevier, 2017: pp. 21–71. https://doi.org/10.1016/B978-0-12-803550-4.00003-3.

[2] S. Damodaran, K.L. Parkin, Fennema's Food Chemistry, Fifth Edition, CRC Press, 2017. https://doi.org/10.1201/9781315372914.

[3] D.L. Nelson, M. Cox, Lehninger Principles of Biochiemistry, 4th ed., 2005. https://doi.org/10.1016/0016-7037(83)90289-2.

[4] Z. Chi, B. Hong, X. Ren, K. Cheng, Y. Lu, X. Liu, Investigation on the conformational changes of bovine serum albumin in a wide pH range from 2 to 12, Spectrosc. Lett. 51 (2018) 279–286. https://doi.org/10.1080/00387010.2018.1471092.

[5] J. Mariam, S. Sivakami, P.M. Dongre, Elucidation of structural and functional properties of albumin bound to gold nanoparticles, J. Biomol. Struct. Dyn. 35 (2017) 368–379. https://doi.org/10.1080/07391102.2016.1144223.

[6] A.J.F. Griffiths, S.R. Wessler, S.B. Caroll, J. Doebley, Introduction to genetic analysis, Tenth edition., 2012.

[7] J. Parker, Peptide Bond, in: Encycl. Genet., Elsevier, 2001: pp. 1429–1430. https://doi.org/10.1006/rwgn.2001.0969.

[8] N.V. Bhagavan, C.-E. Ha, Three-Dimensional Structure of Proteins and Disorders of Protein Misfolding, Essentials Med. Biochem. (2015) 31–51. https://doi.org/10.1016/b978-0-12-416687-5.00004-x.

[9] G.N. Ramachandran, C. Ramakrishnan, V. Sasisekharan, Stereochemistry of polypeptide chain configurations, J. Mol. Biol. 7 (1963) 95–99. https://doi.org/10.1016/S0022-2836(63)80023-6.

[10] S.C. Lovell, I.W. Davis, W.B. Arendall, P.I.W. de Bakker, J.M. Word, M.G. Prisant, J.S. Richardson, D.C. Richardson, Structure validation by Cα geometry: ϕ,ψ and Cβ deviation, Proteins Struct. Funct. Bioinforma. 50 (2003) 437–450. https://doi.org/10.1002/prot.10286.

[11] V.E. Koteliansk, M.A. Glukhova, M. V. Bejanian, V.N. Smirnov, V. V. Filimonov, O.M. Zalite, S.Y. Venyaminov, A Study of the Structure of Fibronectin, Eur. J. Biochem. 119 (1981) 619–624. https://doi.org/10.1111/j.1432-1033.1981.tb05652.x.

[12] L. Pauling, R.B. Corey, H.R. Branson, The structure of proteins: Two hydrogen-bonded helical configurations of the polypeptide chain, Proc. Natl. Acad. Sci. 37 (1951) 205–211. https://doi.org/10.1073/pnas.37.4.205.

[13] N.V. Bhagavan, C.-E. Ha, Three-Dimensional Structure of Proteins, Essentials Med. Biochem. (2011) 29–38. https://doi.org/10.1016/b978-0-12-095461-2.00004-7.

[14] J.S. Richardson, The Anatomy and Taxonomy of Protein Structure, in: Structure, 1981: pp. 167–339. https://doi.org/10.1016/S0065-3233(08)60520-3.

[15] J.A.A. Sillince, M. Sillince, Molecular Databases for Protein Sequences and Structure Studies, Springer Berlin Heidelberg, Berlin, Heidelberg, 1991. https://doi.org/10.1007/978-3-642-76809-5.

[16] Schoolworkhelper Editorial team, Protein Structures: Primary, Secondary, Tertiary, Quaternary, (n.d.). https://schoolworkhelper.net/protein-structures-primary-secondary-tertiary-quaternary/ (accessed March 23, 2020).

[17] S. Adam-Day, Protein Structure , (n.d.). https://alevelnotes.com (accessed March 18, 2020).

[18] W.T. Godbey, Proteins, in: An Introd. to Biotechnol., Elsevier, 2014: pp. 9–

33. https://doi.org/10.1016/B978-1-907568-28-2.00002-2.
[19] C.M. Gomes, P.F.N. Faísca, Protein Folding: An Introduction, 2019. https://doi.org/10.1007/978-3-319-00882-0_1.
[20] G. Markus, F. Karush, The Disulfide Bonds of Human Serum Albumin and Bovine γ-Globulin, J. Am. Chem. Soc. 79 (1957) 134–139. https://doi.org/10.1021/ja01558a034.
[21] P. David Eckersall, Proteins, Proteomics, and the Dysproteinemias, in: Clin. Biochem. Domest. Anim., Elsevier, 2008: pp. 117–155. https://doi.org/10.1016/B978-0-12-370491-7.00005-2.
[22] G. Fermi, M.F. Perutz, B. Shaanan, R. Fourme, Image of 2HHB (The crystal structure of human deoxyhaemoglobin at 1.74 Å resolution) created with NGL (A.S. Rose, A.R. Bradley, Y. Valasatava, J.D. Duarte, A. Prlić, P.W. Rose (2018) NGL viewer: web-based molecular graphics for large complexes. Bioinforma, J. Mol. Biol. 175 (1984) 159–174. https://doi.org/10.1016/0022-2836(84)90472-8.
[23] C. Tanford, Protein Denaturation, in: Cold Spring Harb. Symp. Quant. Biol., 1968: pp. 121–282. https://doi.org/10.1016/S0065-3233(08)60401-5.
[24] C.B. Anfinsen, Principles that Govern the Folding of Protein Chains, Science (80-.). 181 (1973) 223–230. https://doi.org/10.1126/science.181.4096.223.
[25] T.E. Creighton, The biophysical chemistry of nucleic acids & proteins, Helvetian Press, 2010. http://dla.library.upenn.edu/dla/franklin/record.html?q=Biophysical%2A AND %28nucleic acid%2A OR rna OR dna%29 AND %28protein%2A OR peptide%2A%29&filter.access_facet.val=Online&qt=dla-advanced&id=FRANKLIN_5313306&.
[26] T. Peters, All About Albumin, Elsevier, 1995. https://doi.org/10.1016/B978-0-12-552110-9.X5000-4.
[27] A. Bujacz, Structures of bovine, equine and leporine serum albumin, Acta Crystallogr. Sect. D Biol. Crystallogr. 68 (2012) 1278–1289. https://doi.org/10.1107/S0907444912027047.
[28] B.X. Huang, H.-Y. Kim, C. Dass, Probing three-dimensional structure of bovine serum albumin by chemical cross-linking and mass spectrometry, J. Am. Soc. Mass Spectrom. 15 (2004) 1237–1247. https://doi.org/10.1016/j.jasms.2004.05.004.
[29] R. Raoufinia, A. Mota, N. Keyhanvar, F. Safari, S. Shamekhi, J. Abdolalizadeh, Overview of albumin and its purification methods, Adv. Pharm. Bull. 6 (2016) 495–507. https://doi.org/10.15171/apb.2016.063.
[30] D.C. Carter, J.X. Ho, Structure of serum albumin, Adv. Protein Chem. 45 (1994) 153–176. https://doi.org/10.1016/S0065-3233(08)60640-3.
[31] C.M. Gruian, C. Rickert, S.C.T. Nicklisch, E. Vanea, H.-J. Steinhoff, S. Simon, Conformational Changes and Competitive Adsorption between Serum Albumin and Hemoglobin on Bioceramic Substrates, ChemPhysChem. 18 (2017) 634–642. https://doi.org/10.1002/cphc.201600886.
[32] B. Meloun, L. Morávek, V. Kostka, Complete amino acid sequence of human serum albumin, FEBS Lett. 58 (1975) 134–137. https://doi.org/10.1016/0014-5793(75)80242-0.
[33] X.M. He, D.C. Carter, Atomic structure and chemistry of human serum albumin, Nature. 358 (1992) 209–215. https://doi.org/10.1038/358209a0.
[34] S. Sugio, A. Kashima, S. Mochizuki, M. Noda, K. Kobayashi, Crystal structure of human serum albumin at 2.5 Å resolution, Protein Eng. 12 (1999)

439–446. https://doi.org/10.1093/protein/12.6.439.
[35] T. Peters, Serum Albumin, Adv. Protein Chem. 37 (1985) 161–245. https://doi.org/10.1016/S0065-3233(08)60065-0.
[36] L. Karami, E. Tazikeh-Lemeski, A.A. Saboury, Molecular dynamics simulation and free energy studies on the interaction of salicylic acid with Human Serum Albumin (HSA), Phys. Chem. Res. 5 (2017) 483–496. https://doi.org/10.22036/pcr.2017.63757.1315.
[37] E. Retnaningtyas, S.B. Sumitro, D.W. Soeatmadji, E. Widjayanto, Molecular dynamics simulation for revealing the role of water molecules on conformational change of human serum albumin, Int. J. Pharm. Clin. Res. 8 (2016) 158–161.
[38] Y.L. Jeyachandran, E. Mielczarski, B. Rai, J.A. Mielczarski, Quantitative and qualitative evaluation of adsorption/desorption of bovine serum albumin on hydrophilic and hydrophobic surfaces, Langmuir. 25 (2009) 11614–11620. https://doi.org/10.1021/la901453a.
[39] R. Li, Z. Wu, Y. Wangb, L. Ding, Y. Wang, Role of pH-induced structural change in protein aggregation in foam fractionation of bovine serum albumin, Biotechnol. Reports. 9 (2016) 46–52. https://doi.org/10.1016/j.btre.2016.01.002.
[40] E. Edri, O. Regev, pH effects on BSA-dispersed carbon nanotubes studied by spectroscopy-enhanced composition evaluation techniques, Anal. Chem. 80 (2008) 4049–4054. https://doi.org/10.1021/ac800124x.
[41] K. Takeda, A. Wada, K. Yamamoto, Y. Moriyama, K. Aoki, Conformational change of bovine serum albumin by heat treatment, J. Protein Chem. 8 (1989) 653–659. https://doi.org/10.1007/BF01025605.
[42] V.A. Borzova, K.A. Markossian, N.A. Chebotareva, S.Y. Kleymenov, N.B. Poliansky, K.O. Muranov, V.A. Stein-Margolina, V. V. Shubin, D.I. Markov, B.I. Kurganov, Kinetics of thermal denaturation andaggregation of bovine serum albumin, PLoS One. 11 (2016) e0153495. https://doi.org/10.1371/journal.pone.0153495.
[43] H.M. Zhang, K. Lou, J. Cao, Y.Q. Wang, Interaction of a hydrophobic-functionalized pamam dendrimer with bovine serum albumin: Thermodynamic and structural changes, Langmuir. 30 (2014) 5536–5544. https://doi.org/10.1021/la501129y.
[44] R. Pankov, K.M. Yamada, Fibronectin at a glance, J. Cell Sci. 115 (2002) 3861–3863. https://doi.org/10.1242/jcs.00059.
[45] E. Österlund, The secondary structure of human plasma fibronectin: conformational changes induced by acidic pH and elevated temperatures; a circular dichroic study, Biochim. Biophys. Acta (BBA)/Protein Struct. Mol. 955 (1988) 330–336. https://doi.org/10.1016/0167-4838(88)90212-9.
[46] H. Kosmehl, A. Berndt, D. Katenkamp, Molecular variants of fibronectin and laminin: Structure, physiological occurrence and histopathological aspects, Virchows Arch. 429 (1996) 311–322. https://doi.org/10.1007/BF00198435.
[47] K. Skorstengaard, M.S. Jensen, P. Sahl, T.E. Petersen, S. Magnusson, Complete primary structure of bovine plasma fibronectin, Eur. J. Biochem. 161 (1986) 441–453. https://doi.org/10.1111/j.1432-1033.1986.tb10464.x.
[48] I. Wierzbicka-Patynowski, J.E. Schwarzbauer, The ins and outs of fibronectin matrix assembly, J. Cell Sci. 116 (2003) 3269–3276. https://doi.org/10.1242/jcs.00670.
[49] J.R. Potts, I.D. Campbell, Structure and function of fibronectin modules,

Matrix Biol. 15 (1996) 313–320. https://doi.org/10.1016/S0945-053X(96)90133-X.

[50] B. Fernández-Montes Moraleda, J.S. Román, L.M. Rodríguez-Lorenzo, Influence of surface features of hydroxyapatite on the adsorption of proteins relevant to bone regeneration, J. Biomed. Mater. Res. - Part A. 101 A (2013) 2332–2339. https://doi.org/10.1002/jbm.a.34528.

[51] D.E. MacDonald, B. Markovic, A.L. Boskey, P. Somasundaran, Physico-chemical properties of human plasma fibronectin binding to well characterized titanium dioxide, Colloids Surfaces B Biointerfaces. 11 (1998) 131–139. https://doi.org/10.1016/S0927-7765(98)00030-7.

[52] J. van der Valk, K. Bieback, C. Buta, B. Cochrane, W.G. Dirks, J. Fu, J.J. Hickman, C. Hohensee, R. Kolar, M. Liebsch, F. Pistollato, M. Schulz, D. Thieme, T. Weber, J. Wiest, S. Winkler, G. Gstraunthaler, Fetal Bovine Serum (FBS): Past - Present - Future, ALTEX. 35 (2018) 99–118. https://doi.org/10.14573/altex.1705101.

[53] T. Yao, Y. Asayama, Animal-cell culture media: History, characteristics, and current issues, Reprod. Med. Biol. 16 (2017) 99–117. https://doi.org/10.1002/rmb2.12024.

[54] M. Johnson, Fetal Bovine Serum, Mater. Methods. 2 (2012). https://doi.org/10.13070/mm.en.2.117.

[55] T. Gstraunthaler, Gerhard, Lindl, Composition of FBS, Zell- Und Gewebekultur. (2002) 2. http://radio.cuci.udg.mx/bch/EN/Forschung/FBS.pdf%0Afile:///D:/Users/Ludmilla/Documents/FBS componets.pdf.

Chapter 2

Protein adsorption on biomaterials

2.1. Driving forces in the adsorption process

As all processes, the protein adsorption on surfaces is ruled by thermodynamic laws. In particular, it happens spontaneously when the following relation is fulfilled:

$$\Delta G_{ads} = \Delta H_{ads} - T\Delta S_{ads} < 0 \qquad (2.1)$$

Where ΔG_{ads} is the variation in Gibbs free energy of the adsorption process, ΔH_{ads} is the variation in enthalpy, and ΔS_{ads} is the difference in entropy. T is the temperature. Eq. 2.1 is the Gibbs function [1], and it states the principle that spontaneous processes are those who minimize the free energy of the systems.

In spite of Eq 2.1 simple apparency, both enthalpic and entropic terms are the results of a large number of contributing factors, which are not of any simple explanation. Since long time, several authors have reviewed scientific literature about adsorption driving forces [2–8], trying to find a comprehensive explanation for this "common but very complicated phenomenon", as Nakanishi described it 20 years ago [3].

The main driving forces in protein adsorption are hydrophobic interactions, electrostatic interactions and van der Waals forces.

2.1.1. Hydrophobic interactions

As consequence of the Gibbs' relation, one possibility to decrease the free energy of the system is to increase its entropy. Hydrophobic interactions play a major role in this picture.

As discussed in Chapter 1, proteins tertiary structure is maintained mainly thanks to hydrophobic interactions between hydrophobic amino acid residues.

When a protein comes in close contact with a hydrophobic surface, one of its sides is no more interacting with water molecules, thus the balance maintaining protein stability, among intra-protein and protein-solvent interactions, might be deranged. More, a hydrophobic surface provides a region where hydrophobic residues in the peptide chain can be accommodated without interacting with water. As consequences, proteins tend to undergo conformational changes upon adsorption on hydrophobic sorbent, increasing its entropy. Energy gain due to unfolding of adsorbed protein has been regarded as one of the strongest forces that drive adsorption [9]. Protein denaturation during adsorption is widely reported, and, as a rule of thumb, extent of denaturation is greater on hydrophobic surfaces with respect to hydrophilic ones [10,11].

Further contributions in minimizing the Gibbs' free energy are to be researched in the water component of the system, mainly affecting the entropic part [2]. In fact, when a hydrophobic surface is immersed into a water medium, solvent molecules close to surface are perturbed. Bulky water molecules tend to self-associate through a 3D network of hydrogen bonds [12,13]. This network can be disrupted by the presence of a solute or a solvent that shows no ability to form hydrogen bonds. Water molecules in the interface will therefore organize and structure themselves in order to optimize and maximize hydrogen bonding. The structured water zone comprehend some atomic layer in height [14]. Structured water has less entropic energy with respect to bulky water molecules, thus, the molecules displacement during the adsorption of proteins results in entropy gains, which increases the reduction of Gibbs free energy. Since proteins are large molecules, a great number of water molecules have to be removed from the sorbent surface. Thus, dehydration of hydrophobic surfaces has a strong contribute in spontaneous adsorption of proteins [2].

2.1.2. Electrostatic and van der Waals interactions

Even though electrostatic forces have a minor role regarding adsorption on non-polar and/or hydrophobic surfaces, due to great energetic contributions of hydrophobic interactions, the relation is reversed considering hydrophilic and/or charged surface. These interactions affect mainly the enthalpic part of Gibbs' relation [4].

When a charged surface is immersed into a liquid solution, positive or negative ions gather onto the surface and arrange themselves to form the so called electrical double layer (Figure 2.1). A first layer of ions of opposite charge with respect to the material form the Stern layer, while the second layer, known as Gouy-Chapman diffuse layer, extends through the bulk exhibiting an abundance of ions in order to compensate the surface charge. The electrical potential at the shear plane, dividing Stern and diffuse layers, is the zeta potential (ζ). A scheme of the double layer is reported in Figure 2.1 [15].

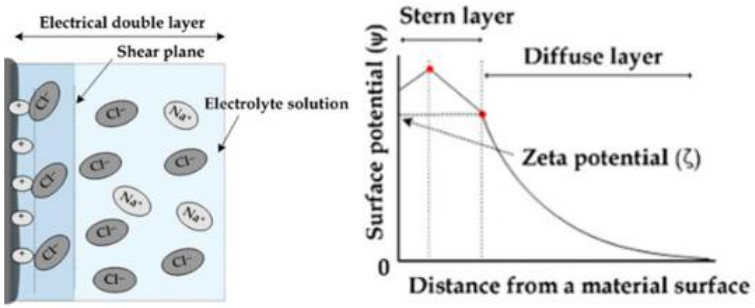

Figure 2.1 Double layer representation and electrical potential evolution. Modified from ref. [15]**.**

The extension of the diffuse layer determines the distance at which two immersed bodies can interact electrostatically. Thickness of the diffuse layer (λ) is independent of the material, but it is determined by the ionic strengths of the liquid medium. λ is known as the Debye length and is defined by the following equation [4]:

$$\lambda = \sqrt{\frac{\varepsilon\varepsilon_0 kT}{e^2 \sum_i c_i q_i^2}} \qquad (2.2)$$

Where:

ε is the medium dielectric constant
ε_0 is the vacuum permittivity
k is the Boltzman constant
T is the temperature in Kelvin degrees
e is the electron charge
q and c are the ionic valency and the concertation, of the i^{th} electrolyte in solution respectively.

As two corps in solution approach, their diffuse layers overlap and generate attractive or repulsive electrostatic interactions, according to the respective sign of the surface charges. The energy of these interactions, U_{electr}, are dependent on the surface potential (ψ_S) and on the protein potential (ψ_P), and it is give by the following equation, stating the boundary condition that surface potential is constant [4]:

$$U_{electr} = \varepsilon\pi R\left[(\psi_S + \psi_P)^2 \ln(1 + e^{-x/\lambda}) + (\psi_S - \psi_P)^2 \ln(1 - e^{-x/\lambda})\right] \qquad (2.3)$$

Where:

R is the curvature radius of the protein
x is the distance between the surface and the protein

As well as colloidal particles, proteins experience forces due to dipole-dipole interactions, commonly referred as van der Waals forces. They are constituted of three different contributions: Keesom and Debye interactions and London forces. The former two arise from electrostatic interactions, dipole-dipole interaction and dipole-dipole induced interaction respectively. They involve polar molecules. London forces, on the other hand, arise from induced dipole-induced dipole interactions generated by the polarization of interacting non-polar molecules. Van der Walls interactions are usually attractive on short distances. In fact, they are proportional to $1/r^6$ [16]. The energy due to overall contributions of van der Waals forces is expressed through the Hamaker constant (A), which is empirical and

depends on the examined system (materials, particles geometry and liquid medium), and it follows the relation [4]:

$$U_{vdWaals} = -\frac{AR}{6x} \tag{2.4}$$

The combination of contributions from electrostatic interactions and van der Waals forces constitute the well-knonw DLVO (Derjaguin, Landau, Verwey Overbeek) theory. This theory can predict whether the resulting force is attractive or repulsive depending on the distance and the energy barrier for aggregation of particles (Figure 2.2) [16].

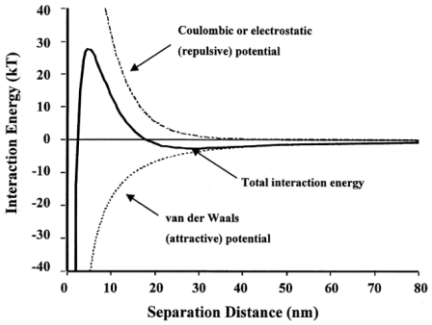

Figure 2.2 Graphical representation of the DLVO theory. Total interaction energy is plotted versus the distance as sum of electrostatic repulsive interactions and van deer Waals attractive forces [16]

2.2. Factors influencing protein adsorption

2.2.1. Protein characteristics

As briefly discussed before, the adsorption process of proteins is deeply affected by several features of proteins themselves. Water-protein interactions, electrostatic attraction with the sorbent surface and extent of conformational modifications are in strict correlation with the peptide chain chemistry and charge and protein structure stability. Regarding a protein mixture, as biological fluids are, diffusivity of proteins determines which one moves faster in the liquid medium. Thus, also protein masses ratios are of interest discussing factors influencing adsorption.

2.2.2. Structural stability

It is widely reported that proteins can undergo conformational transitions after adsorption on hydrophobic or hydrophilic/charged surfaces both [17,18]. In the former case, larger structural deformations generate entropy gains. On the second kind of surfaces, rearrangements in the protein structure allow optimization of electrostatic interactions. Thus, charged amino acid residues can be close to oppositely-charged surface. This fact explains the counter-intuitive adsorption of protein on likely-charged surfaces. Therefore, proteins with lower structural stability are prone to adsorb in greater amount with respect to the more stable ones. The concept of *soft* and *hard* protein was introduced by Norde [17] to easily

visualize this concept. Soft protein family includes intermediate size proteins such as albumin, transferrin, immunoglobulins [7]. Albumin configurations after adsorption have been intensively researched. BSA was proven to undergo conformational modification after adsorption on ceramics and bioceramics substrates [19,20], on nanoparticles [21,22], hydrophilic or hydrophobic polymers [23,24], and on metals, such as Ti alloys [25,26]. Conformational modifications have been reported also for immunoglobulins [27,28] and transferrin [29]. Small proteins usually account as the hard ones: β-Lactoglobulin, α-chymotrypsin and lysozyme [7]. In these cases, very little structural rearrangements occur upon adsorption [30,31].

Despite wide spread of Norde approach [17], as in many general concepts regarding protein adsorption, protein behavior predictions based on soft/hard classification shall be intended as a rule of thumb since exceptions to it have been reported in literature [32,33].

2.2.3. Protein charge

As discussed in section 1.1, protein-surface electrostatic interaction might heavily contribute to the adsorption process, especially regarding adsorption on hydrophilic surfaces. Protein charge is defined by acid/basic behavior of surface amino acid residues and it is strictly dependent on the pH of the liquid phase [34]. Protein overall surface is negatively charged at pH above the IEP and positively charged at pH below the IEP. IEP of different proteins varies on a very wide pH range. For instance, lysozyme shows an IEP around 11 [35], while fibronectin IEP occur at lower pH, about 5.6-6 [36] and the one of BSA is even at the more acidic pH of 4.7 [37]. However, it is necessary to keep in mind that surface charge is not homogeneous on protein. Depending on the amino acid residues sequence and on the secondary and tertiary structures, charge distribution can assume a patch-like aspects, with positive and negative regions, as shown in Figure 2.3.

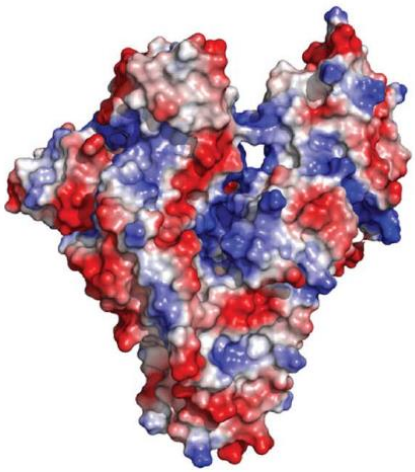

Figure 2.3 BSA molecule charge distribution. Positive domains are represented in blue, negative in red and neutral in grey [38]

The influence of the exposed charge on the adsorption process needs to be addressed taking into account also the charge borne by the adsorbent surface.

Proteins adsorbs easily on substrates that have opposite net charge due to electrostatic attractive interactions [39]. Thanks to charge inhomogeneous distribution, proteins are able also to adsorb also on surfaces that have a net charge of the same kind. At pH 7, BSA has been proven to adsorb on negative charged surfaces, despite its overall negative net charge. Albumin can still interact with the surface thanks to its positive residues, if they are close enough to the surface. Structural modifications can improve attractive electrostatic interactions [40].

Furthermore, protein-protein lateral interactions depend on protein charge, too. It is accepted and confirmed that the higher amount of protein adsorbed happens in correspondence of the IEP of the protein [41,42]. Electrostatic repulsion of likewise-charged proteins, as usually are protein of the same kind in solution away from the IEP, results in lower adsorption on the surface [43]. Protein-protein interactions and their behavior on surfaces will be discussed in more detailed manner later in this chapter.

Molecular weight

Protein mass influences different aspects of adsorption mechanisms. At first, once an interface is created between the protein solution and a sorbent surface, diffusion of proteins from the bulk at the interfacial region takes place. As it is reasonable, smaller molecules diffuse faster than larger one, therefore they can reach the surface faster. In first approximation, proteins in solution can be considered as sphere. Thus, considering two proteins *i* and *j* , the ratio between their diffusion coefficient, D, and their molecular weight, MW, can be expressed as [8]:

$$\frac{\mathrm{D}_i}{\mathrm{D}_j} = \frac{\mathrm{MW}_j^{\,1/3}}{\mathrm{MW}_i} \tag{2.5}$$

The equation 2.5 applies to a wide range of MW, fitting several different proteins.

Differences in diffusion coefficients partially explain why smaller proteins adsorb at first, in larger amount than bigger ones [7]. However, time scale and distances of protein diffusions towards the surface are too short to explain the preliminary selectivity in size of protein adsorption[44]. A complementary effect of protein mass is that larger proteins need to displace a larger amount of hydration water, from the surface and the proteins themselves both, in order to get in contact with the surface. Higher energies are needed for larger molecules to enter the interface region, therefore promoting adsorption of smaller ones in first place [44].

Nevertheless, larger proteins usually exhibit stronger adhesion forces with the surface. Protein adsorption is a dynamic process, proteins with higher MW can eventually displace the smallest ones, adsorbing on the surface. This is referred as the Vroman effect [7].

2.2.4. Surface features

Protein adsorption is influenced on one side by properties of proteins and liquid medium, on the other side by properties of adsorbent surface. Both long- and short-range protein surface interactions are affected by surface chemistry, wettability, charge and topography, also. Surface modifications have been vastly employed by researchers to study the different role played by substrates in the adsorption process from several different points of view.

Surface charge and wettability

As it happens for proteins, chemical groups exposed on sorbent surfaces have a role in defining the electrostatic interactions with proteins and hydration energy, which contribute heavily and in both ways to the overall variation of Gibbs' free energy. Wettability is one of the main players in determining the interactions between proteins and substrates. Hydrophobic or hydrophilic adsorbent can lead to a whole different outcome of the adsorption process. It is widely recognized that hydrophobic materials adsorbs more proteins that hydrophilic ones [7,45,46]. Furthermore, other aspects of protein adsorption are affected by surface wettability. Xu and Siedlecki investigated the effect of change in wettability by adsorbing different proteins on low density polyethylene (LDPE), treated at different intensities with glow discharge plasma. They found that a pivotal water contact angle (CA)(θ) for protein behavior is about 65°. Adhesion forces of proteins are lager for poorly wettable surface, while they decrease at θ below 65°[47]. This value is in agreement with other researchers, who found contact angle values near θ = 65° as dividing line between hydrophilic and hydrophobic surfaces [12]. Interestingly, a threshold for adhesion of cells on surfaces is also located around 60° as contact angle (surface energy equal to 40 mN/m): in this case, cell adhesion is enhanced for larger surface energy, that means lower contact angle values. Cell adhesion is larger on hydrophilic biomaterials, surfaces with surface energy just around the threshold value are biocompatible, but non-adhesive, while highly hydrophobic surfaces are usually cytotoxic.

Hydrophobicity/hydrophilicity of surfaces, combined with structural stability of proteins, have influence also on unfolding mechanisms. Usually, higher hydrophobicity corresponds to larger structural changes [18]. FN structural changes have been investigated after adsorption on surfaces with well-defined properties obtained by self-assembled monolayer (SAM). Hydrophobic surfaces induce heavier structural changes with respect to the hydrophilic ones [48]. Albumin adsorption on CH_3- and HO-terminated SAM substrate was investigated as well, confirming this general rules [49].

Hydrophobic materials are usually non-polar, while hydrophilic ones exhibit electrical charges on their surfaces. As well as wettability, surface charge has an important influence on surface-proteins interactions. Depending on the pH of the solution and proteins contained within, surfaces can be charged in the same way as proteins or not. Thus, the electrostatic forces between proteins and the surface can

be attractive or repulsive [4]. Negatively charged surfaces, such as bioglasses in physiological environment, hinder the process and decrease the total amount of protein adsorbed [50]. Proteins with net negative charge can still adsorbs on surfaces with overall negative charge thanks to positive charged region on the protein surfaces, such as in the case of BSA [40], or thanks to positive charged groups or molecules on the surface of the sorbent materials, as for example positive ions in bioactive glasses[50] or positive portion of copolymers [51]. Whether negative charged surfaces usually repel proteins, it has been demonstrated that increasing positive charge presence promotes protein adhesion in larger amount. Titanium and its alloys are usually negatively charged at pH = 7.4. Recent studies demonstrated that positively charged Ti surfaces can be obtained through lithium ion-containing coating, and that protein adsorption is enhanced [52].

Surface topography and chemistry

Controlling protein adsorption is not only matter of control the surface chemistry or charge. It is well established that surface features in the micrometric scale impact growth and proliferation of several different types of cells. Less understood and investigated is the impact that micro and nanometric topographical elements exert on protein adsorption [53]. As it is quite obvious, more proteins adsorb on larger surface areas due to increased surface roughness. Surprisingly, some proteins adsorb on appreciably larger amount than that expected just for increased surface areas. Fibrinogen was observed to exhibit this fact, probably due to anisotropy of its structures and changes in protein orientation on the surface. BSA, on the other hand, was less affected by nanometric surface roughness [54]. As usual, protein adsorption is a complex phenomenon, and it is necessary to bear in mind that a single parameter is not the only one acting on it. Several studies pointed out that varying surface roughness means also to modify other surface property, namely surface wettability. Increased protein uptake had been co-addressed also to increased hydrophobicity of rough polymeric surfaces [55,56]. On bioceramics, such as hydroxyapatite, besides surface roughness, crystallinity and grain size have been found crucial in establishing protein-surface interactions [36].

In order to control protein adsorption, surface can be modified to larger extent than with respect to only surface roughness. Protein adsorption can be reduced by grafting the surfaces with polymers such as poly(ethylene oxide), poly(ethylene glycol) or zwitterionic polymers. It has been reported that adsorption is suppressed thanks to steric repulsion [7,57]. Another remarkable way of gaining control on protein uptake is to functionalize the surface with a so-called polyelectrolyte brush. Grafted brushes may vary the degree of adsorption thanks to use of stimuli responsive polymers (Figure 2.4).

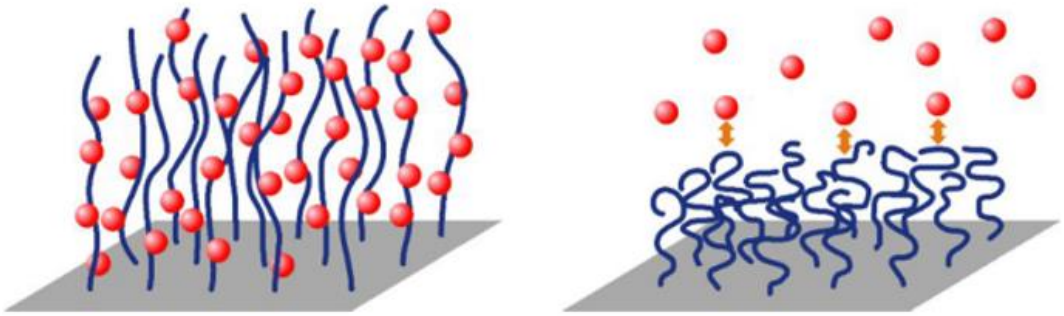

Figure 2.4 polyelectrolite grafting can modulate protein adsorption on the surface. Brushes can uptake a large amount of proteins (red spheres)(left) or they can act as a protein-repellent layer for the surface (right). The change in conformation can be achieved by varying temperature, pH or solution ionic strength [57]

If weak polyelectrolytes are used, such as poly(acrylic acid), protein affinity for the surface can be modified by varying pH and ionic strength of the solution [36]. Fibrinogen adsorption control was obtained thanks to a thermosensitive polymer such as poly(N-isopropylacylamide), which has a protective effect at temperatures below the lower critical solution temperature whist being adsorbent at T above it [58].

2.2.5. Temperature

Protein adsorption is ruled by the Gibbs' relation (eq. 2.1), where the negative contribute is represented by the term $-T\Delta S_{ads}$. Thus, it is clear that temperature has a direct role in lowering the free energy of the system. Actually, temperature affects the process in other ways, than just being a multiplier of the entropy variation, namely, the adsorption rate and the equilibrium state plus increasing protein mobility in solution [7]. Several authors claim that both adsorption kinetic [59] and equilibrium surface concentration [60,61] increase with higher temperature. A very interesting study on the effect of temperature on protein adsorption and desorption was carried out by Kiesel et al. [62]. Higher temperatures increase the mobility of protein at solid-liquid interface, thus influencing desorption of proteins. Desorption is kinetically driven. In this process, structural stability of proteins has a crucial role. In fact, hard proteins, such as lysozyme are more mobile at the interface, while soft proteins, such as BSA, desorb less due to denaturation and increased contact area. The adsorption, on the other hand, is mainly driven by entropy gain due to higher mobility of protein chains at higher temperature, causing conformational changes. If adsorption is obtained at temperatures above the protein denaturation temperature, unfolding can lead to multilayer formation on the surface.

2.2.6. Solution parameters

The environment at which the adsorption experiments are conducted is fundamental to determine the fate of proteins, almost as much as surfaces and protein themselves. Physical properties, namely electrostatic states, of players in the process are determined through the liquid medium they are immersed in and presence of different elements in solution can affect also other characteristic of

proteins (e.g. structural stability). pH, ionic strength, salt ions in solutions and protein concentration play important roles in protein adsorption.

pH and ionic strength

When it comes to adsorption of proteins onto hydrophilic/polar surfaces, electrostatic interactions may overtake the hydrophobic effect as principal driving force in the adsorption process. Electrostatic states of proteins and solids are determined by the environment in which the adsorption experiment is conducted, in particular, they are affected by pH and ionic strength of buffer solutions.

As already discussed, pH controls whether acidic or basic surface groups are in a protonated or deprotonated state. Therefore, pH variations can induce negative, positive or neutral net charge on proteins and surfaces, generating attractive or repulsive forces between them. It's well established that the highest adsorption degrees can be obtained in solution with a pH values corresponding to the IEP of proteins. Usually, proteins of the same type are likewise charged in solution, therefore protein-protein electrostatic interactions are repulsive, preventing very close packing on the surface. At the IEP, protein surface net charge is null, so protein-protein repulsion is at minimum, maximizing the adsorption. This was observed for several different protein-surface systems, such as BSA on ultrafiltration membranes [41] and titanium dioxide (TiO_2) [59]. Kubiak-Ossowska et al. [42] observed how egg lysozyme absorbs onto silica in dependence of the pH. Lysozyme IEP is at pH 10. Below this value, protein and SiO_2 are oppositely charged and adsorption is favored by electrostatic attraction. This until the negative charge on the surface decrease, approaching zero around pH 4, and decreasing adsorption. As expected, adsorption is maximal at lysozyme IEP and it decrease at higher pH, when protein and surface are negatively charged both and the process is driven by hydrophobic interactions. As reported by Demanèche et al. [63], pH has also an influence on the conformation of adsorbed layer, as consequence of pH-induced protein unfolding. Through atomic force microscopy measurements, they observed that layer height of BSA adsorbed onto mica decreased at acidic pH, corresponding to an extended isomer of the protein. The same effect was not observed for a hard protein, such as α-Chymotrypsin.

Solution pH determines the kind of electrostatic interactions, but it is not enough to fully describe their effectiveness. Another important parameter is the ionic strength of the solution. In fact, it determines the distance at which electrostatic interactions are not negligible, according to the Debye length (eq 2.2). Higher ionic strength of the protein containing solution reduces electrostatic interactions, by decreasing the thickness of the diffusive layer of counterions [4]. This means that repulsive forces that may rise due to likewise charged surface of proteins and solids are less relevant in driving the adsorption. Different studies agreed that increasing the ionic strength of the solution results into increased protein uptake on surfaces [64,65].

Influence of solution composition and protein concentration

Overviewing factors influencing protein adsorption, the effects of protein solutions are "Not only pH", as Salis et al. said [66]. In fact, apart from the impact on electrostatic interactions due to pH and ionic strength, buffers result in a wider range of consequences. At first, different salt compositions and concentration within the buffer affect proteins directly in the liquid medium. It is known since long time, since pioneering studies by Hofmeister in 1880s', that salt ions in solution can have effects on solubility of proteins, namely, "salt in" if they increase the solubility, and "salt out" whenever they decrease it, provoking aggregation and precipitation [67]. These effects on solubility are related with the influence of ions on protein structural stability. Ions that are water-structure breakers (i.e. SO_4^{2-}, Mg^{2+}, Ca^{2+}) are called chaotropic and they destabilize structures of proteins. At revers, polar water-structure makers ions that stabilize proteins (i.e. SCN^-, NH_4^+, ClO_4^-) are referred as kosmotropic [68]. Hofmeister series for anions and cations, with their principal and more common effects, are represented in Figure 2.5. As usual, enormous protein variability leads to a number of exceptions to these general rules and difficulties in predicting adsorption on a salt type-bias. A reverse order of anionic Hofmeister series for positively charged proteins, for instance lysozyme, [67] or similar effects of lowered adsorption by chaotropic and kosmotropic salts [69] have been found.

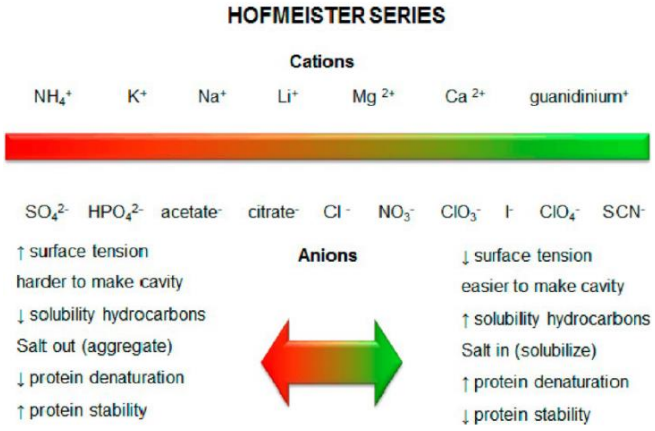

Figure 2.5 Hofmeister series of salt ions and cations accompanied by their effects on proteins in solutions [67].

Over the years, it has been reported that buffer choice affects different aspects of protein adsorption, with different results obtained with respect to different proteins. Gondim et al. [70] observed how buffers, such as trizma-hydrocloric acid (TRIS-HCl) or sodium phosphate, change the amount of HSA and human immunoglobulin G (IgG), adsorbed and how an appropriate choice can produce selective adsorption of one protein with respect to the other.. Wei et al. [71] compared adsorption of different proteins using TIRS-HCl and phosphate buffered saline (PBS) buffers. PBS depresses adsorption in a more extensive manner than TRIS-HCl, possibly due to competitive adsorption of phosphate ions $H_2PO_4^-$ and HPO_4^{2-}. Interestingly, secondary structures of adsorbed proteins resulted unaltered

by buffer choice. Nevertheless, other researchers, in disagreement with before, claim a little influence by the buffer on the adsorbed amount, stating that the main discriminant factors on adsorption are pH and ionic strength [72].

Another aspect of solutions employed in adsorption studies is the initial protein concentration. Researchers employ solution with different concentrations dictated by different reasons: physiological concentration, costs, availability and so on. Anyhow it is necessary to keep in mind that protein concentration in solution can heavily affect the adsorption process, in particular when comparing different experiments or studies. In their paper, Gondim and his group [70] evaluated the effect of protein concentration in solution on adsorption isotherms, noticing that total adsorbed amount increases with increasing quantity of proteins in solution until reaching a plateau. Similar results have been obtained also in other studies [73,74]. Furthermore, if there are not enough proteins in solution to saturate the surface, higher degree of structural changes of adsorbed biomolecules is to be expected. In sub-saturated surfaces there is room for proteins to denature after adsorption [8].

2.3. Protein adsorption on titanium-based biomaterials

This paragraph has been published as part of the review article: Titanium and protein adsorption: An overview of mechanisms and effects of surface features. J. Barberi, S. Spriano, *Materials (Basel).* **2021**, *14*, DOI 10.3390/ma14071590.

2.3.1. General Consideration on Protein Adsorption on Titanium Based Materials

Titanium peculiar properties have made it one of the most world widespread biomaterials [75]. With respect to other metals, titanium and its alloys possess excellent osseointegration capability, proper mechanical properties, and soft tissue compatibility. They have been extensively described elsewhere, therefore here only the ones of interest for discussing protein adsorption will be briefly reported [76–78]. Being a very reactive element, titanium does not exist in its metal form onto its surface, but it is immediately passivated by oxygen and its surface is covered by a thin native oxide layer, which is mainly amorphous TiO_2 about 3–7 nm thick [79]. This layer confers chemical stability, biological inertness and corrosion resistance to the surface. To understand how this biomaterial interacts with the biological environments, it is mandatory to notice that titanium surfaces are highly hydroxylated. OH groups can form by dissociation of water molecules at the five-coordinated Ti sites. Several kinds of hydroxyls can thus form on the surface, differing in their position (terminal or bridging) and in their chemical behavior (acidic or basic). As a consequence, when the surface gets in contact with water, acidic OH groups deprotonate, while basic OH groups protonate themselves, forming both positive and negative charges (Figure 2.6).

Acidic OH deprotonation: $Ti\text{-}OH + H_2O \leftrightarrow [Ti\text{-}O]^- + H_3O^+$

Basic OH protonation: $Ti\text{-}OH + H_2O \leftrightarrow [Ti\text{-}OH]^+ + OH^-$

As consequence of the dissociation constants of both the OH groups, IEP of titanium lies around 5 [80].

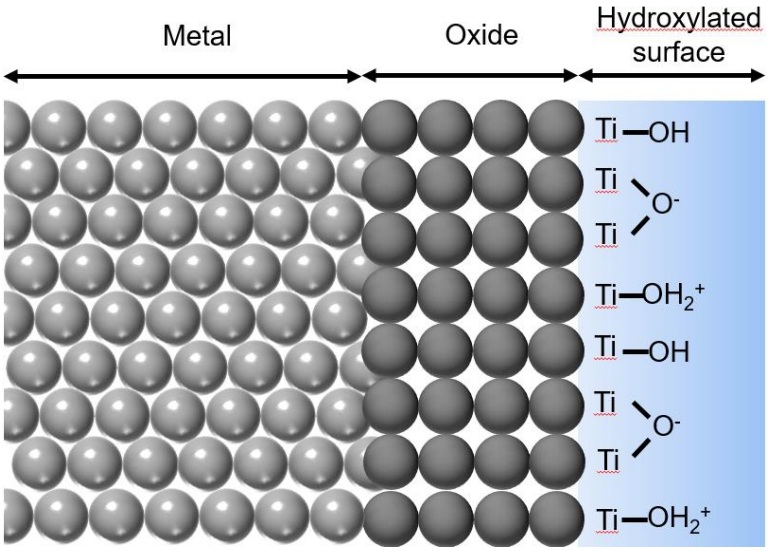

Figure 2.6 Scheme of hydroxylation of Ti surface and surface charge generation during contact with aqueous solutions.

Titanium affinity for proteins is well acknowledged. A stable protein layer was found to form in vivo after just three hours [81]. This was observed to prevent precipitation of compound like HA after a week. Ti-based materials can interact with many different proteins, such as serum albumin [82,83], FIB [84], or FN [85]. Many researchers have tried to unveil the mechanisms of interaction between proteins and titanium substrates. By studying the adsorption isotherms of several different proteins (such as human serum albumin (HSA), BSA, lysozyme (LYS), pepsin, myoglobin, and others) at different pH values, Imamura et al. [86] ascribed pseudo-irreversible adsorption of protein to electrostatic interactions between the OH_2^+ groups on the titanium surface and COO^- groups of proteins. Furthermore, negatively charged carboxyl groups can also induce protonation of the OH groups of the surface around the IEP of titanium. Another research group proposed a slightly different interaction mechanism between HSA and titanium [83,87]. They proposed that HSA has a similar effect to a local change of the pH, acting like a reduction of $[H^+]$ and affecting the thickness of the H^+ diffusion layer on the Ti surface. Interactions between albumin and a titanium surface followed the proposed two steps mechanism, which involves a first hydrogen bonding and a subsequent proton transfer.

Hydrogen bonding:

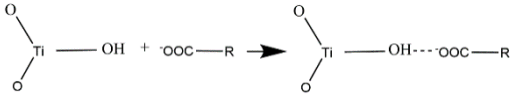

Proton transfer:

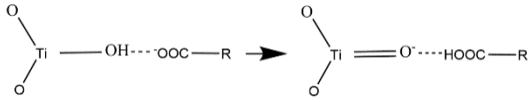

Even though the interaction mechanisms proposed by Imamura and Camàra are different, they underline the importance of the OH groups on driving protein adsorption. Molecular dynamic simulations observed that an increased density of the OH groups on rutile (1 1 0) means higher affinity for the subdomain IIIb of HSA [88]. Electrostatic interactions with the COO^- and NH_3^+ groups of proteins were greatly enhanced. A key role of the local electrostatic interactions between opposite charges respectively on TiO_2 and organic molecules was also observed for peptides [89]. The charge effect of hydroxyls on the strength of protein adsorption was investigated in another interesting computational studies by Sun et al. [90]. They tuned the hydrophobicity/hydrophilicity of rutile surface by scaling the OH charges of different factors. Lower surface charge, related to higher hydrophobicity, turned out to adsorb lactoferrin and bone morphogenetic protein-2 (BMP-2) in a stronger manner than a hydrophilic surface. Being a soft protein, BMP-2 is also more denaturated. At the same time, protein–surface interactions on hydrophilic TiO_2 surfaces are hindered due to water-surface interactions [91]. Thus, spreading and denaturation of certain adsorbed proteins are limited. OH groups generated onto TiO_2 by vacuum annealing can prevent FIB denaturation by avoiding electron transfer, from the protein to the surface. In this case, hydrophilic TiO_2 surface denatures less proteins than the hydrophobic ones [92]. Less FIB denaturation is related to lower platelet activity and better blood compatibility of biomaterials.

In order to predict the biological behavior of biomaterials, alongside the amount and type of protein adsorbed, it is necessary to be aware of their spatial configuration and orientation with respect to the surface. Proteins can adsorb in a "side-on" or "end-on" orientation, according to the positioning of their main axis [7].

Furthermore, denaturation can occur to different extents with different proteins. As already mentioned, adsorption on titanium substrates lead to denaturation of FIB. Several authors found that FIB can interact with titanium surfaces through αC domains. Since they are positively charged at pH = 7.4, electrostatic attraction between the surface and the protein can occur [93,94]. The strong protein–surface interactions lead to denaturation of FIB. This was confirmed by Zhao et al. [95]. Furthermore, even though binding via αC domains shall result in side-on orientation of the proteins on the surface, FIB was found with preferred end-on orientation. Bimodal adsorption isotherms of immunoglobulin (IgG) suggest that adsorbed proteins may undergo structural rearrangements and orientation modification according to saturation level of the surface [96]. While in some cases no denaturation of BSA was observed upon adsorption on titanium oxide [97], others had observed conformational changes of albumin. Hydrophobicity of titanium may lead to spreading of adsorbed HSA onto its surface [98]. Conformation and adsorption mechanisms are strictly dependent on both surface features and protein composition. Different structures were found for proteins that shall be analogous, such as chicken and human albumin [99]. Adsorption mechanism was also profoundly different: HSA adsorbs as a continuous thin film, while chicken albumin forms adherent flakes on the titanium surface. In addition, relevant peptide

sequences, such as RGD domains of FN, may change their spatial configuration after adsorption on rutile or anatase [100].

Surface roughness is a parameter that very often is addressed as pivotal in determining the outcome of protein adsorption, and more in general, cell behavior [101]. It does not only change the effective surface area available for interaction with proteins, but it can also affect the wettability of the materials. It has been acknowledged that roughness in the micro-range enhanced protein adsorption due to increase of specific surface area [102]. Several authors have tried to understand the extent of roughness, in particular in the nano-range, influence on the protein adsorption on titanium-based surfaces. Roughness variations from few to some tens of nm were found not to have a unique effect on all proteins and some results in literature may disagree. BSA adsorption is slightly influenced by roughness between R_a values of 1.57 and 16.44, while in the same range FIB adsorption is increased to a slightly larger extend [103]. Controversially, in a more recent study, Rockwell et al. [104] observed that the increment in the surface area ratio (SAR) due to increased roughness, in the same range as previously reported [103], along sample profile, was not sufficient for explain the increased of normalized adsorption of both FIB and BSA (Figure 2.7 a). Increments on proteins and SAR were up to 50% and 15%, respectively. Instead, the increment in curvature of surface features accounted better for the increment in adsorption (Figure 2.7 b): Higher curvature, meaning smaller features radii, favors end-on FIB adsorption and stabilizes protein secondary structures. Besides, increased roughness, from less than 1 nanometer to about 11, resulted in increased surface free energy (SFE) that promoted better adsorption of FN and VN from fetal bovine serum [105]. These results were confirmed also on TiO_2 when other proteins, such as BSA [106] or casein [107], were adsorbed.

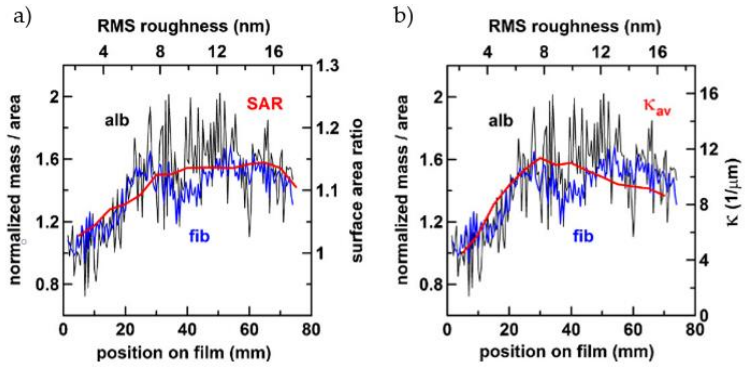

Figure 2.7 Normalized adsorption profile of bovine serum albumin (BSA) (black) and fibrinogen (FIB) (blue) on Ti with roughness gradient (left y-axes). The overlaid red lines are the SAR profile (a) **and the curvature profile** (b) **(right y-axes). Adapted from ref** [104].

Roughness of titanium substrates is also capable of influencing the mechanisms of adsorption. While adsorption of BSA, FIB, and streptavidin on flatter substrates occurs mainly as protein monolayers, roughness values about R_{ms} = 29.5 nm can increase protein–protein interactions, resulting in a multilayer type adsorption [108]. Surface features such as protuberances and peaks are not the only topographical characteristics that have influence on proteins adsorption. Surface pores in the meso- and nano-range need to be accounted when the effect of surface

roughness on this matter is discussed. Proteins are not able to enter pores smaller than their hydrodynamic radius. In the case of BSA, of which hydrodynamic diameter is about 7.2 nm, mesopores need to be at least about 9 nm for albumin to enter them [109]. Larger mesopores can accommodate more than one BSA molecule, with very little conformational changes, and protein-surface adhesion forces were stronger with respect to smaller pores [110]. Singh et al. [111], due to protein tendency to aggregate into nanopores, concluded that nanometer scale morphology is the main reason for increased protein adsorption, more than the modest increase in wettability of surface with different roughness.

Titanium and its oxide exhibit different adsorption properties with respect to other materials, such as other metals or metal oxides clinically used polymers or dental enamel. In comparison with other metal surfaces such as Au, Pt, and Ir, titanium adsorbs the largest amount of plasma proteins. This is because Ti presents the highest SFE and roughness, as a result of the deposition process of metal thin films [112]. At the opposite, when TiO_2 is compared with other oxides such as ZrO_x, TaO_x, and NbO_x, it showed the least adsorption capability [113] and it is also the flattest and the least energetic surface. ZrO_x interacts the most with albumin being a hydrophobic surface, while the amount of adsorbed BSA correlates well with roughness and polar component of the SFE on the hydrophilic oxides. Similar evidence of different mechanisms of adsorption on hydrophobic or hydrophilic surfaces was found with FIB, investigating fibrinogen adsorption on the same set of oxides. Titanium shows also different retention capability of the adsorbed proteins with respect to the other oxides. Its negative charge makes HSA displacement from its surface faster than on positive charged alumina, at pH 7 [114]. Al_2O_3 adsorbs more BSA than TiO_2 also because of its higher number of OH groups that can form H-bonds with proteins [115]. Adsorption of positively charged proteins such as lactoferrin was enhanced on titanium with respect to stainless steel, ZrO_2, and polymethylmethacrylate (PMMA) thanks to the higher negative surface charge [116]. Still, stronger interactions were found on hydrophobic substrates. In order to better understand why different materials have different behavior during their life as implants, titanium was widely compared to other surfaces of interest in the dental field. Titanium's poor adhesion to gingival tissue may be explained by the fact that, with respect to dentin, it adsorbs less key basal lamina proteins, such as laminin (LAM) α, a protein with a key role in tooth-epithelium adhesion, and nidogen-1 [117]. It was also observed that hydrophobic polymeric materials used in dental field, such as polytetrafluoroethylene (PTFE), polyethylene (PE), and PMMA, adsorb more salivary proteins than Ti, for instance salivary mucins and proline-rich proteins [118,119]. This also reflects in higher adhesion forces between albumin and polymers as PMMA and PTFE with respect to titanium [120]. Interestingly, the interaction force between BSA and Ti is about twofold more than on enamel.

2.3.2. Effect of Surface Modifications on Titanium: How Topography, Roughness and Surface Chemistry Change Protein Adsorption

Surface Modification by Sand Blasting and Acid Etching (SLA)

Surface roughness and wettability are the main parameters influenced by SLA treatments, thus changes in protein adsorption are mainly ascribed to these materials features. According to our findings in literature, the studies on this kind of surfaces are not in complete agreement. Some of them observed that SLA treatments increases the total amount of adsorbed proteins [121,122], while, in different conditions of adsorption, others observed a neglectable difference [123]. In a remarkable work of Kohavi et al. [122], the authors studied the influence of SLA and acid treatments on Ti64. Proteins adsorption was carried out in vivo during dental implantation surgery. A titanium rod was implanted into the osteotomy and removed after 10 min. Albumin, fibronectin, fibrinogen, and immunoglobulin were quantified by enzyme-linked immunosorbent assay (ELISA). The SLA surfaces adsorbed more than fourfold more of each protein with respect to an untreated surface. Acid etched (AE) titanium surfaces adsorbed only twice more. SLA surfaces were rougher than both AE and flat surfaces (R_a equal to 287.5, 214.5 and 26.8 nm, respectively). Roughness was addressed as the main factor influencing in vivo protein uptake. Prewetting of surfaces also increases protein adsorption. Similar findings on the same surfaces were obtained in vitro [122]. FN resulted the major protein found on a surface in case of adsorption both from a single protein solution and whole plasma. The effect of roughness and increased surface area on protein adsorption was also highlighted by SLA treatment followed by secondary etching [124]. Protein adsorption is only increased to a certain time of etching, since after about 30 min decreasing in specific surface area is experienced. MC3T3 pre-osteoblastic cells viability also correlate well with this observation. Kopf and co-workers [102] put effort in isolate the effect of wettability and roughness. Hydrophilic and hydrophobic SLA surfaces were obtained through proper storage in air or NaCl solutions. On some samples, the storage in NaCl resulted in further nanostructuration of the surface. WCA of hydrophilic and hydrophobic SLA surfaces ranged between less than 10° to 120°, respectively. Simply, SLA-treated surfaces showed no influence of the WCA on adsorption of both FIB and FN. On the contrary, the hydrophilic nanostructured (NS)-SLA samples adsorbed much more than the hydrophobic ones. In both cases, they adsorbed more than the SLA specimens. Thus, it seems that protein adsorption is mainly driven by roughness at the microscale and by a synergistic effect of hydrophilicity and roughness when it comes to nanostrcutures. As an interesting fact, in the same study, it is observed that blood clotting is more improved by hydrophilicity than surface topography. H_2O_2 hydrothermal treatments on SLA-treated dentals screws can promote bioactivity through surface nanostructuration and formation of many OH groups

[98]. Better protein adsorption, in particular increased selectivity towards FN, resulted from increased wettability of the implants. Hydroxylation of the surface does not only account for improved wettability and enhanced protein adsorption. SLA-induced OH groups are also responsible for denaturation of proteins, such as statherin [125]. Hydroxyls can bond with proteins through hydrogen bonds, disrupting the equilibrium of forces that maintains the native conformation of proteins. Statherin adsorbed onto polished titanium showed less denaturation.

Some studies focused on how SFE influences the adsorption of proteins. Simple sandblasting of cp-Ti resulted in very different values of surface energy, according to dimension of the blasting particles and even to their composition [126]. On rough surfaces, the authors found a linear correlation between surface energy and amount of adsorbed FN (Figure 2.8 b). Interestingly, the samples treated with SiC particles showed higher SFE, in particular the dispersive component, than the ones processed with alumina particles. As a consequence, FN adsorbed preferably on SiC-blasted samples, regardless of roughness (Figure 2.8 a). The importance of SFE on SLA treatments was also observed very recently by Mussano et al. [127]. Adsorption of different proteins, namely collagen (COL) I, FN, and BSA, was depressed by blasting with alumina if compared with machined surface. SLA treatment restored titanium adsorptive properties, though without enhancement with respect to untreated surface. Blasted surfaces showed lower SFE, while machined and SLA specimens had similar values. This correlates well with the results obtained for alumina blasting particles in ref. [126].

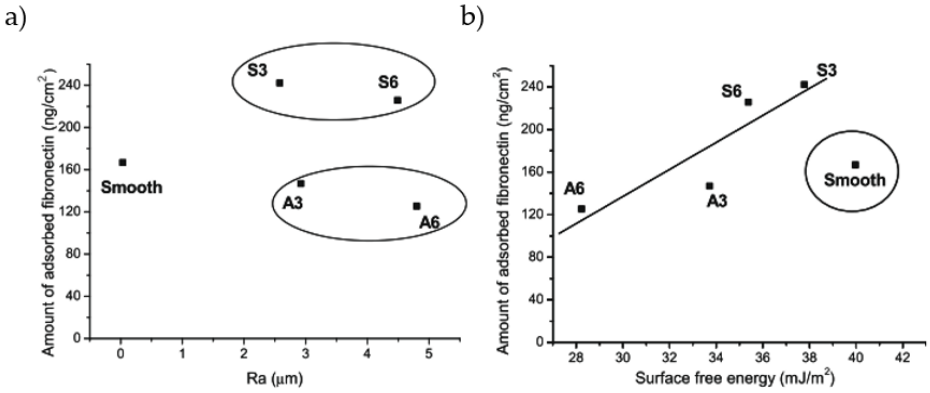

Figure 2.8 Correlation of FN adsorption with roughness (a) and surface free energy (SFE) (b) on cp-Ti blasted with different particles: S, SiC particles; A, Al_2O_3 particels; 3, particles of 212–300 μm; 6, 425–600 μm. Adapted from ref [126].

As previously said, the debate on the effective enhancement of protein adsorption by SLA treatments is an open issue. A recent study observed no difference in adsorption from FBS on machined or SLA cp-Ti [123]. Still, microrough surfaces elicit murine MC3T3-E1 osteoblastic cell spreading and adhesion. Similar findings were observed also in adsorption kinetics and total amount of adsorbed proteins when FN and BSA are adsorbed from single protein solutions, even when wettability was increased by heat treatment [128]. As an interesting fact, heat treatment promoted selective adsorption of fibrinogen and fibronectin from human serum. Even though hydrophilicity may not increase protein adsorption on SLA surfaces, it can promote the formation of a more

homogeneous protein layer [129]. SLA did not seem to enhance adsorption of salivary proteins neither [130].

Surface Modification by Chemical and Hydrothermal Treatments

Acid etching is a very simple kind of chemical treatment employed to enhance biological response of titanium surfaces [77]. Nanopatterning by acid etching was found to affect in different ways adsorption of different proteins [131]. Nanopits, generated by simultaneous acid etching and oxidation with H_2O_2, act as physical traps for proteins that can be accommodated within, such as LYS and growth/differentiation factor 5. Adsorption of larger proteins, such as FN, is hindered due to steric limitations. Acid etching of microgrooved titanium resulted in increased hydrophilicity and consequent enhancement of BSA adsorption and human osteoblast proliferation [132].

Hydrothermal treatments are widespread techniques to obtain surfaces with enhanced cytocompatibility [77]. Immersion in solutions with different chemicals and subsequent heating results in nanostructuration of the surface and modification of its chemistry.

Hydrothermal treatments on Ti64 can also be obtained using simply distilled water [133]. In this way, higher hydrophilicity is obtained without changing surface roughness. Increased wettability led to higher laminin adsorption and consequent improved adhesion of cells through integrins. Hydrogen peroxide is a common reactant for hydrothermal modification of titanium surfaces. Nanoporous structures can be obtained in this way [134]. The increased roughness and SFE of H_2O_2-treated Ti64 results in evident decrease of the WCA, from 49° to 16°, and in a sixfold increase of cytochrome C adsorption. Enhanced serum protein adsorption on this kind of surfaces is also due to the generation of OH groups on titanium surfaces [135]. BSA adsorbs also in a different conformation on H_2O_2-treated Ti64 with respect to the polished surfaces [80]. The higher amount of OH on the treated surface produced adsorption of albumin in a more hydrophilic orientation. FN was proven to adsorb in an island-like manner on this kind of surfaces, by positioning mainly in the surface valleys and forming multilayered globular structures ranging from 55 to 83 nm in diameters [136]. Titanium oxide grown using H_2O_2 treatment adsorbs FN in a more irreversible manner than sputtered TiO_2. On the other side, adsorbed HSA is more easily exchanged by HSA molecules in solution [137].

Bioactive titanium surfaces can be obtained by acid-alkali (AA) treatments, which involve a step of acid etching and a subsequent treatment in alkali solution, mainly NaOH. Both the steps can be performed at temperatures ranging from 30 °C [138] up to 70 °C [139]. These treatments allow to obtain surfaces with nanostructures, enhanced wettability, and different charges with respect to untreated titanium. Nanoscale topography was found responsible for increased protein adsorption of albumin and fibronectin in particular [138]. Treatments in NaOH result in a formation of Ti-O-Na layer that changes the surface electrical charge further increasing adsorption of negatively charged proteins such as

albumin. AA treatments are more effective in promoting protein adsorption when compared to other surface treatments, such as alkali-heat (AH) [25] or anodic oxidation treatments (AO)[140] and also SLA modification [141]. Better BSA adsorption capability of AA-Ti than AH-Ti, where samples are heated at 600 °C for 1 h after alkali treatment, relied on the higher number of OH groups and on the positive surface charge of AA-Ti [25]. Hu and Yang observed that the NH_3^+ groups of albumin mainly interact with AA and untreated samples, exposing more COO^- groups while the orientation is different on AH-Ti. Secondary structures of albumin are also affected by the charge of the surfaces and OH groups. Interestingly, they found that BSA preadsorption elicited higher mouse osteoblast proliferation on polished Ti (P-Ti), due to higher content of cell binding α-helices. The same research group observed that AA-Ti adsorbs more osseointegration-relevant proteins, such as FN and bone morphogenetic protein 2 (BMP-2) than AO- and P-Ti [139,140]. They observed that morphology was more relevant than wettability in determining the amount of protein adsorbed: Nanopits on AO-Ti are not able to accommodate large proteins, while grooves on P-Ti and network structure of AA-Ti offers more interaction sites. The latter can act as reservoir for BMP-2. On the other hand, protein conformation on the surface is dictated by hydroxylation of surfaces. Thus, proteins retained their native structure better on AO-Ti than on AA-Ti. Biological activity of BMP-2 is related to its α-helix content, thus AO-Ti promoted bone formation to a longer extend than AA-Ti, despite adsorbing less. Contrary, adhesive properties of FN are more related to β-sheets, which are consistent with the amount of RGD sequences. In this case, AA-Ti can increase FN effect thanks to the disruption of α-helices and the formation of β-sheets [140]. AA-treatments were also found to increase protein adsorption of SLA modified surfaces by turning the surface from hydrophobic to super-hydrophilic [141]. On hydrophobic samples, air bubbles may be trapped in micropores in a Cassie-Baxter regime, hindering solution-surface interactions thus reducing protein adsorption. Moreover, AA-treatments increase SFE. Alkali-acid treatments were employed also to increase protein adsorption ability of porous titanium scaffolds [142,143]. Various morphology can be easily obtained by changing the treatment parameters such as temperature, time, and solution compositions. Nanoneedles [144], nanopores, or nanoleaves [145] can be obtained on the surfaces. Since nanoneedles showed much higher BSA adsorption than the untreated surfaces, Yu et al. [144] obtained very specific adsorption patterns by texturing nanostructured titanium with laser irradiation (Figure 2.9).

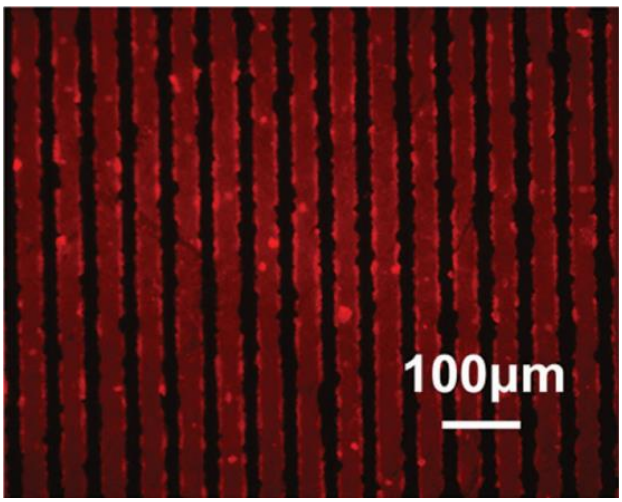

Figure 2.9 Fluorescent image of BSA adsorbed onto a patterned nanostructured surface: The protein is adsorbed on zones with titanium nanoneedles (red) and not in the zones, which were irradiated with laser. Adapted from ref [144]**.**

Morphology has also effect on adsorption selectivity. They present different surface area ratios, SFE, or they can generate physical nanotraps for proteins of certain dimensions [145]. Thus, nanoneedles may overall adsorb less proteins from FBS than nanoleaf or octahedral structures, but still have an equal if not higher number of adhesive proteins such as FN and VN. As result, focal adhesion of human osteoblasts turned out to be larger on this kind of nanostructured surface than on others. Depending on the kind of protein, adsorption may be mainly driven by the contact angle or by roughness. In the case of FIB, adsorption on hydrothermally treated cp-Ti and Ti64 resulted affected more by topography than WCA [146]. Protein adsorption on different morphologies obtained by hydrothermal treatments was also related to their surface potential [147]. High treating temperature, 140 °C, allows to obtain nano-wires on the surface, which exhibit the lowest zeta potential, about −50 mV at pH 7.4, among other nano-structures, such as a nano-network or nano-plate, about −30 and −35 mV at pH 7.4, respectively. Adsorption of BSA and FN was higher on nanowires than on all the other surfaces. Moreover, mouse bone marrow MSCs (BMSCs) had spread better on this kind of surface.

Growth of Titania Nanotubes (TNTs)

A common and easy way to obtain nanotextured titanium surfaces is formation of nanotubes by anodic oxidation [76]. TNTs geometrical features such as diameters, in the range of 15–300 nm, and length are easily tunable with the process parameters. Such surfaces have higher biological response than untreated Ti and can induce cellular differentiation.

At first glance, the enhancement of protein adsorption on TNTs can be ascribed to a much larger surface area than a flat sample [148,149]. At the same time, the oxidized surfaces have higher wettability and SFE, which are factors that contribute to BSA adsorption. The diameters of TNTs further influence the amount of protein adsorbed [150,151]. Increasing diameters from 30 to 100 nm increase adsorption of both FN and COL [150]. Osteoblast viability is higher on 30 nm TNTs when no proteins are adsorbed, while they have the same viability on 30 and 100 nm tubes

after adsorption of FN and COL. Computational studies showed that larger diameters correspond to higher interaction energy with collagen, thus increasing protein adsorption [152]. Conformation of the proteins is not affected by TNT's diameters, and collagen lies across several nanotubes. Changes in the 3D structure of other proteins were reported. Smaller diameters correspond to higher α-helix and β-turn content of adsorbed BSA and FIB, while β-sheet showed the inverse behavior. Since the bigger the diameter, the larger flat area on the top of TNTs is, conformation is similar to the proteins adsorbed onto a flat surface. With smaller nanotubes, proteins are more likely to interact with the edge of them, generating differences [151]. A very interesting study by Kulkarni and co-workers [153] defines the synergistic effect of dimensions and charge distribution of TNTs on protein adsorption. The surface charge density is affected by radius of curvature, therefore there is a difference between the outer convex surface and the inner concave surface of TNT. The former presents higher density than the latter. Anyway, the points with higher curvature are the edges at the top of TNTs. Small proteins like histone and albumin can enter TNT with diameter ranging from 15 to 100 nm. Being positively charged, histone can adsorb twofold BSA and also penetrate the space between nanotubes. Albumin cannot do that because of electrostatic repulsion with titanium oxide. Edges at the top of nanotubes are preferential adsorption sites for histone due to higher charge density, as shown in Figure 2.10.

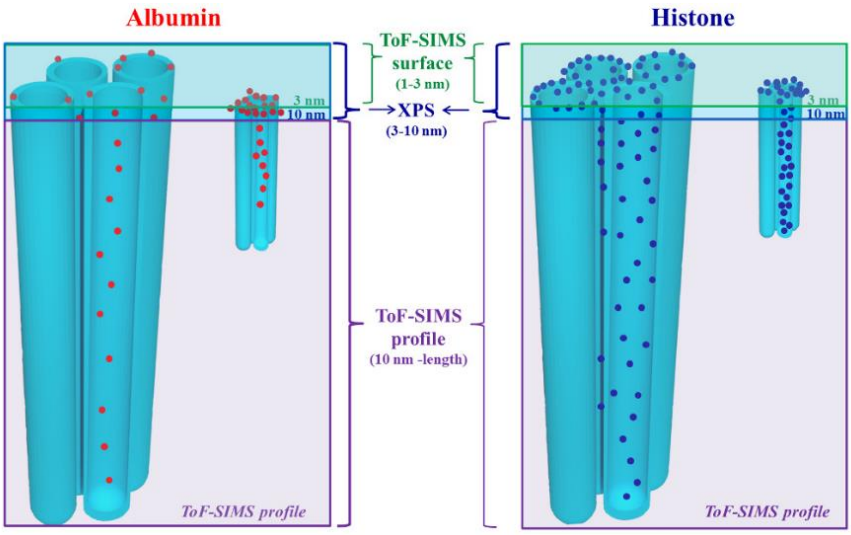

Figure 2.10 Spatial distribution of albumin and histone adsorbed on titania nanotubes reconstructed by different techniques: Time of flight-secondary ion mass spectroscopy (ToF-SIMS) (1–3 nm depth); X-ray photoelectron spectroscopy (XPS) (3–10 nm depth); Tof-SIMS depth profile (from 10 nm to bottom). Reprinted from ref[153]**.**

Adsorption from platelet rich plasma resulted in lower FIB on TNT surfaces with respect to flat cp-Ti [154]. This is because on more hydrophilic surfaces, such as nanotubes, fibrinogen can be more easily replaced by other proteins, like kininogen, through "the Vroman effect". Adsorption of proteins can be selectively controlled by tuning the diameters of the tube. Smaller TNTs, about 27 nm of diameter, adsorbed more VN from FBS than larger ones, diameters of about 88 nm [155]. Similar effect was obtained for other adhesive proteins such as laminin and

fibronectin. Protein adsorption on TNT can be further enhanced by chemical modification of the surface. Hydrogenation of the surface can be achieved by thermal treatments in hydrogenated atmosphere [156]. This is because hydrogenation increase hydrophilicity of TNT and liquid penetration as consequence. Since TNTs substrates can be used as drug-carrier materials, hydrogenation treatment is intriguing because of its effect in changing the release profile of the different proteins.

Other Surface Modification Techniques

SLA, chemical treatments, and growth of TNTs are the most common surface modification techniques for Ti-based biomaterials. Beside those, studies regarding how other kind of surface modifications affect protein adsorption were found.

Electrochemical methods such anodic oxidation allows to grow oxide layers with different nanostrucutres: nanopores[157], nanonetworks [158], or nanorods [159]. By increasing the applied voltage, thickness, micro-roughness, and porosity of the oxide layer increase, resulting in higher BSA adsorption[157]. Higher anodizing voltages resulted, on the other hand, in a rutile layer, which is less biocompatible than anatase. On similar surfaces, no enhancement of adsorbed protein was found when high protein concertation solution as FBS was used [160]. This is a useful reminder that protein adsorption on surfaces is not only dictated by the biomaterials properties but also, and in a significant manner, by the adsorption environment. Subsequent hydrothermal modification of the anodized surfaces highlighted the effect of the surface charge on protein adsorption [161]. Anatase nano-spikes lowered the surface potential of titanium and showed inhomogeneous charge distribution (higher negative charge density on titania tips due to higher curvature). Thus, adsorption of positively charged histone was increased. Au and Ag- nanoparticles (NPs) were successfully embedded into the titanium oxide layer by sequential anodization and soaking in NPs precursor solution and it was found that their presence further increases BSA adsorption[162]. Increased adsorption capability of surfaces with nanonetwork porosity was addressed as result of increased surface area, where pores can easily accommodate BSA and FN [158]. On nanorods, adsorption was found to be mainly driven by the density of the rods. When there are too many or too less structures, adsorption was found to be lower than on untreated titanium. Only intermediate rod density was beneficial for protein adsorption, MC3T3-E1 cell proliferation, and bone formation in vivo [159].

Surface texturing with laser beam is a rather novel way of obtain specific surface pattern in order to increase biological response to biomaterials [163]. It is possible to obtain very complex surface structures, such as micro-pits with nano-ripples at the bottom or at the top, selectively. This results in an accelerated adhesion of MSCs and in a more enhanced osteogenic behavior of the cells [164]. Laser patterning changes surface properties, such as roughness, wettability, chemistry, and charge, to a great extent. Thus, its effect on protein adsorption may vary largely according to the process parameters. Patterning of Ti64 was demonstrated to increase FIB adsorption due to increasing in surface roughness

[165]. Furthermore, affinity for FN seemed increased, in particular due to increase in the polar component of the SFE [166]. For the same reason, adsorption of HSA decreased. Lower affinity of textured Ti64 for albumin was also ascribed to a reduction of available binding sites and to chemical modifications and formation of less active titanium oxide forms [167]. Controversy, in a series of studies by Kuczyńska et al. [163,168], an increased adsorption of both BSA and FN was observed. This is the combined result of modified wettability and SFE, morphology, and increased negative charge of the treated surfaces. Conformation of proteins was also affected.

2.3.3. Effect of Alloying Elements and Surface Ion Doping

Despite being the most widespread materials for orthopedic and dental implants, properties of pure titanium and Ti6Al4V alloy, such as Young's modulus, are not the optimum for instance to avoid stress shield effect. Thus, titanium alloying with several different metals have been developed in order to reduce the elastic modulus or to get other interesting mechanical properties. Nickel is one of the most common alloying elements, TiNi alloys, such as Nitinol (about 50% Ti 50% Ni), possess shape memory and super-elastic properties. Nitinol is largely used in the manufacturing of vascular stent, for example [169].

Alloying elements not only modify the bulk properties of titanium, but also the surface ones. This affect adsorption of proteins. Higher Ni content, from 49.5% to 50.5%, in TiNi alloy results in lower albumin adsorption (from about 90 to 30 ng/cm^2), while FN is quite unaffected. Both resulted in being largely lower than on cp-Ti, twofold and almost 4 times, respectively. Albumin adsorption was found to be proportionally related to the polar component of surface energy, and Ni can reduce it. Fibronectin is more affected by other factors, such as surface charge [170]. Regarding albumin, different results were obtained by Clarke at al. [169]y modifying the composition of the oxide layer on TiNi alloy. They obtained higher adsorption with higher Ni and lower O content in the oxide, regardless of contact angle and roughness. According to Bai studies with binary alloy of Ti with Cr, Al, or Ni oxide layer composition has a larger control on protein adsorption than the bulk ones [171]. In addition, FIB was found to be adsorbed less on Nitinol than on cp-Ti [172]. In both cases, it adsorbs with a "side-on" orientation. FN was found to adsorb in similar manner on cp-Ti also when Zr is introduced into TiNi alloy [74].

Niobium is another very common alloying element for titanium. Nb lowers the Young's modulus of titanium, getting closer to the bone value[173]. β-alloys Ti-Nb-Zr and Ti-Zr showed very little differences in BSA adsorption with cp-Ti and Ti64, but a slight increase can be observed thanks to higher Zr content [174]. The oxide layer drives interactions with proteins also for this kind of alloys. In fact, introduction of boron ions causes a reduction of oxide thickness and hydroxide groups, hindering adsorption of proteins from FBS. This is also detrimental for MG63 human osteosarcoma cells proliferation [175]. Niobium is a beneficial element for proteins also when it is introduced into more complex alloys. The Ti-Zr-Pd-Si-Nb alloy showed enhanced adsorption of BSA and FN with respect to the

Nb-free alloy thanks to improved hydrophilicity [176]. The importance of non-polar component in the adsorption of FN was highlighted by Herranz-Diez et al. [177]. They observed that very different Ti-based materials, namely cp-Ti, Ti64, and Ti25Nb21Hf, adsorbed very similar amount of fibronectin, despite various contact angels. Analyzing the components of SFE, they notice different values in the total SFE and polar component, cp-Ti showed the lowest ones. Instead, no variations were found in the dispersive components.

Several metallic ions are well known for being able to stimulate different biological responses, particularly in the field of bioactive glasses. As an example, Ca^{2+} favors osteoblast proliferation and differentiation, Zn^{2+} possess anti-bacterial and anti-inflammatory properties, and Mg^{2+} increase bone cell adhesion and new bone formation[178]. Thus, surface treatments of titanium materials have been developed over past years in order to introduce different ions, in particular within the oxide layer [76]. Presence of ions in the surface results in changes of biomaterials physio-chemical properties and, obviously, this affects protein adsorption. According to several authors, enhancement of protein adsorption is due to increased surface charge of ion-doped titanium materials [52,179] or the bridging effect of divalent ions. Some of the most common methods to produce ion-containing titanium surfaces are hydrothermal treatments [179–182], which allows to obtain at the same time a nanostructured surface and ionic doping. Higher adsorption of albumin was found on treated cp-Ti with Mg^{2+} or Ca^{2+} ions with respect to Na^{+}. Additionally, increased adsorption was obtained by increasing ions concentration [179]. Magnesium bridging effect towards protein was confirmed in other studies [181] and treated titanium turned out to be bioactive, inducing hydroxyapatite precipitation, and promoting osteoblast attachment and spreading [183]. Anyway, cell adhesion can be depressed by too high Mg concentration in the TiO_2 layer due to much higher content of BSA, which reduces cell focal adhesion [184]. Similar results were obtained by lithium ions [52]. Treated surfaces showed super-hydrophilicity, ascribed to increase in surface energy, charge, or OH groups due to Li^{+}. Maximum adsorption of different proteins was found at different lithium concentration, such as FN and BSA. Therefore, it is possible to selectively regulate proteins uptake on the surface and, consequently cellular response. Besides increased protein adsorption, ion presence in a biomaterial is beneficial due to eventual ions release. Co-implantation of Mg and Zn and their release as ions improve adhesion, proliferation, and motility of human gingival fibroblasts [185]. Bridging effect with proteins was confirmed also for trivalent ions such as Fe^{3+} [186], with benefits both in vitro and in vivo. Calcium ions showed further improved protein adsorption, also with respect to other divalent ions such as Mg^{2+} and Sr^{2+} [179,180,187]. Thanks to specific Ca-binding site on some proteins, such as laminin, osteopontin, which is a major non-collagenous bone protein [180], and BSA [187], they adsorb in higher amount on Ca-containing surfaces. Protein adsorption and, more important regarding implants, osteointegration were enhanced also by doping of titanium materials with phosphate ions on TNT[188] or on hydrothermal treated cp-Ti [182]. Growth of TNTs on Ti-Zr-Sn-Mo-Nb alloy resulted into sparse nanotubes due to alloying elements. Spacing between TNTs

increased both protein adsorption and rat primary osteoblasts adhesion, proliferation, and activity [189].

All the doping treatments result also in morphological modification of the surface, which may also have a strong effect on protein adsorption. In fewer cases, mainly in the case of doping with monovalent ions such as Na^+[190], researchers found that morphology had a stronger effect than surface chemistry. Monovalent ions do not possess bridging capability towards proteins. Still, many more studies showed how ions presence in titanium-based biomaterials improved biological properties beyond surface nanostructurations [181,187,188].

2.3.4. Grain Size and Crystalline Phase

Among the factors that influence surface properties such as wettability and surface energy, grain size, and crystalline form of the oxide layer on titanium surface play a major role. It is known that ultrafine-(UG) and nano-grain (NG) metallic surfaces show beneficial behavior with respect to coarse-grain structure. On 301LN stainless steel, grain size of a few nanometers was able to improve BSA adsorption and murine pre-osteoblast cells response [191]. Similar findings, along with improved mechanical properties were obtained on stainless steel 316L[192]. The effect of grain size on protein adsorption has been investigated by several studies, including several types of titanium-based materials such as cp-Ti [193,194], Ti64 [195], and titanium alloy [196,197]. Literature about the effect of nanocrystallization on protein adsorption is not in good agreement. Still, it is important to keep in mind that different results may arise from very different factors, such as surface chemistry, protein concentration in solution, and adsorption conditions. NGs on titanium were mainly obtained by surface mechanical attrition treatment (SMAT) or severe plastic deformation (SPD). The former treatment consists of bombarding the material surface with hardened steel balls [193,196]. The latter is obtained by mechanical stresses such as hydrostatic extrusion [170], sliding friction treatment [195], or high-pressure torsion [197]. All authors assessed that both treatments result in an increased volume of grain boundaries (GBs). They are highly defective sites that contributes to increase the surface energy and the hydrophilicity of titanium-based materials. Usually this resulted in augmented protein adsorption. Bahl et al. [193] applied SMAT to cp-Ti, obtaining nano-grains on the surface. Contrary to other studies, nanocrystallization obtained by SMAT decreases BSA adsorption due to changes in electronic and physicochemical properties of the oxide. Still, this is beneficial for attachment and proliferation of human MSCs (hMSCs) and also improved material hemocompatibility thanks to a reduced platelets attachment and corrosion resistance. Corrosion of metallic implants can be enhanced by proteins in solution [198]. Contrary to the adsorption behavior observed by Bahl, Kubacka et al. [194] observed an increase in BSA adsorption on cp-Ti after nanocrystallization through SPD. They found that adsorption from FBS results in increase of BSA uptake and in reduction of FN. GBs are regions where atoms are prone to be charged, resulting in increase of the acid-base component of the surface energy that is related to adsorption through

electrostatic interactions. Thus, authors claimed that in this way non-specific protein adsorption, as BSA, is enhanced. Anyway, higher FN adsorption from FBS, along with VN was obtained on nano-grained Ti64 and Ti-Nb-Mo-Sn-Zr alloys. Huo et al. [195]ascribed enhanced protein adsorption on treated Ti64 to the smaller contact angle of NG surface with respect to coarse-grain and to higher surface energy. Thanks to a greater amount of RGD-containing proteins, these surfaces develop a suitable microenvironment for osteoblasts. β-alloy Ti-Nb-Mo-Sn-Zr subjected to SMAT treatment was found to adsorb twofold more FN and VN than the untreated surfaces [196]. Interestingly, the authors claimed that enhanced cell behavior on these surfaces is also related to proteins being adsorbed in a more active state with respect to coarse-grain surface. RGD groups are better exposed for cell attachment. Similar results were also obtained on Ti-Ni alloy subjected to high-pressure torsion [197]. VN adsorption increased more than BSA. Furthermore, Ni release was found to be hindered after SPD.

Along with grain size, the crystalline phase of titanium surface oxide layer also plays a fundamental role in determining protein–surface interactions. Different titania phases, such as amorphous, rutile, and anatase, and their orientation change surface properties and protein adsorption. TiO_2 phase is easily controlled through heat treatment: By increasing the treating temperature, amorphous titania is transformed into anatase at first and then to rutile, at about 600 °C [199]. The effect of different crystalline phases of titanium on protein adsorption has been investigated largely on TNT substrates [151,199–201]. Native oxide on flat cp-Ti was turned from amorphous to mainly anatase by annealing, showing almost no differences in the adsorption of BSA and FIB [151]. Nevertheless, the crystalline phase has different effects when adsorption from different proteins is investigated. Gong et al. [200] and Li et al. [201] agreed on the fact that anatase showed the lowest adsorption of COL I and FN compared with amorphous titania and rutile, as possible to see in Figure 2.11. The latter has the highest adsorption capability. On the other hand, adsorption of BSA or FBS were increased by higher annealing temperature [199].

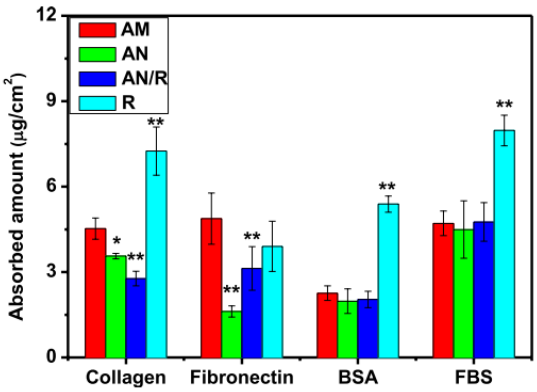

Figure 2.11 Adsorption of different proteins on Titania Nanotube (TNT) substrates with different crystalline phase: AM, amorphous; AN, pure anatase; AN/R, mainly anatase with rutile presence; R, pure rutile. Statistical difference by ANOVA: **ρ < 0.01 and *ρ < 0.05. Reprinted from ref [177].

Phase transformation highly affect the number of hydroxyl groups on the surface: Anatase has fewer OH groups than amorphous TiO_2 and rutile has the

highest number of all [199]. OH groups are fundamental to drive protein–surface interactions, in particular, basic OH groups can promote protein adsorption, and amorphous titania as more of them with respect to anatase [202]. Furthermore, anatase phase is more negatively charged than non-crystalline oxide or rutile, thus less proteins are adsorbed due to electrostatic repulsion [201]. Raffaini and Ganazzoli [203], through molecular modelling, observed that, among titanium oxide polymorphs, anatase provided the highest interaction energy for both BSA and FN. After initial contact, where the adsorption is driven by dipolar and dispersive interactions, both proteins tend to spread on the surface, in order to maximize amino acid residues interacting with the surface. BSA was found to do that on both anatase and rutile, while FN was more compact onto anatase. Higher crystallization obtained by heat treatment was beneficial for protein adsorption also on hydrothermally grown rutile nanoneedles [204]. Beside crystalline phase, also orientation of crystals may affect how proteins arrange on the surface. Molecular dynamic (MD) study allows to investigate protein adsorption by changing crystal's Miller indexes. Myoglobin adsorbs on rutile (1 1 0) or (0 0 1) faces with different orientation [205]. Due to electrostatic repulsion, the HEME group is away from the oxygen rich (1 1 0) rutile face, while it is closer to the (0 0 1) one. Keller et al. [206] proved the effect of anatase orientation on conformation of adsorbed fibrinogen. Low SFE facets, such as the {1 0 0} family, behave as hydrophobic surfaces, favoring protein–protein interactions and formation of FIB networks. (1 0 1) and (1 1 0) crystals have higher hydrophilicity, the latter due to higher surface polarity, and favor adsorption of proteins in a globular-like shape. Globular conformation of FIB may reduce the inflammatory response to a foreign body since it is more similar to its native state.

2.3.5. Surface Activation

UV-light or plasm activations are very well reported to be a way of improve biological activity of biomaterials surfaces [207,208]. Increase of surface activity is achieved by a three-step mechanism: Removal of hydrocarbon contaminants; induced surface hydrophilicity; change of the surface charge from negative to positive. Medical devices would probably be stored for a very long time before usage, up to 5 years [209], therefore removal of atmospheric contaminants is a priority. This will be discussed deeply later in Section 4.1.

Protein adsorption on cp-Ti, in particular of BSA and FN was found to be strictly correlated to hydrocarbon level [210]. When contaminants are removed by UV, Ti^{4+} sites are exposed, increasing interaction with both protein and cell (Figure 2.12 a).

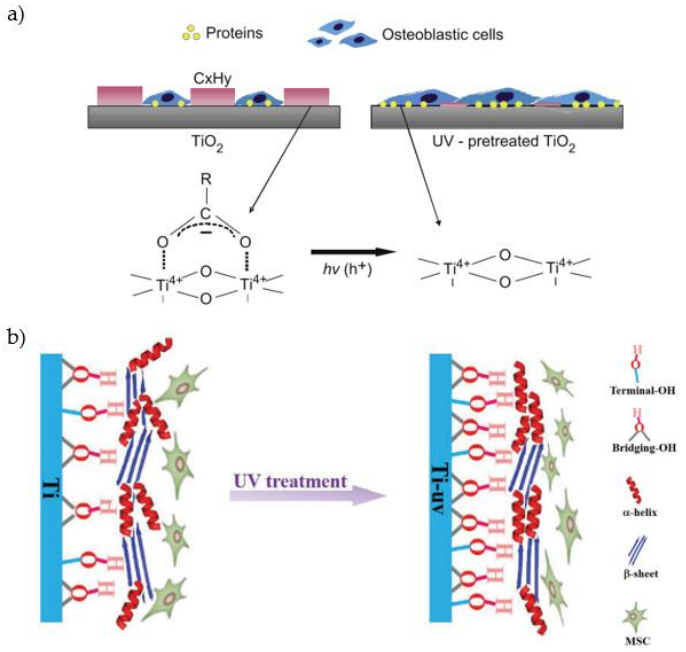

Figure 2.12 Schematic representation of UV effects on protein adsorption and cell attachment: (a) Removal of hydrocarbon contamination results in increased protein adsorption and osteoblast adhesion and spreading, adapted from ref [186]; (b) effect of number and type of UV-generated OH groups on protein conformation and subsequent mesenchymal stem cell (MSC) proliferation, adapted from ref [187].

Hydrophilicity and positive surface charge of UV-activated surface arise from the same physiochemical modifications of TiO_2 layer, formation of oxygen vacancies, and terminal OH groups. Exposure to UV-light promotes an electron from the valence band to the conduction band. This causes a reduction of Ti^{4+} to Ti^{3+} and, as a consequence, oxygen vacancies are formed [211,212]. Other than increasing positive surface charge, Ti^{3+} are favorable sites for water dissociation, leading to generation of terminal OH groups [213]. Positive surface charge is also promoted by the basic behavior of UV-generated OH groups [214]. On titania nanoparticles, it was proven that basic hydroxyls can form hydrogen bonds with $-NH_3^+$ groups on proteins [202]. Electrostatic nature of protein adsorption enhancement was confirmed by Hori et al. [212]. They observed that more BSA adsorbed onto UV-activated surface from solution at pH 7 but a smaller increase was found at pH 3, compared with untreated Ti. At pH 7, both BSA and Ti are negatively charged. Thus, UV-generated positive charges can attract albumin molecules. At pH 3, BSA is below its IEP, as untreated Ti. Therefore, UV-activation is not as effective. Conformation of proteins is also affected by surface UV-activation, in particular by the terminal OH groups. Yu and coworkers [213] observed an increase of α-helix and a decrease of β-sheet contents in albumin, with respect to adsorption on an untreated surface. They discussed that these conformational changes can be related to increased osteogenic differentiation of MSCs(Figure 8b). Remarkably, while cell adhesion and proliferation on UV treated surfaces are increased, bacteria colonization of surface was hindered [215,216].

Different plasma system can be used in order to obtain activation of the surface: Different kinds of glow discharge plasma, such as atmospheric (APGD)[217], radio frequency (RFGD)[218], vacuum [219]; nonthermal atmospheric pressure plasma

(NTAPP)[208]; or argon atmospheric pressure dielectric barrier discharge (APDBD)[220]. As well as UV treatments, plasma can increase protein adsorption thanks to the removal of hydrocarbon contamination [208] but, unlike UV, surface charge become more negative [208,218]. Specifically, employing NTAPP creates -COOH, -OH, and NH_2 groups on the surface [221]. Oxygen-containing groups can generate reactive oxygen species during plasma treatments [208]. NTAPP treatments were found to have analogous effect to UV surface activation in terms of reduction of Ti surface negative charge and adsorption of BSA [222]. To the authors best knowledge, plasma effect was mostly investigated on fibronectin adsorption. Noticeably, FN adsorption was selectively increased in case of single protein solution [218,221] and when mixed to other proteins such as BSA [223] or even from plasma serum [219,224]. FN, as an adhesive protein, is beneficial for cell attachment and spreading *per se*. On plasma-treated Ti, negative plasma-induced charges affect FN conformation, promoting a more bioactive configuration of the protein on the surface. Integrin-binding sites on FN, namely the tripeptide sequence RGD, are more exposed due to conformational changes of the proteins. Thus, interactions with $\alpha_5\beta_1$ integrin on cells are promoted, increasing osteoblast spreading and differentiation [218,221]. Controversy, Santos et al. [225] observed that low-pressure glow discharge plasma did not affect the total amount of adsorbed HSA, IgG, or LAM, nor the adsorption isotherms, when single protein solutions were used. Instead, plasma treatments affected the layer composition of proteins adsorbed from a mixture of the three of them. Adsorption of HSA and LAM were selectively increased and decreased, respectively, while IgG was not changed.

UV photoactivation and plasma treatments are effective ways to promote protein adsorption and surface properties in general. Since surface morphology is not modified, these techniques can provide useful information on adsorption mechanisms, by isolating the effect of surface charges and functional groups. Despite not being addressed as the main adsorption driving force, electrostatic interactions have been proved to play an important role, in particular regarding selective adsorption of proteins and their biological activity.

2.3.6. External Parameters Affecting Protein Adsorption on Titanium Surfaces

Aging and Storage: Contamination of Titanium Surfaces

Biological properties of titanium need to be preserved even through the long-lasting storage of the biomedical devices, up to five years. Implants and dental screw are usually enclosed in a sterile gas-permeable packaging, which keeps the contents sterile but allows contamination of the surfaces by the carbonaceous organic impurities in the atmosphere [209,226]. Very recent molecular dynamic studies performed by Wu et al. [227] demonstrated that carbon contaminants expose C-H bonds, thus greatly reducing surface polarity and dipole–dipole interactions with proteins. Protein adsorption drastically decreases after four-week storage when titanium is placed in sealed container [228]. Proportional correlation between

increased WCA and reduced protein adsorption was observed. The same authors observed that inclusion of divalent ions like Ca^{2+} within Ti surface through chemical treatments may hinder depression of bio-properties due to aging [229]. After four weeks, BSA adsorption, and rat BMCs attachment resulted in being higher with respect to untreated surface. Therefore, it is necessary to limit surface contamination of implants during their shelf-life. As described in the previous paragraph, plasma treatments are an effective way to remove carbon contaminants form titanium surface. Despite being very efficient in removal of carbon contaminants, UV and plasma might be time-consuming processes and require delicate equipment. Miki et al. [230] found that simple cleaning of titanium devices with electrolytic reducing ionic water, which has high OH^- concentration, led to similar results in protein adsorption compared with UV. Bone contact is also much higher than the control surfaces. This process can be easily performed in a generic dentistry facility, for example. In the past 10 years, great efforts have been made by researchers to find a suitable storage method. It shall maintain intact the biological properties of a newly manufactured Ti surface and it needs to withstand sterilization. Storage in wet conditions seems to be the most promising way [231]. Choi and co-workers observed that soaking in distilled water may retain properties of titanium surface after UV and plasma activation for periods up to eight weeks [232]. UV treatment and wet storage on SLA-modified Ti surface allow to obtain the best results, in terms of protein adsorption and murine osteoblast cells adhesion. Interestingly, storage in water is not only suitable for avoiding carbon contamination, but also it is capable of maintaining the more positive surface charge of the UV-treated titanium [226]. Protein adsorption and cell adhesion can be even increased upon storage by using ion-containing solution [231]. Ca-containing solution can benefit from the protein bridging effects of adsorbed ions and the cellular affinity for these ions. Vacuum storage proved to retain biological activity of alkali-heat treated titanium eve after one year [209]. Wilhelmi et al. [73] confirmed, through time of flight secondary ions mass spectroscopy (Tof-SIMS) analysis, that the maximum adsorption of BSA on cp-Ti is obtained for solution at pH 5.2, and decrease with increasing pH values. This confirm that protein–protein latera interactions play a major role in adsorption mechanisms.

Influence of the Solution: pH, Temperature and Ions

As discussed in paragraph 2.4, the parameters of the protein solution have a major role in determining various aspect of protein adsorption, such as amount of the protein adsorbed, surface–protein interactions, and adsorption kinetic. The pH value determines charge distribution on both the surface and protein [4]. As a consequence, protein–surface interactions may vary to a great extent by changing pH. This fact also reflects to loosely bound proteins. At pH close to the IEP of a protein, repulsive interactions between BSA molecules are at the lowest, therefore the loosely bound portion of proteins adsorbed is increased [233]. The highest adsorption was observed near the IEP of the BSA, as it is possible to see in Figure 2.13 [234]. The mechanisms that can explain the pH effect on protein adsorption

on Ti was proposed by Imamura et al. [235]. At pH around 4, that is below the IEP of Ti, acidic residues in the proteins, with COO^- groups, are attracted by OH^+ groups on surface. Above pH = 5, the functional groups on the Ti surface turn negatively charged and can interact with $-NH_2^+/-NH=NH_2^+$ groups of the amino acids. They also observed that thickness of the adsorbed protein layer may vary by changing pH. Similar behavior was observed also for titania.

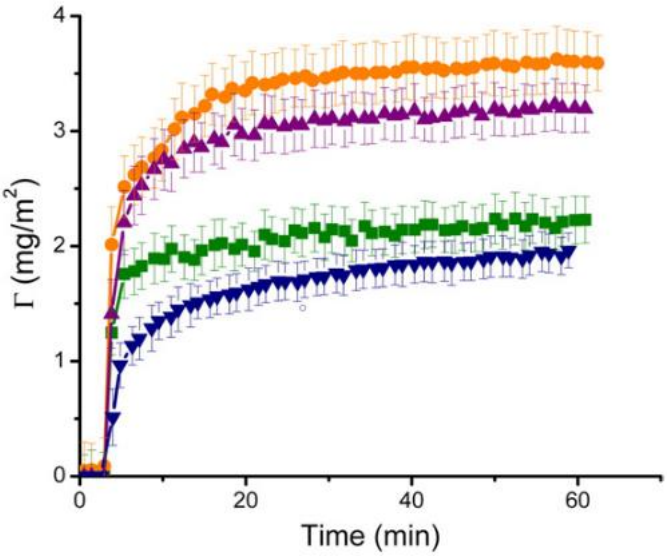

Figure 2.13 BSA adsorption on TiO_2 thin film at different pH values: 3.55 (■), 4.60 (●), 5.60 (▲), and 7.51 (▼). Reprinted with permission from ref [234]**. Copyright 2009 Elsevier B.V.**

Still, due to the high adsorption even under adverse electrostatic condition, namely at pH 3.55 and 7.51, the authors claimed that the main driving force for albumin adsorption on titania is hydrophobic interaction. LYS adsorption was also observed to be strongly dependent on pH [236]: When titania is positively charged, at pH lower than 5, almost no adsorption was observed due to electrostatic repulsion, as expected, because at this pH value, LYS is positively charged. In this study, correlation between protein uptake and temperature was also discussed. Increased temperatures lead to higher amount of adsorbed proteins. Combined effect of pH and temperature was studied by Kopac et al. [59]. By fitting adsorption isotherms with Langmuir or Freundlich curves, they observed that the highest adsorption of BSA onto titania can be obtained at 40 °C and pH 4. These data show that adsorption from different solution may results in very different protein layer on the surface of biomaterials.

Ions dissolved within the protein solution compete with protein for interacting with the surface and hinder or elicit protein adsorption. Phosphate ions can easily adsorb on titanium surfaces [82] and they alter BSA adsorption kinetic and conformation on TiO_2 [237]. Positive mono- and divalent ions are electrostatically attracted by the negative charges on titanium, subsequently mediating the interaction between the surface and proteins. Monovalent ions, such as K^+ and Na^+, do not influence to a great extend protein adsorption [85] since once their single positive charge is attracted by the surface, they have no more for proteins to be attracted. On the other hand, divalent ions, Ca^{2+} and Mg^{2+} in particular have a bridging effect toward proteins thanks to spare positive charges after interaction

with titanium [238,239]. Kohavi et al. [85] observed that electrostatic interactions may play a major role than surface wettability on protein adsorption. Adsorption of HSA and FN was enhanced by prewetting Ti64 surfaces, with solutions containing divalent ions or not. Wetted surface were hydrophilic, and non-wetted ones were hydrophobic. After being dried, surfaces turned hydrophobic again, and adsorption was still enhanced on the samples that were wetted with Ca^{2+} containing solutions. The interplay between pH and ions dissolved in determining the electrostatic interactions between proteins and surfaces was well described by Hori et al. [212]. Around physiological pH, when both titanium and albumin are negatively charged, divalent ions are effective in increasing protein adsorption. At pH 3, below the IEP of surface and protein both, ions did not alter amount of adsorbed BSA. In the same study, it was also found that anions, as Cl^-, can mask UV-generated positive charges and annihilate the beneficial effect of UV treatments. The fact that ions co-adsorption can reduce benefits of positive surface potential on the adsorption of proteins was recently confirmed [240].

After all these considerations, it is possible to state that attention must be paid to the solution parameters, in particular when discussing protein adsorption and comparing results from different studies.

2.3.7. Protein Concentration in Solution

Human plasma and biological fluids in general contain proteins in a very high concentration. The amount of proteins in human plasma is in the range of 60–80 mg/mL[241]. It is not trivial to reproduce this high concentration in laboratory experiment, mainly due to the high cost of proteins and their availability for purchase. Thus, researchers investigating protein adsorption used to lower protein concentration in solution, from some mg/mL [242] down to small fraction of the biological one [170], for example BSA was employed in concentration ranging from 0.4 to 4 mg/mL while its biological concentration is reported to be as high as 33–52 mg/mL [243]. As pointed out by Hemmersam and co-workers [244], adsorption of proteins from low concentrated solution has a stronger dependence from the substrate than what happens using higher protein concentrations. Using quartz crystal microbalance (QCM) analysis, they found that adsorption of FIB from 0.03 mg/mL solution to Au-, Ti-, or Ta-sensors showed larger differences, both in layer structure and protein amount, than in the case where 1 mg/mL solution was used. In the former case, FIB molecules had time to spread on the surface and to interact with it using both αC and D domains, adhering more strongly. In the latter case, adsorption rate is too fast for this to happen. Strong denaturation of proteins adsorbed from low concentrated solution was observed also for FN on Ti64 [245]. Protein unfolding is also hindered by surface hydrophilicity obtained through UV activation. Reducing the amount of proteins used during an experiment, paying the price of be further away from real physiological conditions, may be necessary to appreciate the influence of the material features on adsorption mechanisms. Beneficial effect on protein adsorption obtained by Argon plasma or UV treatments of pure titanium turns insignificant when adsorption was carried out using 10% FBS

solution instead of 2% one [246]. Researchers need to bear in mind that surface effects observed using solution with a very low content of proteins can be reduced, different, or, in the worst case, annihilated in case of the real, biological fluids. This fact applies also for properties and characteristics of the protein adsorbed layers.

2.3.8. Protein Co-Adsorption and Competition for the Surface

Human plasma contains about 3020 distinct proteins [247]. As for protein concentration, it is nearly impossible to replicate this enormous complexity on a lab scale. In addition, it would be extremely complex to understand adsorption mechanisms and the specific role of the biomaterial surface in it. Thus, most of researchers conduct their experiments using a single protein solution, as shown previously. Unfortunately, it is not possible to predict the adsorption of proteins from complex mixture just knowing how it happens from the single protein solutions. Researchers tried to expand knowledge of the protein adsorption on titanium-based biomaterials by mostly using binary protein mixture or subsequent adsorption.

Adsorption of BSA on cp-Ti was found to be enhanced when obtained from BSA-LYS containing solutions [248,249]. $BSA^{-}LYS^{+}$ agglomerates can form in solution and adsorb on the surface, thus increasing the total mass of adsorbed proteins (Figure 1.14). Relative amounts of adsorbed proteins are influenced both by solution composition and pH, as possible to see in Figure 2.14. Interestingly, residual enzymatic activity of LYS is not much influenced on protein content in solution [248]. BSA, due to its larger mass, cannot be displaced by LYS in case of sequential adsorption, thus limiting LYS amount on the surface [249].

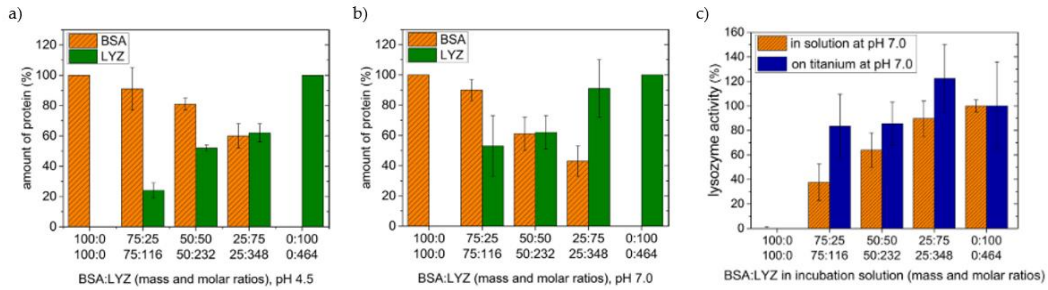

Figure 2.14 Adsorption on cp-Ti from BSA-LYS mixture: Relative amounts of adsorbed proteins form mixtures with different ratios (BSA: LYS 100:0, 75:25, 50:50, 25:75, 0:100) at different pH, 4.5 (a), 7.0 (b) (amount is expressed as percentage of adsorbed protein from a pure solution); LYS enzymatic activity, relative to pure LYS solution, in mixture with BSA and after adsorption from same mixture (c). Adapted from ref [248]**.**

Physiochemical characteristics of surfaces have a strong role in determining protein competition for the surface. Hydrophilic titanium surfaces, such as SLA-treated substrates, have been found to promote FN adsorption during competition with albumin, even when a biological BSA:FN ratio of about 100:1 is maintained in the solution [250]. The first protein to adsorb on the surface can inhibit sequential adsorption of other proteins [251], but higher affinity with the surface can result in protein displacement and substitution [251,252]. Felgueiras et al. [251]showed that FN and COL I can block sequential albumin adsorption on Ti64 due to their larger

mass, and that they are able to displace albumin when adsorbed as second proteins. Interaction between FN and COL I are dependent on the kind of the surface. As in the case of LYS, albumin can form complexes with COL I in solution resulting in higher number of proteins adsorbed with respect to the single protein solutions. Contrary to these results, BSA was found to be able to displace larger proteins such as FIB or FN on TiO_2 surfaces [253] due to higher affinity for the surface. On a pre-existing BSA layer, FIB and FN forms a layer on the albumin instead of displacing it.

Being quite simple, binary protein solutions are still not very much representative of actual biological fluids. Some researchers moved further on in complexity of systems by investigating through proteomic analysis the exact composition of protein layers adsorbed on several titanium surfaces from real and whole biological fluids such as plasma [247,254,255] or saliva [256–258]. Among the thousands of proteins present in human plasma, the most adsorbed was FN, followed by albumin, alipoprotein, and fibrinogen [247]. From saliva, which contains about 750 different proteins, less than half of them were found on titanium [258], mainly amylase and lysozyme [256]. The effect of surface modification on the protein pellicle composition was also evaluated. In case of adsorption from saliva, very low specificity was observed for different titanium surfaces, smooth, SLA-treated, and SLA-treated+stored in ionic solution [257]. On the contrary, differences were observed between smooth and SLA surfaces by using human serum [255]. One hundred and eighty-one and 162 proteins were identified on smooth and blasted/acid-etched surfaces, respectively. Proteins adsorbed onto smooth Ti are involved in a higher number of biological pathways, such as clotting, cytokines-mediated inflammation response, integrin signaling, and glycolysis, the latter being absent on SLA-treated titanium. SLA treatments were also found to affect the proteome on Ti-Zr alloy, from both plasma and saliva [259]. Adsorption from saliva resulted in 389 common adsorbed proteins, 40 adsorbed uniquely on the machined samples, and 14 on the SLA treated ones. The proteome from blood plasma was much more similar with only three unique proteins, on both machined and SLA surfaces, and 145 common proteins. Even though UV activation of the surface has been reported to improve adsorption of proteins [212], proteomic analyses found that light treatment on cp-Ti, hydrothermally coated with nano-structured TiO_2, depress proteins adsorption from plasma [254]. Much lower content of FIB, immunoglobulins, and other proteins were found on pre-activated surfaces. Authors addressed this decrease to a mutual combination of surface properties: Roughness, charge, intrinsic, and photo-induced wettability. Reduction of inflammation-promoting proteins such as immunoglobulins and FIB may be beneficial for osseointegration. Even if adsorption from complex biological fluids can be more significant than adsorption from a single protein solution for understanding the fate of biomaterials, this might not be still enough. Jager et al. [260] studied the composition of the protein layer formed onto explanted hip implants. They found that proteome formed onto a titanium implants is different with respect of the one that forms from plasma. Among the 2802 unique proteins founded on the implant, cell-free hemoglobin was the most abundant, almost two-

fold albumin. Most of them were of intracellular origin and, interestingly, fibronectin was absent.

Adsorption from single protein solution can be useful for a preliminary understanding of how the different surface features may interact with biological fluids after being implanted. Anyhow, it is evident that this is not sufficient and it is quite necessary to test protein-biomaterials interactions using complex solutions.

2.3.9. Key Concepts

Protein adsorption is a fundamental step in the interaction of implantable biomaterials, such as titanium and titanium alloys, with the biological environment. The positive or negative outcome of tissue integration of an implant depends on the interplay between the body and the implant surface. How cells and bacteria adhere, proliferate, and compete is strongly dictated by the protein layer that forms on the device surface within the first minutes after implantation. The understanding of these phenomena is necessary to develop always better implants and to reduce possible adverse reactions. Thus, in past years, great efforts have been put to gain knowledge about the aspects that regulate proteins adsorption on titanium. A large variety of different surface–protein combinations have been investigated, including different type of titanium, titanium oxide, and titanium alloys, several kinds of surface treatments aimed to improve Ti osseointegration and a wide range of proteins in a simpler or more complex environment. Due to the enormous variability and complexity of the protein adsorption processes, a unique and fully agreed explanation of adsorption on titanium was not found in literature, some aspects being clearer than others. Impact of surface properties, such as roughness, morphology, chemistry, surface energy, wettability, and charge, need further investigation. The main effects of titanium surface features are summarized in Table 2.1.

Table 2.1 Effect of titanium surface properties on protein adsorption (amount of adsorbed proteins, protein conformation on surface, and mechanism of protein–surface interaction) and impact of each feature on adsorption. ≈: no clear impact; ↑: mild impact; ↑↑: high impact; n.r.: effect not reported.

Surface Characteristic	Impact on Protein Adsorption	Conformation	Mechanism	Examples
Microroughness	↑	n.r.	Higher interaction area, physical adsorption	SLA surfaces adsorb fourfold more of albumin, fibronectin, fibrinogen and immunoglobulin vs. untreated surface because of roughness. Laser patterning increases adsorption of FIB.
Nanoroughness	≈	↑	Dependent on other characteristics. Aspect ratio of nanofeatures can influence protein conformation.	BSA aggregates into nanopores larger than its hydrodynamic radius with a strong interaction with the surface, while FN is too large. BSA/FIB adsorb as multilayer with stronger protein-protein interaction on nano-rough surfaces
Hydroxylation	↑↑	↑↑	According to the specific adsorbed proteins, OH can promote or hinder interaction with the surface	BSA adorbs through hydrogen bonding and proton transfer with interaction with OH surface groups. FIB adsorbs through positive charged αC domains. Rutile adsorbs more COL, FN and BSA than anatase or amorphous titania due to higher OH density
SFE	↑↑	n.r.	High surface energy, in particular the polar component, increases adsorption	Ti adsorbs larger amount of plasma proteins vs. other metals with lower SFE, but TiO_2 adsorbs less proteins and in a weaker manner than other oxides with higher SFE. Ti adsorbs less basal lamina and salivary proteins than polymers for dentistry. Sandblasting with SiC induces higher SFE and preferential adsorption of FN. Laser patterning induces higher adsorption of FN by increasing the polar component of SFE. Nanograined surfaces have higher volumes of grain boundaries, which increase the SFE and adsorption of FN and VN
Charge	↑↑	↑	Can promote or limit protein adsorption, depending on charge of both surface and proteins	BSA is adsorbed in a lower amount on negatively charged surfaces while it is the opposite for histone that is positively charged. UV-generated positive surface can adsorb more BSA at pH 7, when the protein is negatively charged.
Chemistry (alloying metals, ions)	↑	n.r.	Increase protein adsorption, divalent ions in particular	TiNi alloys results in lower BSA (dependent on Ni content), FIB, and FN adsorption vs. cp-Ti. Ion-doped Ti has increased surface charge and protein adsorption because of bridging effect of divalent ions or specific chemical bonds (Ag)

Increased surface roughness in the micro scale seems to be capable of increasing the adsorption due to a greater number of active sites and features such as pores, nanotubes, or pits can accommodate proteins. On the other hand, no clear effect was found for nano-roughness. In this case, topography effect is mediated by other properties, such as charge or wettability. Electrostatic attraction may increase protein adsorption, while repulsion seems not enough to completely avoid protein binding with the surface. The role of wettability in adsorption is the most controversial. As a rule of thumb, proteins prefer to adsorb on hydrophobic surfaces, since water is more easily displaced from the surface and hydrophobic interactions between amino acid residue and surface can be strong. In fact, this has been reported in some cases for adsorption on titanium surfaces. On the other hand, hydrophilic surfaces usually present more OH groups, higher surface charge, and SFE. These factors can promote surface–protein interactions, making adsorption favorable also on wettable surfaces. Furthermore, wettability can enhance solution-surface contact by turning it from a Cassie-Baxter to a Wenzel regime. These factors are able to promote protein adsorption against the generally accepted rule of thumb. The ongoing research on development of new and more bioactive surfaces had introduced more factors that can influence protein adsorption: The presence of ions within the oxide layer or of metals as alloying elements, the control over grain size, and surface activation treatments. All these features strongly change surface properties, namely wettability, hydroxylation, charge, SFE, roughness, making it less trivial to discriminate what features influence proteins adsorption and how. Conformation and orientation of adsorbed proteins are also heavily affected by surface properties in a non-unique way. Aspect ratio of surface features can change how proteins accommodate on the surface, higher hydroxylation may promote denaturation and spreading of certain proteins, while in other cases, OH groups increase wettability consequently reducing protein–surface interactions.

Besides, the poor standardization and use of testing protocols among researchers led to different conclusions about protein adsorption. The wide variety of protein concentrations, solution composition, and experimental methods make it very difficult to compare different works and to state if a system is an effective representation of the real adsorption process as occurring in vivo, within the human body. The complexity level of the system used can completely change how proteins interact with a surface, and scaling up from a simple single protein solution seems not to be an effective way to understand how materials behave when put in contact with biological fluids.

Today, knowledge about protein adsorption on actual implant surface is also limited by the fact that it is not trivial to find characterization techniques that can provide information about adsorption mechanisms on real surfaces. In the literature, a lot of techniques have been used to investigate protein adsorption on titanium materials, but some of them may not be applicable on a bulky and surface treated titanium sample because they need specific characteristics, such as surface flatness, planar specimen or surfaces need to be grown on the instrument sensors. These kinds of model surfaces may not be representative of the surface of a real implant.

2.4. Protein adsorption on bioactive glasses

2.4.1. General Consideration on Protein Adsorption on bioactive glasses

Bioactive glasses (BG) have been the first class of third generation biomaterials, meaning that they can express biochemical and biological signal for the stimulation of an appropriate host response [261]. From the creation of Hench's 45S5 Bioglass more than 50 years ago, those materials have been extensively investigated and an unaccountable number of bioactive compositions, based on different forming oxides such as silica, phosphate and borate glasses, have been developed [262]. The incredible variability of chemical composition, plus the different manufacturing possibility, melting of raw precursors or sol-gel synthesis [263], results in all kind of different surface properties that may affect protein adsorption: for instance surface energy, wettability, and surface charge. According to the manufacturing methodology, bulk or meso-porous materials, in the range of 10-30 nm [264], can also be obtained. Besides, the overall picture is further complicated by the high reactivity of such materials, on which is based their bioactivity. On silica-based systems, which are the one investigated in this work, hydroxyapatite precipitation is obtained through the following steps: Na^+/Ca^{2+} cation exchange and formation of Si-OH groups; pH increase and release of soluble silica $Si(OH)_4$; repolymerization of silica and formation of a hydrated gel layer; precipitation of amorphous $CaO\text{-}P_2O_5$ layer; hydroxyapatite crystallization [262]. Even if those reactions fully occur in hours or even days, they begin as soon as the glass get in contact with a solution, including physiological fluids and protein solutions used for adsorption experiments. Thus, glass reactivity heavily affects protein adsorption and the surface itself is extensively modified during the process, leading to a highly dynamic phenomenon.

Protein adsorption on bioactive glasses has been recently reviewed by Zheng et al. [50], where they made a comprehensive report of how glass properties affect protein adsorption and vice versa, alongside with an overview of possible surface modification for controlling protein adsorption and application of protein-coated BG. According to what concerns this thesis, here the influence of BG surface properties on the resulting protein layer will be covered.

2.4.2. Surface properties affecting BG-protein interactions

Surface chemistry

The possible compositions of bioactive glasses are virtually infinite, both regarding the bulk chemistry and eventual surface modifications. For a better development of novel BG, and to understand the *in vivo* biological activity of the ones that already exist, it is mandatory to understand how the presence of different chemical elements in the glass surfaces affect protein adsorption. The matter is further complicated by the fact that changes in the chemical composition of BGs

deeply affect surface reactivity, surface charge and also the structure of sol-gel derived mesoporous glasses, and it is not always trivial to discriminate what parameters is affecting the protein-surface interactions.

Calcium is an element practically always present in the composition of BGs, being one of the mineral constituents of bones, and it was found to have a great effect on protein adsorption. Increasing Ca content at the expenses of Si can reduce BSA adsorption, in particular at increasing albumin concentration in solution [265]. Calcium can also limit the denaturation of proteins: BG with higher CaO than 45S5 Bioglass, and no Na_2O, denature less methemoglobin with respect to Hench composition [266]. The presence of calcium greatly affects the reactivity of the bioactive glasses, concurring to create a dynamic environment that change during protein adsorption. Albumin adsorbed more on biocomplatible soda-lime glass than on a BG with higher Ca content: on the bioactive glass, adsorption is in competition with the formation of the calcium-phosphate rich layer, while on unreactive glasses proteins can adsorb directly on the SiO_2 surface [267]. Similar conclusions were drawn also by other authors [265]. Interestingly, if released calcium from BG is removed from the solution, allowing only the formation of a silica-gel layer, protein uptake is greatly enhanced [268]. The surface specific area and pore volumes of mesoporous glasses is reduced by higher Ca/Si ratios, resulting in a consequent decrease of albumin adsorption. Furthermore, the presence of calcium reduces Si-OH groups, which can bond with proteins through hydrogen interactions, due to the transformation of silica to $CaSiO_3$ [269]. Similar results can be obtained also when Si is increased alongside with potassium oxide [270]. Ca^{2+} and Na^{+} release by BG network dissolution in solution contributes to build up a more negative charge and hydrophilic surface, which can limit adsorption of certain proteins such as fibrinogen. This effect is absent on pure silica, where adsorption is higher [271]. As well as calcium, also Sr molar content is inversely proportional to the adsorption capability of silica glass when normalized with the specific surface. Nevertheless, Sr addition greatly increases the specific surface and pore size, resulting in overall higher adsorbed albumin amount [272].

Incorporation of transition metals in BG composition has been widely investigated in order to provide bioactive glasses with other properties such as angiogenesis, antibacterial capacity or cellular stimulation [178], with an effect on protein adsorption as well. In a series of studies, Krajewski et al. [273,274] investigated the effect of small quantities of Ta and La on protein adsorption. The presence of La^{3+} and Ta^{5+} positive ions results in a positive zeta potential at physiological and inflammatory pH, 7.4 and 4.5 respectively. As consequence, the amount of adsorbed albumin increased at higher pH thanks to favorable electrostatic interactions and decreases at lower pH due to Culombic repulsion. The opposite fact happen with an undoped bioactive glass, which has always a negative surface potential [275]. Interestingly, the presence of Ta and La do not change the adsorbed protein profile, thus the different biological activity of BG containing these elements with respect to other BG systems may be related to the amount of adsorbed proteins [274]. Molybdenum and zinc can also increase the protein affinity of

mesoporous sol-gel derived BG, in particular by increasing the pore volume and the specific surface [276,277].

Thanks to its antibacterial properties, silver is a very popular doping element for bioactive glasses. As demonstrated by Gruian and co-worker, both melt-derived and sol-gel Ag-doped glasses shows augmented binding affinity towards different proteins [278–280]. Furthermore, the presence of Ag^0 and Ag^+ increases the denaturation of proteins: the thiol groups of protein Cys residues has a high affinity for metals, easily bonding with them causing also cleavage of protein disulfide bonds. The same happens in case of AuNP-BG composites [281].

Structure and crystallinity

As already mentioned, BG structures highly affect protein adsorption, in particular pore dimension and specific surface of mesoporous glasses. Pore dimensions detain the main control in increasing protein adsorption. For enhanced adsorption, proteins must have the possibility to infiltrate the mesopores, thus they shall have a suitable dimension. On the other hand, specific surface area is also increased by pores too small for proteins, not resulting in more proteins adsorbed [271,282]. The possibility to load mesoporous BG with bioactive and pharmaceutical molecules is also very promising and investigated for *in situ* drug delivery [263], and the selective loading capacity that can be achieved by tuning the mesostructured dimension is of great interest. Small proteins, such as lysozyme, can be adsorbed into structures that hamper the uptake of bigger molecules, such as albumin, achieving also a controlled release over time [283].

Pores are not the only topographical features that can affect protein adsorption. As in the case of titanium, nanostructures can be obtained on BG with surface treatments. Needle-like, with different length, plate-like and flower-like hydroxyapatite/carbohydroxyapatite structures can be obtained by soaking BG in PBS solution in different conditions. Those structures can influence the adsorption from serum supplemented medium of relevant proteins, such as FN, VN, and BSA, according to the net charge on the crystalline structures [284]. The surface structure changes also the conformation of adsorbed proteins, leading to a different attachment of MC3T3-E1 pre-osteoblasts.

Bioactive glasses can be employed both as fully amorphous material or as glass-ceramic. The degree of crystallinity can be tuned by thermal treatment or by changing manufacturing conditions in order to modulate BG properties such as mechanical strength or surface reactivity [264]. As it is obvious, the presence of crystalline domains on the BG surface affects protein adsorption as well. In a series of studies, El-Ghannam et al. [285,286] investigated the influence of crystallization of 45S5 Bioglass on protein adsorption. Crystallization induced by thermal treatment provoked an increment of the zeta potential towards more negative values and a consequent reduction of adsorbed proteins [285]. Concurrently, protein adsorbed on the glass-ceramic surface showed a limited expression of unordered structure and an increased presence of β-structure with respect to adsorption on the amorphous BG. The higher presence of unordered structure was also related to

limited cell spreading [286]. Conversely, other authors suggested that the crystallinity of Bioglass did not affect much the total amount of proteins adsorbed, but it greatly changes the protein profile: even though in both cases albumin is the most abundant proteins in the adsorbed layer, amorphous systems showed also the presence of C3 complement and α-antitrypsin, which were much decreased after devitrification. On the other hand, sol-gel BG adsorbed a much larger variety of proteins [287]. Phase separation has also a determining effect on protein adsorption. By changing the casting equilibration temperature, different phase separated morphologies on 45S5 Bioglass can be obtained: silica rich spinodal phases or silica depleted droplet phase (Figure 2.15). BSA was observed to adsorb more on spinodal type than on droplet one, even in case of pre-incubation in PBS and consequent formation of a HA layer [288]. β-sheet/β-turns ratio, usually correlated to increased biocompatibility, was also increased by adsorption on spinodal morphology.

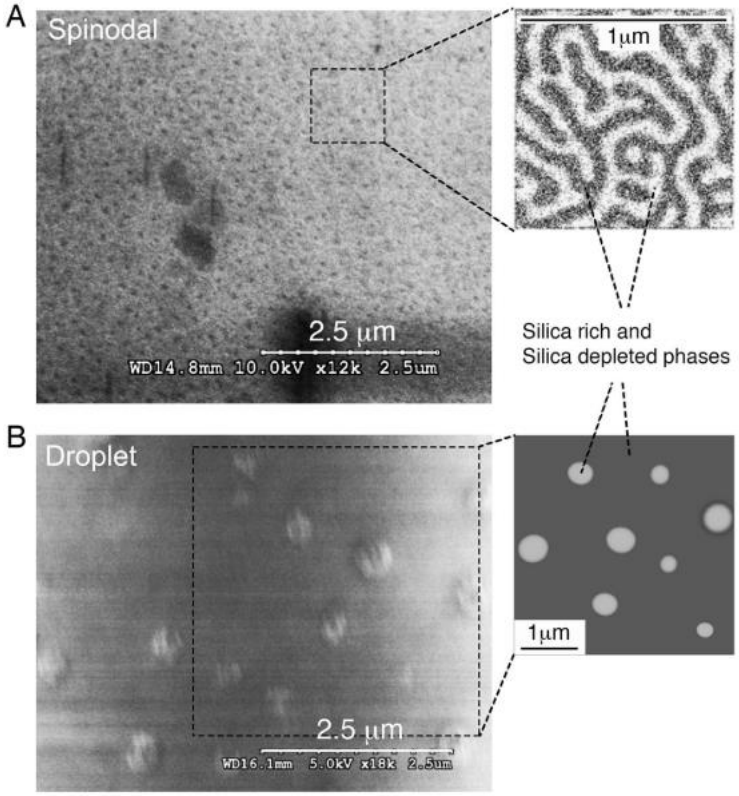

Figure 2.15 Phase separation on 45S5 Bioglass: a) spinodal morphology; b) droplet morphology [288]

Surface reactivity

The strict correlation between protein adsorption and BG surface reactions have been briefly covered in the paragraphs above. Some studies have been specifically performed in order to better clarify the modification events that occur during the interactions with protein containing solutions.

As previously discussed, pre-treatment of BG surface, with the formation of the silica-rich gel-layer or the deposition of the amorphous Ca-P layer deeply affect protein adsorption. These effects were related to the surface charge of the reaction

layer. The higher stability of 13-93 glass, compared to S53P4 and phosphate glasses, was addressed as the main reason for increased protein adsorption on that surface [289]. Silica-gel layer has a negative surface potential, while the presence of Ca-P precipitates increases it, providing better electrostatic interactions with proteins from FBS supplemented Eagle's medium, which are usually negatively charged at physiological pH [290]. Furthermore, the formation of a protein layer on BG surfaces within the first minutes can prevent the dissolution of the glass and delay further bioactive reactions. On this matter, there is no unanimous consensus. Lobel and Hench have reported that cytochrome c adsorption is limited by the nucleation and crystallization of Ca-P on the BG surface [291]. In another study, it was observed that glass pre-treatment did not affect the amount of fibronectin adsorbed, but it changed the conformation of the proteins towards a more cell adhesion simulating structure [292]. As always, when confronting results from different studies, it is necessary to carefully compare the adsorption conditions. In this case, it is possible that the changes in surface potential selectively affect uptake of different proteins. When BGs react in contact with protein solutions, the resulting layer, both the silica-gel and the amorphous Ca-P, may embed inside the adsorbed proteins [293,294].

2.4.3. Key concepts

The already complex matter of protein adsorption on biomaterial surfaces it is further convolute when bioactive glasses are involved, for several reason. At first, it is very intricated to discriminate the effect of the different glass parameters: changes in glass composition affect many other surface parameters, such as wettability, surface charge and even topography and mesostructure, therefore making almost impossible to exactly determine which parameters are mainly influencing protein adsorption. Furthermore, the surface of bioactive glasses is a dynamic entity, specifically designed to react and transform upon contact with biological fluids or simulated solutions. Glass reactions do not only change the surface properties, since the products, such as the silica-rich gel layer, the amorphous calcium-phosphate precipitates and the later crystalline hydroxyapatite, are very different from one another and from the pristine BG, but also because the release of ions from the glass affects the protein solution, by changing its pH and/or ionic strength.

Nevertheless, some insight on the mechanisms of protein adsorption on bioactive glasses have been obtained thanks to the extensive studies performed on the matter in the past 25 years. The main findings are reported in Table 1.2. As in the case of adsorption on titanium based substrates, some aspects are more clear with higher consensus about scientists, while some others are less understood. It is generally accepted that the presence of ions of the first and second groups, such as calcium, is detrimental for protein adsorption, as consequence of less Si-OH groups and competition between adsorption and HA precipitation process. Conversely, the incorporation of transition metals, which have many positive charges, may favor the electrostatic interactions with the usually negative protein surface. Furthermore,

the presence of metallic ions or NPs, mainly Ag and Au, enhances adsorption thanks to the great affinity of proteins for such elements, in particular through the binding with thiol groups. Besides surface chemistry, the presence of different elements may also affect the morphology of the BG, in particular in case of mesoporous sol-gel derived materials. The dimensions of the mesopores are fundamental in controlling protein uptake: adsorption can be selectively hampered by mesopores with reduced dimensions. To achieve control on the adsorbed molecules through dimensional screening is a very interesting and promising features, in particular for drug release purposes. Bioactive glasses can be produced with a fully amorphous structure or as glass-ceramic, usually with improved mechanical strength. Crystalline domains have very different properties than the amorphous phase, and obviously they affect protein adsorption, even though it is not clear in which terms: some authors suggested that crystallinity reduces the amount of protein adsorbed, as consequence of more unfavorable Columbic interactions, while some others pointed out that the main effect is a change of the protein profile in the adsorbed layer. Different processing parameters can also result in phase separation, which a different composition for each phase. Different adsorption mechanisms have been highlighted for BGs with different microstructures. At last, each step of the reaction cascade of bioactive glasses has its own peculiar behavior with respect to proteins. The formation of the silica-gel may limit protein adsorption in first place, but as calcium and phosphate species precipitate, more favorable interactions may occur. In the end, adsorption on crystalline hydroxyapatite shall be the highest. It is still necessary and noteworthy to notice that there is not an overall consensus on this. On the other hand, it seems confirmed that adsorbed proteins are embedded in the growing reaction layer.

Table 2.2 Effect of bioactive glass surface properties on protein adsorption (amount of adsorbed proteins, protein conformation on surface, and mechanism of protein–surface interaction) and impact of each feature on adsorption. ≈: no clear impact; ↑: mild impact; ↑↑: high impact; n.r.: effect not reported.

Surface Characteristic	Impact on Protein Adsorption	Conformation	Mechanism	Examples
Chemistry	↑↑	↑↑	Ions affect the surface properties, glass network structure and reactivity	Ca increases the glass reactivity, leading to lower amount of BSA adsorbed. Ta^{5+} and La^{3+} increases the adsorption thanks to favorable electrostatic interactions. Ag and Au ions or NPs provoke an extended denaturation of BSA by bonding with the thiol group in Cys resides.
Crystallinity	↑	↑	Crystalline domains are less reactive and have different chemistry and morphology than the amorphous phases	Crystalline BG binds less type of proteins than amorphous BG. Adsorption on amorphous BG results in a more unordered conformation of FN.
Phase separation	↑↑	↑↑	Different phases have different chemistry and surface properties	Spinodal 45S5 Bioglass adsorbs more than droplet phased Bioglass, with a favourable protein conformation for cell attachement
Pore dimension	↑↑	n.r.	Proteins can adsorb only in pores with adequate dimensions	BSA and LYS selective adsorption on nanorods can be modulated by changing the rod dimensions
Reactivity	↑↑	↑	Surface reactions may be in competition with protein adsorption and different stages have different properties	The formation of amorphous calcium phosphates or hydroxyapatite modifies the conformation of adsorbed FN, with respect to pristine BG. 45S5 Bioglass pre-treatment increases protein adsorption in case of formation of Ca-P species and not if only the silica-gel is present

2.4.4. Methods for Investigating Protein Adsorption

During the past years, researchers have developed and optimized a huge number of experimental techniques in order to overcome the challenges of investigating adsorption of proteins on surfaces with very different features. Characterization techniques for proteins adsorption, and biomolecules adsorption in general, are extensively reviewed elsewhere [295,296]. Here, a brief overview is reported of the techniques used in literature with a focus on the characterization of adsorption on titanium-based biomaterials and bioactive glasses. There is not a unique characterization technique that can provide information on all the aspects of protein adsorption, such as protein quantification, conformation after adsorption, interaction with the surface, and transient matrix compositions, therefore, different analyses shall be performed to address them all. Experimental methodologies that have been applied to study protein adsorption on biomaterials will be described considering the kind of information provided, alongside with their characteristics, advantages and drawbacks, summarized in Table 1.3.

Protein quantification can be obtained by following mainly two different strategies: the use of unlabeled proteins and labeled proteins. Label-free techniques involves the use of analytical assay such as the bicinchoninic acid protein assay (BCA) or the Bradford method [250,297]. The main drawbacks with these methods are that proteins need to be detached from the surface, for example by the use of surfactants, leading to possible underestimation of the total amount of protein adsorbed. Proteins can be labeled and quantified with radioactive iodine Isotope ^{125}I or with fluorophores [102,170,271]. The use of fluorescent marked proteins allows also the imaging of the adsorbed layer, by traditional or confocal laser microscopy(CLSM) [126,289]. Specific protein quantification may be obtained by targeting them with labeled antibodies [133] or by the well-established enzyme-linked immunosorbent assay (ELISA)[130,153]. The determination of the protein profile in the transient matrix is another aspect of interest, and can be investigated with common biochemical assay, such as Western blot or sodium dodecyl sulphate-polyacrylamide gel electrophoresis (SDS-PAGE)[135,287]. Liquid chromatography electrospray ionization tandem mass spectrometry (LC-ESI-MS/MS) is also employed to identify proteins within a complex layer [117,247]. Chemical analysis of the surface may be also used to detect protein on surfaces: XPS and ToF-SIMS can be employed on both titanium and bioactive glass to detect protein functional groups, identify specific proteins and determine protein-surface interactions [25,153,298,299]. Similar information can be obtained also by site-directed spin labeling combined with electron paramagnetic resonance spectroscopy (SDSL-EPR)[20]. X-ray wavelength dispersion spectroscopy (WSD) can be effectively employed for detecting adsorbed proteins in a large concentration range, from ng/cm^2 to µg/cm^2 [172,300]. Atomic force microscopy (AFM) can be also used for imaging of protein disposition on the surface and eventual agglomeration [93,168]. By properly modifying the tip, it is possible to evaluate the interaction strength between the surface and the proteins [110,278]. Direct visualization of the adsorbed protein layer, or the protein corona on NPs, can be

obtained by transmisison electron microscopy (TEM)[204]. Zeta potential measurement have been recently applied to obtain titration curves of protein adosrbed on bulky samples [80], even though it is usually applied for investigation of colloids [222]. The shape of the curve and the IEP may be used to provide information on surface coverage and protein three dimensional configuration. QCM is a powerfull technique to obtain real-time weighting of proteins adsorption on standard materials [138]. According to the insturment set-up, more information can be obtained, for example the stifness and water content of the adsorbed layer, by QCM with dissipation [152], or electrochemical and impedence measurement can be performed with EQCM [94]. Beside quantification and protein detection, it is also necessary to understand other aspect of the adsorption mechanisms, such as protein denaturation and layer thicnkess: spectroscopic techniques are suitable to investigate them. Secondary sturcture, such as α-helix, β-sheet, and random coils, have very specific vibrational bands, active both in Fourier transform infrared (FTIR) and Raman spectroscopy. The Amide I band (≈1650 cm^{-1}), which arises from stretching of C=O bonds, has a direct and straightforward correlation with the secondary structure of the proteins; on the other hand, the Amide II band (≈1550 cm^{-1}) is composed by the in-plane bend of NH and stretching vibration of CN and its relation with the protein secondary structure is far less obvious [301]. Deconvolution of Amide I band is often used to determine the protein secondary structure [148,299], while both Amide I and Amide II may be helpful to obtain quantitative information [36]. Raman spectroscopy can be used to investigate protein denaturation mainly on nanoparticles [302,303]. The protein denaturation can also be investigated by circular dichroism (CD)[213]. Changes in the intrinsic fluorescence of certain amino acids, such as tryptophan and tyrosine, which are related to mutation in the chemical environment of the residues, can be measured by synchronous fluorescent spectroscopy (SFS) for investigating protein conformation [139]. The thickness of the protein layer can be measured in real-time and in situ by spectroscopic ellipsometry (SE)[235] At last, protein-surface interactions can be evaluated by investigating the electrochemical behavior of the transient matrix interface with electrochemical impedance spectroscopy (EIS)[83,87].

Table 2.3 Characterization techniques commonly used for protein investigation on biomaterials. The output about protein adsorption, the kind of substrates that can be analyzed, the possibility of in situ (without protein detachment) and real-time measurement, main advantages and drawbacks, and eventual application on titanium or bioactive glasses are reported. Adapted and modified from [50,295,296,304].

Technique		Output	Substrate	In Situ/ Real Time	Advantages	Drawbacks	Substrate investigated
Labeled proteins	^{125}I-labeling	Quantification	Any	Yes/no	Direct quantification	Change of protein properties, handling issues	Ti
	Fluorescent labeling	Quantification and imaging	Any	Yes/no	Direct quantification, competitive adsorption evaluation	Change of protein properties, expensive reagents	Ti/BG
	CLSM	Imaging, relative quantification	Any	Yes/no	High resolution, 3D distribution into surface features	Expensive reagents	Ti/BG
UV-vis spectroscopy	BCA	Quantification	Any	No/no	Low cost, large range of concentrations	Protein detachment needed	Ti/BG
	Bradford assay	Quantification	Any	No/no	Low time consume	Protein detachment needed, sensible to surfactant	Ti/BG
Labeled antibodies		Quantification, protein recognition and imaging	Any	Yes/no	Targeting of specific proteins	Time consuming, specific reagents	Ti
ELISA		Quantification and protein recognition	Any	Yes/no	High specificity High throughput	Time consuming, specific reagents	Ti/BG
Gel electrophoresis	Western blot	Quantification and protein recognition	Any	No/no	No toxic chemicals	Sample preparation, poor band separation	Ti/BG
	SDS-PAGE	Quantification and protein recognition	Any	No/no	High sensitivity, small samples needed	Poor band resolution, toxic chemicals	
LC-EIS-MS/MS		Proteomic analysis	Any	No/no	High specificity and sensitivity	High costs	Ti
XPS		Quantification, protein-surface interaction	Any	Yes/no	High sensitivity, simultaneous evaluation of surface chemistry, depth profiling	No absolute quantification, complex data analysis	Ti/BG
Tof-SIMS		Quantification, protein recognition	Any	Yes/no	High sensitivity, possible orientation and conformation analysis, depth profiling	No absolute quantification, complex data analysis	Ti/BG
SDSL-EPR		Quantification, protein recognition	Any	Yes/yes	Conformation analysis in different conditions,	Complex data analysis, protein labeling needed	BG

				recognition of different proteins		
WSD	Quantification	Any	Yes/no	Sensitive to a wide range of protein surface concentration	Thorough calibration needed	Ti
AFM	Imaging, adhesion forces, conformation	Flat substrates	Yes/no	High resolution, customizable tip	Low throughput, time consuming, difficult imaging of soft films, tip preparation needed	Ti/BG
TEM	Imaging, thickness measurement	Any	Yes/no	Direct visualization of protein layer	Complex sample preparation, possible protein damage	Ti/BG
Zeta potential	Adsorption evaluation, protein conformation	Powder or planar samples	Yes/no	Simple measurement	No protein recognition, preliminary information needed	Ti
QCM	Quantification, viscoelastic properties of layer, changes in conformation	Sputtered sensors	Yes/Yes	High sensitivity, real time measurement, possibility to change the uptake solution	Co-adsorbed solvent weighted. mass calculation affected by energy dissipation	Ti/BG
FTIR (ATR)	Secondary structure, relative quantification	Planar samples	Yes/no	Very specific protein band	Not highly sensitive, data deconvolution needed	Ti/BG
Raman spectroscopy	Secondary structure, relative quantification	Any	Yes/no	Very specific protein band	Not highly sensitive, complex data interpretation	Ti/BG
CD	Protein conformation	Planar samples	Yes/no	Specific bands for secondary structures	Band deconvolution needed, measured in solution	Ti/BG
SFS	Protein conformation	Any	Yes/no	Sensitive, high selectivity towards specific amino acids	Possible instrument artifacts	Ti
SE	Layer thickness measurement	Flat surfaces	Yes/yes	High sensitivity, low cost, fast measurement	Difficult optical modeling of rough and structured surfaces	Ti
EIS	Layer evolution, protein-surface interactions	Planar samples	Yes/yes	High sensitivity, possible to study adsorption in different condition	Complex modelling and data interpretation	Ti

2.5. Bibliography

[1] I.N. Levine, Physical Chemistry, 6th ed., McGraw Hill Educaiton, 2011.

[2] W. Norde, Driving forces for protein adsorption at solid surfaces, Macromol. Symp. 103 (1996) 5–18. https://doi.org/10.1002/masy.19961030104.

[3] K. Nakanishi, T. Sakiyama, K. Imamura, On the adsorption of proteins on solid surfaces, a common but very complicated phenomenon, J. Biosci. Bioeng. 91 (2001) 233–244. https://doi.org/10.1016/S1389-1723(01)80127-4.

[4] T.S. Tsapikouni, Y.F. Missirlis, Protein–material interactions: From micro-to-nano scale, Mater. Sci. Eng. B. 152 (2008) 2–7. https://doi.org/10.1016/j.mseb.2008.06.007.

[5] J.J. Gray, The interaction of proteins with solid surfaces, Curr. Opin. Struct. Biol. 14 (2004) 110–115. https://doi.org/10.1016/j.sbi.2003.12.001.

[6] V. Hlady, J. Buijs, Protein adsorption on solid surfaces, Curr. Opin. Biotechnol. 7 (1996) 72–77. http://link.springer.com/10.1007/978-3-662-04352-3_10.

[7] M. Rabe, D. Verdes, S. Seeger, Understanding protein adsorption phenomena at solid surfaces, Adv. Colloid Interface Sci. 162 (2011) 87–106. https://doi.org/10.1016/j.cis.2010.12.007.

[8] E.A. Vogler, Protein adsorption in three dimensions, Biomaterials. 33 (2012) 1201–1237. https://doi.org/10.1016/j.biomaterials.2011.10.059.

[9] C. Czeslik, Factors Ruling Protein Adsorption, Z. Phys. Chem. 218 (2004) 771–801.

[10] M.M. Browne, G.V. Lubarsky, M.R. Davidson, R.H. Bradley, Protein adsorption onto polystyrene surfaces studied by XPS and AFM, Surf. Sci. 553 (2004) 155–167. https://doi.org/10.1016/j.susc.2004.01.046.

[11] Y.F. Yano, Kinetics of protein unfolding at interfaces, J. Phys. Condens. Matter. 24 (2012) 503101. https://doi.org/10.1088/0953-8984/24/50/503101.

[12] E.A. Vogler, Structure and reactivity of water at biomaterial surfaces, Adv. Colloid Interface Sci. 74 (1998) 69–117. https://doi.org/10.1016/S0001-8686(97)00040-7.

[13] L.F. Scatena, Water at Hydrophobic Surfaces: Weak Hydrogen Bonding and Strong Orientation Effects, Science (80-.). 292 (2001) 908–912. https://doi.org/10.1126/science.1059514.

[14] C. Lee, J.A. McCammon, P.J. Rossky, The structure of liquid water at an extended hydrophobic surface, J. Chem. Phys. 80 (1984) 4448–4455. https://doi.org/10.1063/1.447226.

[15] S. Metwally, U. Stachewicz, Surface potential and charges impact on cell responses on biomaterials interfaces for medical applications, Mater. Sci. Eng. C. 104 (2019) 109883. https://doi.org/10.1016/j.msec.2019.109883.

[16] J.H. Adair, E. Suvaci, J. Sindel, Surface and Colloid Chemistry, in: Encycl. Mater. Sci. Technol., Elsevier, 2001: pp. 1–10. https://doi.org/10.1016/B0-08-043152-6/01622-3.

[17] W. Norde, My voyage of discovery to proteins in flatland ...and beyond, Colloids Surfaces B Biointerfaces. 61 (2008) 1–9. https://doi.org/10.1016/j.colsurfb.2007.09.029.

[18] L. Yu, L. Zhang, Y. Sun, Protein behavior at surfaces: Orientation, conformational transitions and transport, J. Chromatogr. A. 1382 (2015)

118–134. https://doi.org/10.1016/j.chroma.2014.12.087.
[19] S. Servagent-Noinville, M. Revault, H. Quiquampoix, M.-H. Baron, Conformational Changes of Bovine Serum Albumin Induced by Adsorption on Different Clay Surfaces: FTIR Analysis, J. Colloid Interface Sci. 221 (2000) 273–283. https://doi.org/10.1006/jcis.1999.6576.
[20] C.M. Gruian, C. Rickert, S.C.T. Nicklisch, E. Vanea, H.-J. Steinhoff, S. Simon, Conformational Changes and Competitive Adsorption between Serum Albumin and Hemoglobin on Bioceramic Substrates, ChemPhysChem. 18 (2017) 634–642. https://doi.org/10.1002/cphc.201600886.
[21] D.H. Tsai, F.W. Delrio, A.M. Keene, K.M. Tyner, R.I. MacCuspie, T.J. Cho, M.R. Zachariah, V.A. Hackley, Adsorption and conformation of serum albumin protein on gold nanoparticles investigated using dimensional measurements and in situ spectroscopic methods, Langmuir. 27 (2011) 2464–2477. https://doi.org/10.1021/la104124d.
[22] N. Dasgupta, S. Ranjan, D. Patra, P. Srivastava, A. Kumar, C. Ramalingam, Bovine serum albumin interacts with silver nanoparticles with a “side-on” or “end on” conformation, Chem. Biol. Interact. 253 (2016) 100–111. https://doi.org/10.1016/j.cbi.2016.05.018.
[23] Y.L. Jeyachandran, E. Mielczarski, B. Rai, J.A. Mielczarski, Quantitative and qualitative evaluation of adsorption/desorption of bovine serum albumin on hydrophilic and hydrophobic surfaces, Langmuir. 25 (2009) 11614–11620. https://doi.org/10.1021/la901453a.
[24] H.M. Zhang, K. Lou, J. Cao, Y.Q. Wang, Interaction of a hydrophobic-functionalized pamam dendrimer with bovine serum albumin: Thermodynamic and structural changes, Langmuir. 30 (2014) 5536–5544. https://doi.org/10.1021/la501129y.
[25] X.N. Hu, B.C. Yang, Conformation change of bovine serum albumin induced by bioactive titanium metals and its effects on cell behaviors, J. Biomed. Mater. Res. - Part A. 102 (2014) 1053–1062. https://doi.org/10.1002/jbm.a.34768.
[26] D.R. Jackson, S. Omanovic, S.G. Roscoe, Electrochemical studies of the adsorption behavior of serum proteins on titanium, Langmuir. 16 (2000) 5449–5457. https://doi.org/10.1021/la991497x.
[27] C. Zhou, J.M. Friedt, A. Angelova, K.H. Choi, W. Laureyn, F. Frederix, L.A. Francis, A. Campitelli, Y. Engelborghs, G. Burghs, Human immunoglobulin adsorption investigated by means of quartz crystal microbalance dissipation, atomic force microscopy, surface acoustic wave, and surface plasmon resonance techniques, Langmuir. 20 (2004) 5870–5878. https://doi.org/10.1021/la036251d.
[28] K. Awsiuk, A. Budkowski, A. Psarouli, P. Petrou, A. Bernasik, S. Kakabakos, J. Rysz, I. Raptis, Protein adsorption and covalent bonding to silicon nitride surfaces modified with organo-silanes: Comparison using AFM, angle-resolved XPS and multivariate ToF-SIMS analysis, Colloids Surfaces B Biointerfaces. 110 (2013) 217–224. https://doi.org/10.1016/j.colsurfb.2013.04.030.
[29] U. Dembereldorj, E.O. Ganbold, J.H. Seo, S.Y. Lee, S.I. Yang, S.W. Joo, Conformational changes of proteins adsorbed onto ZnO nanoparticle surfaces investigated by concentration-dependent infrared spectroscopy, Vib. Spectrosc. 59 (2012) 23–28. https://doi.org/10.1016/j.vibspec.2011.12.002.

[30] M.H. Baron, M. Revault, S. Servagent-Noinville, J. Abadie, H. Quiquampoix, Chymotrypsin adsorption on montmorillonite: Enzymatic activity and kinetic FTIR structural analysis, J. Colloid Interface Sci. 214 (1999) 319–332. https://doi.org/10.1006/jcis.1999.6189.

[31] C.F. Wertz, M.M. Santore, Adsorption and Reorientation Kinetics of Lysozyme on Hydrophobic Surfaces, Langmuir. 18 (2002) 1190–1199. https://doi.org/10.1021/la0108813.

[32] T. Zoungrana, G.H. Findenegg, W. Norde, Structure, stability, and activity of adsorbed enzymes, J. Colloid Interface Sci. 190 (1997) 437–448. https://doi.org/10.1006/jcis.1997.4895.

[33] T. Wei, M.A. Carignano, I. Szleifer, Lysozyme adsorption on polyethylene surfaces: Why are long simulations needed?, Langmuir. 27 (2011) 12074–12081. https://doi.org/10.1021/la202622s.

[34] A. Blanco, G. Blanco, Proteins, in: Med. Biochem., Elsevier, 2017: pp. 21–71. https://doi.org/10.1016/B978-0-12-803550-4.00003-3.

[35] B. Bharti, Adsorption, Aggregation and Structure Formation in Systems of Charged Particles, Springer International Publishing, Cham, 2014. https://doi.org/10.1007/978-3-319-07737-6.

[36] B. Fernández-Montes Moraleda, J.S. Román, L.M. Rodríguez-Lorenzo, Influence of surface features of hydroxyapatite on the adsorption of proteins relevant to bone regeneration, J. Biomed. Mater. Res. - Part A. 101 A (2013) 2332–2339. https://doi.org/10.1002/jbm.a.34528.

[37] R. Li, Z. Wu, Y. Wangb, L. Ding, Y. Wang, Role of pH-induced structural change in protein aggregation in foam fractionation of bovine serum albumin, Biotechnol. Reports. 9 (2016) 46–52. https://doi.org/10.1016/j.btre.2016.01.002.

[38] A. Bujacz, Structures of bovine, equine and leporine serum albumin, Acta Crystallogr. Sect. D Biol. Crystallogr. 68 (2012) 1278–1289. https://doi.org/10.1107/S0907444912027047.

[39] G. Greene, H. Radhakrishna, R. Tannenbaum, Protein binding properties of surface-modified porous polyethylene membranes, Biomaterials. 26 (2005) 5972–5982. https://doi.org/10.1016/j.biomaterials.2005.03.025.

[40] K. Kubiak-Ossowska, B. Jachimska, M. Al Qaraghuli, P.A. Mulheran, Protein interactions with negatively charged inorganic surfaces, Curr. Opin. Colloid Interface Sci. 41 (2019) 104–117. https://doi.org/10.1016/j.cocis.2019.02.001.

[41] K.L. Jones, C.R. O'Melia, Protein and humic acid adsorption onto hydrophilic membrane surfaces: Effects of pH and ionic strength, J. Memb. Sci. 165 (2000) 31–46. https://doi.org/10.1016/S0376-7388(99)00218-5.

[42] K. Kubiak-Ossowska, M. Cwieka, A. Kaczynska, B. Jachimska, P.A. Mulheran, Lysozyme adsorption at a silica surface using simulation and experiment: Effects of pH on protein layer structure, Phys. Chem. Chem. Phys. 17 (2015) 24070–24077. https://doi.org/10.1039/c5cp03910j.

[43] A. Ithurbide, I. Frateur, A. Galtayries, P. Marcus, XPS and flow-cell EQCM study of albumin adsorption on passivated chromium surfaces: Influence of potential and pH, Electrochim. Acta. 53 (2007) 1336–1345. https://doi.org/10.1016/j.electacta.2007.04.109.

[44] N. Barnthip, P. Parhi, A. Golas, E.A. Vogler, Volumetric interpretation of protein adsorption: Kinetics of protein-adsorption competition from binary solution, Biomaterials. 30 (2009) 6495–6513. https://doi.org/10.1016/j.biomaterials.2009.08.016.

[45] E. Brynda, N.A. Cepalova, M. Štol, Equilibrium adsorption of human serum albumin and human fibrinogen on hydrophobic and hydrophilic surfaces, J. Biomed. Mater. Res. 18 (1984) 685–693. https://doi.org/10.1002/jbm.820180609.

[46] H.P. Felgueiras, J.C. Antunes, M.C.L. Martins, M.A. Barbosa, Fundamentals of protein and cell interactions in biomaterials, Elsevier Ltd., 2018. https://doi.org/10.1016/B978-0-08-100803-4.00001-2.

[47] L.C. Xu, C.A. Siedlecki, Effects of surface wettability and contact time on protein adhesion to biomaterial surfaces, Biomaterials. 28 (2007) 3273–3283. https://doi.org/10.1016/j.biomaterials.2007.03.032.

[48] K.E. Michael, V.N. Vernekar, B.G. Keselowsky, J.C. Meredith, R.A. Latour, A.J. García, Adsorption-induced conformational changes in fibronectin due to interactions with well-defined surface chemistries, Langmuir. 19 (2003) 8033–8040. https://doi.org/10.1021/la034810a.

[49] P. Roach, D. Farrar, C.C. Perry, Interpretation of protein adsorption: Surface-induced conformational changes, J. Am. Chem. Soc. 127 (2005) 8168–8173. https://doi.org/10.1021/ja042898o.

[50] K. Zheng, M. Kapp, A.R. Boccaccini, Protein interactions with bioactive glass surfaces: A review, Appl. Mater. Today. 15 (2019) 350–371. https://doi.org/10.1016/j.apmt.2019.02.003.

[51] H.G. Xie, X.X. Li, G.J. Lv, W.Y. Xie, J. Zhu, T. Luxbacher, R. Ma, X.J. Ma, Effect of surface wettability and charge on protein adsorption onto implantable alginate-chitosan-alginate microcapsule surfaces, J. Biomed. Mater. Res. - Part A. 92 (2010) 1357–1365. https://doi.org/10.1002/jbm.a.32437.

[52] K. Isoshima, T. Ueno, Y. Arai, H. Saito, P. Chen, Y. Tsutsumi, T. Hanawa, N. Wakabayashi, The change of surface charge by lithium ion coating enhances protein adsorption on titanium, J. Mech. Behav. Biomed. Mater. 100 (2019) 103393. https://doi.org/10.1016/j.jmbbm.2019.103393.

[53] P. Roach, D. Eglin, K. Rohde, C.C. Perry, Modern biomaterials: A review - Bulk properties and implications of surface modifications, J. Mater. Sci. Mater. Med. 18 (2007) 1263–1277. https://doi.org/10.1007/s10856-006-0064-3.

[54] K. Rechendorff, M.B. Hovgaard, M. Foss, V.P. Zhdanov, F. Besenbacher, Enhancement of protein adsorption induced by surface roughness, Langmuir. 22 (2006) 10885–10888. https://doi.org/10.1021/la0621923.

[55] T. Khampieng, V. Yamassatien, P. Ekabutr, P. Pavasant, P. Supaphol, Protein adsorption and cell behaviors on polycaprolactone film: The effect of surface topography, Adv. Polym. Technol. 37 (2018) 2030–2042. https://doi.org/10.1002/adv.21861.

[56] T. Akkas, C. Citak, A. Sirkecioglu, F.S. Güner, Which ismore effective for protein adsorption: Surface roughness, surface wettability or swelling? Case study of polyurethane films prepared from castor oil and poly(ethylene glycol), Polym. Int. 62 (2013) 1202–1209. https://doi.org/10.1002/pi.4408.

[57] C. Czeslik, A. Wittemann, Adsorption mechanism, secondary structure and local distribution of proteins at polyelectrolyte brushes, Colloid Polym. Sci. (2020). https://doi.org/10.1007/s00396-019-04590-7.

[58] E. Psarra, U. König, Y. Ueda, C. Bellmann, A. Janke, E. Bittrich, K.J. Eichhorn, P. Uhlmann, Nanostructured Biointerfaces: Nanoarchitectonics of Thermoresponsive Polymer Brushes Impact Protein Adsorption and Cell Adhesion, ACS Appl. Mater. Interfaces. 7 (2015) 12516–12529.

https://doi.org/10.1021/am508161q.

[59] T. Kopac, K. Bozgeyik, J. Yener, Effect of pH and temperature on the adsorption of bovine serum albumin onto titanium dioxide, Colloids Surfaces A Physicochem. Eng. Asp. 322 (2008) 19–28. https://doi.org/10.1016/j.colsurfa.2008.02.010.

[60] R.C.F. Bonomo, L.A. Minim, J.S.R. Coimbra, R.C.I. Fontan, L.H. Mendes da Silva, V.P.R. Minim, Hydrophobic interaction adsorption of whey proteins: Effect of temperature and salt concentration and thermodynamic analysis, J. Chromatogr. B Anal. Technol. Biomed. Life Sci. 844 (2006) 6–14. https://doi.org/10.1016/j.jchromb.2006.06.021.

[61] C. Valero Vidal, A. Olmo Juan, A. Igual Muñoz, Adsorption of bovine serum albumin on CoCrMo surface: Effect of temperature and protein concentration, Colloids Surfaces B Biointerfaces. 80 (2010) 1–11. https://doi.org/10.1016/j.colsurfb.2010.05.005.

[62] I. Kiesel, M. Paulus, J. Nase, S. Tiemeyer, C. Sternemann, K. Rüster, F.J. Wirkert, K. Mende, T. Büning, M. Tolan, Temperature-driven adsorption and desorption of proteins at solid-liquid interfaces, Langmuir. 30 (2014) 2077–2083. https://doi.org/10.1021/la404884a.

[63] S. Demanèche, J.P. Chapel, L.J. Monrozier, H. Quiquampoix, Dissimilar pH-dependent adsorption features of bovine serum albumin and α-chymotrypsin on mica probed by AFM, Colloids Surfaces B Biointerfaces. 70 (2009) 226–231. https://doi.org/10.1016/j.colsurfb.2008.12.036.

[64] L. Tercinier, A. Ye, A. Singh, S.G. Anema, H. Singh, Effects of Ionic Strength, pH and Milk Serum Composition on Adsorption of Milk Proteins on to Hydroxyapatite Particles, Food Biophys. 9 (2014) 341–348. https://doi.org/10.1007/s11483-014-9360-5.

[65] K. Szewczuk-Karpisz, M. Wiśniewska, Adsorption properties of the albumin-chromium(III) oxide system - Effect of solution pH and ionic strength, Soft Mater. 12 (2014) 268–276. https://doi.org/10.1080/1539445X.2014.890940.

[66] A. Salis, M. Monduzzi, Not only pH. Specific buffer effects in biological systems, Curr. Opin. Colloid Interface Sci. 23 (2016) 1–9. https://doi.org/10.1016/j.cocis.2016.04.004.

[67] H.I. Okur, J. Hladílková, K.B. Rembert, Y. Cho, J. Heyda, J. Dzubiella, P.S. Cremer, P. Jungwirth, Beyond the Hofmeister Series: Ion-Specific Effects on Proteins and Their Biological Functions, J. Phys. Chem. B. 121 (2017) 1997–2014. https://doi.org/10.1021/acs.jpcb.6b10797.

[68] S.O. Ugwu, S. p Apte, The Effect of Buffers on Protein Conformational Stability, Pharm. Technol. (2004) 86–113.

[69] F. Evers, R. Steitz, M. Tolan, C. Czeslik, Analysis of hofmeister effects on the density profile of protein adsorbates: A neutron reflectivity study, J. Phys. Chem. B. 113 (2009) 8462–8465. https://doi.org/10.1021/jp904065w.

[70] D.R. Gondim, J.A. Cecilia, S.O. Santos, T.N.B. Rodrigues, J.E. Aguiar, E. Vilarrasa-García, E. Rodríguez-Castellón, D.C.S. Azevedo, I.J. Silva, Influence of buffer solutions in the adsorption of human serum proteins onto layered double hydroxide, Int. J. Biol. Macromol. 106 (2018) 396–409. https://doi.org/10.1016/j.ijbiomac.2017.08.040.

[71] T. Wei, S. Kaewtathip, K. Shing, Buffer Effect on Protein Adsorption at Liquid/Solid Interface, J. Phys. Chem. C. 113 (2009) 2053–2062. https://doi.org/10.1021/jp806586n.

[72] M. Parkes, C. Myant, P.M. Cann, J.S.S. Wong, The effect of buffer solution

choice on protein adsorption and lubrication, Tribol. Int. 72 (2014) 108–117. https://doi.org/10.1016/j.triboint.2013.12.005.

[73] M. Wilhelmi, C. Müller, C. Ziegler, M. Kopnarski, BSA adsorption on titanium: ToF-SIMS investigation of the surface coverage as a function of protein concentration and pH-value, Anal. Bioanal. Chem. 400 (2011) 697–701. https://doi.org/10.1007/s00216-011-4833-6.

[74] H. Lefaix, A. Galtayries, F. Prima, P. Marcus, Nano-size protein at the surface of a Ti-Zr-Ni quasi-crystalline alloy: Fibronectin adsorption on metallic nano-composites, Colloids Surfaces A Physicochem. Eng. Asp. 439 (2013) 207–214. https://doi.org/10.1016/j.colsurfa.2013.04.009.

[75] J. Wilson, Metallic biomaterials: State of the art and new challenges, in: P. Balakrishnan, S. M S, T. Sabu (Eds.), Fundam. Biomater. Met., 1st ed., Elsevier, 2018: pp. 1–33. https://doi.org/10.1016/B978-0-08-102205-4.00001-5.

[76] S. Spriano, S. Yamaguchi, F. Baino, S. Ferraris, A critical review of multifunctional titanium surfaces: New frontiers for improving osseointegration and host response, avoiding bacteria contamination, Acta Biomater. 79 (2018) 1–22. https://doi.org/10.1016/j.actbio.2018.08.013.

[77] T. Hanawa, Titanium-tissue interface reaction and its control with surface treatment, Front. Bioeng. Biotechnol. 7 (2019). https://doi.org/10.3389/fbioe.2019.00170.

[78] D.M. Brunette, P. Tengvall, M. Textor, P. Thomsen, eds., Titanium in Medicine, 1st ed., Springer-Verlag Berlin Heidelberg, Berlin, Heidelberg, 2001. https://doi.org/10.1007/978-3-642-56486-4.

[79] M. Textor, C. Sittig, V. Frauchiger, S. Tosatti, D. Brunette, Properties and Biological Significance of Natural Oxide Films on Titanium and Its Alloys, in: D.M. Brunette, P. Tengvall, M. Textor, P. Thomsen (Eds.), Titan. Med., 1st ed., Springer-Verlag Berlin Heidelberg, Berlin, Heidelberg, 2001.

[80] S. Ferraris, M. Cazzola, V. Peretti, B. Stella, S. Spriano, Zeta potential measurements on solid surfaces for in Vitro biomaterials testing: Surface charge, reactivity upon contact with fluids and protein absorption, Front. Bioeng. Biotechnol. 6 (2018) 1–7. https://doi.org/10.3389/fbioe.2018.00060.

[81] K. Watanabe, S. Okawa, M. Kanatani, K. Homma, Surface analysis of commercially pure titanium implant retrieved from rat bone. part 1: Initial biological response of sandblasted surface, Dent. Mater. J. 28 (2009) 178–184. https://doi.org/10.4012/dmj.28.178.

[82] D. Ionita, R. Popescu, T. Tite, I. Demetrescu, The Behaviour of Pure Titanium in Albumin Solution, Mol. Cryst. Liq. Cryst. 486 (2008) 166/[1208]-174/[1216]. https://doi.org/10.1080/15421400801917957.

[83] O.R. Cámara, L.B. Avalle, F.Y. Oliva, Protein adsorption on titanium dioxide: Effects on double layer and semiconductor space charge region studied by EIS, Electrochim. Acta. 55 (2010) 4519–4528. https://doi.org/10.1016/j.electacta.2010.03.003.

[84] D. Roberts, R. Keeling, M. Tracka, C.F. Van Der Walle, S. Uddin, J. Warwicker, R. Curtis, Specific ion and buffer effects on protein-protein interactions of a monoclonal antibody, Mol. Pharm. 12 (2015) 179–193. https://doi.org/10.1021/mp500533c.

[85] D. Kohavi, L. Badihi Hauslich, G. Rosen, D. Steinberg, M.N. Sela, Wettability versus electrostatic forces in fibronectin and albumin adsorption to titanium surfaces, Clin. Oral Implants Res. 24 (2013) 1002–1008. https://doi.org/10.1111/j.1600-0501.2012.02508.x.

[86] K. Imamura, M. Shimomura, S. Nagai, M. Akamatsu, K. Nakanishi, Adsorption characteristics of various proteins to a titanium surface, J. Biosci. Bioeng. 106 (2008) 273–278. https://doi.org/10.1263/jbb.106.273.

[87] F.Y. Oliva, O.R. Cámara, L.B. Avalle, Adsorption of human serum albumin on electrochemical titanium dioxide electrodes: Protein-oxide surface interaction effects studied by electrochemical techniques, J. Electroanal. Chem. 633 (2009) 19–34. https://doi.org/10.1016/j.jelechem.2009.04.024.

[88] Y. Kang, X. Li, Y. Tu, Q. Wang, H. Ågren, On the Mechanism of Protein Adsorption onto Hydroxylated and Nonhydroxylated TiO 2 Surfaces, J. Phys. Chem. C. 114 (2010) 14496–14502. https://doi.org/10.1021/jp1037156.

[89] C.M. Mao, J. Sampath, K.G. Sprenger, G. Drobny, J. Pfaendtner, Molecular Driving Forces in Peptide Adsorption to Metal Oxide Surfaces, Langmuir. 35 (2019) 5911–5920. https://doi.org/10.1021/acs.langmuir.8b01392.

[90] T. Sun, G. Han, M. Lindgren, Z. Shen, A. Laaksonen, Adhesion of lactoferrin and bone morphogenetic protein-2 to a rutile surface: dependence on the surface hydrophobicity, Biomater. Sci. 2 (2014) 1090–1099. https://doi.org/10.1039/C4BM00021H.

[91] T. Utesch, G. Daminelli, M.A. Mroginski, Molecular dynamics simulations of the adsorption of bone morphogenetic protein-2 on surfaces with medical relevance, Langmuir. 27 (2011) 13144–13153. https://doi.org/10.1021/la202489w.

[92] A. Zhao, Z. Wang, S. Zhou, G. Xue, Y. Wang, C. Ye, N. Huang, Titanium oxide films with vacuum thermal treatment for enhanced hemocompatibility, Surf. Eng. 31 (2015) 898–903. https://doi.org/10.1179/1743294414Y.0000000367.

[93] I. Van De Keere, R. Willaert, A. Hubin, J. Vereecken, Interaction of human plasma fibrinogen with commercially pure titanium as studied with atomic force microscopy and X-ray photoelectron spectroscopy, Langmuir. 24 (2008) 1844–1852. https://doi.org/10.1021/la7016566.

[94] Q. Yang, Y. Zhang, M. Liu, M. Ye, Y. Zhang, S. Yao, Study of fibrinogen adsorption on hydroxyapatite and TiO2 surfaces by electrochemical piezoelectric quartz crystal impedance and FTIR–ATR spectroscopy, Anal. Chim. Acta. 597 (2007) 58–66. https://doi.org/10.1016/j.aca.2007.06.025.

[95] A. Zhao, Z. Wang, X. Zhu, M.F. Maitz, N. Huang, Real-Time Characterization of Fibrinogen Interaction with Modified Titanium Dioxide Film by Quartz Crystal Microbalance with Dissipation, Chinese J. Chem. Phys. 27 (2014) 355–360. https://doi.org/10.1063/1674-0068/27/03/355-360.

[96] S.E. Moulton, J.N. Barisci, A. Bath, R. Stella, G.G. Wallace, Investigation of Ig.G adsorption and the effect on electrochemical responses at titanium dioxide electrode, Langmuir. 21 (2005) 316–322. https://doi.org/10.1021/la0487242.

[97] A. Bouhekka, T. Bürgi, In situ ATR-IR spectroscopy study of adsorbed protein: Visible light denaturation of bovine serum albumin on TiO 2, Appl. Surf. Sci. 261 (2012) 369–374. https://doi.org/10.1016/j.apsusc.2012.08.017.

[98] I. Van De Keere, R. Willaert, E. Tourwé, A. Hubin, J. Vereecken, The interaction of human serum albumin with titanium studied by means of atomic force microscopy, Surf. Interface Anal. 40 (2008) 157–161. https://doi.org/10.1002/sia.2673.

[99] A. Wesełucha-Birczyńska, E. Stodolak-Zych, W. Piś, E. Długoń, A. Benko, M. Błażewicz, A model of adsorption of albumin on the implant surface titanium and titanium modified carbon coatings (MWCNT-EPD). 2D correlation analysis, J. Mol. Struct. 1124 (2016) 61–70. https://doi.org/10.1016/j.molstruc.2016.04.050.

[100] H.P. Zhang, X. Lu, L.M. Fang, J. Weng, N. Huang, Y. Leng, Molecular dynamics simulation of RGD peptide adsorption on titanium oxide surfaces, J. Mater. Sci. Mater. Med. 19 (2008) 3437–3441. https://doi.org/10.1007/s10856-008-3498-y.

[101] D.D. Deligianni, N. Katsala, S. Ladas, D. Sotiropoulou, J. Amedee, Y.F. Missirlis, Effect of surface roughness of the titanium alloy Ti-6Al-4V on human bone marrow cell response and on protein adsorption, Biomaterials. 22 (2001) 1241–1251. https://doi.org/10.1016/S0142-9612(00)00274-X.

[102] B.S. Kopf, S. Ruch, S. Berner, N.D. Spencer, K. Maniura-Weber, The role of nanostructures and hydrophilicity in osseointegration: In-vitro protein-adsorption and blood-interaction studies, J. Biomed. Mater. Res. Part A. 103 (2015) 2661–2672. https://doi.org/10.1002/jbm.a.35401.

[103] K. Cai, J. Bossert, K.D. Jandt, Does the nanometre scale topography of titanium influence protein adsorption and cell proliferation?, Colloids Surfaces B Biointerfaces. 49 (2006) 136–144. https://doi.org/10.1016/j.colsurfb.2006.02.016.

[104] G.P. Rockwell, L.B. Lohstreter, J.R. Dahn, Fibrinogen and albumin adsorption on titanium nanoroughness gradients, Colloids Surfaces B Biointerfaces. 91 (2012) 90–96. https://doi.org/10.1016/j.colsurfb.2011.10.045.

[105] J. Lu, C. Yao, L. Yang, T.J. Webster, Decreased Platelet Adhesion and Enhanced Endothelial Cell Functions on Nano and Submicron-Rough Titanium Stents, Tissue Eng. Part A. 18 (2012) 1389–1398. https://doi.org/10.1089/ten.tea.2011.0268.

[106] T. Kopac, K. Bozgeyik, Effect of surface area enhancement on the adsorption of bovine serum albumin onto titanium dioxide, Colloids Surfaces B Biointerfaces. 76 (2010) 265–271. https://doi.org/10.1016/j.colsurfb.2009.11.002.

[107] L. Liu, R. Bhatia, T. Webster, Atomic layer deposition of nano-TiO2 thin films with enhanced biocompatibility and antimicrobial activity for orthopedic implants, Int. J. Nanomedicine. Volume 12 (2017) 8711–8723. https://doi.org/10.2147/IJN.S148065.

[108] P.E. Scopelliti, A. Borgonovo, M. Indrieri, L. Giorgetti, G. Bongiorno, R. Carbone, A. Podestà, P. Milani, The effect of surface nanometre-scale morphology on protein adsorption, PLoS One. 5 (2010) 1–9. https://doi.org/10.1371/journal.pone.0011862.

[109] C. Liu, Y. Guo, Q. Hong, C. Rao, H. Zhang, Y. Dong, L. Huang, X. Lu, N. Bao, Bovine Serum Albumin Adsorption in Mesoporous Titanium Dioxide: Pore Size and Pore Chemistry Effect, Langmuir. 32 (2016) 3995–4003. https://doi.org/10.1021/acs.langmuir.5b04496.

[110] R. An, W. Zhuang, Z. Yang, X. Lu, J. Zhu, Y. Wang, Y. Dong, N. Wu, Protein adsorptive behavior on mesoporous titanium dioxide determined by geometrical topography, Chem. Eng. Sci. 117 (2014) 146–155. https://doi.org/10.1016/j.ces.2014.06.004.

[111] A.V. Singh, V. Vyas, R. Patil, V. Sharma, P.E. Scopelliti, G. Bongiorno, A. Podestà, C. Lenardi, W.N. Gade, P. Milani, Quantitative Characterization of

the Influence of the Nanoscale Morphology of Nanostructured Surfaces on Bacterial Adhesion and Biofilm Formation, PLoS One. 6 (2011) e25029. https://doi.org/10.1371/journal.pone.0025029.

[112] J. Selvakumaran, J.L. Keddie, D.J. Ewins, M.P. Hughes, Protein adsorption on materials for recording sites on implantable microelectrodes, J. Mater. Sci. Mater. Med. 19 (2008) 143–151. https://doi.org/10.1007/s10856-007-3110-x.

[113] P. Silva-Bermudez, S. Muhl, S.E. Rodil, A comparative study of fibrinogen adsorption onto metal oxide thin films, Appl. Surf. Sci. 282 (2013) 351–362. https://doi.org/10.1016/j.apsusc.2013.05.133.

[114] S. Arvidsson, A. Askendal, P. Tengvall, Blood plasma contact activation on silicon, titanium and aluminium, Biomaterials. 28 (2007) 1346–1354. https://doi.org/10.1016/j.biomaterials.2006.11.005.

[115] L. Song, K. Yang, W. Jiang, P. Du, B. Xing, Adsorption of bovine serum albumin on nano and bulk oxide particles in deionized water, Colloids Surfaces B Biointerfaces. 94 (2012) 341–346. https://doi.org/10.1016/j.colsurfb.2012.02.011.

[116] E. Yoshida, T. Hayakawa, Adsorption Analysis of Lactoferrin to Titanium, Stainless Steel, Zirconia, and Polymethyl Methacrylate Using the Quartz Crystal Microbalance Method, Biomed Res. Int. 2016 (2016) 1–7. https://doi.org/10.1155/2016/3961286.

[117] M.-N. Abdallah, G. Abughanam, S.D. Tran, Z. Sheikh, M.A. Mezour, T. Basiri, Y. Xiao, M. Cerruti, W.L. Siqueira, F. Tamimi, Comparative adsorption profiles of basal lamina proteome and gingival cells onto dental and titanium surfaces, Acta Biomater. 73 (2018) 547–558. https://doi.org/10.1016/j.actbio.2018.04.017.

[118] H. Schweikl, K.-A. Hiller, U. Carl, R. Schweiger, A. Eidt, S. Ruhl, R. Müller, G. Schmalz, Salivary protein adsorption and Streptococccus gordonii adhesion to dental material surfaces, Dent. Mater. 29 (2013) 1080–1089. https://doi.org/10.1016/j.dental.2013.07.021.

[119] A. Miyake, S. Komasa, Y. Hashimoto, Y. Komasa, J. Okazaki, Adsorption of Saliva Related Protein on Denture Materials: An X-Ray Photoelectron Spectroscopy and Quartz Crystal Microbalance Study, Adv. Mater. Sci. Eng. 2016 (2016) 1–9. https://doi.org/10.1155/2016/5478326.

[120] C. Müller, A. Lüders, W. Hoth-Hannig, M. Hannig, C. Ziegler, Initial bioadhesion on dental materials as a function of contact time, pH, surface wettability, and isoelectric point, Langmuir. 26 (2010) 4136–4141. https://doi.org/10.1021/la903299y.

[121] D. Kohavi, L. Badihi, G. Rosen, D. Steinberg, M.N. Sela, An in vivo method for measuring the adsorption of plasma proteins to titanium in humans, Biofouling. 29 (2013) 1215–1224. https://doi.org/10.1080/08927014.2013.834332.

[122] M.N. Sela, L. Badihi, G. Rosen, D. Steinberg, D. Kohavi, Adsorption of human plasma proteins to modified titanium surfaces, Clin. Oral Implants Res. 18 (2007) 630–638. https://doi.org/10.1111/j.1600-0501.2007.01373.x.

[123] L. Parisi, A. Toffoli, M. Cutrera, M.G. Bianchi, S. Lumetti, O. Bussolati, G.M. Macaluso, Plasma Proteins at the Interface of Dental Implants Modulate Osteoblasts Focal Adhesions Expression and Cytoskeleton Organization, Nanomaterials. 9 (2019) 1407. https://doi.org/10.3390/nano9101407.

[124] Y. Huang, G. Zha, Q. Luo, J. Zhang, F. Zhang, X. Li, S. Zhao, W. Zhu, X.

Li, The construction of hierarchical structure on Ti substrate with superior osteogenic activity and intrinsic antibacterial capability, Sci. Rep. 4 (2015) 6172. https://doi.org/10.1038/srep06172.

[125] X. Lu, S. Xiong, Y. Chen, F. Zhao, Y. Hu, Y. Guo, B. Wu, P. Huang, B. Yang, Effects of statherin on the biological properties of titanium metals subjected to different surface modification, Colloids Surfaces B Biointerfaces. 188 (2020) 110783. https://doi.org/10.1016/j.colsurfb.2020.110783.

[126] M. Pegueroles, C. Aparicio, M. Bosio, E. Engel, F.J. Gil, J.A. Planell, G. Altankov, Spatial organization of osteoblast fibronectin matrix on titanium surfaces: Effects of roughness, chemical heterogeneity and surface energy, Acta Biomater. 6 (2010) 291–301. https://doi.org/10.1016/j.actbio.2009.07.030.

[127] F. Mussano, T. Genova, M. Laurenti, D. Gaglioti, G. Scarpellino, P. Rivolo, M.G. Faga, P.A. Fiorio, L. Munaron, P. Mandracci, S. Carossa, Beta1-integrin and TRPV4 are involved in osteoblast adhesion to different titanium surface topographies, Appl. Surf. Sci. 507 (2020) 145112. https://doi.org/10.1016/j.apsusc.2019.145112.

[128] A. Toffoli, L. Parisi, M.G. Bianchi, S. Lumetti, O. Bussolati, G.M. Macaluso, Thermal treatment to increase titanium wettability induces selective proteins adsorption from blood serum thus affecting osteoblasts adhesion, Mater. Sci. Eng. C. 107 (2020) 110250. https://doi.org/10.1016/j.msec.2019.110250.

[129] S. Tugulu, K. Löwe, D. Scharnweber, F. Schlottig, Preparation of superhydrophilic microrough titanium implant surfaces by alkali treatment, J. Mater. Sci. Mater. Med. 21 (2010) 2751–2763. https://doi.org/10.1007/s10856-010-4138-x.

[130] M. Martínez-Hernández, V.I. García-Pérez, A. Almaguer-Flores, Potential of salivary proteins to reduce oral bacterial colonization on titanium implant surfaces, Mater. Lett. 252 (2019) 120–122. https://doi.org/10.1016/j.matlet.2019.05.089.

[131] L. Richert, F. Variola, F. Rosei, J.D. Wuest, A. Nanci, Adsorption of proteins on nanoporous Ti surfaces, Surf. Sci. 604 (2010) 1445–1451. https://doi.org/10.1016/j.susc.2010.05.007.

[132] M.H. Lee, N. Oh, S.W. Lee, R. Leesungbok, S.E. Kim, Y.P. Yun, J.H. Kang, Factors influencing osteoblast maturation on microgrooved titanium substrata, Biomaterials. 31 (2010) 3804–3815. https://doi.org/10.1016/j.biomaterials.2010.01.117.

[133] Y. Sakamoto, Y. Ayukawa, A. Furuhashi, M. Kamo, J. Ikeda, I. Atsuta, T. Haraguchi, K. Koyano, Effect of hydrothermal treatment with distilled water on titanium alloy for epithelial cellular attachment, Materials (Basel). 12 (2019). https://doi.org/10.3390/ma12172748.

[134] Y. Yoneyama, T. Matsuno, Y. Hashimoto, T. Satoh, In vitro evaluation of H2O2 hydrothermal treatment of aged titanium surface to enhance biofunctional activity, Dent. Mater. J. 32 (2013) 115–121. https://doi.org/10.4012/dmj.2012-087.

[135] J. Yang, J. Wang, T. Yuan, X.D. Zhu, Z. Xiang, Y.J. Fan, X.D. Zhang, The enhanced effect of surface microstructured porous titanium on adhesion and osteoblastic differentiation of mesenchymal stem cells, J. Mater. Sci. Mater. Med. 24 (2013) 2235–2246. https://doi.org/10.1007/s10856-013-4976-4.

[136] S.R. Sousa, M.M. Brás, P. Moradas-Ferreira, M.A. Barbosa, Dynamics of Fibronectin Adsorption on TiO 2 Surfaces, Langmuir. 23 (2007) 7046–7054.

https://doi.org/10.1021/la062956e.
[137] S.R. Sousa, M. Lamghari, P. Sampaio, P. Moradas-Ferreira, M.A. Barbosa, Osteoblast adhesion and morphology on TiO 2 depends on the competitive preadsorption of albumin and fibronectin, J. Biomed. Mater. Res. Part A. 84A (2008) 281–290. https://doi.org/10.1002/jbm.a.31201.
[138] Y. Zeng, Y. Yang, L. Chen, D. Yin, H. Zhang, Y. Tashiro, S. Inui, T. Kusumoto, H. Nishizaki, T. Sekino, J. Okazaki, S. Komasa, Optimized Surface Characteristics and Enhanced in Vivo Osseointegration of Alkali-Treated Titanium with Nanonetwork Structures, Int. J. Mol. Sci. 20 (2019) 1127. https://doi.org/10.3390/ijms20051127.
[139] M. Xiao, M. Biao, Y. Chen, M. Xie, B. Yang, Regulating the osteogenic function of rhBMP 2 by different titanium surface properties, J. Biomed. Mater. Res. Part A. 104 (2016) 1882–1893. https://doi.org/10.1002/jbm.a.35719.
[140] M.N. Biao, Y.M. Chen, S.B. Xiong, B.Y. Wu, B.C. Yang, Synergistic effects of fibronectin and bone morphogenetic protein on the bioactivity of titanium metal, J. Biomed. Mater. Res. - Part A. 105 (2017) 2485–2498. https://doi.org/10.1002/jbm.a.36106.
[141] S. Jia, Y. Zhang, T. Ma, H. Chen, Y. Lin, Enhanced hydrophilicity and protein adsorption of titanium surface by sodium bicarbonate solution, J. Nanomater. 2015 (2015). https://doi.org/10.1155/2015/536801.
[142] Y. Chen, B. Feng, Y. Zhu, J. Weng, J. Wang, X. Lu, Preparation and characterization of a novel porous titanium scaffold with 3D hierarchical porous structures, J. Mater. Sci. Mater. Med. 22 (2011) 839–844. https://doi.org/10.1007/s10856-011-4280-0.
[143] Y. Yao, S. Liu, M. V. Swain, X. Zhang, K. Zhao, Y. Jian, Effects of acid-alkali treatment on bioactivity and osteoinduction of porous titanium: An in vitro study, Mater. Sci. Eng. C. 94 (2019) 200–210. https://doi.org/10.1016/j.msec.2018.08.056.
[144] P. Yu, X. Zhu, X. Wang, S. Wang, W. Li, G. Tan, Y. Zhang, C. Ning, Periodic Nanoneedle and Buffer Zones Constructed on a Titanium Surface Promote Osteogenic Differentiation and Bone Calcification In Vivo, Adv. Healthc. Mater. 5 (2016) 364–372. https://doi.org/10.1002/adhm.201500461.
[145] V. V.D. Rani, K. Manzoor, D. Menon, N. Selvamurugan, S. V. Nair, The design of novel nanostructures on titanium by solution chemistry for an improved osteoblast response, Nanotechnology. 20 (2009). https://doi.org/10.1088/0957-4484/20/19/195101.
[146] V.K. Manivasagam, K.C. Popat, In Vitro Investigation of Hemocompatibility of Hydrothermally Treated Titanium and Titanium Alloy Surfaces, ACS Omega. 5 (2020) 8108–8120. https://doi.org/10.1021/acsomega.0c00281.
[147] L. Qian, P. Yu, J. Zeng, Z. Shi, Q. Wang, G. Tan, C. Ning, Large-scale functionalization of biomedical porous titanium scaffolds surface with TiO2 nanostructures, Sci. China Mater. 61 (2018) 557–564. https://doi.org/10.1007/s40843-017-9050-0.
[148] J. Shi, B. Feng, X. Lu, J. Weng, Adsorption of bovine serum albumin onto titanium dioxide nanotube arrays, Int. J. Mater. Res. 103 (2012) 889–896. https://doi.org/10.3139/146.110696.
[149] D.P. Zhao, J.C. Tang, H.M. Nie, Y. Zhang, Y.K. Chen, X. Zhang, H.X. Li, M. Yan, Macro-micron-nano-featured surface topography of Ti-6Al-4V

alloy for biomedical applications, Rare Met. 37 (2018) 1055–1063. https://doi.org/10.1007/s12598-018-1150-7.

[150] W. Yang, X. Xi, X. Shen, P. Liu, Y. Hu, K. Cai, Titania nanotubes dimensions-dependent protein adsorption and its effect on the growth of osteoblasts, J. Biomed. Mater. Res. Part A. 102 (2014) 3598–3608. https://doi.org/10.1002/jbm.a.35021.

[151] E. Jia, X. Zhao, Y. Lin, Z. Su, Protein adsorption on titanium substrates and its effects on platelet adhesion, Appl. Surf. Sci. 529 (2020) 146986. https://doi.org/10.1016/j.apsusc.2020.146986.

[152] W. Yang, X. Xi, Q. Ran, P. Liu, Y. Hu, K. Cai, Influence of the titania nanotubes dimensions on adsorption of collagen: An experimental and computational study, Mater. Sci. Eng. C. 34 (2014) 410–416. https://doi.org/10.1016/j.msec.2013.09.042.

[153] M. Kulkarni, A. Mazare, J. Park, E. Gongadze, M.S. Killian, S. Kralj, K. von der Mark, A. Iglič, P. Schmuki, Protein interactions with layers of TiO2 nanotube and nanopore arrays: Morphology and surface charge influence, Acta Biomater. 45 (2016) 357–366. https://doi.org/10.1016/j.actbio.2016.08.050.

[154] R.M. Sabino, K. Kauk, S. Movafaghi, A. Kota, K.C. Popat, Interaction of blood plasma proteins with superhemophobic titania nanotube surfaces, Nanomedicine Nanotechnology, Biol. Med. 21 (2019) 102046. https://doi.org/10.1016/j.nano.2019.102046.

[155] S. Wu, D. Zhang, J. Bai, H. Zheng, J. Deng, Z. Gou, C. Gao, Adsorption of serum proteins on titania nanotubes and its role on regulating adhesion and migration of mesenchymal stem cells, J. Biomed. Mater. Res. - Part A. 108 (2020) 2305–2318. https://doi.org/10.1002/jbm.a.36987.

[156] R. Lu, C. Wang, X. Wang, Y. Wang, N. Wang, J. Chou, T. Li, Z. Zhang, Y. Ling, S. Chen, Effects of hydrogenated TiO2 nanotube arrays on protein adsorption and compatibility with osteoblast-like cells, Int. J. Nanomedicine. 13 (2018) 2037–2049. https://doi.org/10.2147/IJN.S155532.

[157] F. Teng, J. Li, Y. Wu, H. Chen, Q. Zhang, H. Wang, G. Ou, Fabrication and bioactivity evaluation of porous anodised Tio2 films in vitro, Biosci. Trends. 8 (2014) 260–265. https://doi.org/10.5582/bst.2014.01035.

[158] W.E. Yang, H.H. Huang, Multiform TiO2 nano-network enhances biological response to titanium surface for dental implant applications, Appl. Surf. Sci. 471 (2019) 1041–1052. https://doi.org/10.1016/j.apsusc.2018.11.244.

[159] C. Ning, S. Wang, Y. Zhu, M. Zhong, X. Lin, Y. Zhang, G. Tan, M. Li, Z. Yin, P. Yu, X. Wang, Y. Li, T. He, W. Chen, Y. Wang, C. Mao, Ti nanorod arrays with a medium density significantly promote osteogenesis and osteointegration, Sci. Rep. 6 (2016) 19047. https://doi.org/10.1038/srep19047.

[160] Ö. Bayrak, H. Ghahramanzadeh Asl, A. Ak, Protein adsorption, cell viability and corrosion properties of Ti6Al4V alloy treated by plasma oxidation and anodic oxidation, Int. J. Miner. Metall. Mater. 27 (2020) 1269–1280. https://doi.org/10.1007/s12613-020-2020-5.

[161] D.J. Lin, L.J. Fuh, W.C. Chen, Nano-morphology, crystallinity and surface potential of anatase on micro-arc oxidized titanium affect its protein adsorption, cell proliferation and cell differentiation, Mater. Sci. Eng. C. 107 (2020) 110204. https://doi.org/10.1016/j.msec.2019.110204.

[162] S.A. Fadlallah, M.A. Amin, G.S. Alosaimi, Construction of Nanophase Novel Coatings-Based Titanium for the Enhancement of Protein Adsorption,

Acta Metall. Sin. (English Lett. 29 (2016) 243–252. https://doi.org/10.1007/s40195-016-0382-5.

[163] D. Kuczyńska, P. Kwaśniak, M. Pisarek, P. Borowicz, H. Garbacz, Influence of surface pattern on the biological properties of Ti grade 2, Mater. Charact. 135 (2018) 337–347. https://doi.org/10.1016/j.matchar.2017.09.024.

[164] V. Dumas, A. Guignandon, L. Vico, C. Mauclair, X. Zapata, M.T. Linossier, W. Bouleftour, J. Granier, S. Peyroche, J.C. Dumas, H. Zahouani, A. Rattner, Femtosecond laser nano/micro patterning of titanium influences mesenchymal stem cell adhesion and commitment, Biomed. Mater. 10 (2015). https://doi.org/10.1088/1748-6041/10/5/055002.

[165] S. Mukherjee, S. Dhara, P. Saha, Enhancing the biocompatibility of Ti6Al4V implants by laser surface microtexturing: an in vitro study, Int. J. Adv. Manuf. Technol. 76 (2015) 5–15. https://doi.org/10.1007/s00170-013-5277-2.

[166] L. Hao, J. Lawrence, Wettability modification and the subsequent manipulation of protein adsorption on a Ti6Al4V alloy by means of CO2 laser surface treatment, J. Mater. Sci. Mater. Med. 18 (2007) 807–817. https://doi.org/10.1007/s10856-006-0002-4.

[167] V. Parmar, A. Kumar, M. Mani Sankar, S. Datta, G. Vijaya Prakash, S. Mohanty, D. Kalyanasundaram, Oxidation facilitated antimicrobial ability of laser micro-textured titanium alloy against gram-positive Staphylococcus aureus for biomedical applications, J. Laser Appl. 30 (2018) 032001. https://doi.org/10.2351/1.5039860.

[168] D. Kuczyńska, P. Kwaśniak, J. Marczak, J. Bonarski, J. Smolik, H. Garbacz, Laser surface treatment and the resultant hierarchical topography of Ti grade 2 for biomedical application, Appl. Surf. Sci. 390 (2016) 560–569. https://doi.org/10.1016/j.apsusc.2016.08.105.

[169] B. Clarke, P. Kingshott, X. Hou, Y. Rochev, A. Gorelov, W. Carroll, Effect of nitinol wire surface properties on albumin adsorption, Acta Biomater. 3 (2007) 103–111. https://doi.org/10.1016/j.actbio.2006.07.006.

[170] A. Michiardi, C. Aparicio, B.D. Ratner, J.A. Planell, J. Gil, The influence of surface energy on competitive protein adsorption on oxidized NiTi surfaces, Biomaterials. 28 (2007) 586–594. https://doi.org/10.1016/j.biomaterials.2006.09.040.

[171] Z. Bai, M.J. Filiaggi, R.J. Sanderson, L.B. Lohstreter, M.A. McArthur, J.R. Dahn, Surface characteristics and protein adsorption on combinatorial binary Ti-M (Cr, Al, Ni) and Al-M (Ta, Zr) library films, J. Biomed. Mater. Res. - Part A. 92 (2010) 521–532. https://doi.org/10.1002/jbm.a.32398.

[172] Z. Bai, M.J. Filiaggi, J.R. Dahn, Fibrinogen adsorption onto 316L stainless steel, Nitinol and titanium, Surf. Sci. 603 (2009) 839–846. https://doi.org/10.1016/j.susc.2009.01.040.

[173] L. Chen, K. Wei, Y. Qu, T. Li, B. Chang, B. Liao, W. Xue, Characterization of plasma electrolytic oxidation film on biomedical high niobium-containing β-titanium alloy, Surf. Coatings Technol. 352 (2018) 295–301. https://doi.org/10.1016/j.surfcoat.2018.08.025.

[174] J.M. Cordeiro, T. Beline, A.L.R. Ribeiro, E.C. Rangel, N.C. da Cruz, R. Landers, L.P. Faverani, L.G. Vaz, L.M.G. Fais, F.B. Vicente, C.R. Grandini, M.T. Mathew, C. Sukotjo, V.A.R. Barão, Development of binary and ternary titanium alloys for dental implants, Dent. Mater. 33 (2017) 1244–1257. https://doi.org/10.1016/j.dental.2017.07.013.

[175] P. Majumdar, S.B. Singh, S. Dhara, M. Chakraborty, Influence of boron

addition to Ti-13Zr-13Nb alloy on MG63 osteoblast cell viability and protein adsorption, Mater. Sci. Eng. C. 46 (2015) 62–68. https://doi.org/10.1016/j.msec.2014.10.012.

[176] A. Blanquer, J. Musilkova, L. Barrios, E. Ibáñez, M. Vandrovcova, E. Pellicer, J. Sort, L. Bacakova, C. Nogués, Cytocompatibility assessment of Ti-Zr-Pd-Si-(Nb) alloys with low Young's modulus, increased hardness, and enhanced osteoblast differentiation for biomedical applications, J. Biomed. Mater. Res. - Part B Appl. Biomater. 106 (2018) 834–842. https://doi.org/10.1002/jbm.b.33892.

[177] C. Herranz-Diez, F. Gil, J. Guillem-Marti, J. Manero, Mechanical and physicochemical characterization along with biological interactions of a new Ti25Nb21Hf alloy for bone tissue engineering, J. Biomater. Appl. 30 (2015) 171–181. https://doi.org/10.1177/0885328215577524.

[178] A. Hoppe, N.S. Güldal, A.R. Boccaccini, A review of the biological response to ionic dissolution products from bioactive glasses and glass-ceramics, Biomaterials. 32 (2011) 2757–2774. https://doi.org/10.1016/j.biomaterials.2011.01.004.

[179] N. Ren, J. Li, J. Qiu, Y. Sang, H. Jiang, R.I. Boughton, L. Huang, W. Huang, H. Liu, Nanostructured titanate with different metal ions on the surface of metallic titanium: A facile approach for regulation of rBMSCs fate on titanium implants, Small. 10 (2014) 3169–3180. https://doi.org/10.1002/smll.201303391.

[180] T. Haraguchi, Y. Ayukawa, Y. Shibata, T. Takeshita, I. Atsuta, Y. Ogino, N. Yasunami, Y. Yamashita, K. Koyano, Effect of Calcium Chloride Hydrothermal Treatment of Titanium on Protein, Cellular, and Bacterial Adhesion Properties, J. Clin. Med. 9 (2020) 2627. https://doi.org/10.3390/jcm9082627.

[181] X. Shi, M. Nakagawa, G. Kawachi, L. Xu, K. Ishikawa, Surface modification of titanium by hydrothermal treatment in Mg-containing solution and early osteoblast responses, J. Mater. Sci. Mater. Med. 23 (2012) 1281–1290. https://doi.org/10.1007/s10856-012-4596-4.

[182] N. Jiang, Z. Guo, D. Sun, Y. Li, Y. Yang, C. Chen, L. Zhang, S. Zhu, Promoting osseointegration of Ti implants through micro/nanoscaled hierarchical Ti phosphate/Ti oxide hybrid coating, ACS Nano. 12 (2018) 7883–7891. https://doi.org/10.1021/acsnano.8b02227.

[183] X. Lingli, S. Xingling, O. Chun, L. Wen, In vitro Apatite Formation, Protein Adsorption and Initial Osteoblast Responses on Titanium Surface Enriched with Magnesium, Rare Met. Mater. Eng. 46 (2017) 1512–1517. https://doi.org/10.1016/S1875-5372(17)30156-X.

[184] X. Shi, K. Tsuru, L. Xu, G. Kawachi, K. Ishikawa, Effects of solution pH on the structure and biocompatibility of Mg-containing TiO 2 layer fabricated on titanium by hydrothermal treatment, Appl. Surf. Sci. 270 (2013) 445–451. https://doi.org/10.1016/j.apsusc.2013.01.046.

[185] L. Wang, Q. Luo, X. Zhang, J. Qiu, S. Qian, X. Liu, Co-implantation of magnesium and zinc ions into titanium regulates the behaviors of human gingival fibroblasts, Bioact. Mater. 6 (2021) 64–74. https://doi.org/10.1016/j.bioactmat.2020.07.012.

[186] Z. Yuan, P. Liu, Y. Liang, B. Tao, Y. He, Y. Hao, W. Yang, Y. Hu, K. Cai, Investigation of osteogenic responses of Fe-incorporated micro/nano-hierarchical structures on titanium surfaces, J. Mater. Chem. B. 6 (2018) 1359–1372. https://doi.org/10.1039/C7TB03071A.

[187] E. Anbazhagan, A. Rajendran, D. Natarajan, M.S. Kiran, D.K. Pattanayak, Divalent ion encapsulated nano titania on Ti metal as a bioactive surface with enhanced protein adsorption, Colloids Surfaces B Biointerfaces. 143 (2016) 213–223. https://doi.org/10.1016/j.colsurfb.2016.03.009.

[188] P. Soares, M.F. Dias-Netipanyj, S. Elifio-Esposito, V. Leszczak, K. Popat, Effects of calcium and phosphorus incorporation on the properties and bioactivity of TiO 2 nanotubes, J. Biomater. Appl. 33 (2018) 410–421. https://doi.org/10.1177/0885328218797549.

[189] S. Mei, L. Zhao, W. Wang, Q. Ma, Y. Zhang, Biomimetic titanium alloy with sparsely distributed nanotubes could enhance osteoblast functions, Adv. Eng. Mater. 14 (2012) 166–174. https://doi.org/10.1002/adem.201180056.

[190] K.Y. Cai, Surface modification of titanium films with sodium ion implantation: surface properties and protein adsorption, Acta Metall. Sin. (English Lett. 20 (2007) 148–156. https://doi.org/10.1016/S1006-7191(07)60019-2.

[191] R.D.K. Misra, C. Nune, T.C. Pesacreta, M.C. Somani, L.P. Karjalainen, Interplay between grain structure and protein adsorption on functional response of osteoblasts: Ultrafine-grained versus coarse-grained substrates, J. Biomed. Mater. Res. - Part A. 101 A (2013) 1–12. https://doi.org/10.1002/jbm.a.34105.

[192] F. Yin, R. Xu, S. Hu, K. Zhao, S. Yang, S. Kuang, Q. Li, Q. Han, Enhanced Mechanical and Biological Performance of an Extremely Fine Nanograined 316L Stainless Steel Cell-Substrate Interface Fabricated by Ultrasonic Shot Peening, ACS Biomater. Sci. Eng. 4 (2018) 1609–1621. https://doi.org/10.1021/acsbiomaterials.8b00173.

[193] S. Bahl, B.T. Aleti, S. Suwas, K. Chatterjee, Surface nanostructuring of titanium imparts multifunctional properties for orthopedic and cardiovascular applications, Mater. Des. 144 (2018) 169–181. https://doi.org/10.1016/j.matdes.2018.02.022.

[194] D. Kubacka, A. Yamamoto, P. Wieciński, H. Garbacz, Biological behavior of titanium processed by severe plastic deformation, Appl. Surf. Sci. 472 (2019) 54–63. https://doi.org/10.1016/j.apsusc.2018.04.120.

[195] W.T. Huo, L.Z. Zhao, W. Zhang, J.W. Lu, Y.Q. Zhao, Y.S. Zhang, In vitro corrosion behavior and biocompatibility of nanostructured Ti6Al4V, Mater. Sci. Eng. C. 92 (2018) 268–279. https://doi.org/10.1016/j.msec.2018.06.061.

[196] R. Huang, L. Zhang, L. Huang, J. Zhu, Enhanced in-vitro osteoblastic functions on β-type titanium alloy using surface mechanical attrition treatment, Mater. Sci. Eng. C. 97 (2019) 688–697. https://doi.org/10.1016/j.msec.2018.12.082.

[197] D.N. Awang Shri, K. Tsuchiya, A. Yamamoto, Effect of high-pressure torsion deformation on surface properties and biocompatibility of Ti-50.9 mol. %Ni alloys, Biointerphases. 9 (2014) 029007. https://doi.org/10.1116/1.4867402.

[198] M. Talha, Y. Ma, P. Kumar, Y. Lin, A. Singh, Role of protein adsorption in the bio corrosion of metallic implants – A review, Colloids Surfaces B Biointerfaces. 176 (2019) 494–506. https://doi.org/10.1016/j.colsurfb.2019.01.038.

[199] M.F. Dias-Netipanyj, K. Cowden, L. Sopchenski, S.C. Cogo, S. Elifio-Esposito, K.C. Popat, P. Soares, Effect of crystalline phases of titania nanotube arrays on adipose derived stem cell adhesion and proliferation, Mater. Sci. Eng. C. 103 (2019) 109850.

https://doi.org/10.1016/j.msec.2019.109850.
[200] Z. Gong, Y. Hu, F. Gao, L. Quan, T. Liu, T. Gong, C. Pan, Effects of diameters and crystals of titanium dioxide nanotube arrays on blood compatibility and endothelial cell behaviors, Colloids Surfaces B Biointerfaces. 184 (2019) 110521. https://doi.org/10.1016/j.colsurfb.2019.110521.
[201] Y. Li, Y. Dong, Y. Zhang, Y. Yang, R. Hu, P. Mu, X. Liu, C. Lin, Q. Huang, Synergistic effect of crystalline phase on protein adsorption and cell behaviors on TiO2 nanotubes, Appl. Nanosci. 10 (2020) 3245–3257. https://doi.org/10.1007/s13204-019-01078-2.
[202] Y. Hong, M. Yu, J. Lin, K. Cheng, W. Weng, H. Wang, Surface hydroxyl groups direct cellular response on amorphous and anatase TiO2 nanodots, Colloids Surfaces B Biointerfaces. 123 (2014) 68–74. https://doi.org/10.1016/j.colsurfb.2014.08.030.
[203] G. Raffaini, F. Ganazzoli, Molecular modelling of protein adsorption on the surface of titanium dioxide polymorphs, Philos. Trans. R. Soc. A Math. Phys. Eng. Sci. 370 (2012) 1444–1462. https://doi.org/10.1098/rsta.2011.0266.
[204] Y. Liu, K. Cheng, W. Weng, M. Yu, J. Lin, H. Wang, P. Du, G. Han, Influence of rod-surface structure on biological interactions between TiO2 nanorod films and proteins/cells, Thin Solid Films. 544 (2013) 285–290. https://doi.org/10.1016/j.tsf.2013.03.102.
[205] C. Yang, C. Peng, D. Zhao, C. Liao, J. Zhou, X. Lu, Molecular simulations of myoglobin adsorbed on rutile (110) and (001) surfaces, Fluid Phase Equilib. 362 (2014) 349–354. https://doi.org/10.1016/j.fluid.2013.10.052.
[206] T.F. Keller, J. Reichert, T.P. Thanh, R. Adjiski, L. Spiess, L. Berzina-Cimdina, K.D. Jandt, J. Bossert, Facets of protein assembly on nanostructured titanium oxide surfaces, Acta Biomater. 9 (2013) 5810–5820. https://doi.org/10.1016/j.actbio.2012.10.045.
[207] Y. Sugita, J. Saruta, T. Taniyama, H. Kitajima, M. Hirota, T. Ikeda, T. Ogawa, UV-pre-treated and protein-adsorbed titanium implants exhibit enhanced osteoconductivity, Int. J. Mol. Sci. 21 (2020) 1–17. https://doi.org/10.3390/ijms21124194.
[208] W.S. Jeong, J.S. Kwon, E.H. Choi, K.M. Kim, The Effects of Non-Thermal Atmospheric Pressure Plasma treated Titanium Surface on Behaviors of Oral Soft Tissue Cells, Sci. Rep. 8 (2018) 1–13. https://doi.org/10.1038/s41598-018-34402-x.
[209] M. Kamo, M. Kyomoto, F. Miyaji, Time course of surface characteristics of alkali- and heat-treated titanium dental implants during vacuum storage, J. Biomed. Mater. Res. Part B Appl. Biomater. 105 (2016) 1453–1460. https://doi.org/10.1002/jbm.b.33686.
[210] H. Aita, N. Hori, M. Takeuchi, T. Suzuki, M. Yamada, M. Anpo, T. Ogawa, The effect of ultraviolet functionalization of titanium on integration with bone, Biomaterials. 30 (2009) 1015–1025. https://doi.org/10.1016/j.biomaterials.2008.11.004.
[211] N. Hori, F. Iwasa, N. Tsukimura, Y. Sugita, T. Ueno, N. Kojima, T. Ogawa, Effects of UV photofunctionalization on the nanotopography enhanced initial bioactivity of titanium, Acta Biomater. 7 (2011) 3679–3691. https://doi.org/10.1016/j.actbio.2011.06.022.
[212] N. Hori, T. Ueno, H. Minamikawa, F. Iwasa, F. Yoshino, K. Kimoto, M.C. Il Lee, T. Ogawa, Electrostatic control of protein adsorption on UV-photofunctionalized titanium, Acta Biomater. 6 (2010) 4175–4180.

https://doi.org/10.1016/j.actbio.2010.05.006.
[213] M. Yu, J. Gong, Y. Zhou, L. Dong, Y. Lin, L. Ma, W. Weng, K. Cheng, H. Wang, Surface hydroxyl groups regulate the osteogenic differentiation of mesenchymal stem cells on titanium and tantalum metals, J. Mater. Chem. B. 5 (2017) 3955–3963. https://doi.org/10.1039/c7tb00111h.
[214] J. Wu, L. Zhou, X. Ding, Y. Gao, X. Liu, Biological Effect of Ultraviolet Photocatalysis on Nanoscale Titanium with a Focus on Physicochemical Mechanism, Langmuir. 31 (2015) 10037–10046. https://doi.org/10.1021/acs.langmuir.5b01850.
[215] H. Zhang, S. Komasa, C. Mashimo, T. Sekino, J. Okazaki, Effect of ultraviolet treatment on bacterial attachment and osteogenic activity to alkali-treated titanium with nanonetwork structures, Int. J. Nanomedicine. 12 (2017) 4633–4646. https://doi.org/10.2147/IJN.S136273.
[216] C. Dini, B.E. Nagay, J.M. Cordeiro, N.C. da Cruz, E.C. Rangel, A.P. Ricomini-Filho, E.D. de Avila, V.A.R. Barão, UV-photofunctionalization of a biomimetic coating for dental implants application, Mater. Sci. Eng. C. 110 (2020) 110657. https://doi.org/10.1016/j.msec.2020.110657.
[217] I. Han, B. Vagaska, H.J. Seo, J.K. Kang, B.J. Kwon, M.H. Lee, J.C. Park, Promoted cell and material interaction on atmospheric pressure plasma treated titanium, Appl. Surf. Sci. 258 (2012) 4718–4723. https://doi.org/10.1016/j.apsusc.2012.01.065.
[218] B.E. Rapuano, D.E. MacDonald, Surface oxide net charge of a titanium alloy: Modulation of fibronectin-activated attachment and spreading of osteogenic cells, Colloids Surfaces B Biointerfaces. 82 (2011) 95–103. https://doi.org/10.1016/j.colsurfb.2010.08.023.
[219] H. Yamamoto, Y. Shibata, T. Miyazaki, Anode Glow Discharge Plasma Treatment of Titanium Plates Facilitates Adsorption of Extracellular Matrix Proteins, J. Dent. Res. 84 (2005) 668–671.
[220] L. Canullo, T. Genova, H.-L. Wang, S. Carossa, F. Mussano, Plasma of Argon Increases Cell Attachment and Bacterial Decontamination on Different Implant Surfaces, Int. J. Oral Maxillofac. Implants. 32 (2017) 1315–1323. https://doi.org/10.11607/jomi.5777.
[221] E.-J. Lee, J.-S. Kwon, J.-Y. Om, S.-K. Moon, S.-H. Uhm, E.H. Choi, K.-N. Kim, The enhanced integrin-mediated cell attachment and osteogenic gene expression on atmospheric pressure plasma jet treated micro-structured titanium surfaces, Curr. Appl. Phys. 14 (2014) S167–S171. https://doi.org/10.1016/j.cap.2013.12.033.
[222] S.-H. Choi, W.-S. Jeong, J.-Y. Cha, J.-H. Lee, H.-S. Yu, E.-H. Choi, K.-M. Kim, C.-J. Hwang, Time-dependent effects of ultraviolet and nonthermal atmospheric pressure plasma on the biological activity of titanium, Sci. Rep. 6 (2016) 33421. https://doi.org/10.1038/srep33421.
[223] I. Han, B. Vagaska, B. Joo Park, M.H. Lee, S. Jin Lee, J.C. Park, Selective fibronectin adsorption against albumin and enhanced stem cell attachment on helium atmospheric pressure glow discharge treated titanium, J. Appl. Phys. 109 (2011). https://doi.org/10.1063/1.3599885.
[224] W. Zhu, G. Teel, C.M. O'Brien, T. Zhuang, M. Keidar, L.G. Zhang, Enhanced human bone marrow mesenchymal stem cell functions on cathodic arc plasma-treated titanium, Int. J. Nanomedicine. 10 (2015) 7385–7396. https://doi.org/10.2147/IJN.S92733.
[225] O. Santos, I.E. Svendsen, L. Lindh, T. Arnebrant, Adsorption of HSA, IgG and laminin-1 on model titania surfaces – effects of glow discharge treatment

on competitively adsorbed film composition, Biofouling. 27 (2011) 1003–1015. https://doi.org/10.1080/08927014.2011.622440.

[226] S.-H. Choi, W.-S. Jeong, J.-Y. Cha, J.-H. Lee, K.-J. Lee, H.-S. Yu, E.-H. Choi, K.-M. Kim, C.-J. Hwang, Overcoming the biological aging of titanium using a wet storage method after ultraviolet treatment, Sci. Rep. 7 (2017) 3833. https://doi.org/10.1038/s41598-017-04192-9.

[227] X. Wu, P. Hao, F. He, Z. Yao, X. Zhang, Molecular dynamics simulations of BSA absorptions on pure and formate-contaminated rutile (1 1 0) surface, Appl. Surf. Sci. 533 (2020) 147574. https://doi.org/10.1016/j.apsusc.2020.147574.

[228] N. Hori, W. Att, T. Ueno, N. Sato, M. Yamada, L. Saruwatari, T. Suzuki, T. Ogawa, Age-dependent degradation of the protein adsorption capacity of titanium, J. Dent. Res. 88 (2009) 663–667. https://doi.org/10.1177/0022034509339567.

[229] W. Att, N. Hori, M. Takeuchi, J. Ouyang, Y. Yang, M. Anpo, T. Ogawa, Time-dependent degradation of titanium osteoconductivity: An implication of biological aging of implant materials, Biomaterials. 30 (2009) 5352–5363. https://doi.org/10.1016/j.biomaterials.2009.06.040.

[230] T. MIKI, T. MATSUNO, Y. HASHIMOTO, A. MIYAKE, T. SATOMI, In Vitro and In Vivo Evaluation of Titanium Surface Modification for Biological Aging by Electrolytic Reducing Ionic Water, Appl. Sci. 9 (2019) 713. https://doi.org/10.3390/app9040713.

[231] H. Lu, L. Zhou, L. Wan, S. Li, M. Rong, Z. Guo, Effects of storage methods on time-related changes of titanium surface properties and cellular response, Biomed. Mater. 7 (2012). https://doi.org/10.1088/1748-6041/7/5/055002.

[232] S.-H. Choi, J.-H. Ryu, J.-S. Kwon, J.-E. Kim, J.-Y. Cha, K.-J. Lee, H.-S. Yu, E.-H. Choi, K.-M. Kim, C.-J. Hwang, Effect of wet storage on the bioactivity of ultraviolet light- and non-thermal atmospheric pressure plasma-treated titanium and zirconia implant surfaces, Mater. Sci. Eng. C. 105 (2019) 110049. https://doi.org/10.1016/j.msec.2019.110049.

[233] F. Kratz, C. Müller, N. Körber, N. Umanskaya, M. Hannig, C. Ziegler, Characterization of protein films on dental materials: Bicinchoninic acid assay (BCA) studies on loosely and firmly adsorbed protein layers, Phys. Status Solidi Appl. Mater. Sci. 210 (2013) 964–967. https://doi.org/10.1002/pssa.201200642.

[234] J.L. Wehmeyer, R. Synowicki, R. Bizios, C.D. García, Dynamic adsorption of albumin on nanostructured TiO2 thin films, Mater. Sci. Eng. C. 30 (2010) 277–282. https://doi.org/10.1016/j.msec.2009.11.002.

[235] K. Imamura, M. Oshita, M. Iwai, T. Kuroda, I. Watanabe, T. Sakiyama, K. Nakanishi, Influences of properties of protein and adsorption surface on removal kinetics of protein adsorbed on metal surface by H2O2-electrolysis treatment, J. Colloid Interface Sci. 345 (2010) 474–480. https://doi.org/10.1016/j.jcis.2010.01.083.

[236] Y. Forov, M. Paulus, S. Dogan, P. Salmen, C. Weis, T. Gahlmann, A. Behrendt, C. Albers, M. Elbers, W. Schnettger, S. Egger, E. Zwar, H. Rehage, I. Kiesel, T. Riedl, M. Tolan, Adsorption Behavior of Lysozyme at Titanium Oxide-Water Interfaces, Langmuir. 34 (2018) 5403–5408. https://doi.org/10.1021/acs.langmuir.8b00280.

[237] Z. Xu, V.H. Grassian, Bovine serum albumin adsorption on TiO2 nanoparticle surfaces: Effects of ph and coadsorption of phosphate on protein-surface interactions and protein structure, J. Phys. Chem. C. 121

(2017) 21763–21771. https://doi.org/10.1021/acs.jpcc.7b07525.

[238] L. Burgos-Asperilla, M.C. García-Alonso, M.L. Escudero, C. Alonso, Study of the interaction of inorganic and organic compounds of cell culture medium with a Ti surface, Acta Biomater. 6 (2010) 652–661. https://doi.org/10.1016/j.actbio.2009.06.019.

[239] A.M. Sultan, Z.E. Hughes, T.R. Walsh, Effect of calcium ions on peptide adsorption at the aqueous rutile titania (110) interface, Biointerphases. 13 (2018) 06D403. https://doi.org/10.1116/1.5046531.

[240] M. HASHIMOTO, S. KITAOKA, M. FURUYA, H. KANETAKA, K. HOSHIKAYA, H. YAMASHITA, M. ABE, Enhancement of cell differentiation on a surface potential-controlled nitrogen-doped TiO_2 surface, J. Ceram. Soc. Japan. 127 (2019) 636–641. https://doi.org/10.2109/jcersj2.19114.

[241] M. Leeman, J. Choi, S. Hansson, M.U. Storm, L. Nilsson, Proteins and antibodies in serum, plasma, and whole blood—size characterization using asymmetrical flow field-flow fractionation (AF4), Anal. Bioanal. Chem. 410 (2018) 4867–4873. https://doi.org/10.1007/s00216-018-1127-2.

[242] M. Boix, S. Eslava, G. Costa Machado, E. Gosselin, N. Ni, E. Saiz, J. De Coninck, ATR-FTIR measurements of albumin and fibrinogen adsorption: Inert versus calcium phosphate ceramics, J. Biomed. Mater. Res. - Part A. 103 (2015) 3493–3502. https://doi.org/10.1002/jbm.a.35496.

[243] J.D. Hoppe, P.C. Scriba, H. Klüter, 5 Human Albumin, in: Transfus. Med. Hemother., Karger Publishers, 2009: pp. 399–407. http://www.ncbi.nlm.nih.gov/pubmed/21245971%0Ahttp://www.ncbi.nlm.nih.gov/pubmed/21245971 (accessed January 3, 2021).

[244] A.G. Hemmersam, M. Foss, J. Chevallier, F. Besenbacher, Adsorption of fibrinogen on tantalum oxide, titanium oxide and gold studied by the QCM-D technique, Colloids Surfaces B Biointerfaces. 43 (2005) 208–215. https://doi.org/10.1016/j.colsurfb.2005.04.007.

[245] V. Vadillo-Rodríguez, M.A. Pacha-Olivenza, M.L. Gónzalez-Martín, J.M. Bruque, A.M. Gallardo-Moreno, Adsorption behavior of human plasma fibronectin on hydrophobic and hydrophilic Ti6Al4V substrata and its influence on bacterial adhesion and detachment, J. Biomed. Mater. Res. Part A. 101A (2013) 1397–1404. https://doi.org/10.1002/jbm.a.34447.

[246] L. Canullo, T. Genova, M. Tallarico, G. Gautier, F. Mussano, D. Botticelli, Plasma of Argon Affects the Earliest Biological Response of Different Implant Surfaces, J. Dent. Res. 95 (2016) 566–573. https://doi.org/10.1177/0022034516629119.

[247] C.G. Dodo, P.M. Senna, W. Custodio, A.F. Paes Leme, A.A. Del Bel Cury, Proteome analysis of the plasma protein layer adsorbed to a rough titanium surface, Biofouling. 29 (2013) 549–557. https://doi.org/10.1080/08927014.2013.787416.

[248] C. Rösch, F. Kratz, T. Hering, S. Trautmann, N. Umanskaya, N. Tippkötter, C. Müller-Renno, R. Ulber, M. Hannig, C. Ziegler, Albumin-lysozyme interactions: Cooperative adsorption on titanium and enzymatic activity, Colloids Surfaces B Biointerfaces. 149 (2017) 115–121. https://doi.org/10.1016/j.colsurfb.2016.09.048.

[249] J. Wald, C. Müller, M. Wahl, W. Hoth-Hannig, M. Hannig, M. Kopnarski, C. Ziegler, ToF-SIMS investigations of adsorbed proteins on dental titanium, Phys. Status Solidi Appl. Mater. Sci. 207 (2010) 831–836. https://doi.org/10.1002/pssa.200983308.

[250] L. Parisi, B. Ghezzi, M.G. Bianchi, A. Toffoli, F. Rossi, O. Bussolati, G.M. Macaluso, Titanium dental implants hydrophilicity promotes preferential serum fibronectin over albumin competitive adsorption modulating early cell response, Mater. Sci. Eng. C. 117 (2020) 111307. https://doi.org/10.1016/j.msec.2020.111307.

[251] H.P. Felgueiras, N.S. Murthy, S.D. Sommerfeld, M.M. Brás, V. Migonney, J. Kohn, Competitive Adsorption of Plasma Proteins Using a Quartz Crystal Microbalance, ACS Appl. Mater. Interfaces. 8 (2016) 13207–13217. https://doi.org/10.1021/acsami.5b12600.

[252] H. Felgueiras, V. Migonney, S. Sommerfeld, N.. Murthy, J. Kohn, Competitive Adsorption of Albumin, Fibronectin and Collagen Type I on Different Biomaterial Surfaces: A QCM-D Study, in: L.M. Roa Romero (Ed.), IFMBE Proc., Springer International Publishing, Cham, 2014: pp. 563–566. https://doi.org/10.1007/978-3-319-00846-2.

[253] M. Pegueroles, C. Tonda-Turo, J.A. Planell, F.-J. Gil, C. Aparicio, Adsorption of Fibronectin, Fibrinogen, and Albumin on TiO 2 : Time-Resolved Kinetics, Structural Changes, and Competition Study, Biointerphases. 7 (2012) 48. https://doi.org/10.1007/s13758-012-0048-4.

[254] M. Lorenzetti, G. Bernardini, T. Luxbacher, A. Santucci, S. Kobe, S. Novak, Surface properties of nanocrystalline TiO 2 coatings in relation to the in vitro plasma protein adsorption, Biomed. Mater. 10 (2015) 045012. https://doi.org/10.1088/1748-6041/10/4/045012.

[255] F. Romero-Gavilán, N.C. Gomes, J. Ródenas, A. Sánchez, M. Azkargorta, I. Iloro, F. Elortza, I. García Arnáez, M. Gurruchaga, I. Goñi, J. Suay, Proteome analysis of human serum proteins adsorbed onto different titanium surfaces used in dental implants, Biofouling. 33 (2017) 98–111. https://doi.org/10.1080/08927014.2016.1259414.

[256] I.E. Svendsen, L. Lindh, The composition of enamel salivary films is different from the ones formed on dental materials, Biofouling. 25 (2009) 255–261. https://doi.org/10.1080/08927010802712861.

[257] D. Zuanazzi, Y. Xiao, W.L. Siqueira, Evaluating protein binding specificity of titanium surfaces through mass spectrometry–based proteomics, Clin. Oral Investig. (2020). https://doi.org/10.1007/s00784-020-03548-2.

[258] C.X. Wei, M.F. Burrow, M.G. Botelho, H. Lam, W.K. Leung, In vitro salivary protein adsorption profile on titanium and ceramic surfaces and the corresponding putative immunological implications, Int. J. Mol. Sci. 21 (2020) 1–17. https://doi.org/10.3390/ijms21093083.

[259] J.G.S. Souza, M. Bertolini, R.C. Costa, C.V. Lima, V.A.R. Barão, Proteomic profile of the saliva and plasma protein layer adsorbed on Ti–Zr alloy: the effect of sandblasted and acid-etched surface treatment, Biofouling. 36 (2020) 428–441. https://doi.org/10.1080/08927014.2020.1769613.

[260] M. Jäger, H.P. Jennissen, M. Haversath, A. Busch, T. Grupp, A. Sowislok, M. Herten, Intrasurgical Protein Layer on Titanium Arthroplasty Explants: From the Big Twelve to the Implant Proteome, Proteomics - Clin. Appl. 13 (2019). https://doi.org/10.1002/prca.201800168.

[261] L.L. Hench, BIOACTIVE GLASSES: GENE ACTIVATION, in: An Introd. to Bioceram., IMPERIAL COLLEGE PRESS, 2013: pp. 71–85. https://doi.org/10.1142/9781908977168_0004.

[262] J.R. Jones, Review of bioactive glass: From Hench to hybrids, Acta Biomater. 9 (2013) 4457–4486. https://doi.org/10.1016/j.actbio.2012.08.023.

[263] C. Migneco, E. Fiume, E. Verné, F. Baino, A guided walk through the world of mesoporous bioactive glasses (MBGs): Fundamentals, processing, and applications, Nanomaterials. 10 (2020) 1–26. https://doi.org/10.3390/nano10122571.

[264] E. Fiume, J. Barberi, E. Verné, F. Baino, Bioactive Glasses: From Parent 45S5 Composition to Scaffold-Assisted Tissue-Healing Therapies, J. Funct. Biomater. 9 (2018) 24. https://doi.org/10.3390/jfb9010024.

[265] M. Kapp, C. Li, Z. Xu, A.R. Boccaccini, K. Zheng, Protein Adsorption on SiO2-CaO Bioactive Glass Nanoparticles with Controllable Ca Content, Nanomaterials. 11 (2021) 561. https://doi.org/10.3390/nano11030561.

[266] C. Gruian, H.J. Steinhoff, S. Simon, Interaction between methemoglobin and some bioglass systems studied by EPR spectroscopy, Dig. J. Nanomater. Biostructures. 6 (2011) 373–383.

[267] G. Polzonetti, G. Iucci, A. Frontini, G. Infante, C. Furlani, L. Avigliano, D. Del Principe, G. Palumbo, N. Rosato, Surface reactions of a plasma-sprayed CaO-P2O5-SiO2-based glass with albumin, fibroblasts and granulocytes studied by XPS, fluorescence and chemiluminescence, Biomaterials. 21 (2000) 1531–1539. https://doi.org/10.1016/S0142-9612(00)00025-9.

[268] K.D. Lobel, L.L. Hench, In-vitro protein interactions with a bioactive gel-glass, J. Sol-Gel Sci. Technol. 7 (1996) 69–76. https://doi.org/10.1007/BF00401885.

[269] X. Zhang, D. Zeng, N. Li, X. Jiang, C. Liu, Y. Li, Large-pore mesoporous Ca-Si-based bioceramics with high: In vitro bioactivity and protein adsorption capability for bone tissue regeneration, J. Mater. Chem. B. 4 (2016) 3916–3924. https://doi.org/10.1039/c6tb00454g.

[270] M. Shoaib, A. Saeed, J. Akhtar, M.S.U. Rahman, A. Ullah, K. Jurkschat, M.M. Naseer, Potassium-doped mesoporous bioactive glass: Synthesis, characterization and evaluation of biomedical properties, Mater. Sci. Eng. C. 75 (2017) 836–844. https://doi.org/10.1016/j.msec.2017.02.090.

[271] S. Lin, W. Van Den Bergh, S. Baker, J.R. Jones, Protein interactions with nanoporous sol-gel derived bioactive glasses, Acta Biomater. 7 (2011) 3606–3615. https://doi.org/10.1016/j.actbio.2011.06.042.

[272] C. Wu, W. Fan, M. Gelinsky, Y. Xiao, P. Simon, R. Schulze, T. Doert, Y. Luo, G. Cuniberti, Bioactive SrO-SiO2 glass with well-ordered mesopores: Characterization, physiochemistry and biological properties, Acta Biomater. 7 (2011) 1797–1806. https://doi.org/10.1016/j.actbio.2010.12.018.

[273] A. Krajewski, R. Malavolti, A. Piancastelli, Albumin adhesion on some biological and non-biological glasses and connection with their Z-potentials, Biomaterials. 17 (1996) 53–60. https://doi.org/10.1016/0142-9612(96)80755-1.

[274] Å. Rosengren, S. Oscarsson, M. Mazzocchi, A. Krajewski, A. Ravaglioli, Protein adsorption onto two bioactive glass-ceramics, Biomaterials. 24 (2003) 147–155. https://doi.org/10.1016/S0142-9612(02)00272-7.

[275] A. Krajewski, A. Piancastelli, R. Malavolti, Albumin adhesion on ceramics and correlation with their Z-potential, Biomaterials. 19 (1998) 637–641. https://doi.org/10.1016/S0142-9612(97)00153-1.

[276] O. Ponta, R. Ciceo-Lucacel, A. Vulpoi, T. Radu, S. Simon, Molybdenum effect on the structure of SiO2-CaO-P 2O5 bioactive xerogels and on their interface processes with simulated biofluids, J. Biomed. Mater. Res. - Part A. 102 (2014) 3177–3185. https://doi.org/10.1002/jbm.a.34989.

[277] Z. Neščáková, K. Zheng, L. Liverani, Q. Nawaz, D. Galusková, H. Kaňková,

M. Michálek, D. Galusek, A.R. Boccaccini, Multifunctional zinc ion doped sol – gel derived mesoporous bioactive glass nanoparticles for biomedical applications, Bioact. Mater. 4 (2019) 312–321. https://doi.org/10.1016/j.bioactmat.2019.10.002.

[278] K. Magyari, C. Gruian, B. Varga, R. Ciceo-Lucacel, T. Radu, H.J. Steinhoff, G. Váró, V. Simon, L. Baia, Addressing the optimal silver content in bioactive glass systems in terms of BSA adsorption, J. Mater. Chem. B. 2 (2014) 5799–5808. https://doi.org/10.1039/c4tb00733f.

[279] C. Gruian, A. Vulpoi, E. Vanea, B. Oprea, H.J. Steinhoff, S. Simon, The attachment affinity of hemoglobin toward silver-containing bioactive glass functionalized with glutaraldehyde, J. Phys. Chem. B. 117 (2013) 16558–16564. https://doi.org/10.1021/jp408830t.

[280] A. Vulpoi, C. Gruian, E. Vanea, L. Baia, S. Simon, H.J. Steinhoff, G. Göller, V. Simon, Bioactivity and protein attachment onto bioactive glasses containing silver nanoparticles, J. Biomed. Mater. Res. - Part A. 100 A (2012) 1179–1186. https://doi.org/10.1002/jbm.a.34060.

[281] K. Magyari, T. Nagy-Simon, A. Vulpoi, R.A. Popescu, E. Licarete, R. Stefan, K. Hernádi, I. Papuc, L. Baia, Novel bioactive glass-AuNP composites for biomedical applications, Mater. Sci. Eng. C. 76 (2017) 752–759. https://doi.org/10.1016/j.msec.2017.03.138.

[282] C. Covarrubias, F. Arroyo, C. Balanda, M. Neira, A. Von Marttens, P. Caviedes, J.P. Rodríguez, C. Urra, The effect of the nanoscale structure of nanobioceramics on their in vitro bioactivity and cell differentiation properties, J. Nanomater. 2015 (2015). https://doi.org/10.1155/2015/526230.

[283] P. Xie, J. Du, Y. Li, J. Wu, H. He, X. Jiang, C. Liu, Robust hierarchical porous MBG scaffolds with promoted biomineralization ability, Colloids Surfaces B Biointerfaces. 178 (2019) 22–31. https://doi.org/10.1016/j.colsurfb.2019.02.042.

[284] U. Thamma, T.J. Kowal, M.M. Falk, H. Jain, Nanostructure of bioactive glass affects bone cell attachment via protein restructuring upon adsorption, Sci. Rep. 11 (2021) 1–14. https://doi.org/10.1038/s41598-021-85050-7.

[285] A. El-Ghannam, E. Hamazawy, A. Yehia, Effect of thermal treatment on bioactive glass microstructure, corrosion behavior ζ potential, and protein adsorption, J. Biomed. Mater. Res. 55 (2001) 387–395. https://doi.org/10.1002/1097-4636(20010605)55:3<387::AID-JBM1027>3.0.CO;2-V.

[286] L.A. Buchanan, A. El-Ghannam, Effect of bioactive glass crystallization on the conformation and bioactivity of adsorbed proteins, J. Biomed. Mater. Res. - Part A. 93 (2010) 537–546. https://doi.org/10.1002/jbm.a.32561.

[287] M.S. Bahniuk, H. Pirayesh, H.D. Singh, J.A. Nychka, L.D. Unsworth, Bioactive glass 45S5 powders: Effect of synthesis route and resultant surface chemistry and crystallinity on protein adsorption from human plasma, Biointerphases. 7 (2012) 1–15. https://doi.org/10.1007/s13758-012-0041-y.

[288] T.J. Kowal, R. Golovchak, T. Chokshi, J. Harms, U. Thamma, H. Jain, M.M. Falk, Role of phase separation on the biological performance of 45S5 Bioglass®, J. Mater. Sci. Mater. Med. 28 (2017). https://doi.org/10.1007/s10856-017-5976-6.

[289] N.B. Hyunh, C.S.D. Palma, R. Rahikainen, A. Mishra, L. Azizi, E. Verne, S. Ferraris, V.P. Hytönen, A. Sanches Ribeiro, J. Massera, Surface Modification of Bioresorbable Phosphate Glasses for Controlled Protein

Adsorption, ACS Biomater. Sci. Eng. 7 (2021) 4483–4493. https://doi.org/10.1021/acsbiomaterials.1c00735.

[290] E. Söderling, K. Herbst, E. Larmas, A. Yli-Urpo, Protein adsorption to a bioactive glass with special reference to precorrosion, J. Biomed. Mater. Res. 31 (1996) 525–531. https://doi.org/10.1002/(SICI)1097-4636(199608)31:4<525::AID-JBM13>3.0.CO;2-F.

[291] K.D. Lobel, L.L. Hench, In vitro adsorption and activity of enzymes on reaction layers of bioactive glass substrates, J. Biomed. Mater. Res. 39 (1998) 575–579. https://doi.org/10.1002/(SICI)1097-4636(19980315)39:4<575::AID-JBM11>3.0.CO;2-6.

[292] A.J. García, P. Ducheyne, D. Boettiger, Effect of surface reaction stage on fibronectin-mediated adhesion of osteoblast-like cells to bioactive glass, J. Biomed. Mater. Res. 40 (1998) 48–56. https://doi.org/10.1002/(SICI)1097-4636(199804)40:1<48::AID-JBM6>3.0.CO;2-R.

[293] A. El-Ghannam, P. Ducheyne, I.M. Shapiro, Formation of surface reaction products on bioactive glass and their effects on the expression of the osteoblastic phenotype and the deposition of mineralized extracellular matrix, Biomaterials. 18 (1997) 295–303. https://doi.org/10.1016/S0142-9612(96)00059-2.

[294] E.A.B. Effah Kaufmann, P. Ducheyne, S. Radin, D.A. Bonnell, R. Composto, Initial events at the bioactive glass surface in contact with protein-containing solutions, J. Biomed. Mater. Res. 52 (2000) 825–830. https://doi.org/10.1002/1097-4636(20001215)52:4<825::AID-JBM28>3.0.CO;2-M.

[295] M.C.L. Martins, S.R. Sousa, J.C. Antunes, M.A. Barbosa, Protein adsorption characterization, Methods Mol. Biol. 811 (2012) 141–161. https://doi.org/10.1007/978-1-61779-388-2_10.

[296] E. Migliorini, M. Weidenhaupt, C. Picart, Practical guide to characterize biomolecule adsorption on solid surfaces (Review), Biointerphases. 13 (2018) 06D303. https://doi.org/10.1116/1.5045122.

[297] S. Ferraris, A. Bobbio, M. Miola, S. Spriano, Micro- and nano-textured, hydrophilic and bioactive titanium dental implants, Surf. Coatings Technol. 276 (2015) 374–383. https://doi.org/10.1016/j.surfcoat.2015.06.042.

[298] V. Wagener, A.R. Boccaccini, S. Virtanen, Protein-adsorption and Ca-phosphate formation on chitosan-bioactive glass composite coatings, Appl. Surf. Sci. 416 (2017) 454–460. https://doi.org/10.1016/j.apsusc.2017.04.051.

[299] C. Gruian, E. Vanea, S. Simon, V. Simon, FTIR and XPS studies of protein adsorption onto functionalized bioactive glass, Biochim. Biophys. Acta - Proteins Proteomics. 1824 (2012) 873–881. https://doi.org/10.1016/j.bbapap.2012.04.008.

[300] G.P. Rockwell, L.B. Lohstreter, J.R. Dahn, Fibrinogen and albumin adsorption on titanium nanoroughness gradients, Colloids Surfaces B Biointerfaces. 91 (2012) 90–96. https://doi.org/10.1016/j.colsurfb.2011.10.045.

[301] A. Barth, Infrared spectroscopy of proteins, Biochim. Biophys. Acta - Bioenerg. 1767 (2007) 1073–1101. https://doi.org/10.1016/j.bbabio.2007.06.004.

[302] A.E. Ledesma, D.M. Chemes, M. de los A. Frías, M. del P. Guauque Torres, Spectroscopic characterization and docking studies of ZnO nanoparticle modified with BSA, Appl. Surf. Sci. 412 (2017) 177–188.

https://doi.org/10.1016/j.apsusc.2017.03.202.
[303] E. Vanea, V. Simon, XPS and Raman study of zinc containing silica microparticles loaded with insulin, Appl. Surf. Sci. 280 (2013) 144–150. https://doi.org/10.1016/j.apsusc.2013.04.111.
[304] J. Barberi, S. Spriano, Titanium and protein adsorption: An overview of mechanisms and effects of surface features, Materials (Basel). 14 (2021). https://doi.org/10.3390/ma14071590.

Chapter 3

Foreign body reaction and osteoimmunomodulation

3.1. Foreign body reaction: the host response to implants

In case of injury or damages, such as the ones occurring during surgery, our body is programmed to immediately react, in order to defend itself from the external world and to begin the healing process. In case of absence of external bodies inside the injured site, the normal wound repair process takes place. On the other hand, if an external body, which can be a medical device as well, is present in the injured site, the so-called foreign body reaction (FBR) occurs instead (Figure 3.1)[1]. The two processes are constituted by a similar complex cascade of events that involves the formation of a blood clot, the recruitment of cells belonging to the immune system and the inflammatory response. From this point, the normal healing and the FBR take two different paths. During wound healing, the inflammation phase rapidly leave place to cell proliferation and the formation of a granulation tissue, that lead to wound recovery after remodeling. In the case of FBR, the immune system is continuously stimulated, entering a chronic inflammation phase that can lead to the formation of a fibrotic capsule around the foreign body [2].

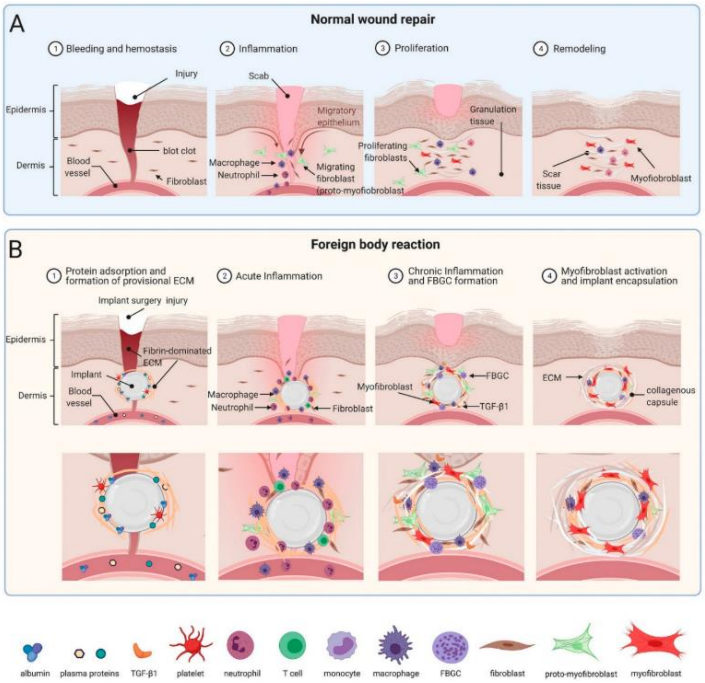

Figure 3.1 Wound repair (a) and FBR (b) phases. They are similar and differs from the formation of a provisional extracellular matrix around the implants, the formation of a foreign body gigantic cells and the final fibrous capsule formation [2]**.**

3.1.1. Blood transient matrix formation

During every surgery, vessels are broken and blood immediately floods into the wound through exudations, thus being the first physiological entity encountered by the implant. As widely discussed before, this provokes the immediate adsorption of plasma proteins, which form a transient matrix on the biomaterial surfaces. Among those, there are proteins responsible for the activation of thrombosis, blood coagulation and complement systems.

The clot formation may proceed through two distinct pathways: the intrinsic pathway, which is surface contact-mediated and initiated by the adsorption and the formation of active forms of proteins such as factor XII (FXII), prekallikrein and kininogen; the extrinsic pathway is activated by tissue factor (TF), collagen and von Willebrand factor (vWF) that are released by cells (activated platelets, endothelial cells and monocytes) following the damage [3]. The activation of FXII is mainly promoted by negatively charged surfaces, which promotes a favorable orientation of the proteins and the cleavage necessary for FXII activation [4]. Both pathways lead to a cascade of enzymatic events that ends in the cleavage of prothrombin in active thrombin. The combination of the two pathways is not enough to provoke clot formation, but platelets adhesion and activation is also necessary. Platelets can be activated by the thrombin released through the intrinsic pathways, and initiating to release themselves pro-coagulation factors, which turn into more thrombin production and more platelet activation, forming a loop [5]. Besides, thrombin initiated the cleavage of fibrinogen in fibrin, forming the clot structure, known also as provisional extracellular matrix, which provides a 3D structure rich in proteins that sustain cells adhesion. Fibrinogen has also a major role in mediate platelet adhesion and activation on biomaterials, through the $\alpha_{IIb}\beta_3$ integrin receptor [6].

In concomitance with the clot formation, a foreign body can also activate the complement system: it is a defense system comprised of more than twenty proteins that are activated by a cascade of enzymatic reactions. The complement system can be activated through three different biochemical pathways, namely the classical pathway, the alternative pathway and the lectin pathway [7]. Biomaterials can trigger the complement system by the alternative pathways, depending also to the adsorbed proteins. For instance, OH and NH_2 functional groups on the surface increase the binding with complement factor C3b, which promotes the assembly of C3 convertase that promotes the formation of more C3b and the generation of an amplification loop. Adsorbed IgG can trigger the classical pathway, by binding C1q and the consequent formation of C1, which is the first enzyme involved in the classical pathway [4]. The complement system has an active role in the onset of the inflammation response. Anaphylatoxins such as C3a and C5a, released after the activation of C3 and C5 factors, are involved in the attraction of leukocytes to the injured site by vascular flow and permeability increase, and infiltration and chemotaxis of immune cells. Furthermore, complement factors can opsonize bacteria and also biomaterials, which can be recognized by monocytes and macrophages as consequence [7]. Complements and coagulation cascade are well interconnected: FXIIa can cleave C1s and C3, triggering the classical activation pathway of the complement system; thrombin can activate C3, C5, and C6 [8].

All these events result in the formation of a transient ECM rich in proteins, chemokines, cytokines and growth factors that are continuously released and stimulate the foreign body reaction process. These molecules are also responsible for the recruitment of immune cells, such as neutrophils and monocytes that initiate the subsequent inflammation response [9].

3.1.2. Inflammation

In the common thinking, inflammation is regarded as something that must be avoided, or at least minimized, by all means. This was true also in the field of biomaterials, where the quest in the past century was for surfaces the most inert as possible in a physiological environment. New knowledge gained in the past decades have shown how inflammation plays a pivotal role in the success of an implant. For instance, osseointegration is regarded as a FBR without the developing of a chronic inflammation [10]. The clinical demand is now on biomaterials that can modulate the interactions with the immune cells and stimulate an appropriate inflammation response. The inflammatory response may be divided into two distinct phases, the acute and the chronic inflammation. The two phases can be distinguished mainly by the predominant cell type: neutrophils for the acute inflammation and macrophages during the chronic phase (Figure 3.2).

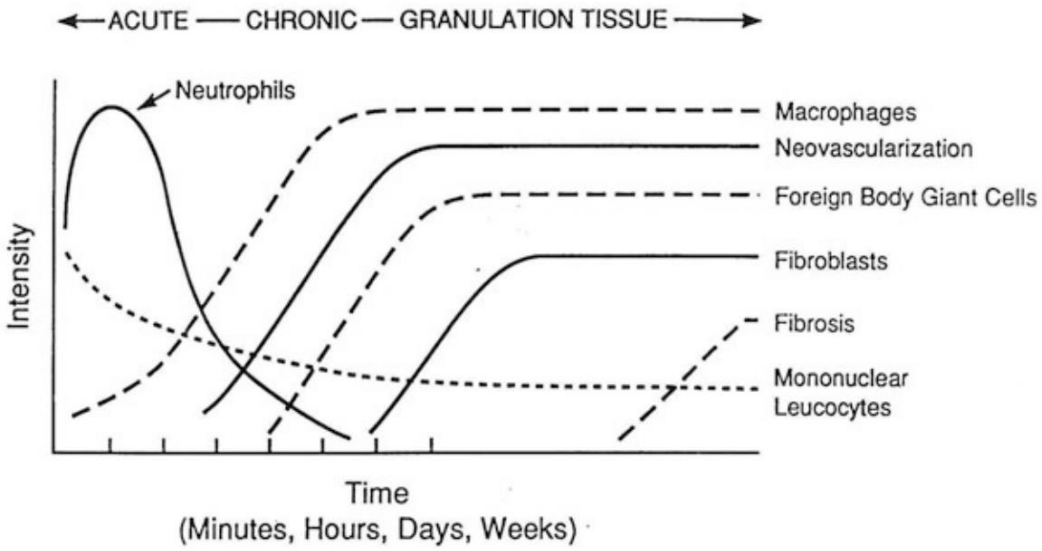

Figure 3.2 Temporal variation of cells population around the implant during FBR [9]**.**

Acute inflammation

The acute inflammation is the first part of the immune response in the injury events of a tissue, and it may span from hours up to a week, according to the extent of the wound. This phase of the inflammation process is characterized by the presence of neutrophils (polymorphonuclear leukocytes, PMNs), which are the first type of leukocytes that gather at the implantation site. PMNs migrate to the injured site from blood vessels, through chemotaxis, induced by exogenous or endogenous molecules, or by "adhesion molecules" on the neutrophils or endothelial surfaces. The expression of those molecules can be increased by pro-inflammatory mediators, such as interleukin (IL)-1 or TNF [11]. At the injury site, the neutrophils phagocyte microorganisms and external bodies. Phagocytosis by PMNs and macrophages occurs in three steps: the first is the recognition of foreign organisms or body via opsonization by IgG or complement C3b; engulfment; killing or degradation by the release of reactive oxygen species (ROI), such as hydrogen peroxyde, antimicrobial proteins or proteases [1]. Biomaterials are usually too large to be ingested and degraded by immune cells, still some of the phagocytosis steps may occur. Leukocytes can recognize and adhere to biomaterials through the adsorption on their surfaces of IgG and C3b, then, they try to degrade the materials by extracellular release of leukocytes products [12]. Adsorbed proteins in the blood transient matrix, such as fibrinogen, fibronectin and vitronectin, have been demonstrated to play an active role in the activation and adhesion of neutrophils. Neutrophils characterize the very first hours of the inflammatory response: in fact, these cells live up to just 48 h. After that, the immune response is entrusted to macrophages, which can last for months.

Along with PMNs, also circulating monocytes are attracted to the wound site by chemokines and factors released by the blood clot and the complement system, but also by factors released by the neutrophils themselves. In fact, PMNs release a large amount of immune-regulatory signals and controls the subsequent

inflammation phases [13]. At the implant site, monocytes differentiate in "classically activated" macrophages. Macrophages are extremely plastic cells and they can adapt their physiology in different phenotypes according to external stimuli, in order to exert the proper response. Usually, the two extreme phenotypes are regarded as M1 and M2 [14]. M1 or classically activated macrophages can increase the inflammatory response, by the release of pro-inflammatory factors and cytokines, such as IL-1, IL-6 and TNF, that can further recruit leukocytes and foster the inflammation process. M2 or alternatively activated macrophages, which are more related to the release of anti-inflammatory and wound-healing factors, such as IL-1 receptor antagonist and IL-10, appear later in the inflammatory process. Macrophage phenotypes are not strictly defined and they can exhibit all the possible variation between the two extremes, according to both external stimuli or factors secreted by the macrophages themselves [15].

After about two days, M1 macrophages are the predominant cells at the infection site, and at that point they have colonized the implant surfaces. Not being able to engulf the implanted device, they undergo "frustrated" phagocytosis, which involve the release of degrading species (ROIs, nitrogen radicals, enzymes)[7]. If the foreign material can be removed in this way, the FBR ends in the acute phase of inflammation, leaving space to the physiological wound healing process; if not, the inflammation turns to chronic. This usually happens in about 1 week.

Chronic inflammation

The continuous release of inflammatory factors by macrophages, and the tissue stimulation by the implanted biomaterial, give birth to the chronic inflammation phase, which is usually confined at the implant site. Macrophages are again the dominant cells in this phase, with the ongoing switch from the M1 to M2 polarization [16].

A hallmark of the chronic phase of FBR is the presence of foreign body giant cells (FBGCs). In order to attempt to engulf big particles (> 10 μm), macrophages can fuse together forming FBGCs, which can stay at the implant surface for all its life [17]. The surface properties of the biomaterial and the adsorbed proteins have an important role in the adhesion, activation and fusion of macrophages. Fibronectin, laminin and fibrinogen can increase the adhesion of macrophages, while vitronectin can induce the formation of FBGCs [7]. The presence of FBGCs and the release of degrading species following frustrated phagocytosis may cause damages to biomaterials, such as polymer oxidation or metal corrosion, that can result in implant failure at the end [17]. FBCGs will persist on the implant surface as long as the foreign body reaction lasts, which can correspond to the whole life of the implant [11].

3.1.3. Fibrous capsule formation

The presence of M2 macrophages and FBGCs is fundamental in driving the final stage of the host response to the implant, which usually consist in the

regeneration of the tissue in the injured site. These cells release factors such as platelet-derived growth factor (PDGF), vascular endothelial growth factor (VEGF), and transforming growth factor-β1 (TGF- β1), which are reported to activate fibroblasts and stimulate the production of blood vessels [18]. Activated fibroblasts result in development of myofibroblasts, which are characterized by the expression of smooth muscle actin (α-SM actin), which generates contractile forces to close the wound, and synthesis of proteins in the ECM, such as collagen I [19]. In normal wound healing, myofibroblasts undergo apoptosis after the successful remodeling of the tissue [1]. The continuous stimulation associated to the presence of an implant leads in excessive production, contraction and crosslinking of collagen I by myofibroblasts, resulting in the formation of the fibrotic capsules [2]. The capsule is a whole new tissue that grows and get vascularized by the continuous deposition of new ECM and the release of PDGF and VEGF, which have angiogenic effects. Once the macrophage activity is not intense enough to sustain the one of fibroblast, the fibrotic capsule reaches a steady state, isolating the FBR site from the rest of the host body [16]. Fibrosis poses a threat to biomedical implants, since it can provoke the failure of the device by isolating it from the rest of the organism, for example avoiding correct tissue-implant contact, drug delivery or osseointegration.

3.2. Osteoimmunomodulation: a new paradigm

Cross talking between immune cells and the rest of the body is very intense and the right immune response during injury events is fundamental for the correct recovery of the wound. When bone trauma are involved, the connection between the cells deputed to host defense and bone remodeling cells, osteoblasts and osteoclasts, is so intense that a whole new field has been developed: “osteoimmunology” [20]. In case of an implant, cells involved in the FBR, such as macrophages, but also other immune cells such as lymphocyte T or B cells, must achieve the right balance in polarization and factors expression to elicit the activity of osteoblast and modulate the bone resorption by osteoclasts (Figure 3.3). The capacity of a material to induce the proper immunological response for a correct osseointegration is called “osteoimmunomodulation” [21]. Osseointegration can be seen as a limited FBR, which does not involve the development of a chronic inflammation and fibrotic capsule but instead it results in the growth of new functional bone tissue at the interface with the implant.

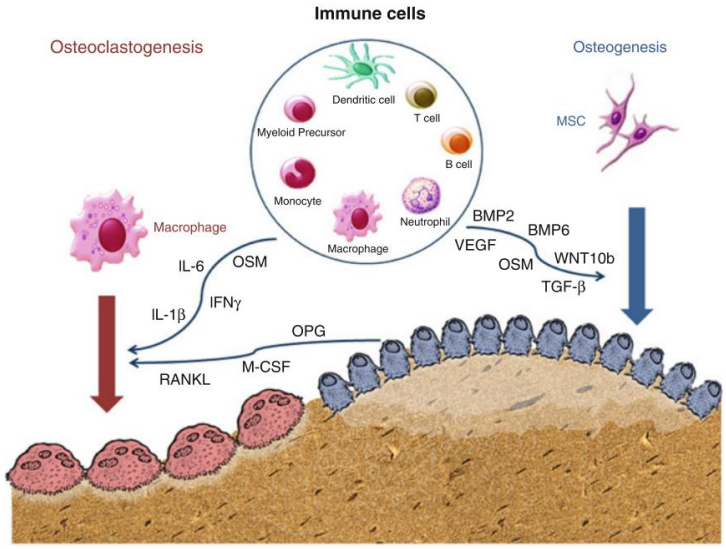

Figure 3.3 Osteoimmunomodulation by immune cells. The released factors that concur to osteogenesis and osteoclastogenesis are indicated [21].

3.2.1. Regulation of bone remodeling by immune cells

As discussed in the previous section of this paragraph, the immune system can react in different manners. The FBR can be more or less severe, with the perdurance in time of a chronic inflammation state, with a predominant M1 macrophages polarization, the continuous stimulation of fibroblasts and the development of a thick fibrotic capsule. The factors released by the immune cells do not only affect the activity of fibroblast, but the activity of bone remodeling cells depends heavily on those products.

The main pathway that controls bone remodeling is the one formed by RANKL/RANK/OPG. Receptor activator of nuclear factor kappa-B ligand (RANKL), at type II membrane protein, regulates osteoclast differentiation and, consequently, bone resorption. It is expressed by both bone cells, such as osteoblast and bone marrow stromal cells (BMSC), and immune cells, such as lymphocytes T and PMNs. Receptor activator of nuclear factor kappa-B (RANK) is expressed by osteoclast precursors and when it bound by RANKL bone resorption processes begin [22]. Osteoprogerin (OPG) is the decoy for osteoclastogenesis expressed by osteoblasts: it binds to RANKL, interrupting the RANKL/RANK interaction and suppressing the activation of osteoclasts [21]. Another indispensable factor for osteoglastogenesis is mesenchymal colony stimulating factors (M-CSF), which can commit MSCs to osteoclast differentiation by induction of RANKL expression [23]. Overexpression of RANKL by T cells is also related to pathological conditions such as rheumatoid arthritis.

Immune cells do not regulate bone metabolism only by through the RANKL/RANK pathway, but other cytokines released by lymphocytes and M1 or M2 macrophages have a pivotal role in directing osteoclast and osteoblast activity. Pro-inflammatory TNF-α and interleukin IL-1α, IL-1β, IL-6, IL-7 can promote osteocalstogenesis, while INF-β, INF-γ and anti-inflammatory IL-4 and IL-10 can suppress osteoclast activity [24,25].

Macrophages, as the predominant cells during the main part of FRB, have a strong effect on the osseointegration, largely dependent on their phenotypic expression. Classically activated macrophages are well recognized to release pro-inflammatory factors related to osteoclastogenesis, and it has been shown that they can directly differentiate into osteoclasts when stimulated by M-CSF and RANKL [26]. On the other hand, M2 macrophages are more often associated to the release of anti-inflammatory cytokines and other factors, such as BMP2 and VEGF, which can enhance osteogenic differentiation of MSCs. However, some studies have highlighted the osteogenic effect of M1 and the fact that a marked M2 polarization can correlate with a severe FBR and fibrosis. These facts bring to light that osseointegration is a complex process, which relies on balanced and time-depended release of factors by immune cells [27].

3.2.2. FBR control: tackling osteoimmunomodulation with biomaterials

Due to the strict interplay between host immune response and bone remodeling around the implant, it is necessary to design bone-contact biomaterials in order to express proper osteoimmunomodulation properties and not only focusing on the response of bone cells. Such results can be achieved by using strategies applied for tuning biomaterial surface properties in order to control the FBR (Figure 3.4)[7]. Surface topography, chemistry, wettability, mechanical properties and the shape of the biomaterials are all features that can affect the immune response, therefore surface modification are effective to modify material interactions with immune cells (Table 3.1)[15].

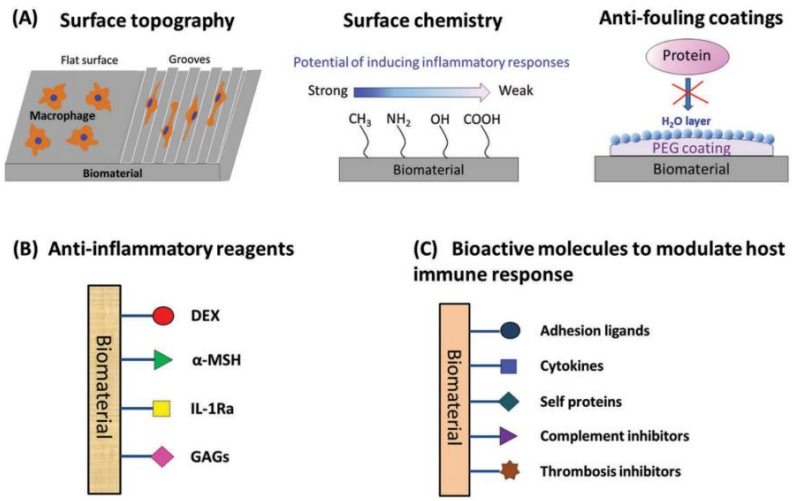

Figure 3.4 Representation of different anti-inflammatory surface modifications: a) physiochemical modification of the biomaterial surface; b) functionalization with anti-inflammatory agents; c) grafting of bioactive molecules for immunomodulation of the host response [7].

Table 3.1 Effec of surface properites of biomaterials on the host immune response. Repoduced from [27].

Tunable properties	Effect of immune cells

Surface chemistry	Wettability	hydrophobicity: ↑monocyte adhesion hydrophilicity: ↓macrophage adhesion
	Charge	anionic/neutral particles: ↓ inflammatory reaction cationic species: ↑ inflammation;
Surface topography	Roughness	induces significant immune reactions, influences immune cell adhesion;
	Particle size	no consensus has been reached on size;
	Porosity/pore size	larger pore size: ↓ inflammation, ↑ angiogenic process;
Delivery of biological molecules		elicit immunoregulatory effects

The physiochemical properties of the surface can be modified to obtain anti-fouling surfaces. At first, surface topography and material size can be modified to elicit the proper response [28]. Porous materials, with pore size in the range 30-40 μm, have been observed to increase the M2 macrophages polarization and elicit a healing process with little fibrosis and high vascularization [29]. The presence of nano- and micro-grooves and grating have been found to change the morphology and cytokine expression of macrophages, with respect to a smooth surface [30]. The size of particles, from micrometers to millimeters, can also influence the FBR and the thickness of the fibrotic capsule [28]. Immune response can be controlled also by modulating the adsorption of proteins, such as albumin, fibrinogen, fibronectin, immunoglobulins and system complements, in order to reduce the adhesion site for cells and the opsonization of the biomaterials, according to the surface properties that have been deeply discussed in the previous chapter. Hydrophilic polymeric brushes have been found to reduce protein adsorption and leukocyte adhesion [31], while anionic materials can limit integrin adsorption, and as consequence, macrophage integrin-mediated adhesion, leading them to apoptosis [4]. It was further observed that the presence of certain functional groups can worsen or improve the inflammatory response: amino groups and hydroxyls increase the infiltration of macrophages and the intensity of the fibrotic response, the former groups may also increase the M2 polarization; on the other hand, carboxyls may induce a more inflammatory M1 phenotype [13]. Coating can be obtain also by the use of natural materials, such as chitosan, collagen, hyaluronan or dextran [32].

Functionalization with biomolecules such as adhesion molecules, drugs, growth factors, or antibodies is another very investigated strategy. Those active elements can be both grafted on the biomaterial surfaces or incorporated into it, such as in the case of hydrogels polymeric scaffolds [33]. A possibility for the creation of immunomodulatory biomaterials is the use of ECM components, which can be combined with other materials, as in case of hip replacement, to create a favorable immune environment [34]. ECM elements, such as hyaluronic acid, collagen or interleukin can be used as coating on the materials or tissue derived de-cellularized ECM can be directly used as immunomodulating scaffold [31]. For instance, both anti-inflammatory drugs, such as dexamethasone or heparin, and cytokines, as TGF-β or IL-10, can be embedded in coatings and hydrogels, for *in situ* releases [31,35]. Growth factors, such as VEGF, PDGF or TGFβ, can be delivered to the implant site with the same strategies [36].

While developing or characterizing materials for osseointegration, the common use is to test their interaction with bone cells, such as MSCs or osteoblast.

According to the concept of osteoimmunomodulation, it is also of equivalent and uttermost importance to investigate the immune response to such biomaterials, even though it is rarely done [21]. The strategies to study the osteoimmunomodulation properties of materials have been developed to mimic as closely as possible what actually happens on the surface of an implant, and are mainly four, accordingly to a recent review by Mestres et al. (Figure 3.5)[37]: simplified method; indirect co-culture by conditioned medium or transwell; direct co-culture. The first method involves the stimulation of bone cells by the use of commercial factors, but lack the real-time interplay between biomaterials and bone or immune cells. The conditioned medium indirect co-culture is obtained by firstly seeding and culturing immune cells on the biomaterial, then the growth medium is withdrawn and employed for cultivating bone cells on the biomaterial again or on culture plates. The use of a conditioned medium was found effective in evaluating osteoimmunomodulation of various materials, such as the effect of titanium surface topography on macrophage polarization and MSCs response [38,39]. Still, again the real-time crosstalk between cells is hindered and released factor accumulation and nutrients depletion in the medium must be accounted for.

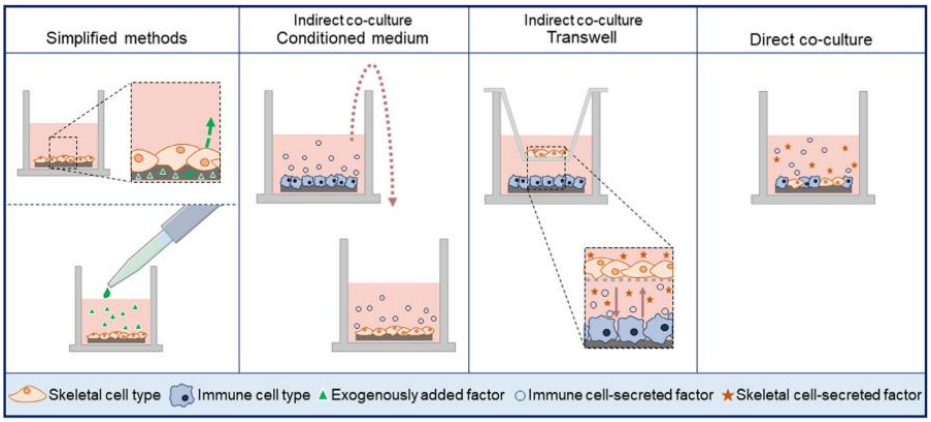

Figure 3.5 Main experimental methodologies for evaluating the immunomodulation of biomaterials [37]**.**

Real-time interaction between immune and bone cells can be achieved by the use of transwell or by direct co-culture. These two methods have the advantage of a direct interaction between cells, but poses great difficulties in the experimental set-up for the proper growth condition of both cell types. Plus, in case of direct co-culture, the analysis of the cell response and the comprehension of the results is more complicated.

3.3. Bibliography

[1] S. Ellis, E.J. Lin, D. Tartar, Immunology of Wound Healing, Curr. Dermatol. Rep. 7 (2018) 350–358. https://doi.org/10.1007/s13671-018-0234-9.

[2] N. Noskovicova, B. Hinz, P. Pakshir, Implant Fibrosis and the Underappreciated Role of Myofibroblasts in the Foreign Body Reaction, Cells. 10 (2021) 1794. https://doi.org/10.3390/cells10071794.

[3] H.T. Shiu, B. Goss, C. Lutton, R. Crawford, Y. Xiao, Formation of blood clot on biomaterial implants influences bone healing, Tissue Eng. - Part B Rev. 20 (2014) 697–712. https://doi.org/10.1089/ten.teb.2013.0709.

[4] S. Franz, S. Rammelt, D. Scharnweber, J.C. Simon, Immune responses to implants - A review of the implications for the design of immunomodulatory biomaterials, Biomaterials. 32 (2011) 6692–6709. https://doi.org/10.1016/j.biomaterials.2011.05.078.

[5] A. De Mel, B.G. Cousins, A.M. Seifalian, Surface modification of biomaterials: A quest for blood compatibility, Int. J. Biomater. 2012 (2012). https://doi.org/10.1155/2012/707863.

[6] L.C. Xu, J.W. Bauer, C.A. Siedlecki, Proteins, platelets, and blood coagulation at biomaterial interfaces, Colloids Surfaces B Biointerfaces. 124 (2014) 49–68. https://doi.org/10.1016/j.colsurfb.2014.09.040.

[7] G. Zhou, T. Groth, Host Responses to Biomaterials and Anti-Inflammatory Design-a Brief Review, Macromol. Biosci. 18 (2018) 1800112. https://doi.org/10.1002/mabi.201800112.

[8] M.B. Gorbet, M. V. Sefton, Biomaterial-associated thrombosis: Roles of coagulation factors, complement, platelets and leukocytes, Biomaterials. 25 (2004) 5681–5703. https://doi.org/10.1016/j.biomaterials.2004.01.023.

[9] J.M. Anderson, S. Jiang, Implications of the Acute and Chronic Inflammatory Response and the Foreign Body Reaction to the Immune Response of Implanted Biomaterials, in: Immune Response to Implant. Mater. Devices, Springer International Publishing, Cham, 2017: pp. 15–36. https://doi.org/10.1007/978-3-319-45433-7_2.

[10] S. Spriano, S. Yamaguchi, F. Baino, S. Ferraris, A critical review of multifunctional titanium surfaces: New frontiers for improving osseointegration and host response, avoiding bacteria contamination, Acta Biomater. 79 (2018) 1–22. https://doi.org/10.1016/j.actbio.2018.08.013.

[11] J.M. Anderson, Mechanisms of inflammation and infection with implanted devices, 1993. https://doi.org/10.1016/1054-8807(93)90045-4.

[12] J. Anderson, S. Cramer, Perspectives on the Inflammatory, Healing, and Foreign Body Responses to Biomaterials and Medical Devices, in: Host Response to Biomater., Elsevier, 2015: pp. 13–36. https://doi.org/10.1016/B978-0-12-800196-7.00002-5.

[13] E. Mariani, G. Lisignoli, R.M. Borzì, L. Pulsatelli, Biomaterials: Foreign bodies or tuners for the immune response?, Int. J. Mol. Sci. 20 (2019). https://doi.org/10.3390/ijms20030636.

[14] D.M. Mosser, J.P. Edwards, Exploring the full spectrum of macrophage activation, Nat. Rev. Immunol. 8 (2008) 958–969. https://doi.org/10.1038/nri2448.

[15] Z. Sheikh, P.J. Brooks, O. Barzilay, N. Fine, M. Glogauer, Macrophages, foreign body giant cells and their response to implantable biomaterials, Materials (Basel). 8 (2015) 5671–5701. https://doi.org/10.3390/ma8095269.

[16] A. Carnicer-Lombarte, S.T. Chen, G.G. Malliaras, D.G. Barone, Foreign

Body Reaction to Implanted Biomaterials and Its Impact in Nerve Neuroprosthetics, Front. Bioeng. Biotechnol. 9 (2021) 1–22. https://doi.org/10.3389/fbioe.2021.622524.

[17] J.M. Anderson, A. Rodriguez, D.T. Chang, Foreign body reaction to biomaterials, Semin. Immunol. 20 (2008) 86–100. https://doi.org/10.1016/j.smim.2007.11.004.

[18] J.M. Anderson, Inflammation, Wound Healing, and the Foreign-Body Response, Third Edit, Elsevier, 2013. https://doi.org/10.1016/B978-0-08-087780-8.00044-9.

[19] B. Rolfe, J. Mooney, B. Zhang, S. Jahnke, S.-J. Le, Y.-Q. Chau, Q. Huang, H. Wang, G. Campbell, J. Campbell, The Fibrotic Response to Implanted Biomaterials: Implications for Tissue Engineering, Regen. Med. Tissue Eng. - Cells Biomater. (2011). https://doi.org/10.5772/21790.

[20] H. Takayanagi, Osteoimmunology: Shared mechanisms and crosstalk between the immune and bone systems, Nat. Rev. Immunol. 7 (2007) 292–304. https://doi.org/10.1038/nri2062.

[21] Z. Chen, C. Wu, Y. Xiao, Convergence of Osteoimmunology and Immunomodulation for the Development and Assessment of Bone Biomaterials, in: B. Corradetti (Ed.), Immune Response to Implant. Mater. Devices, Springer International Publishing, Cham, 2017: pp. 107–124. https://doi.org/10.1007/978-3-319-45433-7_6.

[22] Y. Xie, C. Hu, Y. Feng, D. Li, T. Ai, Y. Huang, X. Chen, L. Huang, J. Tan, Osteoimmunomodulatory effects of biomaterial modification strategies on macrophage polarization and bone regeneration, Regen. Biomater. 7 (2020) 233–245. https://doi.org/10.1093/rb/rbaa006.

[23] C. Guder, S. Gravius, C. Burger, D.C. Wirtz, F.A. Schildberg, Osteoimmunology: A Current Update of the Interplay Between Bone and the Immune System, Front. Immunol. 11 (2020) 1–19. https://doi.org/10.3389/fimmu.2020.00058.

[24] M. Rauner, W. Sipos, P. Pietschmann, Osteoimmunology, Int. Arch. Allergy Immunol. 143 (2007) 31–48. https://doi.org/10.1159/000098223.

[25] M.B. Greenblatt, J.-H. Shim, Osteoimmunology: A Brief Introduction, Immune Netw. 13 (2013) 111. https://doi.org/10.4110/in.2013.13.4.111.

[26] Z. Chen, T. Klein, R.Z. Murray, R. Crawford, J. Chang, C. Wu, Y. Xiao, Osteoimmunomodulation for the development of advanced bone biomaterials, Mater. Today. 19 (2016) 304–321. https://doi.org/10.1016/j.mattod.2015.11.004.

[27] A.M. Negrescu, A. Cimpean, The state of the art and prospects for osteoimmunomodulatory biomaterials, Materials (Basel). 14 (2021). https://doi.org/10.3390/ma14061357.

[28] B. Aktaş, B. Garipcan, Z.B. Ahi, K. Tuzlakoğlu, E. Ergene, P.Y. Huri, Osteoimmunomodulation with Biomaterials, in: Biomater. Immune Response, 2018: pp. 161–190. https://doi.org/10.1201/b22419-8.

[29] B.D. Ratner, The Biocompatibility of Implant Materials, Elsevier Inc., 2015. https://doi.org/10.1016/B978-0-12-800196-7.00003-7.

[30] S. Chen, J.A. Jones, Y. Xu, H.Y. Low, J.M. Anderson, K.W. Leong, Characterization of topographical effects on macrophage behavior in a foreign body response model, Biomaterials. 31 (2010) 3479–3491. https://doi.org/10.1016/j.biomaterials.2010.01.074.

[31] A. Vishwakarma, N.S. Bhise, M.B. Evangelista, J. Rouwkema, M.R. Dokmeci, A.M. Ghaemmaghami, N.E. Vrana, A. Khademhosseini,

Engineering Immunomodulatory Biomaterials To Tune the Inflammatory Response, Trends Biotechnol. 34 (2016) 470–482. https://doi.org/10.1016/j.tibtech.2016.03.009.

[32] J.M. Morais, F. Papadimitrakopoulos, D.J. Burgess, Biomaterials/Tissue Interactions: Possible Solutions to Overcome Foreign Body Response, AAPS J. 12 (2010) 188–196. https://doi.org/10.1208/s12248-010-9175-3.

[33] M. Griffith, M.M. Islam, J. Edin, G. Papapavlou, O. Buznyk, H.K. Patra, The quest for anti-inflammatory and anti-infective biomaterials in clinical translation, Front. Bioeng. Biotechnol. 4 (2016) 1–9. https://doi.org/10.3389/fbioe.2016.00071.

[34] A. Poliakov, V. Pakhaliuk, V.L. Popov, Current Trends in Improving of Artificial Joints Design and Technologies for Their Arthroplasty, Front. Mech. Eng. 6 (2020). https://doi.org/10.3389/fmech.2020.00004.

[35] W.K. Ward, A review of the foreign-body response to subcutaneously-implanted devices: The role of Macrophages and cytokines in biofouling and fibrosis, J. Diabetes Sci. Technol. 2 (2008) 768–777. https://doi.org/10.1177/193229680800200504.

[36] K. Sarkar, Y. Xue, S. Sant, Host Response to Synthetic Versus Natural Biomaterials, in: Immune Response to Implant. Mater. Devices, Springer International Publishing, Cham, 2017: pp. 81–105. https://doi.org/10.1007/978-3-319-45433-7_5.

[37] G. Mestres, S.-S.D. Carter, N.P. Hailer, A. Diez-Escudero, A practical guide for evaluating the osteoimmunomodulatory properties of biomaterials, Acta Biomater. 130 (2021) 115–137. https://doi.org/10.1016/j.actbio.2021.05.038.

[38] Y. Zhu, H. Liang, X. Liu, J. Wu, C. Yang, T.M. Wong, K.Y.H. Kwan, K.M.C. Cheung, S. Wu, K.W.K. Yeung, Regulation of macrophage polarization through surface topography design to facilitate implant-to-bone osteointegration, Sci. Adv. 7 (2021) 1–14. https://doi.org/10.1126/sciadv.abf6654.

[39] B. Chen, Y. You, A. Ma, Y. Song, J. Jiao, L. Song, E. Shi, X. Zhong, Y. Li, C. Li, Zn-Incorporated TiO2 Nanotube Surface Improves Osteogenesis Ability Through Influencing Immunomodulatory Function of Macrophages, Int. J. Nanomedicine. Volume 15 (2020) 2095–2118. https://doi.org/10.2147/IJN.S244349.

Chapter 4

Materials and Methods

4.1. Substrates

In the frame of this work, different materials, three titanium-based surfaces with different chemical treatments, plus their respective untreated surfaces as control, and two bioactive glasses were used as substrates for investigating protein adsorption; those surfaces were chosen due to their relevance as innovative biomaterials for bone regeneration application. In fact, they have been developed by the research groups involved in this work, both at Politecnico di Torino and at Chubu University. Polystyrene was employed as model for a hydrophobic material without specific functional groups.

The substrates investigated, with the respective surface treatments, are listed in Table 4.1.

Table 4.1 Substrates employed in this work, with their names, bulk material and surface treatment employed (-: sample without surface modification)

Substrate	Bulk material	Surface treatment
Ti	Pure titanium	-
Ti64	Ti6Al4V alloy	-
Ti(A-HC-H)	Pure titanium	Acid, alkali and heat treatment
Ti64(SrAg)	Ti6Al4V alloy	Sr ang Ag ionic doping and heat treatment
Ti64(HF-H_2O_2)	Ti6Al4V alloy	HF and H_2O_2 treatment
SBA2	Silica glass	-
AgSBA2	Silica glass	Ag ionic exchange
PS	Polystyrene	-

4.1.1. Titanium samples preparation

Pure titanium, grade 2, (Ti)(ISO5832-2, Nilaco Co., Tokyo, Japan) and titanium alloy Ti6Al4V, grade5, (Ti64)(ASTM B348, Titanium Consulting and Trading, Buccinasco, Italy) were subjected to three chemical treatments in order to enhance their bioactivity. As control surfaces, polished Ti and Ti64 were used.

Ti and Ti64 were supplied as plates, 1 mm thick, or as bars, with 10 mm diameter, and cut in 10x10 mm square samples or 2 mm thick disks respectively. Plates were used for the sample preparation at Chubu University while disks were employed at Politecnico di Torino for the preparation of controls and one of the three chemical treatments (Figure 4.1).

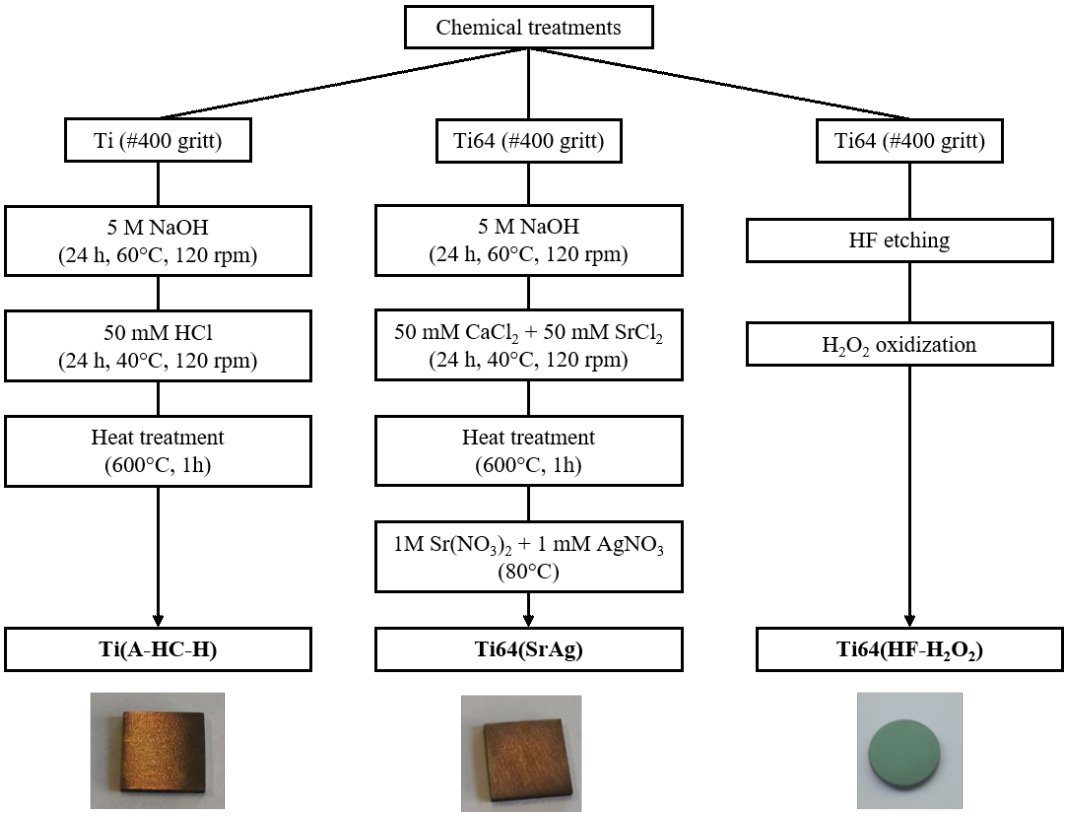

Figure 4.1 Scheme of the chemical treatments on Ti and Ti64 samples

Chemical treatment on pure titanium

Ti square plates were chemically treated via a mixed acid-alkali solution and a subsequent thermal treatment by the group of Prof. Yamaguchi, at the laboratories of Chubu university, where this surface have been developed [1,2]. More precisely, the samples were treated as follows (all reagents form Kanto chemical Co., Inc, Tokyo Japan):

- Gritted with a #400 SiC polishing paper and washed three times in an ultrasonic bath, for 30 min each, with acetone, 2-propanol and MilliQ water and dried overnight at 40°C;
- Soaked for 24 h in a 5 M NaOH solution, in an oil bath at 60°C and shaken at 120 rpm;
- Soaked again for 24 h in a 50 mM HCl solution, in an oil bath at 40°C at 120 rpm;
- Heat treated at 600°C for 1 h, with a heating rate of 5°C/min and leaved to cool inside the furnace.

The samples treated in this way will be referred as Ti(A-HC-H)

Chemical treatment on titanium alloy

Two different chemical treatments were performed on Ti64 samples. One was performed at Politecnico di Torino, following a registered patent [3], the other was made again at Chubu University [4].

The last type of surface modification, besides the generation of a titanium oxide layer with controlled morphology and chemistry, involves also the doping of the surface with strontium and silver ions, and it is obtained with the steps listed below:

- Gritted with a #400 SiC polishing paper and washed three times in an ultrasonic bath, for 30 min each, with acetone, 2-propanol and MilliQ water and dried overnight at 40°C;
- Soaked for 24 h in a 5 M NaOH solution (5 ml), in an oil bath at 60°C and shaken at 120 rpm;
- Soaked for 24 h in a mixed solution 50 mM $CaCl_2$ and 50 mM $SrCl_2$, in an oil bath at 40°C and shaken at 120 rpm;
- Washed and dried as before;
- Heat treated at 600°C for 1 h, with a heating rate of 5°C/min and leaved to cool inside the furnace;
- Immersed in a mixed solution 1M $Sr(NO_3)_2$ and 1 mM $AgNO_3$ at 80°C.

The obtained Ti64 samples will be denoted as Ti64(SrAg).

Due to patent restrictions [3], not all details of the treatment can be disclosed and the process is generally described here. Ti64 disks were treated as follows:

- Gritted with a #400 SiC polishing paper and washed in an ultrasonic bath once with acetone for 5 min and twice for 10 min in MilliQ water and dried under a laminar flow hood;
- Etching of the native oxide in a HF (Sigma Aldrich, St. Louis, USA) solution;
- Soaked in a H_2O_2 solution at 60°C (PanReac AppliChem, Darmstadt, GE).

This kind of specimens will be addressed as Ti64(HF-H_2O_2).

Preparation of the control surfaces

Ti and Ti64 disks were used as control after being mirror polished using subsequent SiC gritting paper (#320, #600, #800, #1000, #2500 and #4000), washed in an ultrasonic bath once with acetone for 5 min and twice for 10 min in MilliQ water and dried under a laminar flow hood (Figure 4.2). Control samples will be simply labeled as Ti and Ti64 respectively. All the samples were stored in closed plastic containers under room conditions.

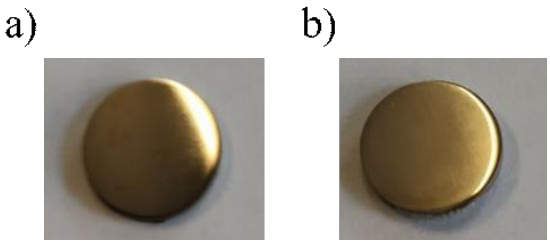

Figure 4.2 Ti (a) and Ti64 (b) samples

4.1.2. Bioactive glass samples preparation

The bioactive glass, called SBA2 and based on silica-systems, was prepared by melting and casting of raw reagents with the following composition (%mol)(all reagents Sigma Aldrich St. Louis, USA): 48% SiO_2, 18% Na_2O, 30% CaO, 3% P_2O_5, 0.43% B_2O_3, 0.57% Al_2O_3 [5]. Oxides and carbonates were pressed in a Pt crucible and melted in a furnace at 1450°C, with an heating rate of 10°C/min and a homogenizing temperature hold at 1450°C for 1 h. For obtaining a bar with diameter of 1 cm, the glass was poured in a bronze mold, preheated at 500°C, annealed at 500°C for 14 h and left cooling naturally in the furnace. The bar was then cut by an automatic cutting machine (IsoMet High Speed Precision Cutter; Buelher, Lake Bluf, USA) in disks 2 mm thick. A smooth surface was obtained by gritting the disks with SiC abrasive disks as follows: #600 for 30 s; #800 for 1 min; #1000 for 2 min. Then the samples were washed for 10 min with an ultrasonic bath with MilliQ water and dried under a laminar flow hood. The glass disk will be referred as SBA2 (Figure 4.3 a).

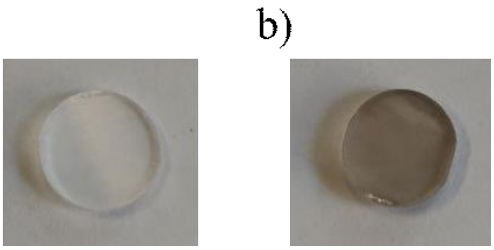

Figure 4.3 SBA2 (a) and AgSBA2 (b) samples

Silver ionic exchange

Silver doping the bioactive glass surface was achieved through an ionic exchange treatment using a silver nitrate solution [6]. SBA2 disks were modified as follows:

- 0.03 $AgNO_3$ (Sigma Aldrich St. Louis, USA) solution was prepared and left stabilizing in an orbital shaker at 37°C and 100 rpm for 30 min in a beaker covered with aluminum foil;
- 20 ml of silver nitrate solution were poured in dark plastic bottles and they are put again in the orbital shaker for 15 min;
- SBA2 disks are put in the bottles and treated for 30 min in the orbital shaker at 37°C and 100 rpm;
- The samples were rinsed with MilliQ water, dried under a laminar flow hood covered with aluminum foil and stored in dark conditions.

The treated glass disks will be referred as AgSBA2 from here on (Figure 4.3 b).

4.1.3. Preparation of the polystyrene samples

Polystyrene square samples, 10x10 mm, were manually cut with an hacksaw from petri dishes for bacterial culture, without any surface activation such as plasma treatments. After cutting, they were washed twice with MilliQ water for 10 min in an ultrasonic bath.

4.2. Proteins

As model proteins for the study of the adsorption mechanisms, albumin and fibronectin from bovine serum have been selected thanks to their relevance in many physiological processes, in particular for being among the most abundant protein in human plasma and being involved in implant osseointegration pathways.

4.2.1. Protein solutions

Bovine serum albumin solution was prepared by dissolving crystallized BSA powder (Sigma Aldrich St. Louis, USA) in phosphate buffered saline (PBS) solution. 0.01 M PBS solution was obtained by dissolving one PBS tablet (Sigma

Aldrich St. Louis, USA) in 200 ml of ultrapure water and stirring upon complete dissolution of the tablet. The solution has a pH of 7.4. Albumin was dissolved in a concertation of 20 mg/ml, which is close to the physiological concentration of the human plasma [7], using a magnetic stirrer. BSA solution was then stored at 4°C and used within few days.

Bovine fibronectin (Sigma Aldrich St. Louis, USA) was received lyophilized and dissolved in PBS, as well as BSA, with a final concentration of 0.2 mg/ml, being similar to the amount of FN in human blood [8]. FN solution was aliquoted and stored at -20°C until usage.

For the adsorption experiments from mixed protein solution, BSA powder was dissolved into thawed FN aliquots in order to obtain a final concentration of 20 mg/ml and 0.2 mg/ml of albumin and fibronectin respectively

4.2.2. Fluorescent protein solutions

For fluorescent quantification and imaging, labeled proteins were purchased. Albumin was obtained in red, tetramethylrhodamine (TMR)-conjugated, and green, Alexa Fluor® 488-conjugated, colour (Invitrogen, Waltham, USA). Labeled BSA was dispersed in PBS to a final concentration of 20 mg/ml, divided into 10 µl aliquots and stored in dark at -20°C till use.

Red colored fibronectin, rodhamine-conjugated (Cytoskeleton, Inc., Denver, USA) was also employed. According to manufacturer instruction, it was firstly dissolved at a concentration of 2 mg/ml and stored at -80°C in 2 µl aliquots. Prior adsorption, the aliquots were thawed and diluted to a final concentration of 0.2 mg/ml.

4.3. Protein adsorption

In order to optimize the adsorption conditions for exploiting at the best all the different techniques that have been employed in this thesis, three different adsorption methodologies have been used. They have been optimized in order to ensure that the adsorption conditions were all the same for the different samples and that the adsorption happened in a similar manner despite the different set up. In particular, that the surface is wetted by the protein solution during all the adsorption and that the amount of proteins in the solution was more than the uptake capacity of the surfaces. Independently of the mode, sample after adsorption will be labeled according to the protein used. When albumin is adsorbed the surface will be addressed with the suffix "_BSA" (e.g. Ti_BSA). In the case of fibronectin, the name of the samples will have the suffix "_FN" (e.g. Ti_FN).

4.3.1. Standard adsorption

For standard adsorption, the surfaces of the samples were completely covered by protein solutions. BSA adsorption was obtained by placing the samples in a 24-well multiwell and soaking them in 1 ml of solution. Due to less FN availability,

for adsorbing fibronectin the samples were put in a humid chamber and a drop of 125 µl of FN solution was casted on them. This volume ensured that all the surface of the different samples was covered and it was enough to avoid evaporation during the process. In both cases, the adsorption was carried out at 37°C for 2 h. After that, the samples were gently rinsed by immersing them three times in ultrapure water, dried under a laminar flow hood and stored at 4°C prior characterization.

4.3.2. Adsorption for Kelvin probe force microscopy

Due to intrinsic characteristic of the technique, the Kelvin probe force microscopy (KPFM) cannot measure the absolute value of the surface potential and, as consequence, the results obtained for two different samples cannot be directly compared. In order to effectively visualize the distribution of the protein on a certain sample, it is therefore necessary to have both a clean area of the surface and a one covered by the protein to be visualized in the same image. This was obtained by adsorbing proteins only on a portion of the surface. To do so, a drop of about 50 µl was deposited on one side of the samples, avoiding to completely cover it (Figure 4.4). Then the samples were incubated in a humid chamber at 37°C for 2 h, rinsed and stored as described before.

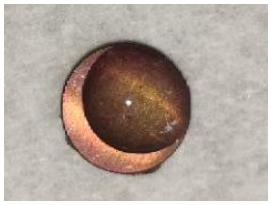

Figure 4.4 Ti64(HF-H_2O_2) with the protein solution drop for KPFM measurement

4.3.3. Adsorption with fluorescent proteins

Fluorescent proteins are available in an extremely limited amount, as consequence it was necessary to limit the amount of solution employed. For fluorescent experiments, 10 µl of solution were dropped on each sample and the surface was covered with a coverslip glass, to ensure the complete spreading of the solution and avoid its drying. The incubation followed as usual. Due to the elevate sensibility of this kind of experiment, it was necessary to perform a more thorough rinse process, in order to eliminate all the loosely bound proteins form the sample surface and obtain reliable results. So, the specimens were rinsed thrice with PBS and thrice with ultrapure water. For the observation, the samples were prepared using a drop aqueous mounting medium (FluoroShield: Sigma-Aldrich, St. Louis, USA) and by putting a coverslip on the top.

4.3.4. Sequential adsorption and co-adsorption from mixed solutions

Sequential adsorptions were obtained by exposing to a protein solution a substrate previously adsorbed with the other protein, i.e. a FN solution for samples

already covered with BSA or vice versa. According to the techniques that can provide information on a layer of mixed proteins, which in our case are the ζ potential, the fluorescent quantification and imaging and water contact angle, the standard adsorption protocol and the protocol for labeled protein adsorption were used. In this case, green BSA and red FN were used. The samples will be referred with the suffix "_BSA-FN" (e.g. Ti_BSA-FN), in case the first protein adsorbed is albumin and the second fibronectin, or with "_FN-BSA" vice versa (e.g. Ti_FN-BSA).

Co-adsorption was investigated only by zeta potential and water contact angle, due some experimental issues noticed with fluorescent quantification in this case. It was performed with the standard adsorption protocol for fibronectin, using instead a mixed protein solution. The suffix used for the samples in this case is "_BSA+FN" (e.g. Ti_BSA+FN).

4.4. Substrate and adsorption characterization

The surface of all the different materials was carefully characterize in order evaluate the different surface properties that may play a role in the formation of the protein transient matrix on the biomaterials. Different techniques were employed to evaluate the surface topography and morphology, chemistry, wettability, surface free energy and its components, the polar and the dispersive ones, and surface charge.

4.4.1. Topography and morphology investigation

The surface of the samples was observed with a field emission scanning electron microscope (FESEM)(Supra™ 40, Zeiss, Oberkochen, Germany). The insulating samples were sputtered with Pt or Cr.

A confocal laser optical profilometer (LSM 900, Zeiss, Oberkochen, Germany) was used to investigate the surface morphology. The height maps collected with the profilometer were elaborated with the software Confomap™ (Zeiss, Oberkochen, Germany). 3D reconstructions of the surface were obtained with z-stacks acquired using a 500x magnification, while morphological parameters were calculated according to the ISO 25178 [9] after acquiring the data with a 200x magnification. According to the ISO standard, a first low pass Fourier filter with cut off wavelength at 2.5 µm was applied to remove the measurement noise and nano-roughness. Then, a high pass Fourier filter was applied to remove the waviness. The critical wavelength cut off depends on the average roughness (S_a) of the surface, being 0.8 mm for a S_a value between 0.1 and 2 µm, or 0.25 for a S_a between 0.02 and 0.1 µm. The calculation of the roughness parameters was carried out in triplicate for each sample, and presented here as average ± standard deviation.

4.4.2. Surface chemical composition

The chemical composition of all the samples was determined with XPS analysis (XPS, PHI 5000 Versaprobe II, ULVAC-PHI, Inc., Kanagawa, Japan). The X-ray source was of Al-K and the take off angle was set at 45°. The survey spectra were collected at an energy step of 1 eV. In order to understand which functional groups are bored on the surfaces, high resolution spectra were collected in different energy regions, according to the element of interest of the particular sample. C1s, O1s and N1s were investigated for all surfaces, being relevant as control for sequent adsorption studies, Ti2p was analyzed on titanium based materials and Ag3d on Ti64(SrAg) and AgSBA2 surfaces. The high resolution spectra were collected with an energy step of 0.1 eV. In order to compensate charging effect, all the spectra were corrected by centering the C1s peaks, relative to hydrocarbon C-C and C-H bonds, at a binding energy (BE) of 284.8 ± 0.1 eV [2]. Deconvolution of the element peaks was performed using the software CasaXPS with mixed Gaussian-Lorentzian (70-30%) curves and applying a background calculated by the Shirley methods for all elements but nitrogen. For the N1s peaks a linear background was used [10].

4.4.3. Wettability and surface free energy

The calculation of the surface free energy and its polar and dispersive components was made by measuring the contact angle of water, hexadecane and ethylene glycol (Sigma Aldrich, St. Louis, USA) by the sessile drop technique (FTA 1000C; First Ten Ångstroms, Newark, USA). The measurement was repeated three times on each surface.

The Owens-Wendt method was employed to calculate the total SFE, γ, and the γ^p and γ^d components of the different surfaces according to the following equations [11]:

$$\gamma = \gamma^d + \gamma^p \tag{4.1}$$

$$(\gamma^d)^{0.5} = \frac{\gamma_h(cos\Theta_h + 1) - \sqrt{(\gamma_h^p/\gamma_w^p)}\gamma_w(cos\Theta_w + 1)}{2(\sqrt{(\gamma_h^d} - \sqrt{(\gamma_h^p(\gamma_h^p/\gamma_w^p))}} \tag{4.2}$$

$$(\gamma^p)^{0.5} = \frac{\gamma_w(cos\Theta_w + 1) - 2\sqrt{\gamma^d/\gamma_w^d}}{2\sqrt{\gamma_w^p}} \tag{4.3}$$

Where γ_h, γ_h^p and γ_h^d are the total SFE, the polar and dispersive components of hexadecane respectively; γ_w, γ_w^p and γ_w^d are the total SFE, the polar and dispersive components of water respectively; Θ_h is the contact angle of hexadecane on the surface; Θ_w is the water contact angle on the surface.

4.4.4. Solid surface ζ potential

ζ potential vs pH titration curves were obtained by electrokinetic measurement on the surface of bulk samples.

The experiments were carried out using an elecrokinetic analyzer (SurPASS, Anton Paar, Gratz, Austria) equipped with an adjustable gap cell and an automatic titration unit. A pair of specimens are mounted on the cells and the measure is performed by fluxing the electrolyte, which is KCl 1 mM, at different pH. Acidic and basic titration were achieved using 0.05 M HCl and NaOH respectively, and 15 point were measured in each range. The two part of the curves were obtained in separate measurement. For reactive samples, such as SBA2 and AgSBA2, two different pairs were used, one for each range, to avoid changes in the zeta potential due to reaction at aggressive pH.

The ζ potential value is calculated at each pH by measuring the streaming current, I_{str}, at the cell ends and applying the Helmholtz-Smoluchowski equation [12]:

$$\zeta = \frac{dI_{str}}{d\Delta P} \cdot \frac{\eta}{\varepsilon \cdot \varepsilon_0} \cdot \frac{L}{A} \tag{4.4}$$

Where ΔP is the pressure variation at the ends of the cell; η is the viscosity and $\varepsilon \cdot \varepsilon_0$ is the dielectric coefficient of the electrolyte; L is the gap in the cell and A the area of the samples.

The IEP of the material is calculated at the intersection of the curve with the X axis, while the onsets, basic or acid, were obtained when possible by calculating the intersection point between a horizontal line at the value of the plateau and the tangent line in the linear range of the curve, around the IEP.

4.5. Protein adsorption characterization

Albumin and fibronectin adsorption were investigated on all surfaces, focusing on the main properties of the adsorbed layer, such as amount of protein bounded on the surface, extension and distribution of the transient matrix and orientation and conformation of the proteins after adsorption. In order to do so, methods that are well established in literature were combined with techniques adapted for the aim of this research or developed during this work.

4.5.1. Quantification of the adsorbed protein Bicinchoninic acid assay

The BCA test is a colorimetric assay that allows the quantification of proteins in solution. The assay is based on the combination of biuret reaction, which is the reduction of copper Cu^{2+} to Cu^{+} by proteins in alkaline medium, and the subsequent chelation of reduced ions by four molecules of bicinchoninic acid, giving birth to the intense purple color. The intensity of the color, quantified by its absorbance at 562 nm, is proportional to the concentration of the protein in solution, which can be measured by using a proper calibration curve. Since the number of reduced ions for protein is strictly dependent on the primary structure of the polypeptide, in particular on the presence of cysteine, cystine, tryptophan and tyrosine residues [13], reliable and accurate quantification data can be obtained if the calibration

curves is done by using standards of the same protein that would like to be quantified. For this reason, BCA assay was performed only after BSA adsorption and not after FN adsorption. The manufacturer of the kit provides BSA standard solutions to build the calibration curve, but albumin and fibronectin are too different to be quantified using the same standard and FN was not available in amount sufficient for obtaining a dedicated calibration curve.

The experimental measures on samples after BSA adsorption were performed according to the following protocol. Firstly, the adsorbed proteins were detached from the surface with sodium dodecyl phosphate 2% vol (SDS)(Fisher Scientific Hampton, USA) by immersing the samples in 300 µl of the surfactant for 2 h at 37°C. The amount of albumin adsorbed on the surface was expected to range from less than 1 µg to few µg [14,15], which is out of the measuring range for the BCA kit employed (Pierce™ BCA Protein Assay Kit; Thermo Fisher Scientific, Waltham, USA), so the standard protocol was properly modified by calculating the calibration standard curve in the range 0-80 µg of BSA, with a particular focus on the range 0-10 µg.

Fluorescent protein quantification

Adsorbed proteins were quantified also by using fluorescent-labeled albumin and fibronectin. After being properly mounted, the fluorescent signal of the labeled proteins on the different surfaces was quantified using a ChemiDoc MP system (Biorad, Hercules, USA). This instrument is capable of exploiting both chemiluminescence and fluorescence to perform quantitative analysis. Images were taken using the proper filter according to the protein used, by the Rhodamine application (excitation source: red epi illumination; emission filter: 602/50 nm) for red proteins and by the Alexa488 (excitation source: green epi illumination; emission filter: 520/545 nm) for green proteins. The signal was quantified over the same area on each sample. Triplicates were used for every substrate.

Due to the intrinsic nature of this techniques, the obtained results are not absolutely quantitative but relatively quantitative, allowing comparison between samples analyzed at the same time. Imaging area of the system and technical experimental limitations made impossible to observe at the same time all the eight surfaces with both albumin and fibronectin. Therefore, it was chosen to quantify simultaneously all the surface adsorbed with the same protein. As consequence, it is possible to discuss about the amount of BSA or FN adsorbed on the different surfaces, but not to compare the amount of the two protein in the same sample.

4.5.2. XPS analysis of samples after adsorption

XPS analysis were performed also on surfaces after protein adsorption, as described in section 4.4.2. Through the increment of nitrogen, it was possible to detect the protein bounded with the surface, since N is highly present in the protein composition and almost absent in environmental contamination, contrary with respect to carbon. In order to gain information about the functional groups of the

proteins after adsorption, deconvolution of the C1s and N1s core peaks was also performed. XPS was also performed on BSA powder to obtain reference spectra for the C1s, O1s and N1s region. Unfortunately, FN is not available in a suitable form, as powder, for performing XPS. Since the type of bonds in proteins are always the same, they just change in concentration, BSA peaks were used as reference also for FN.

4.5.3. Imaging of the adsorbed protein layer

Fluorescent microscopy

Direct imaging of the protein layer was obtained by fluorescent microscopy. Pictures were obtained by using the optical profilometer (LSM900) in the optical microscope operation mode. The images were acquired by using a Xe lamp as a light source and a red filter (excitation wavelength 540 – 562 nm; beamsplitter 560 nm; emission wavelength 515 – 565 nm) and a green filter (excitation wavelength 450 - 490 nm; beamsplitter 510 nm; emission wavelength 515 – 565 nm), for imaging TMR-labeled proteins or AlexaFluor-conjugated proteins respectively. This kind of analysis is purely qualitative and it wants to show the distribution of the proteins on the surface of biomaterials. To obtain the best results, the images have been postprocessed.

Kelvin probe force microscopy

The Kelvin probe force microscopy is a technique that belong to the atomic force microscopy family and it allows to obtain simultaneously a topographical image and a representation of the distribution of the surface potential. The measurements were performed in amplitude modulation mode (AM-KPFM), which based on a double scansion of the surface: the forward scan, performed in tapping mode, is used to acquire the topography of the surface; the backward scan, performed in lift mode, adjusted thanks to the topographical information, allows the determination of the surface potential. In the KPFM set up, the sample and the conductive AFM tip are put in electrical contact: as consequence, when the tip is moved close to the surface, an electrostatic potential difference, the contact potential difference (CDP), V_{CPD}, and a force are generated between the sample and the tip. The V_{CPD} is proportional to the difference between the work function, ϕ, or the surface charge for semiconductors and insulators, of the sample and the tip [16]:

$$V_{CPD} = \frac{\Phi_{tip} - \phi_{sample}}{-e} \tag{4.5}$$

The V_{CPD} can be measured by nullifying the electrostatic forces between the samples and the tip applying a DC external bias, V_{DC}, to the system. When the forces are equal to zero, the V_{DC} is equal to the V_{CPD}. In the backward scan, oscillating electrostatic forces are generated by applying an AC bias, V_{AC}, to the system, caused by the CPD, which can be nullified thanks to a V_{DC}. A lock-in amplifier is used to extract the frequency component of the electrostatic force,

which is proportional to the V_{CPD}, by measuring the oscillation of the cantilever thanks to a laser and a position sensitive detector. A feedback controller applies the V_{DC} in order to minimize the lock-in amplifier signal, resulting in the measure of the surface potential of the sample [17]. A scheme of the instrument is reported in Figure 4.5.

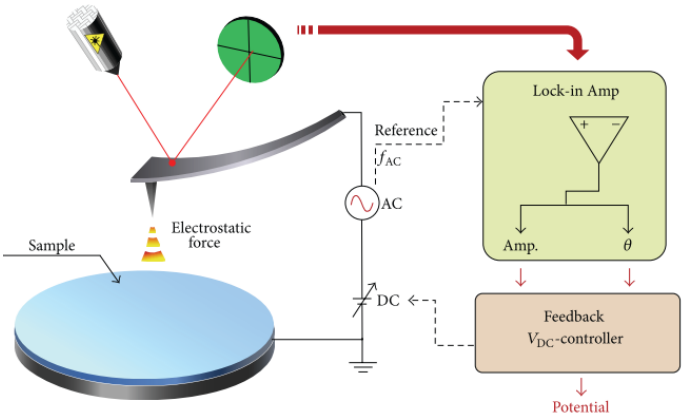

Figure 4.5 Scheme of a KPFM measuring system [17]

KPFM measurement were performed on samples prepared as described in section x.3.2, using a Innova AFM (Bruker, Billerica, USA) and conductive tips, made of Sb-doped silicon (SCM-PIT-V2, Bruker, Billerica, USA), or made of conductive diamond (AD-2.8-AS, ADAMA, Dublin, Ireland). The measuring parameters, such as scanning speed, lift height, KPFM parameters, were adjusted each measure to obtain the best results. The BSA and FN layers were imaged at the border of the area adsorbed with proteins using large 100x100 µm scans. The distribution of the proteins was also investigated at a smaller scale by acquiring images in the center of the area covered by the protein solution. All the samples were analyzed in air after drying. The acquired data were elaborated with the Gwyddion software [18]. It was possible to image all the samples but the polystyrene, due to a too elevate accumulation of charges on the surface that interfered with the measurement.

4.5.4. Protein conformation and orientation

Surface enhanced Raman Scattering by drop casting of AgNPs

Raman spectroscopy was thought to be a suitable candidate for investigating protein secondary structure as complementary technique for ATR-FTIR. In order to increase the sensibility of the measure and to detect the protein on the surfaces of the materials, a new investigation method was developed, exploiting the SERS effect of silver nanoparticle colloids deposited by drop casting on the sample surfaces.

AgNPs preparation

AgNPs with nominal diameter of 30 nm were prepare using a seeding-growth procedure, which consist into synthesize 4 nm particles and then increase their dimensions [19]. Briefly, 20 ml of citrate solution 1% (w/v) were added to 75 ml of water and heated at 70°C in an oil bath for 15 min. Then 1.7 ml of $AgNO_3$ solution 1% (w/v) were added to the solution, with the subsequent quick addition of 2 ml of $NaBH_4$ 0.1% (w/v) ice-cooled solution. The mixture was kept at 70°C for 1 h under vigorous stirring, then cooled down to room temperature and topped up to 100 ml with water. These NPs were used as seeds to obtain 30 nm AgNPs as follows. 2 ml of 1% citrate solution were added to 70 ml of water and heated to the boiling point for 15 min. Then, 10 ml of 4 nm AgNPs solution were added under vigorous stirring. 1.7 ml of 1% $AgNO_3$ solution were subsequently added and the solution was vigorously stirred for 1 h. After, 2 ml of 1% citrate solution and 1.7 ml of 1% silver nitrate solution were added to the mixture and kept under stirring for another hour. This last step was repeated. At the end, the NPs colloid was cooled down and the total volume brought to 100 ml with water.

SERS measurements

Samples for SERS analysis were prepared by drop casting 10 µl of AgNPs colloid, which was left drying in air. Spectra in the range of 50 cm^{-1} to 3400 cm^{-1} were collected with a Raman imaging DXR-Xi apparel (Thermo Fisher, Waltham, USA) equipped with a 532 nm excitation laser operated at 1 mW power and a charge-coupled device (CCD) detector. Maps were collected on an area of 500x500 µm, with a resolution of 25 µm, using a 10x objective, a rectangular aperture of 50 µm, 0.01 Hz collection frequencies and 10 acquisition on each pixel. The resulting spectrum was obtained by averaging all the spectra in the entire map. Reference spectra for the native proteins were collected on pure albumin and fibronectin thick layer deposited on a microscope glass. Spectra of denatured proteins were also collected after thermal denaturation of BSA and FN at 100°C for 1 h. Denatured proteins will be labeled as BSA_h and FN_h.

The interaction between protein and Ag-NPs was also evaluated to avoid artifacts and misinterpretation of the results. Albumin was used as protein model SERS spectra of 1:1 mixed colloid and BSA solution (20 mg/ml) were obtained using an accessory for liquid measurement and a quartz cuvette. UV-Vis absorbance was also used to assess the interaction between albumin and nanoparticles.

All the surface after albumin adsorption were investigated and, due to the unsatisfactory results on certain substrates, only Ti, Ti64 and Ti64(HF-H_2O_2) were analyzed after FN adsorption.

Attenuated Total Reflection FTIR

ATR micro-FTIR was used to investigate the presence of proteins on the surfaces of the samples and their secondary structures. Measurements were performed using a micro-FTIR (Nicolet iN10 Infrared Microscope, Thermo Fischer Scientific, Waltham USA) equipped with ATR Se/Ge crystal tip and a nitrogen cooled MCT (mercury-cadmium-tellurium) detector. The spectra were collected in the rage 700-4000 cm^{-1} with a resolution of 4 cm^{-1} and the background spectra was collected in air before each measurement. 64 scans were performed for each spectrum and three spectra were collected for each sample, in different areas. Before plotting, the collected spectra were averaged. Secondary structures were determined by deconvolution of the Amide I band (1640-1680 cm^{-1}), which is highly conformation sensitive [20]. It was performed with Thermo Scientific Peake Resolve in the OMNIC software, using the Savitsky-Golay second derivative minima identification, using a Voigt function for peak shape. Baseline correction was performed using a linear function. The spectral range considered was in the range of 1750-1350 cm^{-1} to include all the protein signal, but bands were assigned only for the Amide I peak. ATR-FTIR analysis were performed on all the samples after adsorption of BSA and FN but PS, due to intrinsic organic signals that strongly interfere with the protein typical peaks. Spectra were collected also on pure and denatured proteins

ζ potential after protein adsorption

Zeta potential titration curves were obtained on samples after single protein adsorption, after sequential adsorption and after adsorption from mixed protein solutions as described in paragraph 4.4.4. A new pair of samples was used for each titration range, since proteins can detach or be denatured by the flux or the very acid or basic pH of the electrolyte solution. In order to better understand and comment the potential titration curves, XPS analysis were performed on samples after the acidic titration range, which is believed to be the harsher condition for the protein layer on the samples, possibly resulting in detachment of the proteins or their denaturation.

ζ potential of protein in solution

The zeta potential of native proteins in solution was obtained using a dynamic light scattering (DLS) instrument (Ltesizer 500, Anton Paar, Gratz, Austria). Protein solution were prepared by firstly dissolving BSA and FN in PBS, at concentration of 35 mg/ml and 0.2 mg/ml respectively. Then they were further diluted in 1 mM KCl until the final concentration of 5 mg/ml for BSA and 0.01 mg/ml for FN. The zeta potential vs pH curves were obtained by manually titrating the solution at pH of 2.5, 3, 3.5, 4, 5, 6, 7, 8, 9 using 0.05 M NaOH and HCl. Zeta potential of thermally denatured BSA was also measured by heating the protein

solution just below the boiling point for 1 h. Then the measure was performed as in the other cases

4.5.5. Protein effect on surface bioactivity

Bioactivity of Ti64(HF-H_2O_2) surface was tested in presence of proteins. Samples were immersed in simulated body fluid (SBF) solution prepared using the protocol by Kokubo [21], with or without BSA. Albumin was dissolved in SBF with a concentration of 20 mg/ml, the modified solution will be addressed as SBF+BSA. Prior use, the solutions were filtered with a 0.2 µm. The samples were soaked in 25 ml of SBF or SBF+BSA in dark polyethylene bottles, for 1, 3, 7 or 14 days. For the soaking at 14 d, the solution was refreshed at 7 d. The experiment was conducted in triplicate. After being removed from the solutions, the samples were gently rinsed, dried and stored at 4°C.

The precipitation of hydroxyapatite on the samples was investigated by FESEM equipped with energy dispersive spectroscopy (EDS).

4.5.6. Investigation of the osteoimmunomodulation of biomaterials

THP-1 culture and differentiation

As model for immune cells, monocyte-derived macrophages were chosen. Human monocyte cell lines THP-1 (ATCC, Manassas, USA), was grown in suspension in T-75 flasks, using RMPI-1640 medium (ATCC, Manassas, USA) supplemented with 10% FBS (Sigma Aldrich St. Louis, USA) and 1% of penicillin-streptomicin (Sigma Aldrich St. Louis, USA). Macrophages differentiation was stimulated by phorbol 12-myrisate-13-acetate (PMA)(Sigma Aldrich St. Louis, USA). Specifically, $2x10^5$ cells/ml were cultured for 48 h into T-75 flasks with 100 ng/ml of PMA. Subsequently, the stimulation medium was replaced with fresh supplemented RPMI-1640 medium and the differentiated cells were incubated for 48 h more. Prior seeding on samples, cells were detached by using Acutase (Sigma Aldrich St. Louis, USA).

Cell seeding on titanium samples

For the evaluation of osteoimmunomodulation properties, three different surfaces have been chosen: Ti64, Ti64(SrAg) and Ti64(HF-H_2O_2). In order to allows attachment of differentiated THP-1, $2x10^5$ cells were seeded in 75 µl of complete medium on the surface of the samples, placed in a 24-well plate, for 4 h. After that, 1 ml of full medium was added.

MTT viability assay

Cell viability was assessed by MTT assay (Sigma Aldrich St. Louis, USA) performed at 3 and 7 days from the seeding. The test was performed as follows:

after medium removal, the samples were incubated for 3 h in 0.5 mg/ml of MTT, dissolved in complete medium; subsequently, the reagent was removed and formazan salts were dissolved using dimethyl sulfoxide. The optical density (OD) was red at a wavelength of 570 nm and 650 nm (reference) using the Synergy. HTX Multi-Mode Microplate Reader (BioTek, Winooski, VM, USA). The bottom of a plastic well was used as control (CTRL) surface. Each sample was measured in triplicate.

Cell staining

The morphology of cultured THP-1 derived macrophages was assessed by staining the cytoskeleton and the nuclei respectively with phalloidin–Tetramethylrhodamine B isothiocyanate and 4′,6-Diamidino-2-phenylindole dihydrochloride (DAPI)(Sigma Aldrich St. Louis, USA) at 3 and 7 days after cell seeding. Samples were washed with PBS and fixed in 4% paraformaldehyde. Before staining, samples were washed with PBS and then they were incubated in Phalloidin 0.25 μM for 30 minutes. After a further washing with PBS, samples were again incubated in DAPI at the concentration of 0.3 μM for 10 minutes.

Fluorescent microscopy observations on stained samples were performed with the LSM-900 in fluorescent configuration.

Evaluation macrophages response to titanium biomaterials

The inflammatory response of macrophages to the different surfaces was evaluated by investigating the growth factors and cytokines released in the culture medium after 3 days and 7 days. 27 cytokines and growth factors were detected and quantified simultaneously using a multiplex immunoassay, the Bio-Plex Pro Human Cytokine 27-plex assay (BioRad, Hercules, USA). The molecules investigated were: EOTAXIN; Fibroblast Growth Factor-Basic, FGF-basic; Granulocyte colony-stimulating factor/colony-stimulating factor 3, G-CSF; Granulocyte-macrophage colony-stimulating factor/colony-stimulating factor 2, GM-CSF; IFN-γ; IL-1β; IL-1rα; IL-2; IL-4; IL-5; IL-6; IL-7; IL-8; IL-9; IL-10; IL-12(p70); IL-13; IL-15; IL-17°; Interferon gamma-induced protein 10, IP-10; Monocyte chemotactic protein 1/monocyte chemotatic activating factor, MCP-1 (MCAF); Macrophage Inflammatory Protein 1α, MIP-1α; MIP-1β; Platelet Derived Growth Factor BB, PDGF-BB; RANTES; TNF-α; and Vascular endothelial growth factor, VEGF.

300 μl of conditioned medium were stored at -80°C and delivered to the company for performing the analysis with the multiplex assay. The experiment was run in duplicate and for each experiment biological triplicate of each surface were used.

4.5.7. Statistical analysis

When necessary, the statistical significance between data was calculated by applying Student t test and calculating the p-values. Significance was set to a p-value lower than 0.05.

4.6. Bibliography

[1] D.K. Pattanayak, S. Yamaguchi, T. Matsushita, T. Kokubo, Effect of heat treatments on apatite-forming ability of NaOH- and HCl-treated titanium metal, J. Mater. Sci. Mater. Med. 22 (2011) 273–278. https://doi.org/10.1007/s10856-010-4218-y.

[2] S. Ferraris, S. Yamaguchi, N. Barbani, M. Cazzola, C. Cristallini, M. Miola, E. Vernè, S. Spriano, Bioactive materials: In vitro investigation of different mechanisms of hydroxyapatite precipitation, Acta Biomater. 102 (2019) 468–480. https://doi.org/10.1016/j.actbio.2019.11.024.

[3] S. Spriano, E. Verne, S. Ferraris, Multifunctional titanium surfaces for bone integration, EP 2 214 732 B1, 2007.

[4] S. Yamaguchi, P.T. Minh Le, M. Ito, S.A. Shintani, H. Takadama, Tri-functional calcium-deficient calcium titanate coating on titanium metal by chemical and heat treatment, Coatings. 9 (2019). https://doi.org/10.3390/coatings9090561.

[5] M. Miola, G. Fucale, G. Maina, E. Verné, Composites bone cements with different viscosities loaded with a bioactive and antibacterial glass, J. Mater. Sci. 52 (2017) 5133–5146. https://doi.org/10.1007/s10853-017-0750-1.

[6] M. Miola, G. Fucale, G. Maina, E. Verné, Antibacterial and bioactive composite bone cements containing surface silver-doped glass particles, Biomed. Mater. 10 (2015). https://doi.org/10.1088/1748-6041/10/5/055014.

[7] A.M. Merlot, D.S. Kalinowski, D.R. Richardson, Unraveling the mysteries of serum albumin-more than just a serum protein, Front. Physiol. 5 AUG (2014) 1–7. https://doi.org/10.3389/fphys.2014.00299.

[8] E. Österlund, The secondary structure of human plasma fibronectin: conformational changes induced by acidic pH and elevated temperatures; a circular dichroic study, Biochim. Biophys. Acta (BBA)/Protein Struct. Mol. 955 (1988) 330–336. https://doi.org/10.1016/0167-4838(88)90212-9.

[9] Geneva: International Organization for Standardization, ISO 25178-2:2012 BSI Standards Publication Geometrical product specifications (GPS). Surface texture. Areal. Terms, definitions and surface texture parameters, 2012.

[10] J.S. Stevens, A.C. De Luca, M. Pelendritis, G. Terenghi, S. Downes, S.L.M. Schroeder, Quantitative analysis of complex amino acids and RGD peptides by X-ray photoelectron spectroscopy (XPS), Surf. Interface Anal. 45 (2013) 1238–1246. https://doi.org/10.1002/sia.5261.

[11] A. Rudawska, E. Jacniacka, Analysis for determining surface free

energy uncertainty by the Owen–Wendt method, Int. J. Adhes. Adhes. 29 (2009) 451–457. https://doi.org/10.1016/j.ijadhadh.2008.09.008.
[12] T. Luxbacher, The zeta potential for solid surface analysis, Anton Paar GmbH, 2014.
[13] Pierce, BCA Protein Assay Kit 23225, (2020) 0–3.
[14] H.M.W. Uyen, J.M. Schakenraad, J. Sjollema, J. Noordmans, W.L. Jongebloed, I. Stokroos, H.J. Busscher, Amount and surface structure of albumin adsorbed to solid substrata with different wettabilities in a parallel plate flow cell, J. Biomed. Mater. Res. 24 (1990) 1599–1614. https://doi.org/10.1002/jbm.820241205.
[15] D.M. Togashi, A.G. Ryder, G. Heiss, Quantifying adsorbed protein on surfaces using confocal fluorescence microscopy, Colloids Surfaces B Biointerfaces. 72 (2009) 219–229. https://doi.org/10.1016/j.colsurfb.2009.04.007.
[16] W. Melitz, J. Shen, A.C. Kummel, S. Lee, Kelvin probe force microscopy and its application, Surf. Sci. Rep. 66 (2011) 1–27. https://doi.org/10.1016/j.surfrep.2010.10.001.
[17] H. Lee, W. Lee, J.H. Lee, D.S. Yoon, Surface potential analysis of nanoscale biomaterials and devices using Kelvin probe force microscopy, J. Nanomater. 2016 (2016). https://doi.org/10.1155/2016/4209130.
[18] D. Nečas, P. Klapetek, Gwyddion: an open-source software for SPM data analysis, Open Phys. 10 (2012) 181–188. https://doi.org/10.2478/s11534-011-0096-2.
[19] L. Mandrile, I. Cagnasso, L. Berta, A.M. Giovannozzi, M. Petrozziello, F. Pellegrino, A. Asproudi, F. Durbiano, A.M. Rossi, Direct quantification of sulfur dioxide in wine by Surface Enhanced Raman Spectroscopy, (2020). https://doi.org/10.1016/j.foodchem.2020.127009.
[20] A. Barth, Infrared spectroscopy of proteins, Biochim. Biophys. Acta - Bioenerg. 1767 (2007) 1073–1101. https://doi.org/10.1016/j.bbabio.2007.06.004.
[21] T. Kokubo, H. Takadama, How useful is SBF in predicting in vivo bone bioactivity?, Biomaterials. 27 (2006) 2907–2915. https://doi.org/10.1016/j.biomaterials.2006.01.017.

Chapter 5

Results and Discussion

5.1. Substrate characterization

Protein adsorption is deeply affected by the surface properties of the biomaterial. Morphology, wettability, zeta potential and surface functional groups can completely change the transient protein matrix [1]. The first step of this work was to thoroughly characterize the investigated substrates with respect to the aforementioned properties.

5.1.1. Substrate topography

Surface topography was evaluated by FESEM at different magnification, the images are reported in Figure 5.1. Ti and Ti64 have similar featureless surfaces with the signs of the polishing process. At low magnification, the samples are flat, while at higher magnification the defects induced by the gritting SiC particles are visible. The chemical treatments introduce more interesting features on the surface of titanium samples. At low magnification (Figure 5.1), all the three modified surfaces show a similar topography, mainly characterized by the grooves left by the quite rough #400 polishing paper. Their differences can be appreciated at higher enlargement. Ti(A-HC-H) and Ti64(SrAg) have a similar oxide layer, that is characterized by a very opened structure, with highly interconnected pores formed by a web of filamentous-like oxide (Figure 5.1). The pores on the treated pure titanium seems larger than on the treated titanium alloy, with the former ranging between about 500 and 650 nm and the latter being in the range of about 250 to 450 nm. The surface of Ti64(HF-H_2O_2) is more compact and is hierarchically structured. At medium magnification, the surface appears covered by globular structures, which are the grains of the β-phase. In fact, β-phase Ti is less sensible to the HF etching with respect to the α-phase, therefore β-grains can emerge from the surface. At higher magnification (Figure 5.1), it is possible to observe the nanotopography obtained by this treatment, which is a sort of nano-sponge that

covers both α and β-grains, with pores around 100 nm. As published in other works, the oxide layer of Ti(a-HC-H) and Ti64(SrAg) maintains its filamentous structure through all the thickness, which is about 1 µm, while the Ti64(HF-H_2O_2) spongeous layer is just about 400 nm thick [2,3].

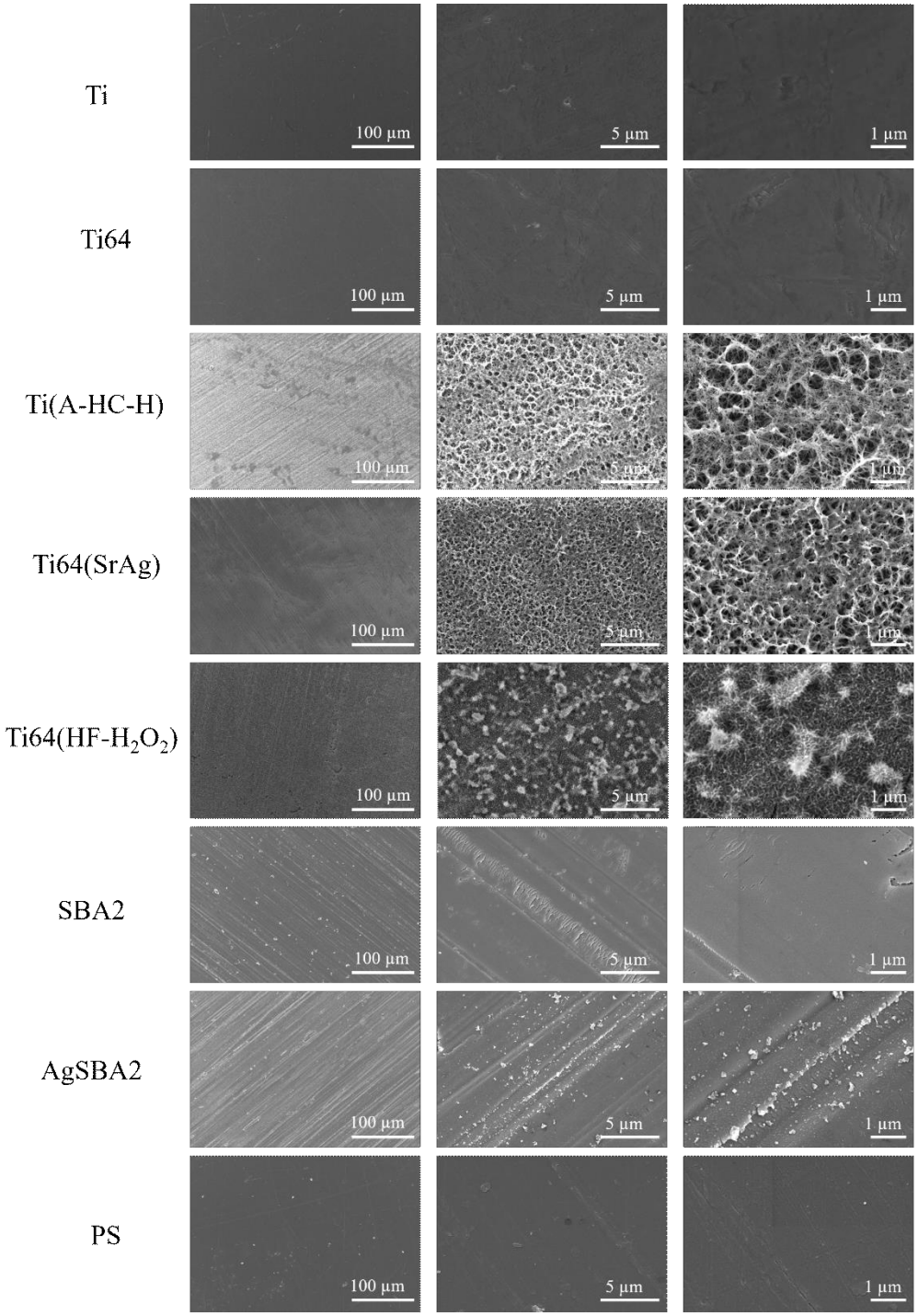

Figure 5.1 FESEM images of the substrates at different magnifications: a) 1000x; b) 20000x; c) 60000x.

The bioactive glasses also show a similar topography. The main features are the gritting scratches, well visible at low magnification (Figure 5.1). The polishing process has caused the formation of some small cracks on the glass surface, as shown in high magnification images. On AgSBA2, it was noticed the presence of

small silver precipitates, as confirmed by EDS analysis. It is possible that some silver particles are formed during the ion-exchange process, giving rise to the metallic signal in the XPS spectra of the ASBA2 glass that will be presented in paragraph 1.1.3.

The PS surface is mostly flat and featureless, with some imperfections that are visible at high magnification (Figure 5.1).

5.1.2. Substrate morphology

The surfaces were studied by evaluating different roughness parameter according to the ISO 25178. In Table 5.1 some of the different roughness parameters evaluated for the surfaces are reported. In particular, they are:

- Average roughness, S_a: arithmetic mean of the distance from the average line of the surface;
- Root mean square roughness, S_p: root mean square value of the distance from the average line of the surface;
- Skewness, S_{sk}: indicates the asymmetry of the probability density function (PDF) of the surface. Values above 0 are typical for asymmetry over the average line, meaning a predominance of peaks; values lower than 0, on the other hand, are typical of surfaces with more valleys than peaks, with a PDF showing a tail below the average line;
- Kurtosis, S_{ku}: indicates the width of the PDF: S_{ku} over 3 result from a narrow PDF, due to surfaces with sharp features; Kurtosis values lower than 3 derives form a wide PDF, due to large features on the surface;
- Developed area, A_s: is the real area of the samples, as result of the area increase due to the surface features with respect to the projected area, A_p.

In Table 5.1, the roughness parameter for Ti64 after gritting with #400 SiC paper is also reported, to evaluate the effect on the morphology of the surface treatment. Pure titanium disks have the same type of morphology after #400 grit and the data are not reported.

As possible to see, the titanium-based surfaces have very different roughness values and the chemical treatments increase the irregularity of the surface. Ti and Ti64 polished surfaces have a very low roughness, both S_a and S_q, as expected from the gritting process. These surfaces are characterized by the narrow lines left from the abrasive papers (Figure 5.2a-b), resulting in a Skewness lower than 0 and $S_{ku} >$ 3. The PDFs are almost gaussian-shaped, with small tails below the average line due to the grooves. Also, the Abbot-Fireston curves, which are the representation of the cumulative probability density function (CPDF), are mostly symmetric with a narrow range between the minima and the maxima, indicating the flatness of the surface themselves. The S_q/S_a ratio correlate with the S_{ku}, in fact a ratio close to 1.25 corresponds to sharp features on the surfaces [4]. For Ti and Ti64 samples, these ratios confirm that the surfaces are very regular.

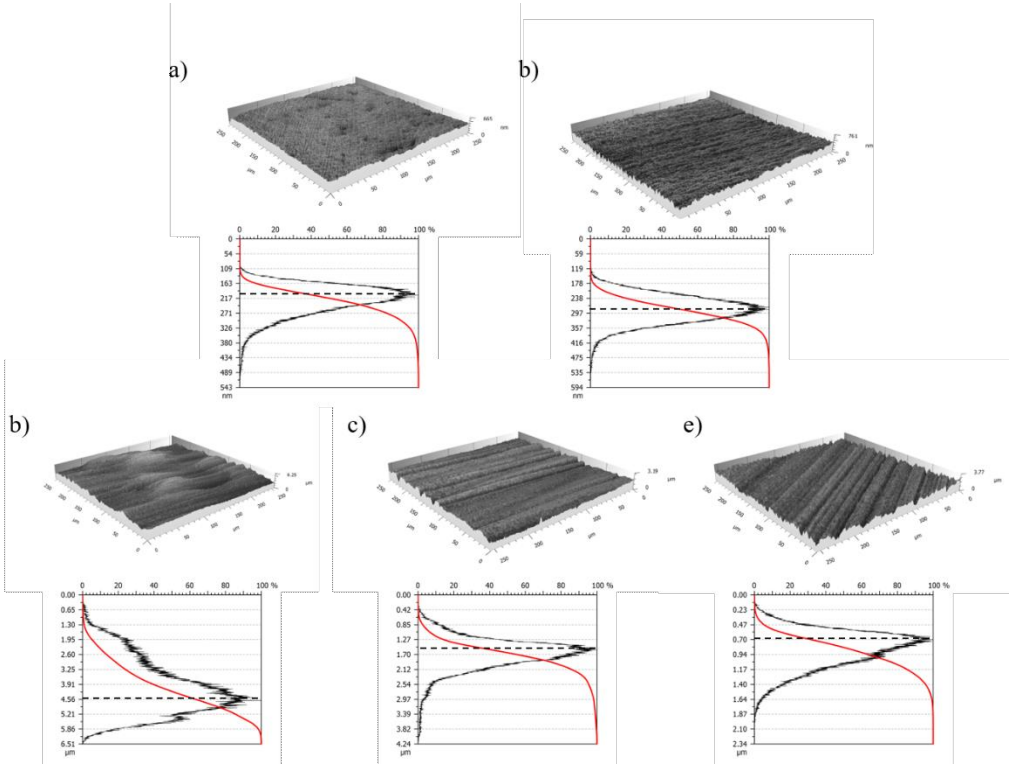

Figure 5.2 3D reconstruction image of titanium surfaces and graph showing the corresponding probability density function (black line) and Abbot-Firestone curve (red line), the abscissa 0 is set at the highest point of the surface and the axis is directed downward, inside the surface: a) Ti; b) Ti64; c) Ti(A-HC-H); d) Ti64(SrAg); e) Ti64(HF-H_2O_2). The average line of the surface is represented by horizontal dashed lines in the graphs.

Table 5.1 Roughness parameters of all the substrates investigated in this work (reported as average ± standard deviation).

	Ti	Ti64	Ti64 #400	Ti(A-HC-H)	Ti64(SrAg)	Ti64(F-H_2O_2)	SBA2	AgSBA2	PS
S_q (µm)	0.05±0.01	0.05±0.01	0.22±0.04	0.96± 0.21	0.48±0.10	0.25±0.03	0.05±0.01	0.07±0.02	0.03±0.00
S_a (µm)	0.03±0.01	0.04±0.01	0.17±0.03	0.77± 0.18	0.36±0.08	0.12±0.02	0.07±0.01	0.09±0.03	0.02±0.00
S_{sk}	-0.76±0.14	-0.49±0.27	-0.79±0.28	0.51± 0.09	-0.83±0.12	-0.56±0.22	-0.51±0.14	-0.48±0.17	-
S_{ku}	5.99±1.92	3.16±0.46	4.61±0.89	3.236±0.141	5.356±0.387	5.646±2.865	3.67±0.65	3.95±1.28	-
S_q/S_a	1.36±0.04	1.26±0.01	1.29±0.05	1.26± 0.02	1.35±0.05	1.28±0.03	1.27±0.01	1.27±0.02	1.50±0.00
A_s/A_p	1.000±0.000	1.000±0.000	1.003±0.001	1.009± 0.002	1.010±0.002	1.006±0.002	1.001±0.0001	1.000±0.000	1.000±0.000

Surface roughness is increased for every sample after surface treatments, with respect to titanium gritted with #400 SiC paper. The roughest surface is the Ti(A-HC-H) one, followed by Ti64(SrAg) and the flattest among the treated samples is the Ti64(HF-H_2O_2). The heat treatments that are performed on Ti(A-HC-H) and TI64(SrAg) makes the oxide layer grew more than what happens during the hydrothermal treatment on Ti64(HF-H_2O_2), in fact the thickness of the final oxide layer is about 1 µm for the former two surfaces and just 400 nm for the latter [2,3]. The difference in the oxide thickness may account for the different roughness in first place, with a role in reducing the final roughness played also by the HF etching on Ti64(HF-H_2O_2). The higher roughness of the Ti(A-HC-H) may be due also to the formation of bulges, as possible to see on the 3D reconstruction in Figure 5.2 c. These bulges may be points where the oxide layer begin to delaminate form the surface, resulting in a high mechanical fragility and easy detachment of the oxide layer, as shown in Figure 5.3 and reported in previous work [5].

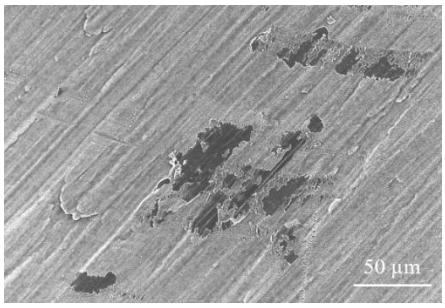

Figure 5.3 FESEM image of a delamination defect on Ti(A-HC-H)

Despite being so different, the roughness values for these surfaces are in the range considered suitable for osteoblast adhesion and proliferation [6]. After the chemical treatments, the surfaces are still deeply characterized by the presence of the grooves due to gritting with coarse abrasive paper (Figure 5.2), as well represented by the S_{sk} and S_{ku} values. In fact, the Skewness values are negative while the Kurtosis ones are greater than 3. The sharpest features can be found on Ti64(SrAg), it has the most negative S_{ku} values and the highest S_q/S_a ratio. The only exception is the S_{sk} of Ti(A-HC-H), which has a positive value probably due to the bulges, which elevate many surface points above the average line, therefore counting as peaks. The PDF and Abbot-Firestone curves reflect what can be observed in the surface reconstruction and agree with the roughness parameter. The PDF of Ti(A-HC-H) has a prominent shoulder above the average line, due to the bulges, reflected by the shape of the CPDF that increases constantly before the average line. On the other hand, the other two kind of surfaces show narrow almost symmetrical distributions, with tails in the lower part of the surfaces, as result of gritting grooves. The different roughness of the surfaces can also be deduced by the different range of the graphs in Figure 5.2, which are the distances between the highest and the lowest point: in fact, Ti(A-HC-H) has a range of more than 6 µm, Ti64(SrAg) interval is about 4.25 µm, while Ti64(HF-H_2O_2) has a height spawn of only 2.34 µm ca.

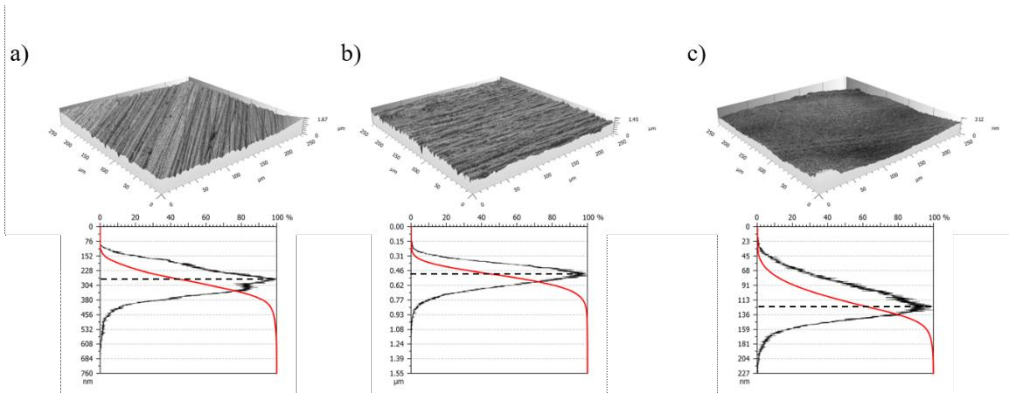

Figure 5.4 3D reconstruction image of bioactive glass surfaces and polystyrene, with graph showing the corresponding probability density function (black line) and Abbot-Firestone curve (red line), the abscissa 0 is set at the highest point of the surface and the axis is directed downward, inside the surface: a) SBA2; b) AgSBA2; c). The average line of the surface is represented by horizontal dashed lines in the graphs.

While the chemical treatments on Ti and Ti64 deeply change the surface topography and morphology, silver ion exchange does not have a similar effect. As possible to see in Table 5.1 and Figure 5.4, SBA2 and AgSBA2 have a very similar surface. The roughness parameters are practically identical, with a slight but not significant increase in the S_a and S_q after the surface treatment. Still, these surfaces result very flat, as expected of the polishing procedure. The little increase in roughness can be attributed to the silica dissolution and reprecipitation as hydrated gel on the glass surface, that is the typical first step of the reaction sequence on which the bioactivity of glasses is based on [7]. Skewness and Kurtosis, lower than 0 and higher than 3 respectively, correlate with the polishing grooves that are present on the surfaces, as in the case of Ti64 #400. The ratios S_q/S_a of BGs agree with the low values of S_{ku}. The slim tails in the PDF curves are due to the presence of some deeper scratches.

As expected, the polystyrene sample has a featureless surface (Figure 5.4) and a very small roughness. The flatness of this surface approach the limit of resolution of the optical profilometer, which can result in measurement noise and artifacts, as the undulations visible in the 3D reconstruction, that can affect the evaluation of parameters such Skewness and Kurtosis. In fact, these values were not reported in Table 5.1 since the variation among the measurements were too high.

The surfaces considered in this work have very different features, from the nanoscale, such as the pores of the treated titanium surfaces, to the microscale. This can change to a great extent the interaction with protein solutions and shall be carefully considered in comparing and discussing the results presented in the rest of this thesis. Surface roughness parameters are often obtained also through AFM. In this work, it was chosen not to do so, since it is not possible to apply the ISO 25178 on AFM images because the image size does not allow the correct application of the Gaussian filters needed for the height map elaboration. The values obtained with the ISO standard are thought to be more representative of the investigated surfaces, since they have also quite large features.

5.1.3. Surface chemistry

The surface composition of the samples was evaluated by XPS, using the survey spectra. The atomic compositions are reported in Table 5.2.

On all the samples, a high level of environmental contaminations was observed, as highlighted by the high amount of C found on all surfaces. This kind of contaminations are inevitable, due to the affinity of the surfaces such as titanium for carbon elements in the atmosphere [8]. These atmospheric contaminations may account also for nitrogen and sulfur on the surfaces.

Besides the contaminants, the compositions of the outer layer of the sample surfaces reflect what was expected. Ti and Ti(A-HC-H) are composed only by titanium and oxygen, as expected for oxide on pure titanium. The small variation in the Ti % may be due to different level of contaminations or the different stoichiometry of the oxide. On Ti64, the alloying elements, Al and V, are also detected. Their amount is less than in the nominal composition because they barely enter the oxide layer, which can mask their presence in the bulk. After treatment, the surface composition changes accordingly. Ca, Ag and Sr were found on the surface of Ti64(SrAg), as result of the formation of the calcium titanate and the incorporation of strontium and silver ions during the treatment. On Ti64(HF-H_2O_2), it was noticed a reduction of the vanadium, which was no more detected. It is possible that this element is not incorporated in the oxide layer, contrary to what happens with Al. The amount of oxygen is the highest among the titanium surfaces and it may be due to the particular stoichiometry of the hydrogen titanate and to the generation of a high number of OH groups during the treatment in hydrogen peroxide, as will be discussed later and as was already observed [2].

Regarding the bioactive glass samples, the principal elements of the glass network, Si and O in particular, were found on SBA2. Other elements of the glass composition were also detected: Ca on both SBA2 and AgSBA2, while Na only on AgSBA2. The remaining elements of the glass recipe, B and Al, were not detected probably due to the contaminations and the low presence in the glass. The observed composition is a bit different from the nominal one of the glass. Some ion release probably occurs during polishing lubricant and ultrasound washes in water, altering the glass composition in the first nanometers from the surface. After the ion exchange treatment, silver was detected, confirming its incorporation in the SBA2 surface. As before, the typical elements of the glass resulted in the composition of the sample. Si and O may be higher on AgSBA2 than SBA2 due to lower contamination, there is less carbon, while Ca% is reduce because it is involved in the ionic exchange with silver during the treatment. Nitrogen can also be a residual of the reactants used during the treatment. Due to lower contaminations, also P, another element of the glass, was detected.

As expected, PS is composed only by carbon and oxygen.

Table 5.2 Atomic composition (%) of the investigated surfaces before protein adsorption (-: non-detected).

	C	N	O	Ti	Si	S	Ag	Al	Na	P	Ca	V	Sr
Ti	28.19	4.07	52.12	15.51	-	0.11	-	-	-	-	-	-	-
Ti64	23.55	3.39	51.84	16.36	-	0.05	-	3.62	-	-	-	1.19	-
Ti(A-HC-H)	22.13	1.68	55.32	20.88	-	-	-	-	-	-	-	-	-
Ti64(SrAg)	20.92	1.62	50.26	18.13	-	-	0.94	1.232	-	-	4.85	-	2.06
Ti64(HF-H_2O_2)	12.73	2.52	60.78	20.29	-	-	-	3.7	-	-	-	-	-
SBA2	46.35	-	34.35	-	5.03	-	-	-	-	-	7.61	-	-
AgSBA2	33.63	0.71	40.88	-	11.70	-	6.88	-	2.85	1.49	2.84	-	-
PS	72.78	1.82	24.47	-	-	0.93	-	-	2.88	-	-	-	-

The sample surface chemistry was further investigated by analyzing the high-resolution spectra of selected elements, in order to obtain information about the functional groups exposed by the different materials.

For titanium substrates, the peaks that are interesting to be deconvoluted are the C1s, the O1s and the Ti2p (Figure 5.5). For all the samples, the C1s peaks is due only to carbonaceous contaminations, as confirmed also by the deconvolution, where a main contribute due to C-C (248.8 eV) is found and low contribution comes from C=O (286-287 eV) and COO (288-289 eV) (Table 5.3) [9,10]. On Ti64(SrAg) a low energy peak, at 279.8 eV, due to Sr 3p1/2 electrons was also detected [11].

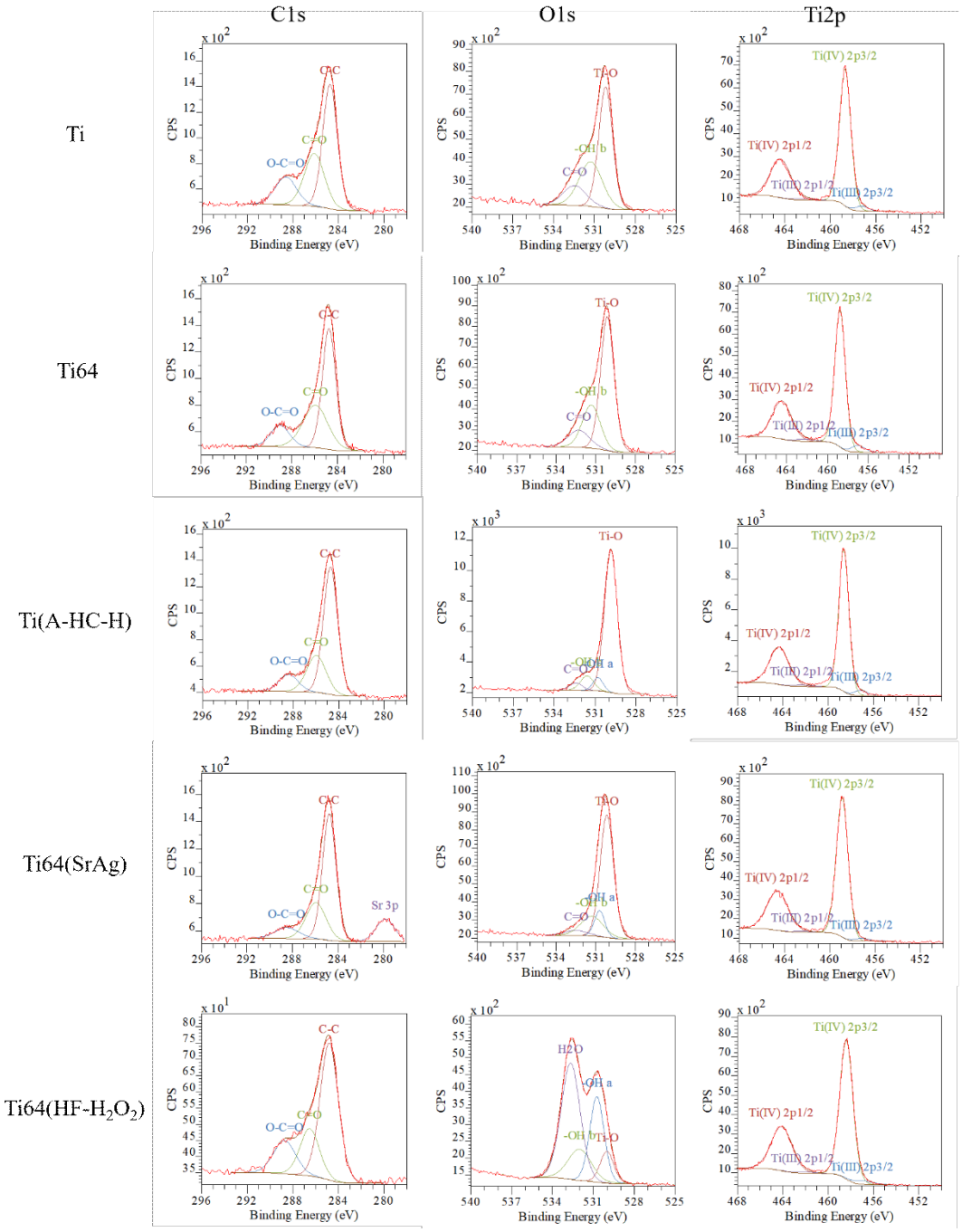

Figure 5.5 Deconvolution of the C1s, O1s and Ti2p region for titanium surfaces.

Table 5.3 Binding energies and composition of the deconvoluted peaks in the C1s, O1s and Ti2p regions for titanium samples. Theoretical energies for each component are reported (-: non-detected). The hydroxylation degree is calculated as the ratio between the total amount of OH and TiO groups.

	C1s			O1s				Ti2p			
	Binding energy (eV)										
	CC (248.8)	C=O (286-287)	COO (288-289)	TiO (529.8)	OHa (530.7)	OHb (531.6)	CO (532.3)/ H_2O (532.8)	Ti(III) 2p3/2 (457.1)	Ti(IV) 2p3/2 (458.7)	Ti(III) 2p1/2 (462.2)	Ti(IV) 2p1/2 (464.4)
Ti	248.7	286.1	288.6	530.2	-	531.6	532.4	457.2	458.7	462.4	464.4
Ti64	284.7	285.9	289.0	530.1	-	531.3	532.3	457.0	458.8	462.2	464.5
Ti(A-HC-H)	284.7	285.9	288.4	529.8	530.8	531.6	532.4	457.1	458.6	462.3	464.6
Ti64(SrAg)	284.8	285.9	288.4	530.2	530.7	531.3	532.5	457.2	458.9	462.4	464.6
Ti64(HF-H_2O_2)	284.8	286.5	288.7	530.1	530.7	532.0	532.7 (H_2O)	457.0	458.4	457.2	464.2
	Peak composition (%)									Hydroxylation	
	CC	C=O	COO	TiO	OHa	OHb	CO /H_2O	Ti(III)	Ti(IV)	OH_{tot}/TiO	
Ti	52.3	30.7	17.0	53.0	-	32.6	14.4	3.8	96.2	0.62	
Ti64	52.5	34.4	13.1	61.3	-	26.3	12.4	5.4	94.6	0.43	
Ti(A-HC-H)	63.7	25.0	11.3	81.3	5.9	8.6	4.2	4.4	95.6	0.18	
Ti64(SrAg)	63.2	27.0	9.8	66.8	10.8	17.8	4.6	2.4	97.6	0.43	
Ti64(HF-H_2O_2)	60.2	22.0	17.8	9.69	26.7	15.4	48.3 (H_2O)	1.5	98.5	4.34	

Table 5.4 Binding energies and composition of the deconvoluted peaks in the C1s, O1s and Si2p region for BG samples. Theoretical energies for each component are reported (-: non-detected).

	C1s					O1s		Si2p
	Binding energy (eV)							
	CC (248.8)	C=O (286-287)	COO (288/289)	CO_3 (289.4)	C-Me (283.5)	Si-O (531.7)	n.b. O (≈530)	Si-O_2 (103)
SBA2	248.8	286.8	288.3	289.6	283.4	531.4	530.1	102.7
AgSBA2	284.7	286.5	288.0	289.3	283.2	531.7	-	102.6
	Peak composition (%)							
	CC	C=O	COO	CO_3	C-Me	Si-O	n.b. O	Si-O_2
SBA2	62.2	2.05	12.2	4.6	19.0	63.6	36.4	100
AgSBA2	74.75	5.7	5.8	5.4	8.43	100	-	100

More informations about the chemistry of the different titanium substrates can be obtained by focusing on the oxigen and titanium peaks. The Ti2p region is characterized by two strong peaks, derived from the 3/2 and 1/2 splitting of the orbital, with an area ratio of 0.5. The different valence state of Ti, Ti(III) and Ti(IV), have a different BE and a precice splitting energy. In particular, Ti(III) 2p3/2 peak is centered at 457.1 eV, with a split energy of 5.2 eV, and Ti(IV) 2p3/1 can be found at 458.7 eV, with a split energy of 5.7 eV [12]. As reported in Table 5.3, the oxidation state of the Ti is mainly as +4 on all samples, but some Ti(III) is also observed. Ti64(SrAg) and Ti64(HF-H_2O_2) have a slighly lower amount of Ti(III) with respect to the other samples, probably due to the complex composition of the oxide layer, being calcium or hydrogen titanate. The O1s peak can be deconvoluted with contribution by Ti-O at 529.8 eV, by OH surface groups, which can be distinguished between acidic OH (OHa) and basic OH (OHb) at a BE of 530.7 eV and 531.6 eV respectively, and by a final contribuition that can be attributed to CO bonds from environmental contaminations, at 532.3 eV, on all samples but Ti64(HF-H_2O_2), where this last peak has higher binding energy (532.7 eV) and is due to adsorbed water on the surface, as observed in previous works [10,13,14]. Looking at the deconvolution and composition of the O1s peak in Figure 5.5andTable 5.3, it can be observed that the untreated Ti and Ti64 expose only basic OH groups, while the threated surfaces expose also acid OH groups with a different hydroxlation degree and ratio of OHa and OHb. The hydroxilation density can be compared between the different surfaces by comparing the ratio of the total amount of OH against the Ti-O (Table 5.3). This ratio is equal to 0.62 for Ti, 0.43 for Ti64, 0.17 for Ti(A-HC-H), 0.43 for Ti64(SrAg) and 4.34 for Ti64(HF-H_2O_2). Pure titanium shows a higher amount of OH with respect to Ti64 alloy. The acid-alkali treament, Ti(A-HC-H), despite increasing the amount of OHa, which are in a ratio with basic OH on this surface of 0.69, results in the lower hydroxylation degrees. It is possible that the final heat treament concur to reduce the number of OH groups. Ti64(SrAg) has the same total amount of OH compared to Ti64, with a higher presence of acidic hyrdoxyls resulting from the chemical treatment, the OHa/OHb ratio is 0.61, similar to Ti(A-HC-H). The highest hydroxilated surface is the Ti64(HF-H_2O_2), which is also the only one that has more OHa than OHb groups, in fact their ratio is 1.73. This very high hydroxylation with respect to all the other titanium surfaces might be related to the fact that this kind of treatment does not involve a high temperature step, but the samples are just hydrothermally modified at low temperature.

On bioactive glass surfaces, the deconvolution was performed on the C1s, O1s and Si2p regions (Figure 5.6). For both samples, the carbon peak is composed by the contribution of carbonaceous contamination, CC, CO and COO as usual, but two more peaks were detected, one at high BE and one at BE lower than the CC peak. The one at high energy, around 289.6 eV, is related to the presence of carbonates on the surface of the glass [15], which can be formed on the glass surface during the polishing and cleaning steps in the samples preparation. The other peak, around 283.5 eV, may arise from C atoms bonded to metals [14]. This kind of contamination may be due to SiC particles detached from the polishing papers that

get stuck in the glass surface and cannot be removed during the washing of the samples. The C-Me signal is reduced on the AgSBA2 surface (Table 5.4), probably due to the fact that a reaction layer is formed on the surface of the glass during the ionic exchange treatment, covering and masking the gritting particles. The O1s peak for SBA2 can be deconvoluted in two distinct component, one at 531.4 eV, attributed to SiO bond [16], and one at 530.1 that can arise from non binding oxygens (n.b. O) [17], that are the oxygens where the Si-O-Si bond of the silica network is interrupted by the modifier elements introduced in the glass. After the surface treatment, the O1s peak of AgSBA2 is due only to Si-O. The reactions on the surface during the soaking in the $AgNO_3$ solution seems to have an effect on the glass structure at the surface, increasing the number of bridging oxygens. The peak at ≈531 has been attributed to SiO according to literature and due to the fact that this kind of bonds are be predominant on glass surface, but it is worthy to notice that the OH groups possess the same BE and that, despite the confirmed presence of hydroxyls on BGs, their contributions might be hidden under the SiO peak. On both BG samples, the Si2p is composed only by the peaks relative to silica, SiO_2, at a BE of ≈102.7 eV [16].

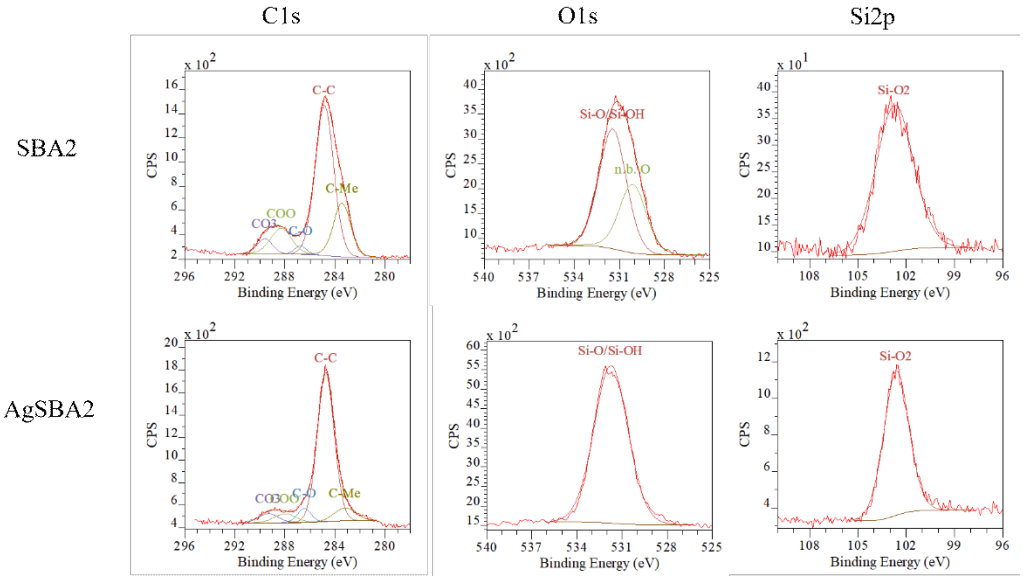

Figure 5.6 Deconvolution of the C1s, O1s and Si2p region for SBA2 and AgSAB2.

On PS surface (Figure 5.7and Table 5.5), the carbon peak is due to the carbon-carbon bonds of the surface and to environmental contaminations, as the other samples. Consequently, in the O1s region, the peak is due only to the C=O bonds.

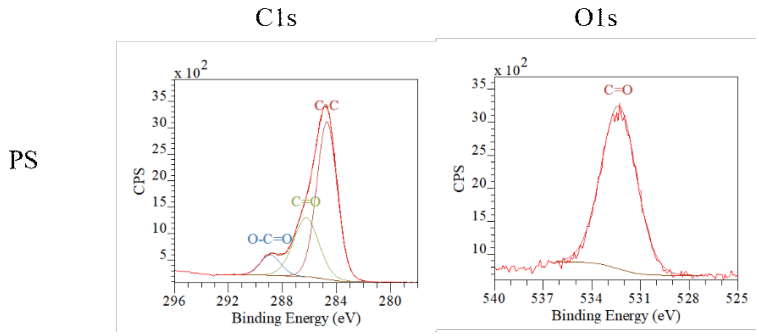

Figure 5.7 Deconvolution of the C1s and O1s for PS.

Table 5.5 Binding energies and composition of the deconvoluted peaks in the C1s and O1s region for PS. Theoretical energies for each component are reported.

	C1s			O1s
	Binding energy (eV)			
	CC (248.8)	C=O (286-287)	COO (288/289)	CO (532.3)
PS	248.7	286.2	288.9	532.3
	Peak composition (%)			
	CC	C=O	COO	CO
PS	62.5	29.3	8.2	100

At last, the Ag3d region was analyzed on Ti64(SrAg) and AgSBA2 in order to evaluate the chemical state of silver on the two surfaces, as metal (Ag^0) or as ion (Ag^+). The 3d5/2 peaks for metallic or ionic Ag have close, but different BE, respectively 368.4 eV and 367.9 eV, while the energy split with the corresponding 3d3/2 peaks is of 6 eV [18,19]. As shown in Figure 5.8and Table 5.6, only ionic silver was found on Ti64(SrAg), while some metallic silver was found on the AgSBA2 sample, probably due to nanoparticles precipitation. In particular, the silver on the glass sample is in the ionic form for the 58% and in the metallic form for the 42%.

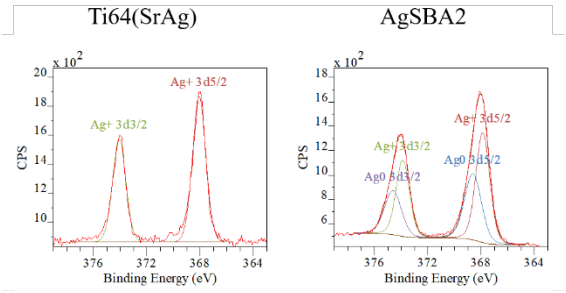

Figure 5.8 Deconvolution of the Ag3d peaks for Ti64(SrAg) and AgSBA2.

Table 5.6 Binding energies and composition of the deconvoluted Ag3d peaks for Ti64(SrAg) and Ag SBA2. Theoretical energies for each component are reported.

	Ag 3d			
	Binding energy (eV)			
	Ag^+ 3d5/2 (367.9)	**Ag^0 3d5/2 (368.4)**	**Ag^+ 3d3/2 (373.9)**	**Ag^0 3d3/2 (374.4)**
Ti64(SrAg)	368.0	-	374.0	-
AgSBA2	367.9	368.6	373.9	374.6

5.1.4. Wettability and surface free energy

Water wettability and the SFE are fundamental properties of biomaterials. Despite the discussion on the effect of implant wettability is still ongoing, there are

evidences that hydrophilic materials can enhance the early interaction of cells with the implants, in terms of adhesion, proliferation and bone mineralization. Still, a high surface energy may hinder cells activity after the adhesion on the surface [20]. As described in chapter 2, wettability and SFE deeply affect also the adsorption of proteins, and the threshold in θ between hydrophobic and hydrophilic materials is set around 60° [21].

The contact angle (CA) with water and hexadecane, and the total SFE with the polar and dispersive components as calculated with the Owens-Wendt method from the contact angles of the two liquids are reported in Table 5.7.

Table 5.7 Contact angle of water and hexadecane and SFE, γ, with the polar, γ^p, and dispersive, γ^d, components of the substrates calculated with the Owens-Wendt method (reported as average ± standard deviation).

	Water CA (°)	Hexadecane CA (°)	Ethylene glycol CA (°)	γ (mN*m^{-1})	γ^p (mN*m^{-1})	γ^d (mN*m^{-1})
Ti	49.2±4.4	6.2±0.5	25.7±1.0	52.43±2.97	25.09±2.95	27.34±0.03
Ti64	53.5±3.0	5.2±0.1	26.0±0.6	49.55±2.02	22.16±2.01	27.39±0.01
Ti(A-HC-H)	44.2±2.8	4.7±1.6	2.7±1.5	55.80±1.87	28.39±1.80	27.41±0.07
Ti64(SrAg)	7.4±0.4	6.8±0.5	5.3±0.6	72.67±0.06	45.37±0.03	27.30±0.03
Ti64(HF-H_2O_2)	28.4±4.8	7.40±0.3	18.0±0.9	65.30±2.59	38.02±2.57	27.27±0.02
SBA2	22.0±2.6	7.7±2.0	15.5±2.1	68.20±1.12	41.69±0.99	26.51±0.13
AgSBA2	22.3±4.5	3.9±0.6	10.3±1.1	68.25±2.36	40.81±2.34	27.43±0.01
PS	71.9±0.1	13.1±0.4	58.1±1.7	37.66±0.07	10.87±0.03	26.79±0.04

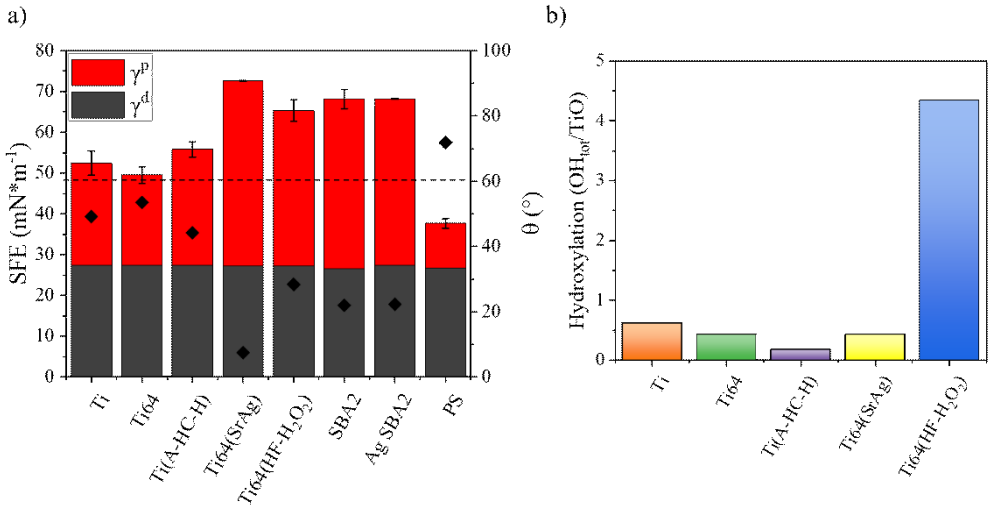

Figure 5.9 a) Polar (red bar) and dispersive (dark gray bar) components of the SFE. The total bar is the value of the SFE (left axis). Water contact angles θ are also reported (♦)(right axis). The dashed line represents the separation between hydrophobic and hydrophilic materials; b) hydroxylation degree of titanium-based substrate, calculated by the OH_{tot}/TiO ratio obtained with XPS.

Contact angles were measured using water, hexadecane and ethylene glycol since they are useful to evaluate the surface free energy and its components with different methods. For instance, the Owens-Wendt method is appropriate to determine the total SFE, with the respective polar and dispersive components, while the acid-base method allows to obtain also the acid and basic component of the SFE. This last method was not deemed suitable to be applied on the investigated samples, therefore the acid and basic component were not calculated. To evaluate the SFE with the Owens-Wendt method, two liquids respectively exhibiting a dominant polar or dispersive component shall be used. The couple water-

hexadecane well fulfill this condition (water: γ^d=21.8 mN/m, γ^p=51 mN/m; hexadecane: : γ^d=27.5 mN/m, γ^p=0 mN/m). On the other hand, ethylene glycol has not a largely dominant component of the SFE (γ^d=29 mN/m, γ^p=19 mN/m), so it was not used for calculating the SFE with the selected method. The hexadecane contact angle values have been reported for completeness.

The surfaces investigated in this work range from hydrophobic surfaces, such as PS, to highly hydrophilic ones, such as treated Ti64 and BGs. It was also confirmed the inverse correlation between the polar component of the surface energy and the water contact angle (Figure 5.9 a) [22]. Interestingly, the γ^d is similar for every kind of sample, independently from the bulk material or the surface treatment, as possible to see in Figure 5.9 a.

Polished Ti and Ti64 have a similar water CA and they can be still considered as hydrophilic surfaces, even though they approach the threshold θ value of 60°. Also, their SFE and its components are very similar. The chemistry of the native oxide on pure titanium and Ti6Al4V alloy is not much different, resulting in the same wettability and surface energy. The chemical treatments on titanium surfaces have different effect on these surface properties. Ti(A-HC-H) shows a small decrease in θ and a slight increase in its polar surface energy, while Ti64(SrAg) and Ti64 (HF-H_2O_2) surfaces have a major increase in both wettability and γ^p, with Ti64(SrAg) being the most hydrophilic, almost super-hydrophilic, and energetic surface of all. The differences may arise from the different crystalline phase growth during the chemical treatments and from the different surface composition and surface OH groups, as previously discussed. As shown by XPS (Table 5.2), Ti(A-HC-H) has a very similar composition to pure titanium, low hydroxylation degree, and its crystalline structure is a mix of anatase, for the most part, and rutile [5], which are natural isomorphs of titanium dioxide. On the other hand, the treated Ti64 have a very different crystalline structure. The oxide layer of Ti64(SrAg) is formed by calcium titanate where some Ca^{2+} ions have been substituted by strontium and silver ions [23], which were found in the surface layer, while Ti64(HF-H_2O_2) is composed of a hydrogen titanate ($H_2Ti_3O_7$)[5] and has a high hydroxylation degree, with mainly acidic -OH groups, strongly affecting the surface wettability. The polar component of the SFE arises from electrostatic interactions and hydrogen bonds, as consequence, a greater number of functional groups and charged ions on the surface are well expected to increase the γ^p and the wettability of the materials. The high hydrophilicity of Ti64(SrAg) can also be ascribed both to the hydroxylation degree and to the presence of strontium, which is reported to greatly decrease θ when present in concentration up to 15 mol% [24]. On the other hand, silver in the ionic form is not expected to change the wettability of titanium surfaces [25].

The bioactive glasses have a strong hydrophilic behavior, related to the many OH groups exposed by the glass surface. What is interesting and unexpected is the fact that the surface treatment and the subsequent incorporation of silver ions in the glass surface does not change neither the wettability nor the SFE of the glass (Figure 5.9 and Table 5.7). It has been previously reported that the hydrophobicity of glasses can be increased by Ag doping using high temperature salt baths [26]. While this process results in a concentration of silver in the order of 20-30 wt%, the ionic

exchange in the silver nitrate solution can introduce about the 3% of silver, evaluated by EDS [27]. Thus, the amount of silver in the glass may not be enough to modify the SFE of the glass.

At last, PS shows a hydrophobic behavior, with low overall SFE and γ^p in particular, which is typical for a polymer that does not bear charged groups, nor in the polymeric chain neither as lateral groups.

A general rule is often reported [28] about a threshold between adhesive and not adhesive surfaces at the critical surface tension of 40 mN/m (aqueous contact angle around 60°), whereby surfaces with lower surface tension are not adhesive for cells: it is interesting to note that the un-treated Ti surfaces are close to this threshold while all the chemical treated surfaces move at a upper level of surface energy. PS is below this threshold.

5.1.5. ζ potential

The zeta potential of a surface provides information about the charge distribution on a surface when it gets in contact with a solution, at a certain pH, and insights on the strength of the acidic or basic nature of surface functional groups and wettability by analyzing the shape of the titration curve. Furthermore, it is a useful characterization technique to evaluate the effect of a surface modification on a certain material [29].

Here, the ζ potential of all surfaces was tested in the pH range between 3 and 9 and, where possible, the IEP and the onsets of the acidic and basic plateau were calculated (Table 5.8). The results will be shown at first by comparing the treated surfaces with their respective untreated samples, then a cross-comparison will be made.

Table 5.8 IEP and acid and basic onset of the substrates (-: not found).

	IEP	Acid onset	Basic onset
Ti	4.1	-	-
Ti64	4.1	-	-
Ti(A-HC-H)	5.6	4.2	-
Ti64(SrAg)	2.9	-	4.7
Ti64(HF-H_2O_2)	-	-	5.1
SBA2	-	-	-
AgSBA2	-	3.2	-
PS	3.74	-	7.3

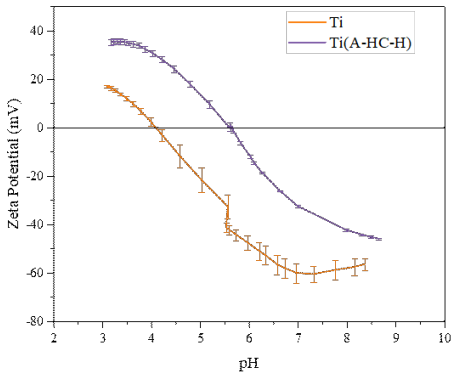

Figure 5.10 ζ potential titration curves of Ti and Ti(A-HC-H).

The titration curves of pure Ti surfaces are shown in Figure 5.10. Ti has an IEP around 4, which fits in the range reported in literature [30]. The Ti zeta potential is characterized by the absence of evident and stable plateaus, both in the basic and in the acidic range, which can evidence that the functional groups on this surface, in particular OH, have not a strong acidic or basic behavior. In fact, the plateaus are reached thanks to the complete protonation or deprotonation of surface groups. When the pH is shifted to low values, basic surface groups protonate themselves, acquiring a positive charge, while the acidic groups may remain in their dissociated form or be protonated, at the rising of H^+ concentration in the solution, depending on their pKa: a concomitant IEP higher than 4 is expected in this case. Once the basic groups are fully protonated and larger in number that eventual acidic groups in their dissociated form, the ζ potential of the surface is stable respect to further lowering of the pH, reaching a positive plateau in the acidic portion of the graph. The stronger is the basicity of the surface groups, the higher is the pH at which the plateau is reached. In a similar manner, the negative basic plateau is reached thanks to the fully deprotonation of acidic surface groups, and it is shifted towards lower pH at the increase of their strength: an IEP lower than 4 is expected in this case. After the chemical treatment, Ti(A-HC-H) has an IEP shifted at 5.6 and a plateau is present in the acidic range, with onset at 4.2. In the basic range, the curve seems to tend towards a plateau, that might be reached at even higher pH. Thus, the OH on the Ti(A-HC-H) are supposed to have a predominant basic behavior, even though some acidic OH are exposed, in agreement with XPS. As consequence of the treatment, the modified titanium surface has a more positive charge with respect to pure titanium. The zeta potential titration curve can also provide information about the wettability of a certain surface thanks to the slope of the linear portion around the IEP: the lower the slope, the more wettable is the surface. Ti and Ti(A-HC-H) have a similar contact angle (Table 0.7) and as possible to see in Figure 1.10, they have also a similar slope of the curve near the IEP.

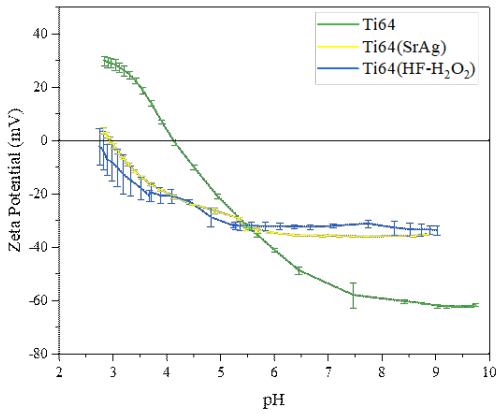

Figure 5.11 ζ potential titration curves of Ti64, Ti64(SrAg) and Ti64(HF-H_2O_2).

The potential titration curves for Ti64 substrate, polished and treated, are reported in Figure 5.11. The curve of the untreated titanium alloy is very similar to the one of Ti (Figure 5.10), with the same IEP and absence of clear plateaus, neither at low pH nor at high pH. Since the native oxide layer of Ti and Ti64 is analogous,

as obtained by XPS, wettability and SFE measures, a similitude in the ζ potential is coherent and expected. After being treated, the Ti64 changes drastically its surface potential and the modified surfaces have practically the same titration curves. The IEP of both Ti64(SrAg) and Ti64(HF-H_2O_2) is heavily shifted towards acidic pH. The point of zero charge of Ti64(SrAg) is barely detected at pH = 2.9, at the end of the measuring range, while the IEP of Ti64(HF-H_2O_2) is even lower and outside the measuring range. By interpolating the curve, it is possible to estimate it around 2.6. The treated surfaces show also marked plateaus, with onset at 4.7 and 5.1 for the ions doped Ti64 and the hydrothermally treated one respectively. These plateaus are at negative potential values and therefore due to deprotonation of acidic OH. The fact that these plateaus have such a low onset is significant of a high acidic strength of such OH, that can remain in the O^- state even at high concentration of H^+ in solution. The presence of acidic OH on the treated Ti64 surfaces was also noticed by XPS deconvolution (Table 5.3). Since the IEP is shifted at acidic pH, the treated surfaces have always a negative net charge, which is lower than Ti64 at pH below 5.5 ca and it is higher at pH above it. At last, the slope of the curves of Ti64(SrAg) and Ti64(HF-H_2O_2) is much lower than respect to Ti64 as expected, since they are more hydrophilic than untreated Ti64 (Table 5.7). Both surfaces are fairly chemically stable, in fact the standard deviations are low almost along all the curves. They increase a bit for the Ti64(HF-H_2O_2) at pH below 3.5, indicating that some corrosion process may began in such environment.

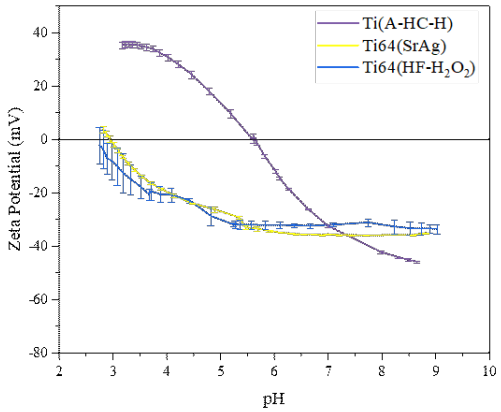

Figure 5.12 ζ potential titration curves of Ti(A-HC-H), Ti64(SrAg) and Ti64(HF-H_2O_2).

By comparing the results for the titanium surfaces after treatment (Figure 5.12), their differences became more evident. While Ti(A-HC-H) is positively charged in almost half of the measurement range, the other two surfaces are always negative. Interestingly, at physiological pH, around 7.4, they have a very similar surface potential, around -40 mV. In the case of Ti(A-HC-H), a local microenvironment effect can be present at physiological pH with a predominant positive zeta potential because of the presence of the basic OH groups, as reported in [2] where the zeta potential was measured in presence of a low amount of liquid in contact with the surface. At last, the different wettability can be noticed looking at the slopes of the curves, which are less steep for the treated titanium alloy samples than for the treated pure titanium.

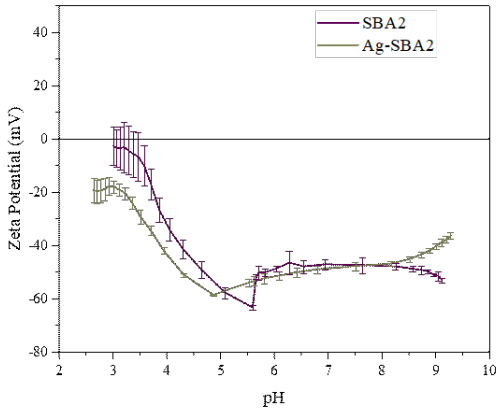

Figure 5.13 ζ potential titration curves of SBA2 and AgSBA2

In figure Figure 5.13 are plotted the titration curves for the two Bg samples. The bioactive glasses have a negative zeta potential in all the pH measured range and the IEP was not detected for both SBA2 and AgSBA2. A very low IEP is typical for silica based bioactive glasses [31]. The surface charge of bioactive glass may be related to the great amount of OH groups that are exposed on the surface of this materials. Interestingly, the addiction of silver ions in the glass surface does not affect the overall behavior of the zeta potential to a great extent. SBA2 and AgSBA2 have identical zeta potential at basic pH, up to about 8.5, where the deviation from the plateaus suggest some degradation of the samples. At acidic pH, they show some differences. The surface of AgSBA2 is slightly more negatively charged and an acidic plateau appears at very low pH, with onset around 3.7. It is possible that the begin of the silica gel formation, that takes place during the soaking in the silver nitrate solution and can change the nature of hydroxyls groups, coupled with the release of positive ions, such as Ca^{2+}, from the glass network, is responsible for this increase in the acidic characteristic of the treated glass surface. For both samples, the determination of the onset of the basic plateau is not possible due to the shape of the curves, with a sort of drop in the potential around pH 5 and its subsequent rise. As expected from glasses, they began to corrode at pH lower than about 3.5, as evidenced by the high standard deviations.

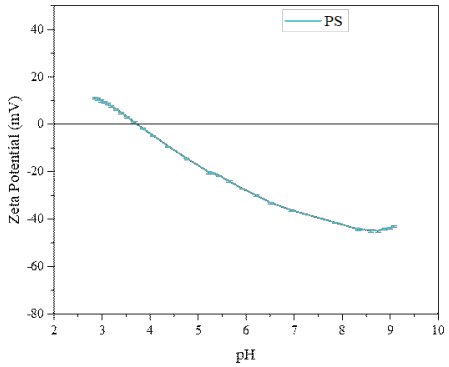

Figure 5.14 ζ potential titration curve of PS

At last, the PS titration curve is presented in Figure 5.14. The IEP of polystyrene was found at 3.7 and the shape of the curve is typical for uncharged surfaces, as previously reported in literature [32]. The small surface potential measured for PS arises from adsorbed hydroxide or hydrogen ions from the electrolyte solution.

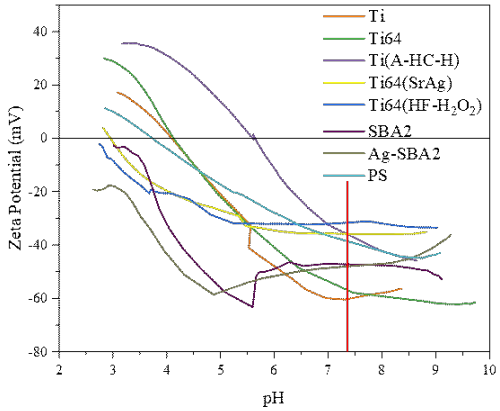

Figure 5.15 Comparison of the ζ potential titration curves of all the surface. pH 7.4 is marked by the red line.

A comparison between all the surfaces is reported in Figure 5.15. In particular, it is interesting to notice the potential value around pH 7.4, which is the pH of the protein solution used for the adsorption experiments. At that pH, albumin and fibronectin are negatively charged (as will be show in paragraph 5.2.4), thus the overall electrostatic interaction between the proteins and the surfaces, which are all negatively charged, are unfavorable to adhesions of proteins on the surface. Still, the higher potential on treated titanium surfaces, Ti(A-HC-H), Ti64(SrAg) and Ti64(HF-H_2O_2), may results in lower electrostatic repulsion with respect to Ti, Ti64 and BGs. As last, the presence/absence of charged functional groups on zwitterionic molecules, as proteins are, and on the surfaces can play a role, despite of the overall electrostatic status.

5.1.6. Consideration on the substrate properties

By merging all the information about the surface characteristics of all the different samples, it is possible to draw an overall picture of the substrates, represented in Figure 5.16. The surface features vary greatly between the materials, but some similarities can be found. To have this general overview about what is different and what is analogous between the substrates used in this work may help to interpret the data about protein adsorption and to discriminate the effect of the different surface features on the protein-surface interaction mechanisms.

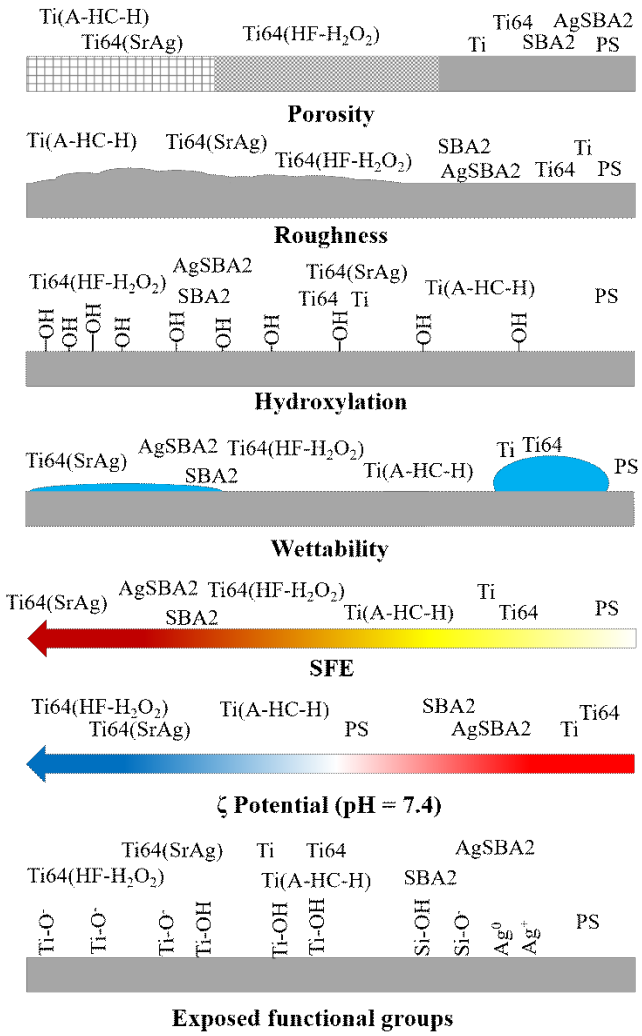

Figure 5.16 Scheme of the different surface properties of the substrates. All the properties decrease from left to right

The surface layers of Ti(A-HC-H) and Ti64(SrAg) are the most porous of all, with quite wide and elongated pores, as suggested by FESEM imaging. The oxide layer of Ti64(HF-H_2O_2) is still porous, but more compact than the others treated titanium samples. All the remaining surfaces, Ti, Ti64, SBA2, AgSBA2 and PS, have non-porous and compact surfaces. The surface roughness follows the same trend as surface porosity, which is quite expected. The compact surfaces have a similar low roughness that increase for Ti64(HF-H_2O_2), Ti64(SrAg) and Ti(A-HC-H). To compare the hydroxylation degree of all surfaces in once is not possible, but

it can be done between similar type of materials. Among titanium samples, the untreated Ti and Ti64 have a similar OH density, which share also the weak basic behavior. Each treatment results in a different hydroxyl concentration and OH type: the mixed acid- alkali treatment (followed by a thermal treatment) highly decrease the number of OH on the surface, in fact Ti(A-HC-H) has the lowest OH/TiO ratio, but it introduces acidic OH; incorporation of strontium and silver in the growth calcium titanate layer does not change the overall concentration of hydroxyls, despite generating strong acidic OH groups; in the end, the peroxide treatment, Ti64(HF-H_2O_2) highly increases the hydroxylation degree and the strong acidic hydroxyls became predominant. Due to the overlapping of SiO and OH BE in the XPS spectra, it is not possible to determine with this technique eventual differences between SBA2 and AgSBA2. Anyhow, looking at the results obtained for the SFE, wettability and surface potential, it is possible to hypophyses that the ion-exchange process does not affect the OH surface groups to an extent that is appreciable with the techniques employed here. PS is not expected to expose OH groups, as confirmed by XPS and zeta potential. Wettability and surface free energy follows the same trend among the different surfaces. Ti64(SrAg) has the highest SFE and the lowest θ, followed by BGs and Ti64(HF-H_2O_2), which have comparable values. Ti(A-HC-H) is less wettable and energetic, still more than the untreated titanium have similar SFE and water contact angle, close to the threshold value of 60°. In terms of biological behavior, all these surfaces can be considered hydrophilic. The only hydrophobic surface is PS, which has the lowest SFE and highest contact angle. At last, the ζ potential, where all the curves have their peculiarities, can be used to order the substrates according to their surface potential at the adsorption pH 7.4 and to understand the acidic-basic reactivity of the hydroxyl groups. In this case, from the lowest values to the highest, there are Ti and Ti64, followed by SBA2 and AgSBA2, PS, Ti(A-HC-H) and Ti64(HF-H_2O_2) and Ti64(SrAg). The treated titanium surfaces can be considered at the same potential, since their difference is less than 10 mV, which is the sensibility of the instrument. In conclusion, adsorption on titanium-based substrates can be influenced by several different parameters, such as surface porosity, hydroxylation and SFE or wettability. On the other hand, SBA2 and AgSBA2 are substantially identical, in terms of tested properties, but for the presence of silver in the treated samples. Therefore, the differences in the glass-protein interactions may be ascribed only to the presence of silver atoms in the glass surface and not to other surface properties.

5.2. Adsorption from a single-protein solution: albumin or fibronectin.

The adsorption of BSA and FN was investigated using the same methodology, trying to evaluate different surface parameters that influences the final protein layer. In order to do so, it was researched a set of techniques that were able to provide information on each of these parameters. Due to the lack of a complete set of

analysis for studying protein adsorption in a roughland, during this work, efforts were spent also to develop and try new methods for achieving such results.

5.2.1. Protein quantification

The first question that was tried to be answered is how much protein each surface is capable to bind. Two techniques were selected for the investigation of this aspect of adsorption: BCA protein assay and the use of fluorescent labeled proteins. The first one can provide quantitative information about the adsorbed proteins, the second qualitative information. The comparison of the results obtained by the two methods allowed to further clarify how the surface features affect the amount of proteins adsorbed.

Albumin quantification by BCA protein assay and labeled proteins

Adsorption of BSA was at first investigated by BCA protein assay. This kind of colorimetric test is based on the reduction of copper ions by proteins and the subsequent chelation of Cu^{+} by the bicinchoninic acid, in a reaction that develops a purple color that can be quantified by measuring the absorbance of light at 562 nm. In order to properly quantify the amount of proteins, it is necessary to build a calibration curves over a concentration range that can include the expected results of the experiments. The first step was to extend the standard calibration range, from 25 µg to 2000 µg, towards lower concentration. In particular, two curves were obtained, one in the range 0-80 µg (Figure 5.17 a) and one in a reduced range, 0-10 µg (Figure 5.17 b). In both cases, a linear trend of the concentration versus the optical density of the solution at 562 nm was observed, confirming that the BCA protein assay is suitable to obtain quantitative data also as such low protein concentration. In particular, a calibration curve in the range 0-80 µg (Figure 5.17 a) was obtained with the following BSA standards: 0, 0.5, 1, 2, 3, 4, 5, 7.5, 10, 20, 40, 60, 80 µg. A good linear regression was observed. Since a very low amount of albumin was expected, the linear correlation between OD and micrograms of BSA was controlled over the range 0-10 µg (Figure 5.17 b). A very good linear regression of the BSA content versus the optical density of the solution at 562 nm was observed, confirming that the BCA protein assay is suitable to obtain quantitative data also as such low protein concentration.

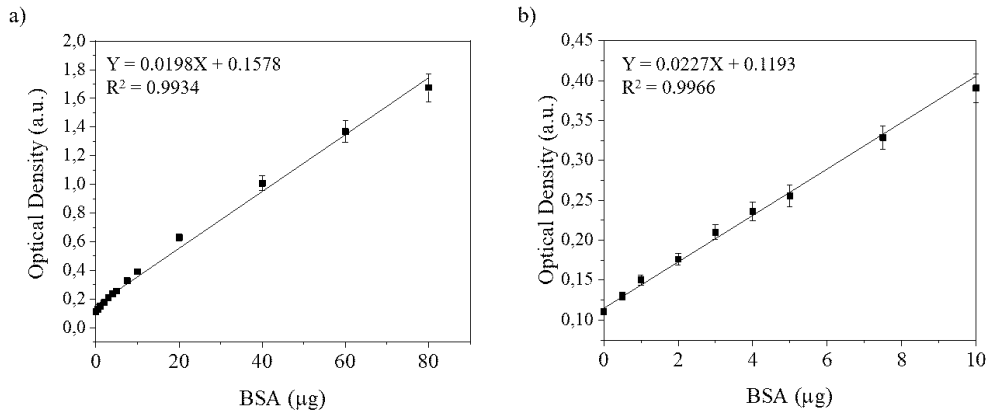

Figure 5.17 a) Calibration curve for the BCA protein assay with BSA standards with linear regression in the range 0-80 µg; b) 0-10 µg range of the calibration curve with the corresponding linear fitting. The equations of the interpolating lines are reported with the respective R^2 value.

The BCA protein assay results are reported in Figure 5.18. The amount of proteins adsorbed varies from 0.07 µg/cm^2 on PS up to 3.27 µg/cm^2 on Ti64(SrAg). The treated titanium surfaces adsorb the highest amount of proteins, which is also statistically confirmed by the p-value. Among them, no significative difference was found, but Ti64(SrAg) seems to adsorb more than Ti(A-HC-H) and Ti64(HF-H_2O_2). The untreated titanium and titanium alloy surfaces can bind a similar amount of albumin, as it is reasonable due to the similarities of their surfaces. Regarding the bioactive glasses, it was not found any statistically significative difference, but the trend of the measure seems to suggest that AgSBA2 can adsorb more BSA than the undoped glass. It is possible that the high error bars invalidate an eventual significance. The SBA2 surface was found to adsorb a low amount of BSA, even lower than Ti, not only lower than the treated titanium surfaces. The same result was obtained for PS, which seems to be the less adsorbing surface with the BCA protein assay.

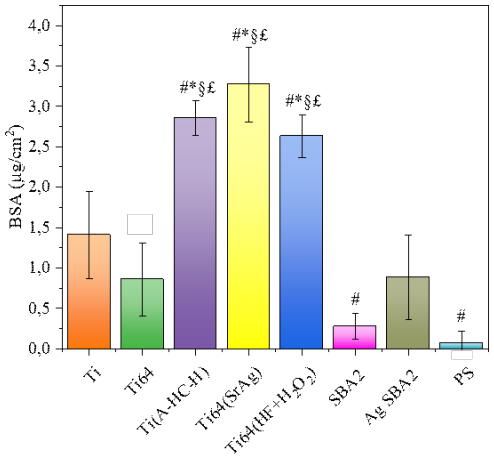

Figure 5.18 Albumin quantified by BCA protein assay. p < 0.05: # vs Ti; * vs Ti64; § vs PS; £ vs SBA2 and AgSBA2.

Before discussing the results obtained with the BCA protein assay, it is fundamental to remember that this kind of test does not quantify the amount of BSA directly on the surface, but it is necessary to previously detach the proteins with a surfactant and perform the assay in solution. It has been previously demonstrated

that SDS is not able to remove all the adsorbed proteins on flat stainless steel [33]. In this study, the surfactant may not have the same efficiency in removing albumin from the different surfaces. Surface porosity or the binding strength with the surface may result in different degree of protein detachment and, as consequence, different level of underestimation of the total amount of protein adsorbed. For drawing conclusions from the BCA experiments, it is necessary to compare them with fluorescent measurements.

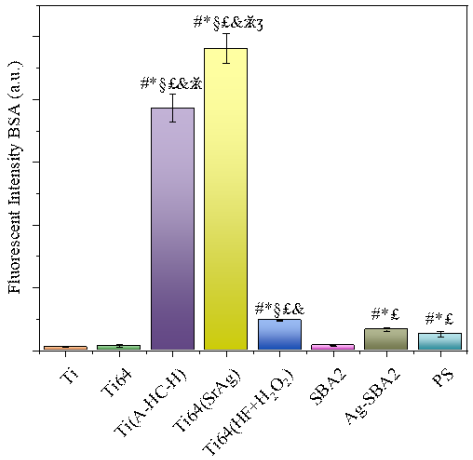

Figure 5.19 Albumin quantified by fluorescent intensity. p < 0.05: # vs Ti; * vs Ti64; ӝ vs Ti64(HF-H_2O_2); ʒ vs Ti(A-HC-H) § vs PS; £ vs SBA2; & vs AgSBA2.

The results obtained by fluorescence quantification are shown in Figure 5.19. The trend of the total amount of protein adsorbed is similar to the one observed for BCA, but some interesting differences can be found. The treated titanium surfaces are still the one adsorbing the most BSA, but in this case the difference between all three is statistically significative. Furthermore, the fluorescent signals of Ti(A-HC-H) and Ti64(SrAg) are respectively eightfold and tenfold more than Ti64(HF-H_2O_2). The difference in fluorescent signal is not proportional to an actual difference in the amount of protein adsorbed, still it suggests a much greater difference in bounded BSA than what was indicated by BCA. Other variations can be found focusing on the glasses and PS. With BCA, the latter resulted in a lower amount of albumin than both Ti and Ti64. Now, the proteins on PS are statistically higher than on the flat titanium substrates. The same thing happens for AgSBA2, which now is statistically different from Ti, Ti64, and even SBA2. The diversity previously found between SBA2 and pure Ti is now annihilated.

Combining the information from the two experiments, it is possible to make some interesting considerations. Since the quantification by labeled-proteins is performed directly on the sample, it is possible to think that the real trend in the total adsorbed proteins is the one observed in Figure 5.19 and not the one in Figure 5.18. This may be because the detachment of proteins with SDS is affected by different parameters, such as protein-surface interaction strength or impossibility to remove proteins from surface pores. Thus, some hypothesis can be drawn. At first, the main surface feature affecting the total amount of adsorbed albumin seems to be surface porosity, as represented in Figure 5.20. Ti(A-HC-H) and Ti64(SrAg) adsorb much more than all the other surfaces and are also the ones with the most

porous oxide layer, with pore some hundreds of nanometers wide and about 1 µm deep. The possibility to physically trap BSA inside the surface overcomes also the presence of more binding sites such as OH or a lower surface energy: Ti(A-HC-H) has very low hydroxylation degree and its surface energy is comparable to the one of Ti and Ti64, smaller than Ti64(HF-H_2O_2). On the other hand, when two surfaces have a similar surface morphology, OH groups and higher wettability and SFE concur to increase the binding capability of the substrates towards BSA. Confronting the results from the two techniques, it seems evident that the surfactant is incapable of detaching the proteins adsorbed at the bottom of the pores and consequently BCA results are largely underestimated for this kind of surfaces. Ti and Ti64 are very similar, both in the total amount of proteins adsorbed and in the SDS detachment efficiency, since the trend between the two techniques is similar. This may results form a similar binding strength.

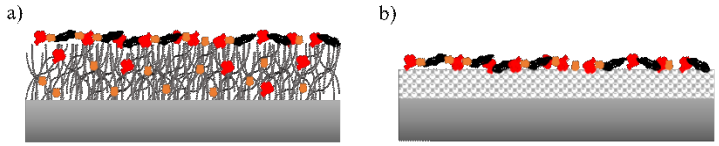

Figure 5.20 Scheme of protein adsorption on titanium samples with highly porous oxide layer, with trapping of proteins, (a) and with more compact oxide layer (b).

In the case of bioactive glasses, the presence of silver increases the amount of proteins adsorbed, possibly thanks to the affinity of metal for the thiol groups of cysteine residues in the albumin chain [34] or to the fact that positive Ag^+ ions provide electrostatically favorable binding sites for the negative COO^- groups of the proteins (Figure 5.21). As described in section 5.1, the only difference in the surface properties of the BGs is the presence of silver, therefore, the increase of BSA adsorption can be attributed only to that. The underestimation of the bound proteins by BCA in the case of SBA2 and AgSBA2 may be related to the complex events that take place on the glass surface during the soaking in the protein solution. In fact, in concomitance with the formation of the protein layer, the glass surface reacts itself, by solubilization and reprecipitation of silica in form of gel. It appears quite obvious that some proteins may adsorb and then subsequently be covered by a layer of gel or that they can diffuse inside the layer. The proteins that are not exposed directly on the surface cannot be removed by the action of the SDS and, as consequence, they are not quantified by BCA protein assay. Even though the biological effect of adsorbed proteins *in vitro* have been largely investigated [35], whether or not the adsorption of proteins affect the formation of the silica-gel or if the proteins inside the gel have a biological impact *in vivo* was not found to be studied previously on literature, but it is worthy of being further investigated.

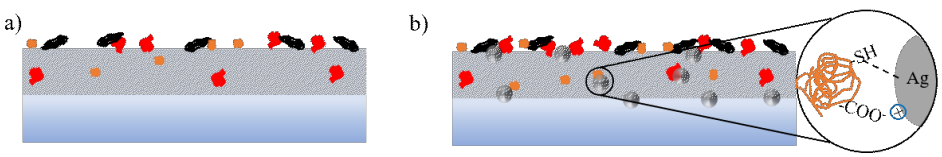

Figure 5.21 Scheme of protein adsorption on SBA2 (a) and AgSBA2 (b) with diffusion of proteins in the silica- gel layer. Interaction between proteins and silver are proposed in the inset.

At last, also in the case of PS, BCA seems to underestimate the total amount of adsorbed proteins, in particular, with respect to Ti and Ti64. In fact, PS adsorbs more than the polished titanium samples, as confirmed by fluorescent quantification. Being all flat and inert surfaces, the ineffectiveness of SDS in removing albumin from PS may be related to the very strong hydrophobic interactions on such surface, while the binding of BSA on Ti and Ti64 may be looser. When the surfaces do not have extremely different topography or high presence of protein-binding groups, as in the case of treated titanium samples, the general rule that hydrophobic surfaces adsorb proteins more and stronger than hydrophilic samples is here confirmed.

Fibronectin quantification by labeled proteins

As previously discussed, for performing BCA protein assay it is necessary to build a calibration curve. Due to the nature of the reaction involved in this test, the amount of reduce copper ions and, as consequence, the intensity of the purple coloration is strictly dependent on the type of protein involved. Since BSA and FN are very different proteins, both in terms of molecular weight, 60 versus 250 kDa respectively, and amino acid composition, it is not appropriate to use the BSA standard calibration curve also for the quantification of fibronectin. Unfortunately, due to the low availability of FN, the preparation of a calibration curve with this protein was not possible. Therefore, it was chosen not to quantify fibronectin adsorption by BCA protein assay, only through fluorescent labeled proteins.

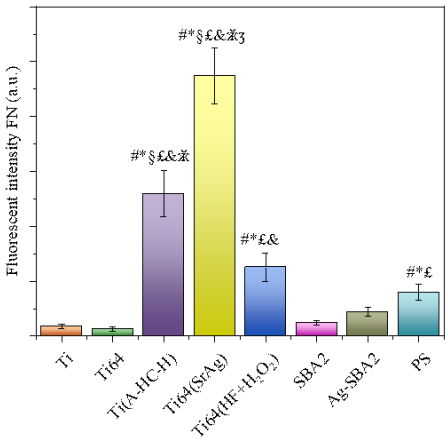

Figure 5.22 Fibronectin quantified by fluorescent intensity. p < 0.05: # vs Ti; * vs Ti64; ӂ vs Ti64(HF-H_2O_2); ʒ vs Ti(A-HC-H) § vs PS; £ vs SBA2; & vs AgSBA2.

Results for fibronectin quantification are reported in Figure 5.22. The trend in the amount of adsorbed protein is similar to the one observed for albumin. The treated titanium surfaces are the ones that adsorb most, with Ti64(SrAg) confirmed as the most protein binding surface. The statistical difference between the treated and untreated titanium surfaces is again significant, as among the modified samples themselves. Ti(A-HC-H) and Ti64(SrAg) adsorb respectively about twofold and fourfold more FN than Ti64(HF-H_2O_2). Contrary, this does not happen for the glasses: even though AgSBA2 signal seems higher than SBA2, the difference is not

statistically different. Again, PS adsorbs more than Ti, Ti64 and SBA2, but in this case, the difference between PS and Ti64(HF-H_2O_2) is reduced with respect to BSA adsorption and not significative.

As in the case of albumin, surface porosity seems to play the major role in determining the total amount of adsorbed proteins, followed by the presence of protein binding sites and increased SFE. For FN, the differences between the various surfaces seems to be reduced with respect to BSA adsorption. This fact may be related to two factors. In first place, FN concentration in the adsorbing solution is a hundredth of BSA solution, so the total amount of proteins available for adsorption is reduced. In second, fibronectin is much larger than BSA (BSA has a globular shape of about 5 nm in diameter and FN a disk like shape of about 14 nm, see Chapter 1) thus its ability to accumulate in surface features or to diffuse in the hydrated silica-gel may be reduced. The topography of the porous surface has a role at this concern. As shown in Table 5.1, the increment of the surface area exposed to the protein solution because of the porosity is almost negligible, while the difference in adsorption is attributable to the presence of a niche and micro-environment within the pores.

Unfortunately, due to experimental limitation and characteristic of the quantification via fluorescent labeled proteins it is not possible to compare the signal obtained for BSA with the signal of FN in order to compare the total amount of the two adsorbed proteins, so it cannot be determined with this technique if Ti64(SrAg) adsorbs more BSA or FN. The fact that the difference between SBA2 and AgSBA2 is not significant in the case of FN may be also interpreted in terms of selective adsorption enhancement by silver. As already discussed, Ag can bound with proteins using the SH groups in the Cys residues, which is very effective in BSA that contains the 6% of cysteine. FN has a much-reduced content of that specific residue, about 2.7%, thus the possible binding sites for silver are few and it is not capable to increase the adsorption of this specific proteins up to a significant amount. In the case of FN, the small increase in adsorption may be attributed to electrostatic interactions between Ag^+ and negative patches of the protein surface. The possibility of a selective modulation of the adsorption of certain proteins is very interesting with the aim of obtaining a protein layer that can stimulates an appropriate cellular response and shall be further clarified and investigated with different proteins. At last, focusing on the behavior of PS, the preference of proteins for adsorbing on hydrophobic flat surfaces than on more hydrophilic ones seems to be confirmed, due to the increased FN adsorption with respect to Ti, Ti64 and SBA2.

5.2.2. Protein adsorption investigated by XPS

XPS is widely reported in literature as powerful tool to investigate protein adsorption, thanks to its capability of determining contemporaneously both the surface chemistry and the bonds in which the atoms are involved [10,36]. Here, XPS was performed on all surfaces after adsorption of albumin and fibronectin.

In Table 5.9 the atomic composition of the substrates after BSA adsorption is reported. With respect to the pristine surfaces (Table 5.2), it is possible to see that the main bulk elements, such as Ti and Si, generally decreased, while the content of C and N were increased. This agrees with the occurrence of protein adsorption on all surfaces, since nitrogen is a typical element of proteins and the formation of a layer on the surfaces limit the detection of the underlying substrates. Also, the presence of sulfur, which is contained in Cys amino acids, indicates the presence of BSA on all the surfaces.

Focusing on the different family of materials investigated, it is possible to notice that on titanium substrates, carbon rises from about 20% to 35% of Ti(A-HC-H)_BSA and up to 67% for Ti_BSA, with the other titanium samples being in the range between 45 and 55%. Contextually, the amount of nitrogen rises from few point percent, which are related to environmental contamination, to 12-13% on Ti, Ti64 and Ti64(HF-H_2O_2) and to a lower amount on Ti(A-HC-H) and Ti64(SrAg), respectively 7 and 9 %. Albumin has a concentration of N equal to 16% [37], still in literature it is reported that a nitrogen level of 9% correspond to a complete coverage of the surface [38]. Therefore, it is possible to conclude that a continuous layer of albumin is formed on all the titanium substrates. The only exception seems to be the Ti(A-HC-H), where N is only 7%. Still, in light of the quantification results and the fluorescent and KPFM imaging that will be discussed later in this work, it is possible to presume that also this surface is fully covered by albumin. Since the penetration depth of XPS is limited to the very first nanometers of the surface, the formation of an additional layer can limit the detection of the elements in the material below. In fact, titanium and the other elements composing the bulk materials, such as Al, V, Sr, Ag and Ca, are much reduced and in some case barely or not detected at all. Oxygen also decreased, since its concentration in titanium oxide is higher than the one in proteins.

Table 5.9 Atomic composition (%) of BSA and the investigated surfaces after BSA adsorption (-: non-detected).

	C	N	O	Ti	Si	S	Ag	Al	Na	P	Ca	V	Sr
BSA	64.11	16.62	18.40	-	-	0.71	-	-	-	-	-	-	-
Ti_BSA	67.08	12.07	20.02	0.20	-	0.64	-	-	-	-	-	-	-
Ti64_BSA	53.03	12.83	28.23	3.81	-	0.87	-	0.88	-	-	-	0.35	-
Ti(A-HC-H) _BSA	35.10	7.03	44.09	13.30	-	0.48	-	-	-	-	-	-	-
Ti64(SrAg) _BSA	43.32	9.07	34.13	9.26	-	0.26	0.13	-	-	-	3.84	-	-
Ti64(HF-H_2O_2) _BSA	48.05	13.27	32.66	5.15	-	0.50	-	0.33	-	-	-	0.04	-
SBA2_BSA	34.10	2.79	41.63	-	0.58	-	-	-	-	11.03	9.87	-	-
AgSBA2_BSA	37.53	9.01	40.83	-	0.99	-	1.03	-	0.25	5.39	8.53	-	-
PS_BSA	71.88	8.40	19.15	-	-	0.57	-	-	-	-	-	-	-

On Ti_BSA, titanium is barely detected, suggesting that the protein layer has a thickness of some nanometers. XPS can detect an element only if the core electron of that particular atoms has enough energy to travel towards the surface and escape without any collision with the surrounding atoms. The depth from which an electron can exit the surface is the inelastic mean free path (IMFP), which depends on the kinetic energy of the electron and on the material it is traveling inside. A Ti2p electron has a kinetic energy about 1025 eV, which corresponds to an IMPF of 3-4 nm through amino acids [39], which is about the dimension of a BSA molecule. Since the protein layer is not completely dense, it may be plausible that the titanium signal can be collected through one or two monolayers of albumin, but not more. For the same reason, O on Ti_BSA has the lowest percentage among the Ti surfaces, since the titanium oxide is almost invisible under the proteins. Ti64_BSA has a slightly higher content of Ti and O than Ti, but a comparable amount of nitrogen. These facts suggest that the amount of albumin on the alloy may be somewhat less than on the pure Ti, as indicated by the BCA protein assay (Figure 5.18).

Contrary to what was expected by quantification experiments, on the treated chemical surfaces, the amount of titanium detected after adsorption, that can be at first inversely correlated with the thickness of the protein layer, is higher with respect to untreated samples, and the N is lower (Table 5.9). Ti64(HF-H_2O_2) has an intermediate behavior, since the N% is higher than Ti64, but also the Ti% is a bit higher. This apparent incoherence between the quantification and the XPS results can be explained considering the topography of the surfaces. As already discussed, proteins can adsorb inside the pores of the treated surfaces, diffusing and accumulating inside them. On flat surfaces, all the proteins adsorbed are exposed on the very top of the samples, being all detected by the XPS. On the other hand, on porous specimens, only the proteins that are adsorbed on the top of the pores might be detected by XPS, while the ones accumulated at the bottom of them cannot be revealed, resulting in an apparent reduced amount of proteins on the surfaces. For a similar reason, Ti may appear in higher concentrations on the treated surface after adsorption.

Similar considerations about the decrease of the bulk element concentration can be made for SBA2 and AgSBA2 (Table 5.9). In fact, Si is hardly detected after adsorption of albumin, along with other glass components such as Ca and Ag, the latter only for AgSBA2. On BGs, the presence of the proteins is not much observed through to the content of C and O, which barely change with respect to pristine surfaces, but the increase in nitrogen confirms BSA adsorption. As it was discussed in paragraph 5.2.1, it is believed that proteins, besides being adsorbed on the surface, may be embedded also in the reaction layer of BGs. As consequence, the proteins inside the silica-gel layer may not be detected by XPS. The IMPF of N1s electrons, which have a kinetic energy around 1088 eV, through silica can be lower than 3 nm [40]. Since the reaction layer is not pure silicon dioxide, but a hydrated gel, it is reasonable to think that the IMPF may be slightly higher, but not enough to make N1s electrons escape through all the reaction layer. Contrary, with fluorescence it may be possible to quantify all the proteins on the BGs thanks to the transparency of the glasses. The formation of a complex reaction layer can be

deduced also by the increase of P and Ca concentration after soaking in the protein solution. It is well known that the second step of glass bioactivity is the diffusion and precipitation of phosphates and calcium ions on the silica-gel. PO_4^{2-} are present in the PBS composition, while Ca^{2+} are released from the glasses themselves and then reprecipitate.

After BSA adsorption, the N content on PS is close to 9% (Table 5.9), so it is possible to conclude that also on this surface BSA forms almost a complete and uniform layer. Due to the polymeric nature of the substrate, C% does not change much, while oxygen decreases, being less present in BSA with respect to the substrate and environmental contaminations.

Deconvolution of high resolution spectra after adsorption were performed to investigate the chemical state of adsorbed BSA. C1s, O1s and N1s region were considered. The deconvoluted components were assigned to specific protein groups, according to literature [10,13,41,42], but it is necessary to bear in mind that in the same regions, contributions from the underlying substrates may arise, changing the peak areas and the ratios among them.

At first, deconvolution of BSA was performed, in order to obtain a reference and to compare it with the literature. The results are reported in Figure 5.23 and Table 5.10.

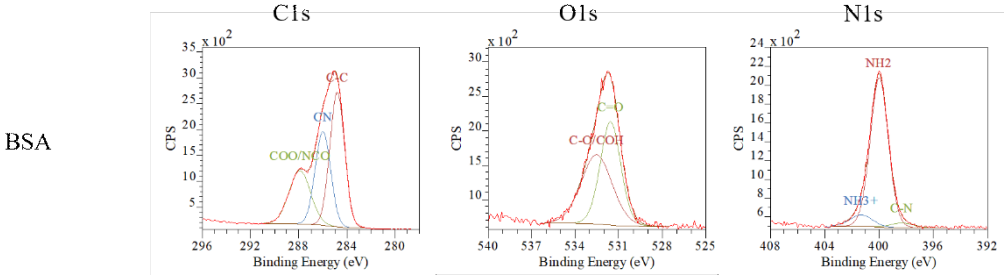

Figure 5.23 Deconvolution of the C1s, O1s and N1s region for BSA.

The C1s peak was deconvoluted using three contributes. The one at lowest energy is related to C-C bonds, at 284.8 eV as usual. By increasing the BE, it was found a contribution from C-N bonds, which is reported to lay in the range of 286-287 eV. And at last, at higher energy there is the peak related to peptidic N=C-O and to COO^- groups, around 288.1 eV. The O1s region is mainly due to the presence of carbon-oxygen bonding, through double and single bonds, at energy of 531.5 eV and 532.6 eV respectively. In the peak related to C-O, contributions related to C-OH are also included, and as consequence the full width half maximum (FWHM) is increased with respect to the C=O peak. At last, also the N1s peak was deconvoluted by using three distinct components. The main one, centered around 400 eV, is related to amine NH_2, while the two minor components, at higher and lower energies, are due to NH_3^+ protonated amine of basic residues, around 401.5 eV, and to C-N bonds, at about 398.8 eV.

Table 5.10 Binding energies and composition of the deconvoluted peaks in the C1s, O1s and N1s region for BSA. Theoretical energies for each component are reported (-: non-detected).

	C1s			O1s		N1s		
	Binding energy (eV)							
	CC (248.8)	C=O/CN (286-287)	COO^-/NCO (288.1)	C=O (531.5)	C-O/C-OH (532.3-532.6)	CN (398.8)	NH_2 (400.0)	NH_3^+ (401.5)
BSA	248.8	286.0	287.9	531.6	532.5	398.3	400.0	401.3
	Peak composition (%)							
	CC	C=O/CN	COO^-/NCO	C=O	C-O/C-OH	CN	NH_2	NH_3^+
BSA	43.3	31.7	25.0	50.2	49.8	3.62	88.0	8.4

Table 5.11 Binding energies and composition of the deconvoluted peaks in the C1s, O1s and N1s region for titanium samples after albumin adsorption. Theoretical energies for each component are reported (-: non-detected).

	C1s			O1s			N1s		
	Binding Energy (eV)								
	CC (248.8)	C=O/CN (286-287)	COO^-/NCO (288.1)	TiO (529.8)	C=O (531.5)	C-O/C-OH (532.3-532.6)	CN (398.8)	NH_2 (400.0)	NH_3^+ (401.5)
Ti_BSA	284.7	286.2	287.9	-	531.5	532.7	398.3	399.7	401.6
Ti64_BSA	284.7	286.1	287.9	529.9	531.2	532.7	398.2	399.7	401.3
Ti(A-HC-H) _BSA	284.8	286.2	288.0	529.7	531.4	532.8	398.5	399.9	401.5
Ti64(SrAg) _BSA	284.7	286.1	288.0	529.7	531.4	532.6	398.6	400.0	401.8
Ti64(HF-H_2O_2) _BSA	284.8	286.2	288.0	529.8	531.5	532.1	398.8	400.0	401.3
	Peak composition (%)								
	CC	C=O/CN	COO^-/NCO	TiO	C=O	C-O/C-OH	CN	NH_2	NH_3^+
Ti_BSA	56.8	23.6	19.6	-	71.2	28.8	5.7	92.5	1.8
Ti64_BSA	53.8	21.9	24.3	17.1	73.2	9.7	10.5	86.7	2.8
Ti(A-HC-H) _BSA	53.5	23.8	22.7	65.4	30.4	4.2	13.7	80.5	5.8
Ti64(SrAg) _BSA	57.7	18.9	23.4	63.6	27.3	9.1	17.3	78.0	4.7
Ti64(HF-H_2O_2) _BSA	46.2	27.3	26.5	28.0	61.8	10.2	13.5	79.9	6.6

The results of the deconvolution performed on the various titanium substrates are reported in Figure 5.24 and Table 5.11.

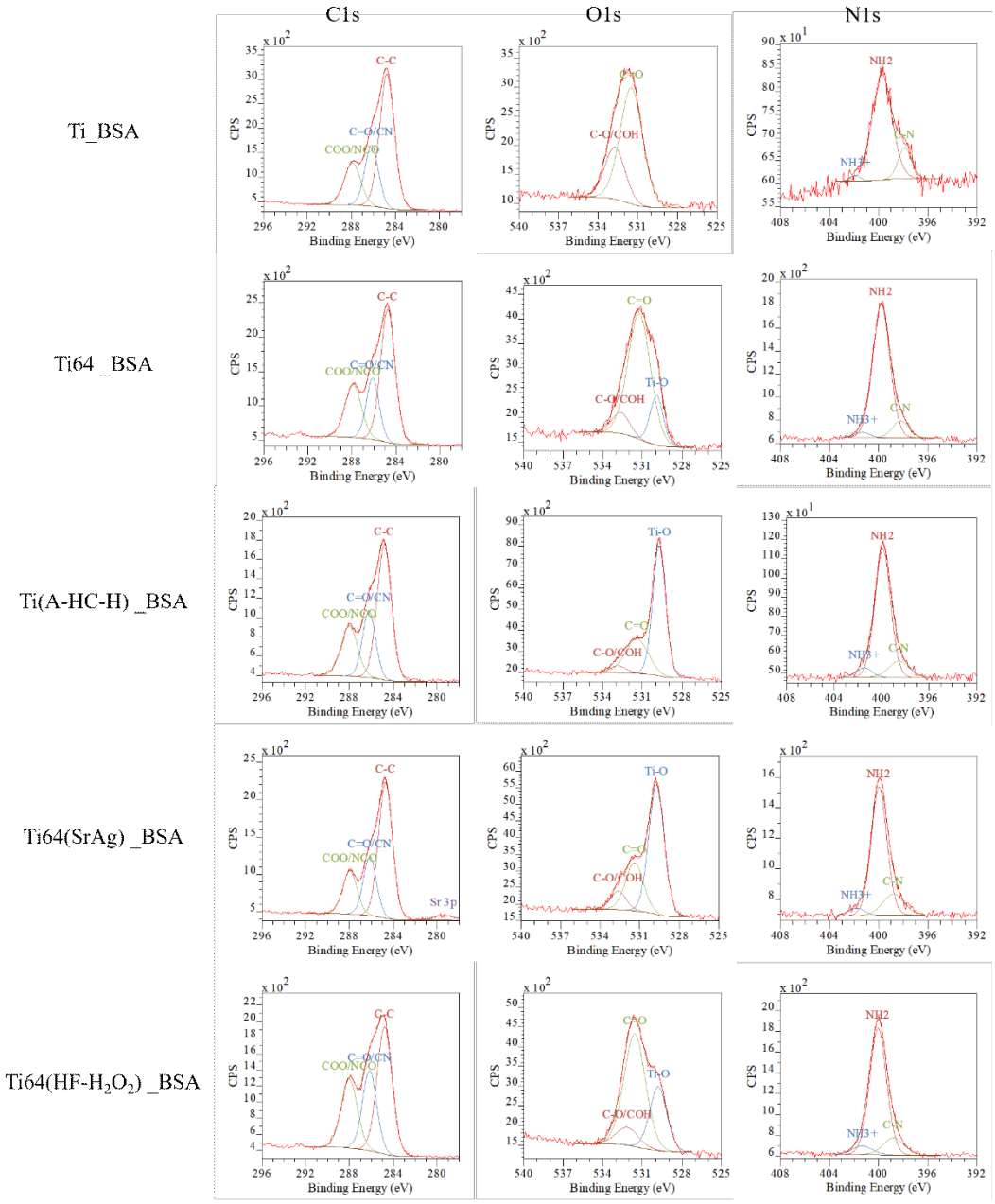

Figure 5.24 Deconvolution of the C1s, O1s and N1s region for titanium surfaces after BSA adsorption.

In the C1s peaks, the contributions related to BSA were observed on each surface, at energies comparable to the ones of the pure protein. This shows that albumin is chemically intact after adsorption. Due to random uptake of environmental molecules, that mainly contribute to the C-C component, and to the effect of surface topography on the detection of adsorbed BSA, the shape of C1s peak on the different surfaces are slightly different. On Ti64(SrAg)_BSA a small contribute from Sr3p in the substrate was also found at low energies, as before adsorption. Despite so, the ratios between CN/CO and COO/NCO components is not much different from the one of pure albumin, which is about 1.2.

The O1s peak was highly affected by the titanium substrates. In fact, the signal from Ti-O is well present and, in some case, dominates the spectra, according to the amount of Ti detected (Table 0.9). The contribution of OHa and OHb, which were well observed in the surface spectra (Figure 1.5), is missing after protein adsorption due to the overlapping with the C=O peaks of proteins. On Ti_BSA, the Ti-O contribute was not found and the O1s peak is due only to C=O and C-O/C-OH groups. The oxide component has a minor contribute on Ti64_BSA and Ti64(HF-H_2O_2)_BSA, on which titanium was found in a small amount. Where Ti was detected in a larger amount, that means on Ti(A-HC-H) and Ti64(SrAg), Ti-O contribution prevails in the O1s region. Despite that, the components related to albumin, C=O and C-O/C-OH, were found on all the samples, at energies similar to the one found in BSA. Since the influence of the substrates is high, and some peaks, such as the one related to titanium OH groups, can be hidden beneath the protein signal, the area ratios between C=O and CO-O/C-OH peaks may not be considered significative and should be not compared to the one of pure BSA. N1s peaks after adsorption are due only to nitrogen from proteins, and they were deconvoluted accordingly, by using the same three peaks of pure BSA. The main contribution on all the samples arises from the amine NH_2 groups, always found around 400.0 eV. The CN related contribution was also found on all the substrates, in the same energy range of pure albumin. Interestingly, the NH_3^+ peak was observed too, again on all the titanium surfaces. This fact suggests that BSA adsorbs in its zwitterionic form, with both charged amino and carboxyl groups that can interact with the charged groups on the surface.

Regarding SBA2 and AgSBA2 after BSA adsorption, deconvolution was performed on C1s and N1s regions. It was not possible to perform a reasonable fitting of the O1s region due to the complexity of the outer layer on such surfaces, formed by the hydrated silica-gel, adsorbed ions from solution and albumin. In fact, there are numerous oxygen containing functional groups that have overlapping XPS energies, such as SiO, non brdging oxygen, carbonates, OH, adsorbed waters, PO_4^{2-}, and C-O and C=O bonds within the proteins. Since it is hard to hypothesize a composition of the glass surfaces, it is not possible to create a reliable model for XPS fitting. The results obtained are shown in Figure 5.25 and Table 5.12.

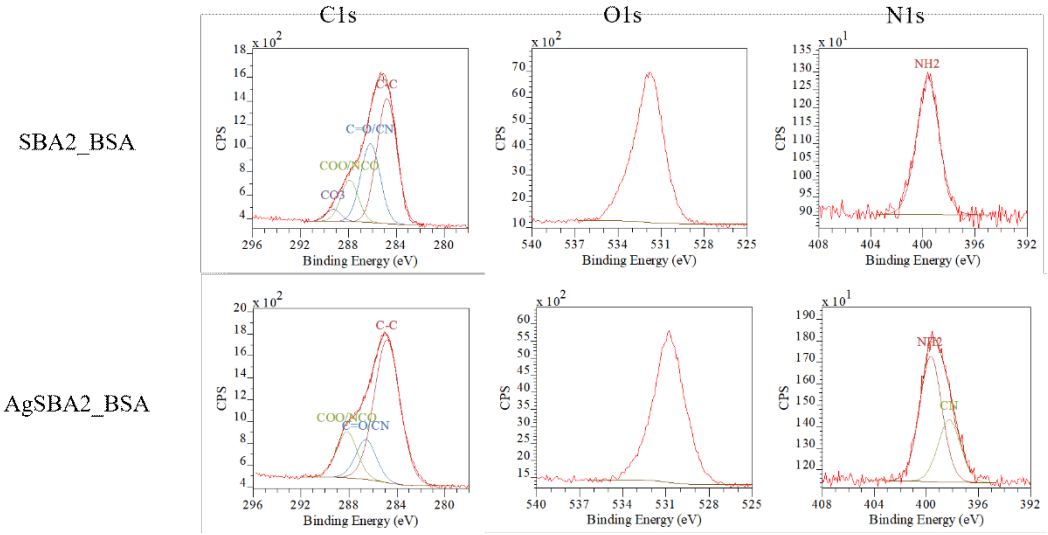

Figure 5.25 Deconvolution of the C1s and N1s region for BGs surfaces after BSA adsorption. O1s peaks are also reported

Table 5.12 Binding energies and composition of the deconvoluted peaks in the C1s, O1s and N1s region for BGs samples after albumin adsorption. Theoretical energies for each component are reported (-: non-detected).

	C1s				O1s		N1s	
	Binding Energy (eV)							
	CC (248.8)	C=O/CN (286-287)	COO^-/NCO (288.1)	CO_3 (289.4)	O1s	CN (398.8)	NH_2 (400.0)	NH_3^+ (401.5)
SBA2_BSA	284.8	286.2	287.9	289.3	531.8	-	399.6	-
AgSBA2_BSA	284.8	286.6	288.2	-	530.8	398.3	399.8	-
	Peak composition (%)							
	CC	C=O/CN	COO^-/NCO	CO_3	O1s	CN	NH_2	NH_3^+
SBA2_BSA	51.0	30.98	14.58	3.48	100	-	100	-
AgSBA2_BSA	67.5	15.0	17.5	-	100	24.9	75.1	-

Table 5.13 Binding energies and composition of the deconvoluted peaks in the C1s, O1s and N1s region for PS after albumin adsorption. Theoretical energies for each component are reported (-: non-detected).

	C1s			O1s		N1s		
	Binding energy (eV)							
	CC (248.8)	C=O/CN (286-287)	COO^-/NCO (288.1)	C=O (531.5)	C-O/C-OH (532.3-532.6)	CN (398.8)	NH_2 (400.0)	NH_3^+ (401.5)
PS	248.8	286.3	288.3	531.6	532.8	398.0	399.7	401.3
	Peak composition (%)							
	CC	C=O/CN	COO^-/NCO	C=O	C-O/C-OH	CN	NH_2	NH_3^+
PS	55.2	32.5	12.3	45.4	54.6	9.7	88.7	1.6

As in the case of Ti-based samples, in the C1s region the typical peaks of albumin were found on both SBA2 and AgSBA2 after adsorption, at comparable energies. On SBA2, a highly energetic contribution was also found, at 289.3 eV, which was attributed to carbonates that may precipitate on the glass as consequence of surface reactions. For the uncertainty of the effective surface composition, to compare the area ratios of BSA peaks before and after adsorption on BGs may lead to wrong conclusions. The O1s peaks were not deconvoluted, as already discussed, still it is possible to notice that on AgSBA2_BSA the peak is shifted at lower energy, 530.8 eV, with respect to SBA2_BSA, which has the O1s peak centered at 531.8 eV. This may be the results of a different surface reactivity, for example, a higher content of non-bridging oxygen or SiO_2, which have low BE, in the reaction layer of AgSBA2 compared with SBA2. Regarding nitrogen, the deconvolution of the N1s peak for SBA2_BSA resulted in just one contribution, at 399.6, attributed to NH_2 groups of the protein. It is possible that the other two peaks for albumin N1s were not found due to the low amount of N detected (Table 0.9) and the high noise in the spectra. Thanks to better condition, the contribution by CN groups was found on AgSBA2, along with the usual NH_2 peak, while the protonated amine signal was still missing. Since the NH_3^+ signal its quite low, it might be that it was not detected for technical issues and not because the adsorbed BSA does not have such groups. In the case of BSA adsorption on bioactive glass surfaces, XPS seems to confirm that albumin adsorbs without any severe modifications to its chemical structure, but also highlight the very complex mechanisms that are involved in the adsorption of proteins on such reactive surfaces.

At last, the results of C1s, O1s and N1s fitting of PS_BSA are reported in Figure 5.26 and Table 5.13.

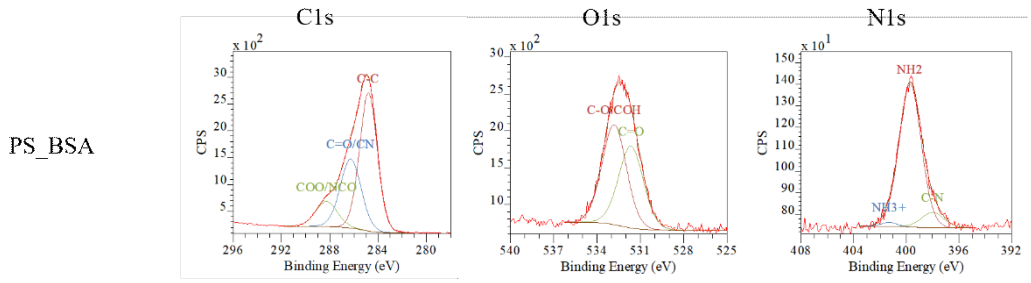

Figure 5.26 Deconvolution of the C1s, O1s and N1s region for PS after BSA adsorption.

The C1s region was deconvoluted with the usual three peaks, corresponding to the CC, C=O/CN and COO^-/NCO protein groups, centered at energies that are comparable to the ones of pure BSA. The CC contribution is quite high due to the polymeric nature of the substrate. The same similarities were observed both in the O1s region, where C-O/COH and C=O contribution were found, and in the N1s region, which was fitted with the same three components as BSA. Also in the case of adsorption on polystyrene, albumin is chemically intact and it is in the zwitterionic conformation, exposing negative COO^- and positive NH_3^+ groups.

The same kind of analysis was performed on samples after fibronectin adsorption. The composition of surfaces with FN is reported in Table 5.14.

Table 5.14 Atomic composition (%) of the investigated surfaces after FN adsorption (-: non-detected).

	C	N	O	Ti	Si	S	Ag	Al	Na	P	Ca	V	Sr
Ti_FN	58.14	12.57	26.54	1.82	-	-	-	-	-	-	-	-	-
Ti64_FN	54.18	10.26	30.53	2.59	-	2.03	-	-	-	-	-	0.4	-
Ti(A-HC-H) _FN	52.76	11.41	29.33	6.49	-	-	-	-	-	-	-	-	-
Ti64(SrAg) _FN	53.50	14.23	26.72	4.55	-	-		-	-	-	3.84	-	-
Ti64(HF-H_2O_2) _FN	54.83	13.66	27.70	3.80	-	-	-	-	-	-	-	-	-
SBA2_FN	42.57	1.55	31.44	-	1.01	-	-	-	-	11.14	12.07	-	-
AgSBA2_FN	51.26	0.79	33.80	-	7.84	-	0.53	-	0.95	-	4.76	-	-
PS_FN	81.52	6.40	12.08	-	-		-	-	-	-	-	-	-

Regarding titanium-based substrates, after adsorption of FN the results are quite similar, much more than in the case of BSA adsorption. All these samples have comparable amount of carbon, nitrogen and oxygen, with C and N increased with respect to the pristine surfaces and O reduced (Table 5.2), as expected. As albumin, FN can penetrate the pores on the treated surfaces, but possibly less with respect to BSA due to bigger dimensions. Thus, the protein can accumulate more on the top of the pores and be detected by XPS, resulting in a similar amount of nitrogen on all the titanium samples. By comparing the quantification results and the XPS chemical analysis for both albumin and fibronectin, it seems that the nitrogen content on the surface is not proportional to the amount of proteins adsorbed and it can not be used as reliable indicator for adsorption quantification. Titanium percentage after FN adsorption has the same trend as in the case of BSA, it increases with increasing surface porosity and structuration, being lower on flat Ti_FN and Ti64_FN and higher on Ti(A-HC-H)_FN and Ti64(SrAg)_FN. This may happen for the same reason as discussed for BSA, due to the fact that on porous surfaces the protein has few niches where to accumulate and therefore more signal from the underlying substrates can be collected. Contrary to BSA, sulfur was not detected on all the samples, including BGs and PS, but Ti64_FN. Fibronectin has a very low amount of cysteine residues, about the 2.7% of the total amino acids [43], and a consequently very low amount of S, possibly too low to be detected by XPS after adsorption. The high value on T64_FN may be due to some environmental contamination. Coherently with the formation of a layer on the surface, the alloying or the doping elements, such as Al, V, Ag and Sr, were no more detected after FN adsorption. On Ti64(SrAg)_FN, Ca was still found due to its high content in the calcium titanate layer.

Concerning fibronectin adsorption on BGs, XPS results are not trivial to discuss. In fact, while C amount increased, suggesting the adsorption of carbonaceous molecules, such as proteins, N content is very low, with almost no increase on AgSBA2_FN with respect to the substrate (Table 5.2). Plus, the highest amount of N found on SBA2_FN compared to AgSBA2_FN seems to suggest a higher adsorption on the undoped BG, at first. Si is also well present in the surface composition after FN adsorption, 1.01% and 7.84% on SBA2_FN and AgSBA2_FN respectively. Considering what was discussed about the interactions between the adsorbing proteins and the growing silica-gel layer, the IMPF of nitrogen and the quantification results showed in the previous paragraph, it may be possible to speculate that FN somehow tends to remain less on the bioactive glass surface, in particular in the case of AgSBA2, while it adsorbs more within the reaction layer of the glass surface. Another possibility is that the binding strength between FN and BGs is reduced with respect to the one between BSA and BGs and that more proteins are removed from the glass surfaces during the rinsing steps.

On PS_FN, the results were similar to what was expected. On this surface, C is not significant of protein adsorption, but the marked increase in N% confirms the presence of fibronectin also on PS. As consequence of protein adsorption, also oxygen is reduced.

As for BSA, peak fitting of C1s, O1s and N1s region was performed for samples after FN adsorption.

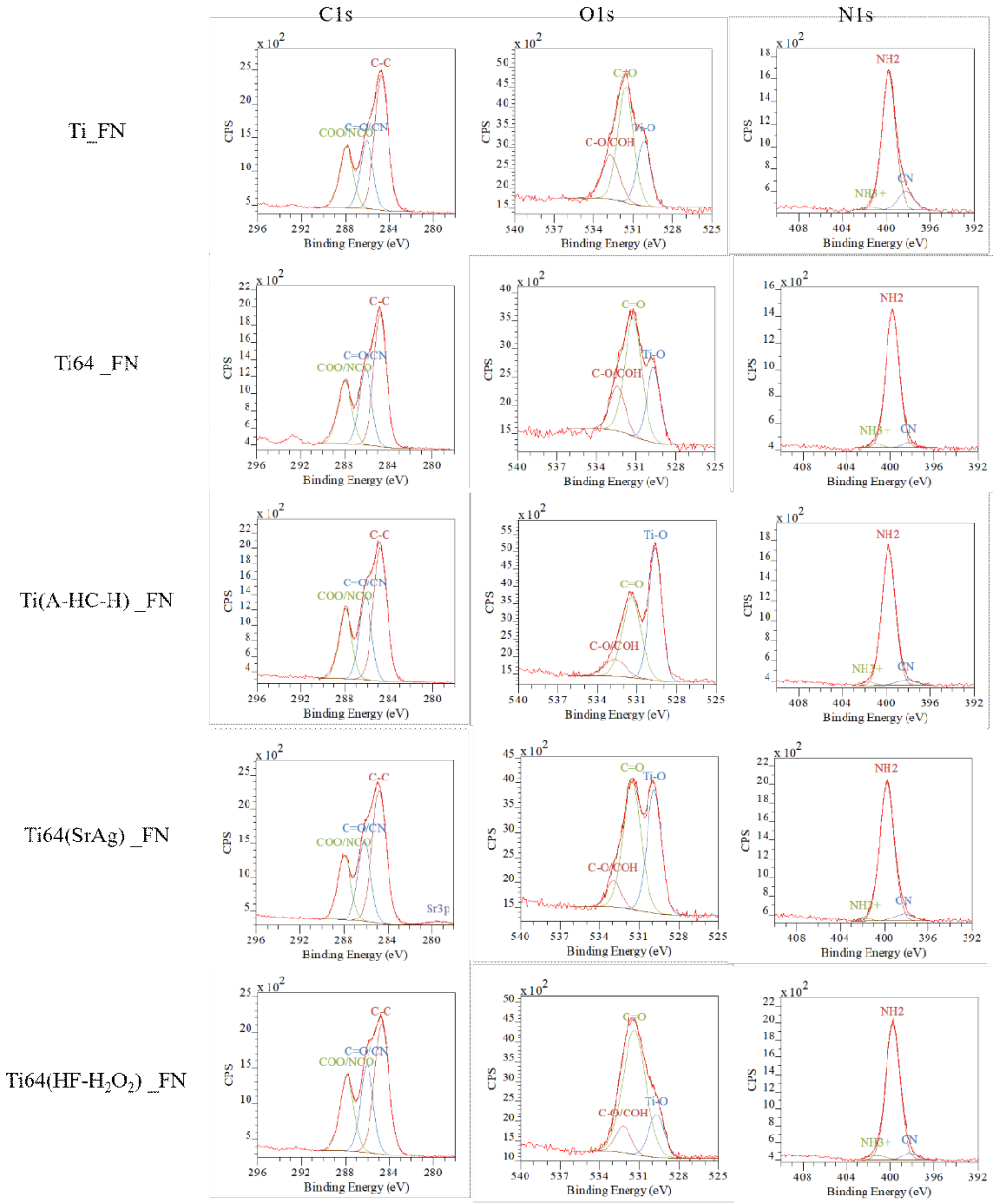

Figure 5.27 Deconvolution of the C1s, O1s and N1s region for titanium surfaces after FN adsorption.

The fitting results for titanium samples are reported in Table 5.15 and Figure 5.27 Deconvolution of the C1s, O1s and N1s region for titanium surfaces after FN adsorption. As for BSA, the C1s peak arises thanks to the contribution of CC, C=O/CN and COO^-/NCO bonds. The binding energies of the different components are similar among the different samples and to pure BSA (Table 0.10), considered as protein model in this case. The shapes of the peaks on the various surfaces are mainly dictated by the intensity of the CC contribution, which may change due to environmental contaminations. On the other hand, the amount of protein related C=O/CN and COO^-/NCO peaks is similar on every surface, indicating that FN is adsorbed in an unaltered chemical state on each surface. The O1s peaks are highly

influenced by the substrate Ti-O signal. In fact, the intensity of such peak was found to vary a lot with respect to the Ti% observed in Table 0.14. Ti(A-HC-H)_FN and Ti64(SrAg)_FN, which have the highest amount of Ti, show an intense peaks related to Ti-O groups. On the contrary, the contribution of Ti-O on Ti_FN and Ti64_FN, having low Ti%, is much reduced. Ti64(HF-H_2O_2)_FN had a peculiar behavior. In fact, despite having a higher Ti content than the untreated titanium substrates, the Ti-O peak is reduced. Considering that the main signal on the pristine surface was the one related to acidic OH, at 530.7 eV (Table 0.3), it is possible that the C=O contribution may be due also to that specific substrate component. Following the supposition that the O1s peaks are determined to some extent also by the substrate and not only by the adsorbed fibronectin, it does not seem reasonable to compare the areas of the different contribution. In the end, the deconvolution of the nitrogen peak led to the expected results. In fact, the main contribution found on all samples, centered at 399.8 eV, is due to NH_2, while two minor components, related to CN and charged NH_3^+ groups, were also observed. As for BSA, fibronectin adsorbs on titanium surfaces in its charged zwitterionic conformation, with COO^- and NH_3^+.

Repeating the same considerations that were made for the deconvolution of albumin on BGs, in the case of FN the fitting of XPS data was performed only on C1s and N1s region. The results, plus the position and the spectra of the O1s peak are reported in Figure 5.28 and Table 5.16.

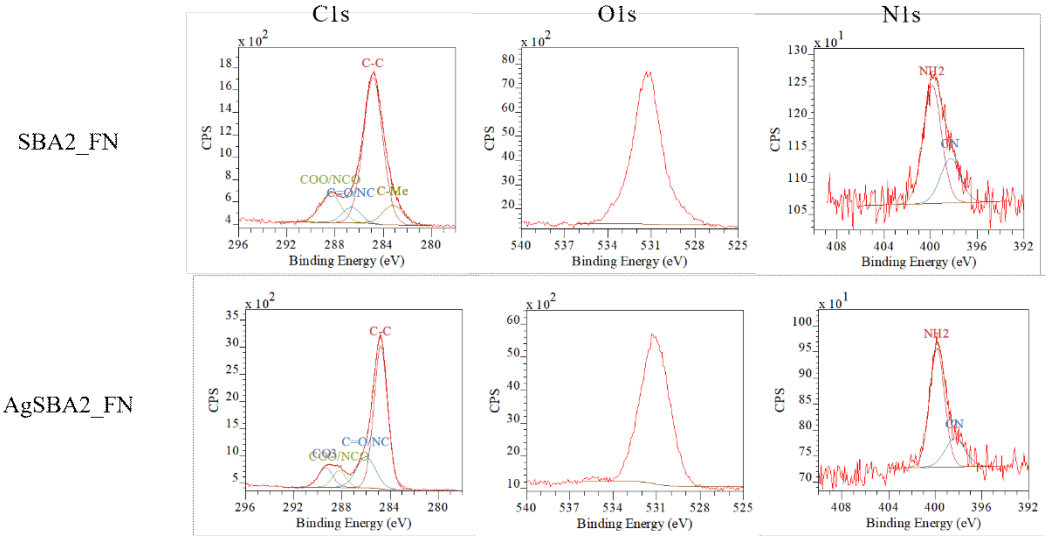

Figure 5.28 Deconvolution of the C1s and N1s region for BGs surfaces after FN adsorption. O1s regions are also reported.

Due to low amount of protein within the first nanometers, the protein signals in the C1s region are quite low, and the spectra is mainly affected by CC peak on both SBA2_FN and AgSBA2_FN. The C=O/CN and COO^-/NCO components were still observed at energies corresponding to the one of protein groups. In order to obtain a good fitting, it was necessary to add one component for both spectra. In case of SBA2_FN, a low energetic peak was found, at 283.2 eV. As in the case of pristine SBA2 (Table 5.4), this peak was attributed to C-Me bonds, deriving from

contaminations during the preparation of the samples. On the other hand, a new high energetic contribution was observed on AgSBA2_FN, at 289.3 eV. Again, in analogy to what was done in the case of pristine BGs surfaces, that peak was assigned to carbonates CO_3 groups, which may be formed as side reactions during the glass soaking. After FN adsorption, the peak in the O1s region is centered around 531.2 for both SBA2 and AgSBA2, and it has a similar shape, indicating some analogies in the products of the combined reaction of the glass surface and FN adsorption, contrary to what happened with albumin (Figure 5.25). The effect of different proteins on the reactions that occur on BGs surfaces once they are put in contact with biological fluids may be a crucial point in order to better understand the actual bioactivity of glass systems *in vivo* and further studies are desirable. Due to the very low amount of nitrogen, the N1s spectra have a very high noise to measurement ratio, as possible to see in Figure 5.28. For both SBA2_FN and AgSBA2_FN, only two contributions were found in this region, one attributed to NH_2 and the other one to CN bonds. The signal from the protonated amines was not found, but it may be due to the low intensity of the total peak. Again, as well as after albumin adsorption, the picture drawn by XPS analysis is one of very complex protein-BGs interaction mechanisms, which depends not only on the composition of the glass but also on the type of adsorbing proteins.

To conclude, deconvolution was performed also on PS_FN and the fitting results are presented in Figure 5.29 and Table 5.17.

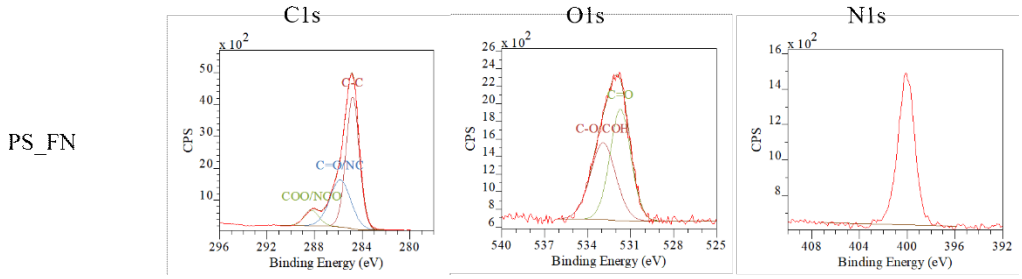

Figure 5.29 Deconvolution of the C1s, O1s and N1s region for PS after FN adsorption.

As usual, the typical peaks of proteins were observed in the C1s, O1s and N1s region. CC, C=O/CN and COO^-/NCO were found at energies corresponding to protein ones, with the CC being the predominant signal due to the carbon content in the substrate. The O1s peak was fitted by the contributes of C-O/COH and C=O, at respectively 531.7 ant 532.9 eV, that arise from oxygen containing groups of FN. In the case of nitrogen, only one contribution at 400 eV, attributed to NH_2, was found. As in the case of BGs, it is possible that the low amount of nitrogen hinders the detection of the minor contributions to N1s region.

Table 5.15 Binding energies and composition of the deconvoluted peaks in the C1s, O1s and N1s region for titanium samples after fibronectin adsorption. Theoretical energies for each component are reported (-: non-detected).

	C1s			O1s			N1s		
	Binding Energy (eV)								
	CC (284.8)	C=O/CN (286-287)	COO^-/NCO (288.1)	TiO (529.8)	C=O (531.5)	C-O/C-OH (532.6)	CN (398.8)	NH_2 (400.0)	NH_3^+ (401.5)
Ti_FN	284.7	286.1	287.9	530.2	531.6	532.7	398.2	399.8	401.4
Ti64_FN	284.8	286.1	288.0	529.7	531.2	532.4	398.5	399.8	401.1
Ti(A-HC-H) _FN	284.8	286.1	288.0	529.6	531.4	532.7	398.2	399.8	401.7
Ti64(SrAg) _FN	284.8	286.1	288.0	529.9	531.5	532.9	398.2	399.8	401.7
Ti64(HF-H_2O_2) _FN	284.7	286.1	287.9	529.8	531.1	532.0	398.3	399.8	401.3
	Peak composition (%)								
	CC	C=O/CN	COO^-/NCO	TiO	C=O	C-O	CN	NH_2	NH_3^+
Ti_FN	52.3	24.1	23.6	25.6	52.4	22.0	13.3	84.9	1.7
Ti64_FN	48.0	26.0	26.0	26.7	54.9	18.4	3.9	91.9	4.2
Ti(A-HC-H) _FN	49.0	27.8	23.2	48.3	41.9	9.8	5.3	92.3	2.4
Ti64(SrAg) _FN	50.5	27.2	22.3	40.0	51.8	8.2	6.3	92.1	2.6
Ti64(HF-H_2O_2) _FN	47.2	27.1	25.7	23.2	32.1	44.7	4.7	91.2	4.1

Table 5.16 Binding energies and composition of the deconvoluted peaks in the C1s, O1s and N1s region for BGs samples after fibronectin adsorption. Theoretical energies for each component are reported (-: non-detected).

	C1s					O1s		N1s	
	Binding Energy (eV)								
	CC (248.8)	C=O/CN (286-287)	COO^-/NCO (288.1)	CO_3 (289.4)	C-Me	O1s	CN (398.8)	NH_2 (400.0)	NH_3^+ (401.5)
SBA2_FN	284.8	286.6	288.4	-	283.2	531.1	398.3	399.8	-
AgSBA2_FN	284.8	286.0	288.2	289.3	-	531.3	398.3	399.8	-
	Peak composition (%)								
	CC	C=O/CN	COO^-/NCO	CO_3		O1s	CN	NH_2	NH_3^+
SBA2_FN	68.8	6.9	14.3	-	10.1	100	24.4	75.6	-
AgSBA2_FN	63.7	19.6	7.4	9.3	-	100	70.5	29.5	-

Table 5.17 Binding energies and composition of the deconvoluted peaks in the C1s, O1s and N1s region for PS samples after fibronectin adsorption. Theoretical energies for each component are reported (-: non-detected).

	C1s			O1s		N1s		
	Binding energy (eV)							
	CC (248.8)	C=O/CN (286-287)	COO^-/NCO (288.1)	C=O (531.5)	C-O/C-OH (532.6)	CN	NH_2	NH_3^+
PS_FN	284.8	285.8	288.2	531.7	532.9	-	400.0	-
	Peak composition (%)							
	CC	C=O/CN	COO^-/NCO	C=O	C-O/C-OH	CN	NH_2	NH_3^+
PS_FN	58.9	33.4	7.7	54.4	45.6	-	100	-

Summarizing the results obtained by XPS measurement after adsorption of albumin and fibronectin on the surfaces investigated in this work, it is possible to conclude that both BSA and FN are not chemically modified after adsorption and that they maintain the negatively charged carboxyl groups and the positively charged amine groups. By comparison with the quantification results, it was not observed a linear or simple correlation between nor the amount of nitrogen, in particular, carbon or oxygen and the quantity of protein adsorbed, neither with the residual signal from the substrate. This effect is further enhanced by complex surface topography, as in the case co Ti(A-HC-H) or Ti64(SrAg), or by surface reactivity, as in the case of BGs. Regarding the bioactive glasses, XPS analysis supports the hypothesis of an extremely complex interplay between proteins, the glass surface and the growing silica-gel layer.

5.2.3. Surface coverage by the protein layer

The second aspect of protein adsorption that was investigated is the extension and distribution of the protein layer on the different surfaces. If the protein layer fully covers the surface, most of the material properties can then be masked to the cells, in particular the surface chemistry, charge, SFE, and wettability. The roughness might still be exposed to cells if the protein layer is not too thick. The protein layer was imaged at two different scales thanks to fluorescent imaging and to a novel approach to Kelvin probe force microscopy, which was never used previously to image proteins on biomaterial surfaces of clinical interest.

5.2.4. Fluorescent imaging

The distribution of albumin and fibronectin at a millimetric scale was investigated thanks to the use of fluorescent labeled proteins.

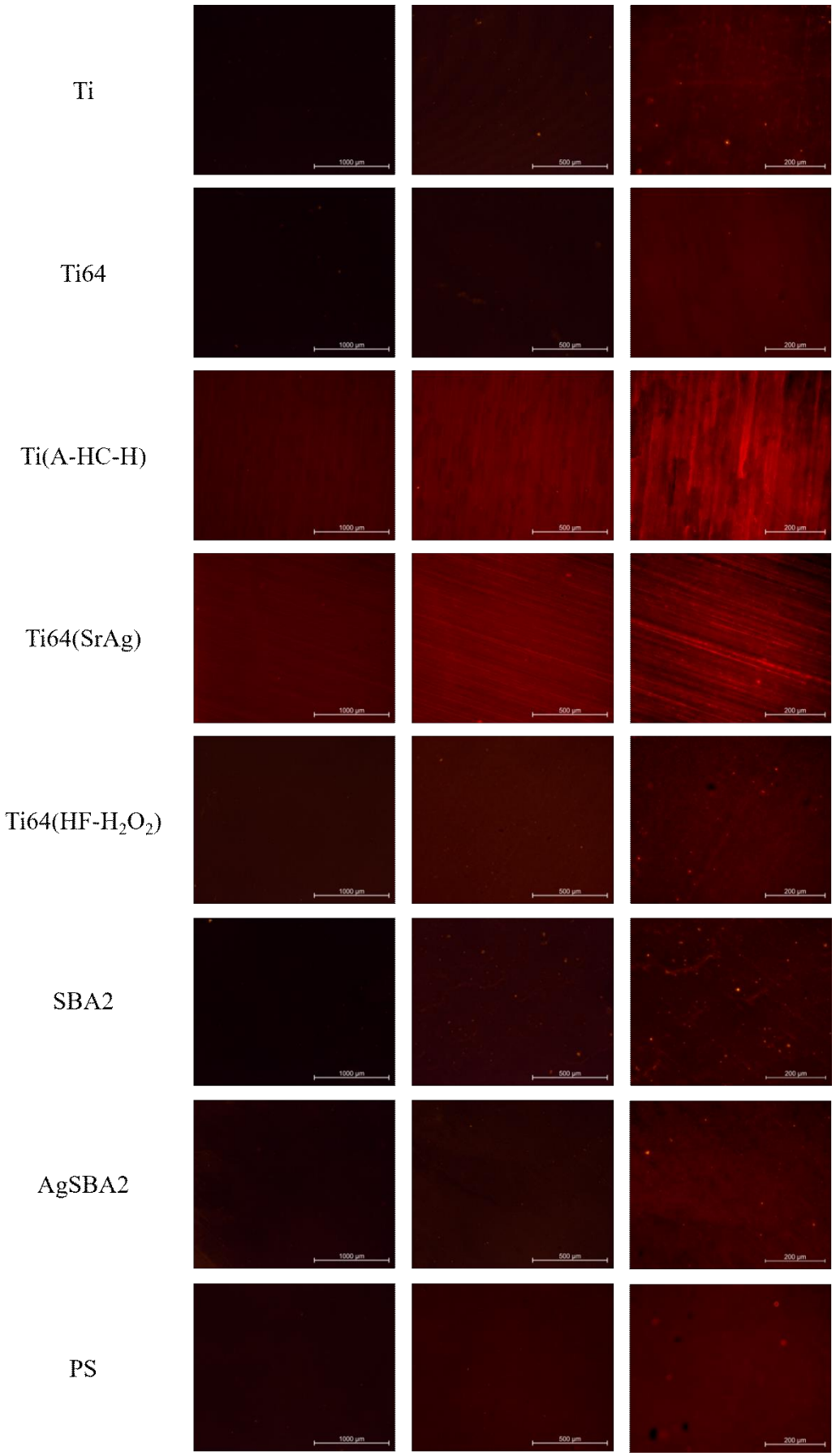

Figure 5.30 Fluorescent images of adsorbed albumin on the different substrates at increasing magnification: 50x (left); 100x (center); 200x (right).

BSA distribution on all the samples is shown in Figure 5.30. At lower magnification (50x, Figure 5.30), albumin is visible only on highly adsorbing surfaces, such as Ti(A-HC-H) and Ti64(SrAg). On the other surfaces, the amount of adsorbed protein is too low to emit enough fluorescent light for being visualized. Increasing the magnification (100x, Figure 5.30) allowed to image the adsorbed protein on almost all the surfaces, but not on Ti and Ti64. BSA seems to form a continuous layer on the samples, even though it can be sometimes inhomogeneous. In particular, on flat surfaces, such as PS and BGs, the protein distribution seems homogeneous at this magnification. The same happens for Ti64(HF-H_2O_2). On the other hand, on Ti(A-HC-H) and Ti64(SrAg), there is an evident effect of the surface features on increasing the local amount of adsorbed protein. In particular, on Ti64(SrAg) albumin accumulates in the deepest polishing grooves. This behavior is confirmed at higher magnification (200x, Figure 5.30). In this case, the protein layer is visible on all the surfaces. On Ti, Ti64, Ti64(HF-H_2O_2) and PS no aggregates were noticed and the substrates were fully and homogeneously covered by the proteins. The image of Ti(A-HC-H) shows a slight uneven coverage of the surface, with some dark spot. As already said, it is known that the oxide layer on this surface is quite unstable and can delaminate spontaneously in some point [5]. When this happens, the underlying pure Ti is exposed, with a much lower protein binding power, resulting in dark areas in the fluorescent images. At high magnification, it was noticed that on SBA2 there are some points where albumin accumulates, such as the grit marks. This was observed in a lesser extent on AgSBA2, where the protein layer is more homogeneous. The presence of silver may induce a more homogeneous adsorption on the surface, or it is possible that, thanks to the increased affinity for BSA limits the effect of the surface features that act as accumulating points.

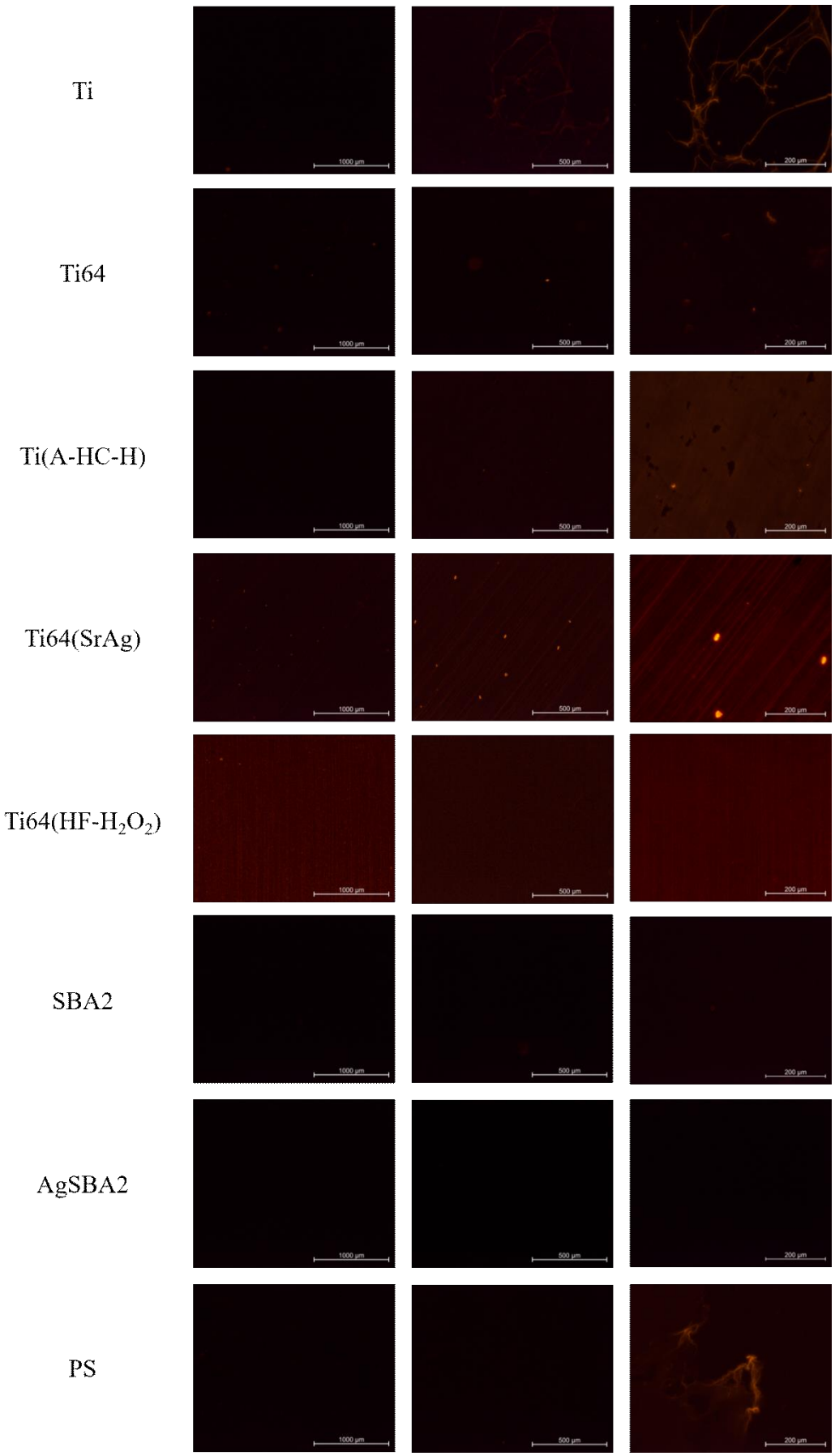

Figure 5.31 Fluorescent images of adsorbed fibronectin on the different substrates at increasing magnification: 50x (left); 100x (center); 200x (right).

The results of the fluorescent imaging study on the fibronectin adsorption are reported in Figure 5.31. As possible to see, on many surfaces the red protein can be barely observed. The presence of the protein on all the samples used for the microscopic analysis was sure, since they are the exact same specimens on which the quantification reported in paragraph 5.2.1 was performed. So, the amount of protein on some samples is low enough that cannot be visualized. Since BSA layer was visible on all the surfaces, at least at high magnification, it is possible to speculate that the total amount of adsorbed fibronectin is quite lower than the adsorbed albumin. With respect to albumin, the fibronectin layer is generally less homogeneous, in particular on the less adsorbing surfaces. On Ti samples, the layer was not visible at low magnification, while by increasing the enlargement (Figure 5.31), it can be noticed that FN adsorbs in a filamentous network, as previously reported by Jia et al. [44]. A similar behavior was observed on PS and on Ti64, on the latter smaller aggregates were found. Such inhomogeneous distribution on low-binding surface might be due to a low number of binding sites. When the affinity of FN for the surface is increased, adsorption seems to take place in a more homogeneous way, since an higher number of binding sites is more distributed on the surface. On Ti(A-CH-H), Ti64(SrAg) and Ti64(HF-H_2O_2) the protein layer covers all the imaged areas. As in the case of BSA, the treated pure titanium Ti(A-HC-H) clearly has some areas where proteins are not adsorbed, that correspond to zone where the porous oxide layer detached. Some aggregates were also found on Ti(A-HC-H) and Ti64(SrAg). On the latter, the aggregates were bigger and sometimes very long filaments, even up to 400 μm, have been found, as shown in Figure 5.32.

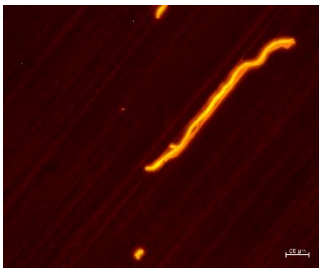

Figure 5.32 Detail of a fibronectin filament found on Ti64(SrAg)

At last, on both SBA2 and AgSBA2 the signal was too low to be imaged.

Based on the fluorescent imaging, it is possible to hypothesize that when the affinity of FN for the surface is low, it adsorbs in a filamentous network, while when the protein adsorbing capability of the surface its high, the protein can adsorb more homogeneously. It is also possible that the structured topography of the treated titanium samples, with pores where the proteins can be entrapped, may hinder the formation of network-like adsorption patterns.

5.2.5. Kelvin probe force microscopy

Protein distribution at the microscale was investigated by imaging the surface potential thanks to KPFM. Potential imaging was already employed to investigate protein adsorption, but, to the best of the authors knowledge, it was employed only

on nanometrically flat metal substrates, such as CoCrMo and Ti6Al4V alloy [45,46]. In this work, KPFM was employed for the first time to investigate BSA and FN adsorption on rough titanium substrates developed specifically for osteointegration and on bioactive glasses. It was not possible to use KPFM on PS due to its strong insulating nature and to the fact that electrostatic charges accumulate easily in its surface, heavily interfering with the instrument.

At first, the distribution of albumin was investigated on a 100*100 μm areas on the several titanium samples, as reported in Figure 5.33. These samples have been prepared by adsorbing only a part of the surface with the protein layer with a known border between the covered and un-covered areas. As general consideration, it is possible to see that on every surface the protein layer is invisible in the topographical images and no aggregates are also deposited on the surface. This means that the overall thickness of the protein layer is in the range of very few nanometers, consistently with what was deduced by XPS measures. Since cells, and osteoblasts in particular, are sensitive to the morphological features of the surface in the micrometric range, it is positive the fact that the transient protein matrix seems not capable to level the surface micrometrical structure, which can still perform their osteoblast adhesion enhancing effect. On the other hand, the potential images can reveal the albumin layer, which is always at lowerpotential (darker areas in the images) with respect to the titanium substrates. This is in accordance to what has been already reported in literature, considering organic molecules, such as proteins or DNA [47,48], even in case of albumin on Ti6Al4V [46]. The albumin layer is mainly homogeneous on all the surfaces, with the only exception of Ti64(SrAg). In this case, there is a variation in the potential distribution of the adsorbed proteins, but it can be due to the potential of the surface itself, which is intrinsically uneven. Interestingly, on Ti64(SrAg), a much lower potential is observed along the deepest grooves of the surface. This confirms the accumulation of adsorbed proteins in correspondence of surface features such as pores or valleys, as observed also by fluorescence imaging. The sharpness of the border between the areas with and without BSA adsorbed is related to the specific preparation of these samples and wettability of the surface, in fact, the samples with lower wettability, Ti, Ti64 and Ti(A-HC-H), shows a net boundary between the bright and the dark areas in the potential images, while the other two substrates have a more unprecise confinement of the protein, due to spreading of the protein solution drop. The potential measured by the KPFM is not the absolute potential of the sample surface, but it depends on the charge distribution in all the system, sample and instrument, which is determined by factors that are extremely hard to control. Thus, the scale of the potential is always set to start from 0 V. What can be considered reliable, it is the difference between the potential of the substrates and the one of the adsorbed proteins. On Ti, this difference is equal to about 180 mV; on Ti64 to 130 mV; on Ti(A-HC-H) it is around 150 mV; on Ti64(SrAg) it is lowered to 20 mV; and at last, on Ti64(HF-H_2O_2), it is around 60 mV. The potential gap between the surface and albumin may be caused by a different orientation of the protein on the samples, but also by a difference between the potential of the titanium surfaces themselves. Since it is reported that the work function, and the surface potential as consequence,

of different types of titanium oxide may vary up to some volts [49], it is not possible to assess if the potential changes are due to a different protein orientation or a variation in the titanium surface.

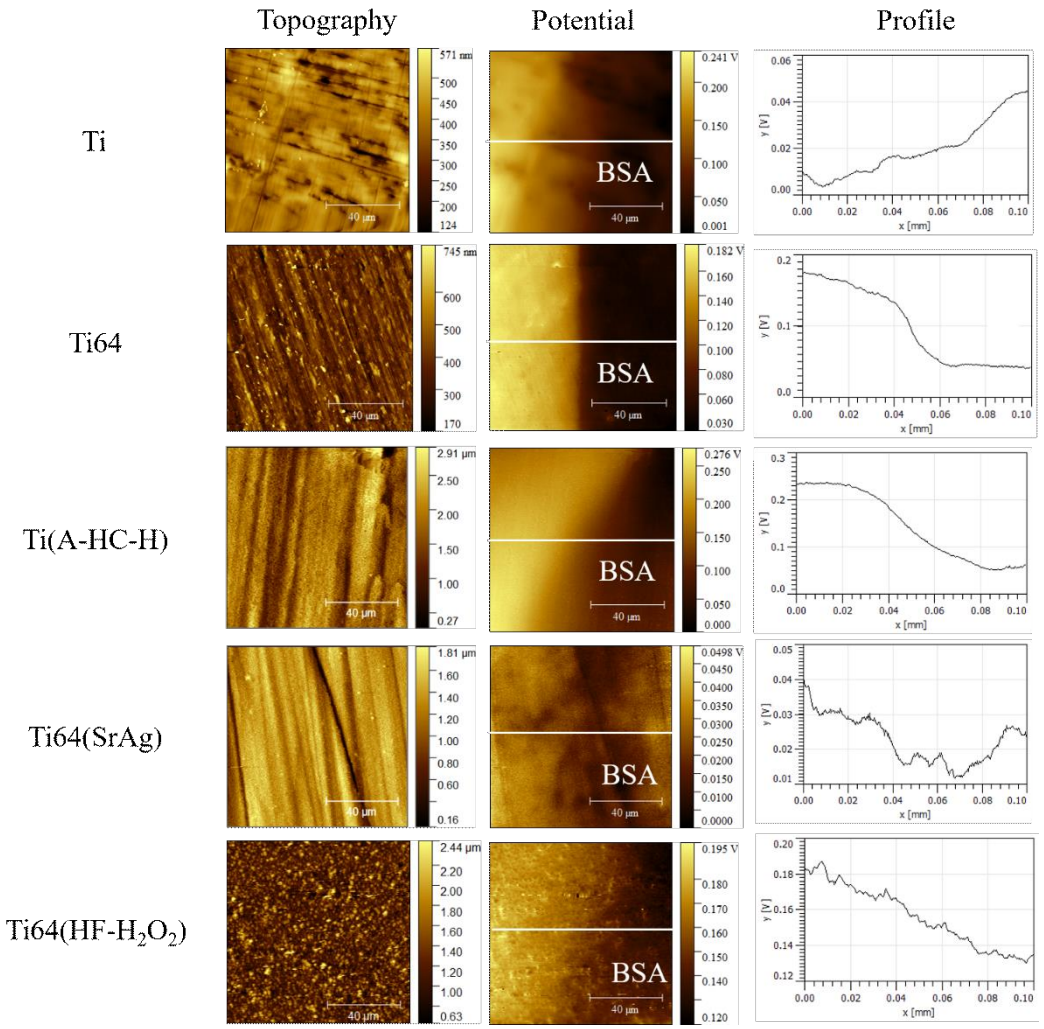

Figure 5.33 Topography and potential 100*100 µm images for titanium surfaces half covered by BSA (lighter areas). The potential profile along the with line is reported in the third column.

Adsorption of albumin was also investigated by increasing the magnification of the KPFM images, by performing 5*5 µm scans (Figure 5.34). The topographical images report the expected morphology, according to SEM observations (Figure 5.1), without signs of proteins agglomerates. Ti and Ti64 have not a particular morphology nor features in the potential. The topography of the treated samples is more complex. On Ti(A-HC-H) and Ti64(SrAg), the porous oxide layer is very well observed in the topographical image. In these cases, the rough surface morphology has an unavoidable effect on the surface potential images, therefore it is not possible to obtain information about the protein distribution.

On Ti64(HF-H_2O_2) there are two grains of β-phase that pop out from the surface and it is possible to observe also the nanostructuration all over the topographical image, due to the nanosponge. The areas in the potential image corresponding to the protruding grains have a higher potential than the surrounding area,which can be attributed to the influence of the β-phase under the protein layer: in fact, β-phase has an higher potential than α-phase, due to higher vanadium content [46]. Similar

results, both the topographical image and potential distribution, were obtained for the pristine substrates (Figure 5.34), avoiding the investigation of protein distribution on such surfaces at a sub-micrometical scale.

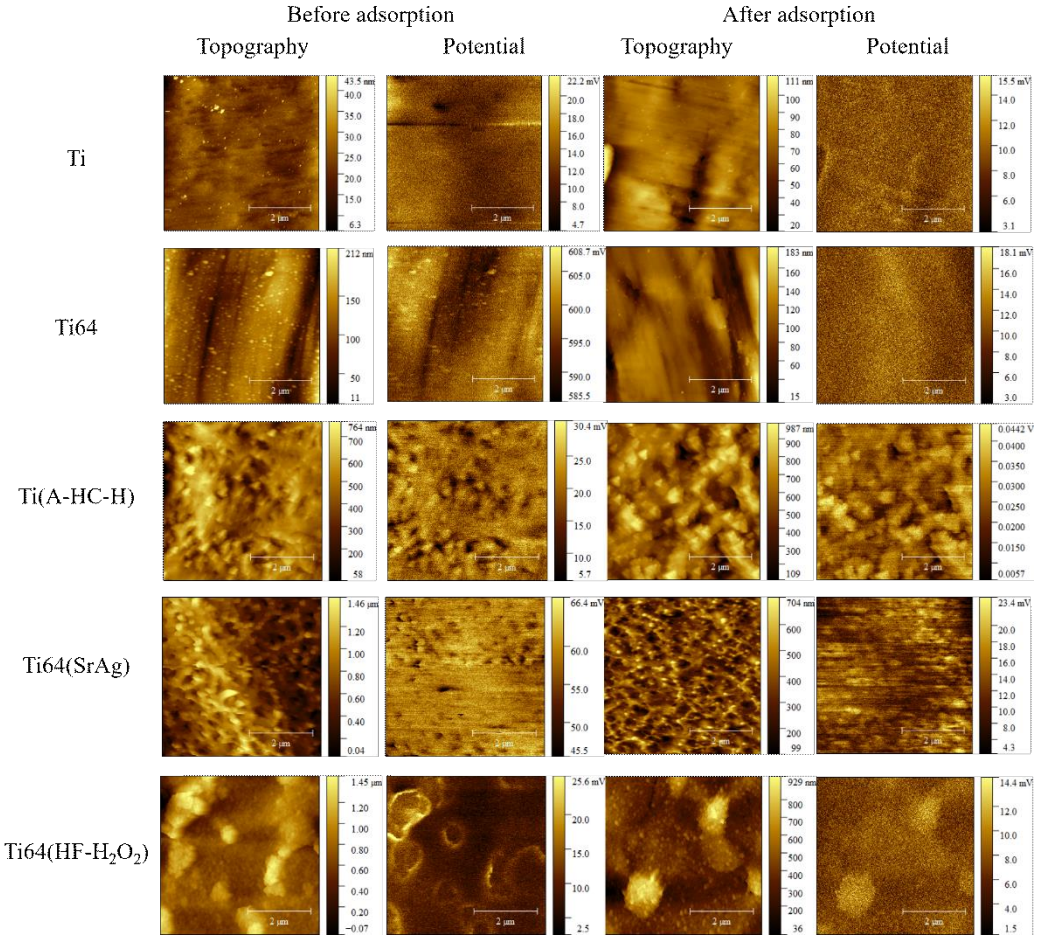

Figure 5.34 Topographical and surface potential 5*5 µm images of titanium surfaces before and after BSA adsorption.

KPFM imaging was performed also on the two glass samples. As usual for BGs, the results are affected by the high reactivity of these surfaces (Figure 5.35). The surfaces of both SBA2 and AgSBA2 are characterized by a net separation in the topography between the area without BSA and the area covered by the albumin solution. Where the solution drop has been deposited, the surface of the glasses is rougher and it is 70-100 nm higher than the area outside the drop. The formation of the silica-gel probably generates an increase in volume of the surface, leading to the height increase observed here. In the potential images, three areas at similar potential can be distinguished. The first corresponds to the pristine surface and has a medium potential. The second, at lower potential, can be found around the boundary of the drops, both on SBA2 and AgSBA2. It is possible that in these areas, the solution evaporated during the adsorption, not hallowing the surface to react much and that here the protein layer is visible in the surface potential. In fact, in the SBA2, these areas can be found also in the grooves, where a small amount of solution was possibly infiltrated due to capillary effects and then evaporated. On AgSBA2, the darker areas in the potential are also found on the left of the lines that divides the unreacted and reacted areas in the topographical image, for the same

reason. The last potential zone is the one at the highest potential, corresponding to the core of the drop, where the silica-gel layer is fully formed. Here it is possible that the potential of is the result of the combined protein-silica gel potentials.

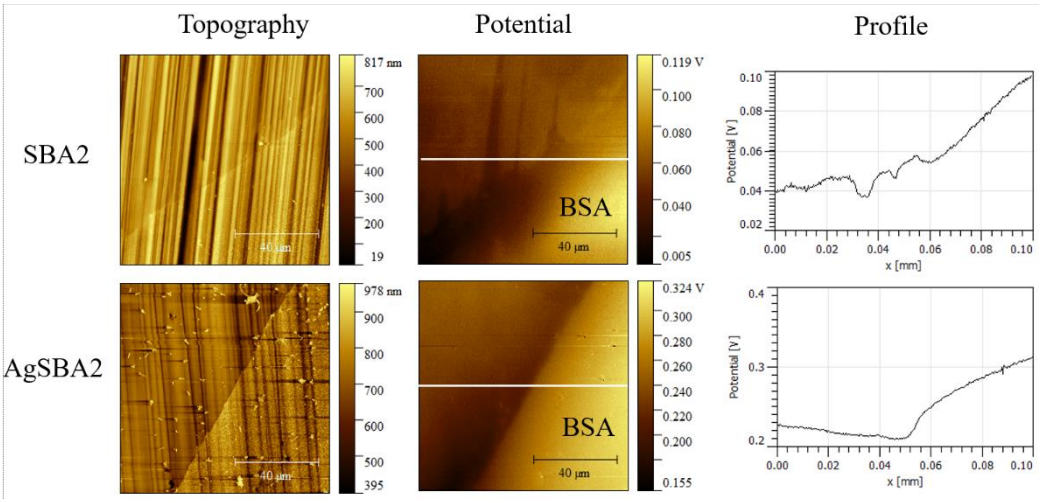

Figure 5.35 Topography and potential 100*100 µm images for bioactive glass surfaces half covered by BSA. The potential profile along the with line is reported in the third column.

The changes in the morphology due to the reaction of the surfaces are well visible at higher magnifications, comparing the outside and the inside of the drop (Figure 5.36). SBA2 before albumin adsorption has a very flat surface, apart from the polishing grooves, while after adsorption the surface appears jagged and rough. AgSBA2 is similar, the pristine surface is less plain than the one of SBA2 since it started to react and change a bit during the ion-exchange process. Due to the surface conformation, it is not possible to observe eventual proteins aggregates. The surface potential was not informative in these cases.

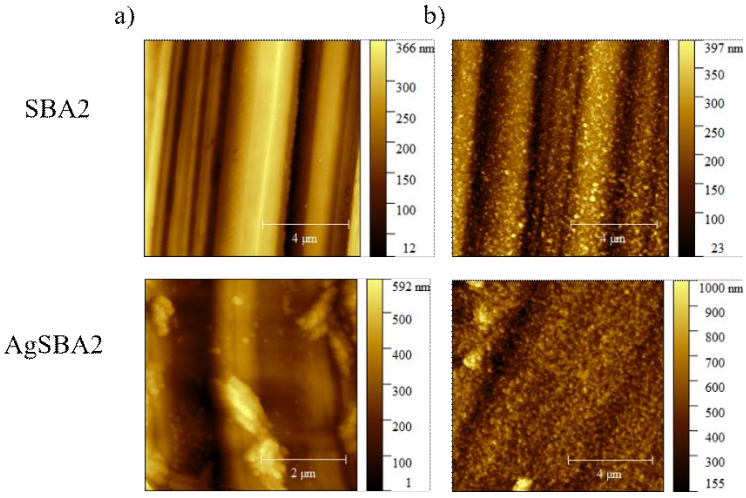

Figure 5.36 Topography 5*5 µm images for SBA2 and AgSBA2 surfaces before (a) and after (b) BSA adsorption.

Similar results were obtained for fibronectin adsorption. As well as BSA, FN forms a continuous layer on all the titanium surfaces (Figure 5.37). Again, the protein layers cannot be distinguished in the topographical images, while they appear clearly imaging the surface potential. The same considerations that have been done for the KPFM investigation of BSA adsorption can be done here to. In

the case of FN, the differences between the surfaces and the adsorbed protein layer are about 35 mV, 140 mV, 65 mV, 25 mV, 80 mV, for Ti, Ti64, Ti(A-HC-H), Ti64(SrAg), and Ti64(HF-H_2O_2), respectively.

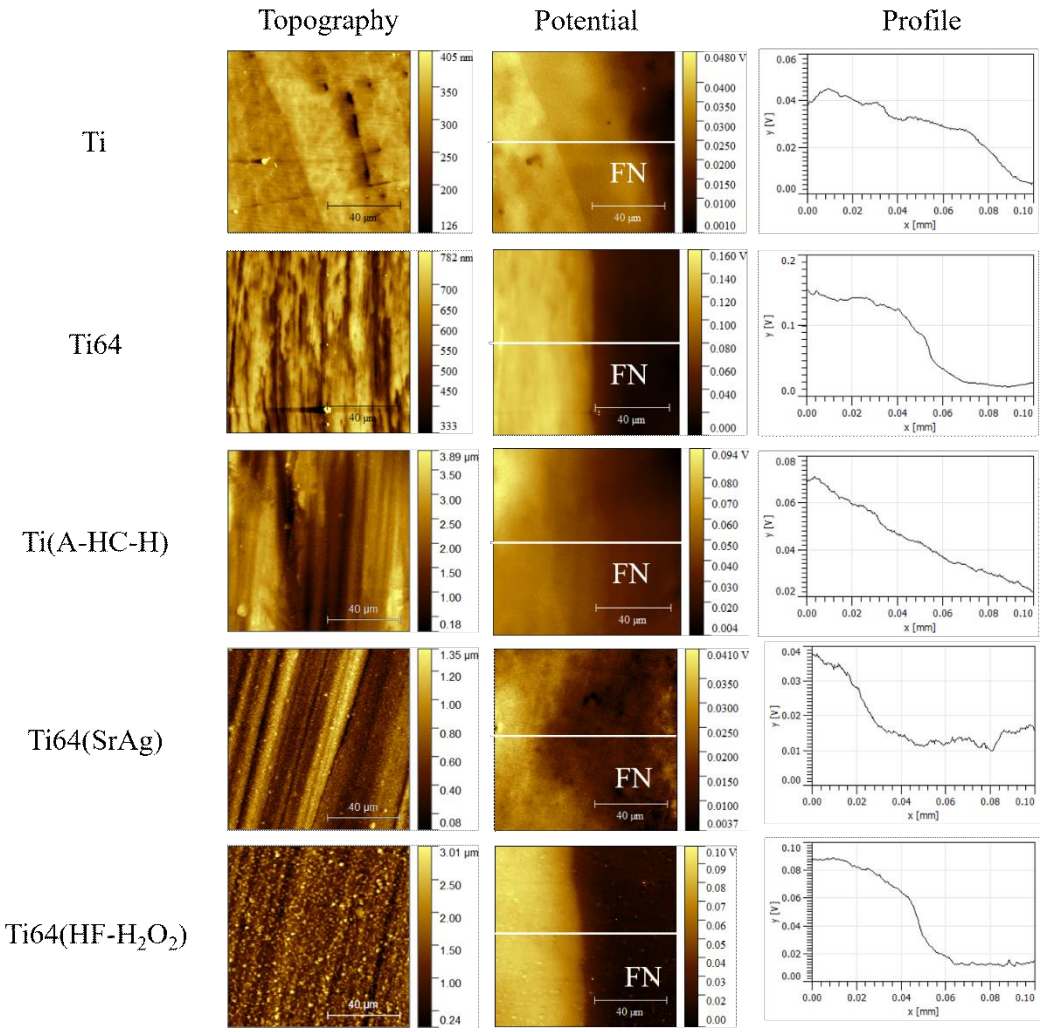

Figure 5.37 Topography and potential 100*100 µm images for titanium surfaces half covered by FN (lighter areas). The potential profile along the with line is reported in the third column.

KPFM analysis of BGs after fibronectin adsorption (Figure 5.38) provide similar results to the case of adsorbed BSA (Figure 5.35). In fact, the areas exposed to the protein solution, both on SBA2 and AgSBA2, are at higher potential than the areas without the protein, as consequence of the reactions that occurs on the surfaces and the formation of the silica-gel. In the case of AgSBA2, a small protein accumulation at the border of the drop may have formed, causing a small decrease of the potential in that area, but which is still lower than the potential of the glass bulk, as possible to notice by the potential profile. On this sample, the potential image has artifacts due to the topography.

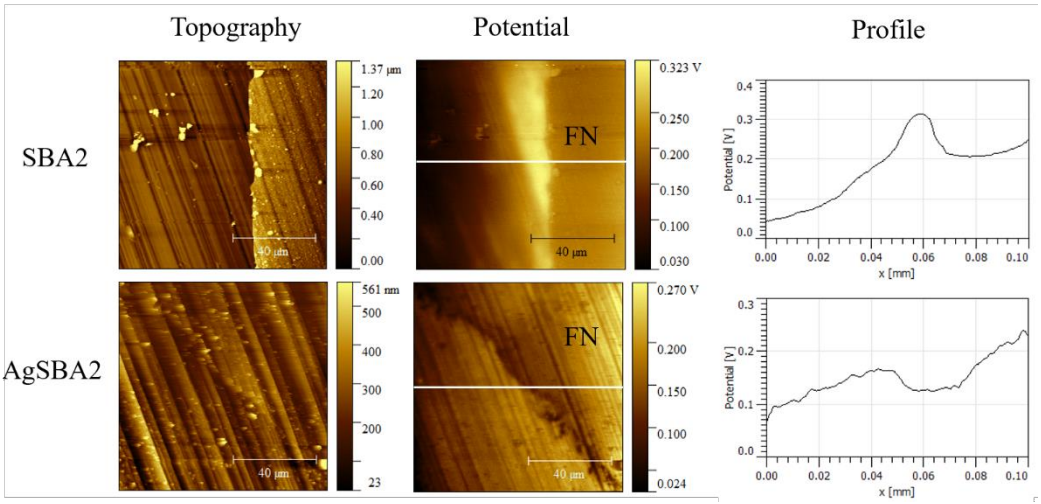

Figure 5.38 Topography and potential 100*100 µm images for bioactive glass surfaces half covered by FN. The potential profile along the with line is reported in the third column.

The results obtained by 5*5 µm on BGs covered by fibronectin were equal to those shown in the case of albumin adsorption (Figure 5.36).

Kelvin probe force microscopy allows to determine the distribution of adsorbed proteins at the microscale. Regarding titanium substrates, albumin and fibronectin form a continuous layer on the surfaces, but it is not thick enough to mask the topographical features of the surface themselves. It was also confirmed that the bioactive glasses react during the adsorption, unfortunately this fact hinder the evaluation of the protein distribution on the BGs. It was also tried to investigate the distribution of the proteins at a submicrometrical scale. On rough surfaces, such as treated titanium and reacted glasses, the surface features are too big for small proteins aggregates to be distinguished. On polished titanium surfaces, the presence of dirt particles, which cannot be cleaned unless removing also the adsorbed proteins, affects and invalidates the measures. The surface potential distribution was not informative on the protein distribution at such scale due to both intrinsic variation of the potential of the substrates or too high topographical interferences from the structured surfaces.

5.2.6. Protein conformation and orientation on the surfaces

The biological activity of proteins is strictly related to the spatial conformation of the polypeptide chain, which can form active and catalytic sites by the reciprocal positions of amino acids or that can expose particular sequences that can be recognized by cells. It is therefore crucial to determine how the surface properties impact on the denaturation properties of proteins during the adsorption. Furthermore, proteins can orient themselves on the surface in different manners, such as side-on or end-on, in order to optimize the interactions with the samples. According to the orientation, the areas on the protein surface exposed to the cells may vary. In this work, the protein conformation and orientation were investigated through different techniques. At first, a novel approach to Surface Enhanced Raman Scattering was proposed. Then the results were supported and extended thanks to

FTIR-ATR. At last, surface ζ potential was employed to gain some information about the orientation and the quaternary structure of BSA and FN.

AgNPs aided SERS of adsorbed proteins

Vibrational spectroscopic techniques, such as Raman or FTIR, are widely employed to investigate protein adsorption thanks to their selectivity to specific vibrational fingerprints of molecules and the absence of molecules labeling or sample preparation. Unfortunately, standard Raman spectroscopy is not sensible enough to detect the low amount of proteins adsorbed on solid samples. In fact, protein adsorption has been studied mainly on metal nanoparticle colloids [50,51] or specific plasmonically-active substrates, for examples by functionalization with gold nanostars [52], by exploiting the Raman enhancing effect of such materials. Here, it was tried to enhance the Raman sensitivity by depositing a drop of metal nanoparticles colloid on the samples after protein adsorption. After evaporation of water, the NPs shall be close enough to the proteins for their Raman signal to be enhanced and detected. At first, it was tried to use AuNPs (40 and 120 nm of diameter), since their plasmonic resonance can be activated with a 780 nm laser, which is suitable for biological samples thanks to its low energy, but no protein signal was detected. The desired enhancing effect was obtained by the use of 30 nm silver NPs, which can be excited by a 532 nm laser.

The first experiments were conducted on samples after albumin adsorption. Preliminary investigations were performed in order to assess the Raman shift of denatured BSA and to determines how AgNPs and proteins interact. In Figure 5.39 the Raman spectra of pure and thermally denatured BSA are reported. The typical bands of proteins, Amide I (≈1650 cm^{-1}), Amide II (≈1450 cm^{-1}), C-H (≈1335 cm^{-1}), Amide III (≈1270 cm^{-1}), vibrations from the skeletal chain (≈900-1000 cm^{-1}) and from aromatic residues (≈1000 and 825-850 cm^{-1}) were assigned according to literature [53]. Focusing on Amide I band, which is highly conformational sensitive, a shift from 1650-1660 cm^{-1}, which is related to protein in its native conformation, to 1670-1680 cm^{-1}, which is related to a more unordered structure, was observed. The increase of the vibrational frequencies in the Amide I band is related to the formation of random coils, aggregated strands and possibly β-sheets during the denaturation process, as reported in literature [54].

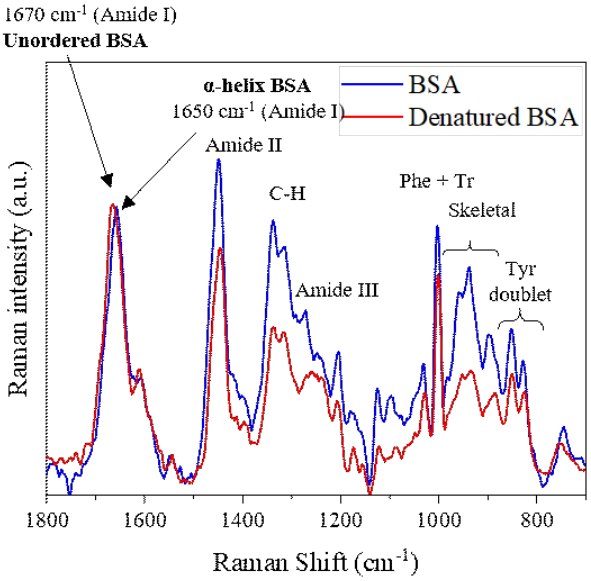

Figure 5.39 Raman spectra of BSA (blue) and BSA_h (red) with band assignment.

The second step was to investigate the interactions between BSA and AgNPs. Those interactions need to happen in order for the proteins to be close enough to the metal NPs, but they shall not affect the secondary structure of the proteins, for not create artifacts in the measurement. The chemical interaction between BSA and AgNPs was investigated by liquid agglomeration test with UV-vis spectroscopy (Figure 5.40 a). Despite not being visible by naked eye (in the figure inset), a shift in the Local Surface Plasmon Resonance (LSPR) adsorption peak of AgNPs was observed after adding albumin. The small red-shift, from 397 to 495 nm, attests the interactions between the proteins and the metallic nanoparticles, probably through the amino groups of BSA and the citrates on the NPs surface, which are used as reductant during the synthesis and stabilizing agent.

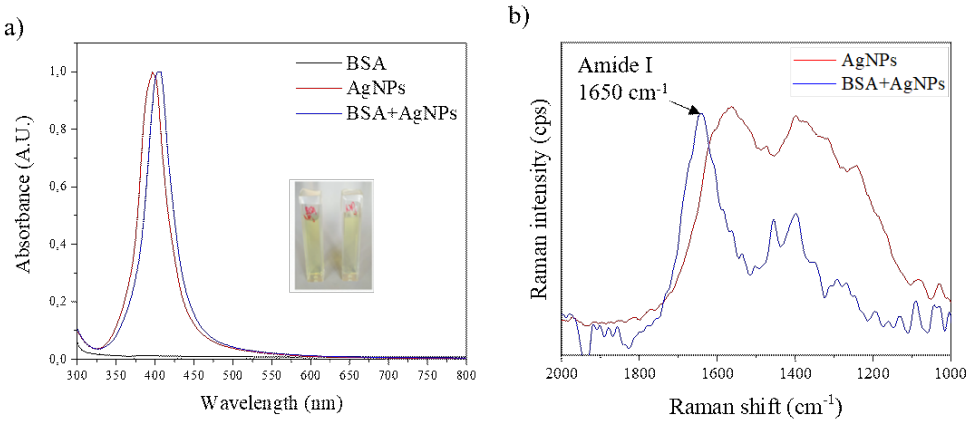

Figure 5.40 a) UV-vis spectra of BSA, AgNPS and AgNPs with BSA suspensions, a picture of the cuvettes in the inset; b) SERS spectra collected in liquid of pure (red) and with BSA (blue) AgNPs suspensions.

The effect of these interactions on the secondary structure of albumin was evaluated by SERS collected in liquid (Figure 5.40 b). As expected by the UV-vis measure, the protein signals are visible in the spectrum thanks to the SERS effect of AgNPs. As hoped, the Amide I band was found at the shift related to the native

α-helical structure of albumin, indicating that the interactions with AgNPs do not provoke denaturation. The AgNPs colloid has also many signals related to the organic molecules, citrates in particular. As usual, those signals are suppressed by the presence of the analyte.

The effect of AgNPs on albumin under experimental conditions were tested by ATR-FTIR and Ti64 was employed as model substrate, since the Amide I band of BSA after adsorption on this surface was found not shifted as it will be discussed in the next paragraph. After spotting of AgNPs colloid, the signal of the amide I band was not changed with respect to Ti64_BSA (Figure 5.41). Consequently, it is possible to conclude that eventual shift in the Amide I band observed by SERS spectroscopy may be ascribed only to denaturation occurred during the adsorption process.

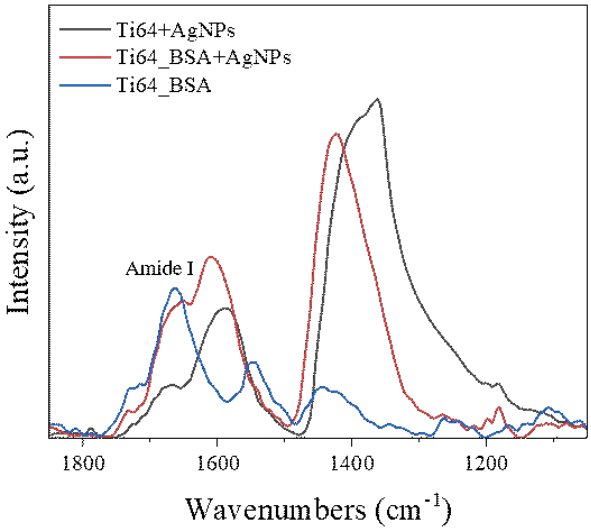

Figure 5.41 ATR-FTIR spectra of Ti64_BSA (red), Ti64_BSA with AgNPs (green) and Ti64 with AgNPs (blue)

After the preliminary characterizations, AgNPs aided SERS spectra were collected on all the samples after BSA adsorption. Unfortunately, the results obtained were not satisfactory in all the cases. In particular, it was possible to investigate the secondary structure of BSA on Ti64 and Ti64(HF-H_2O_2).

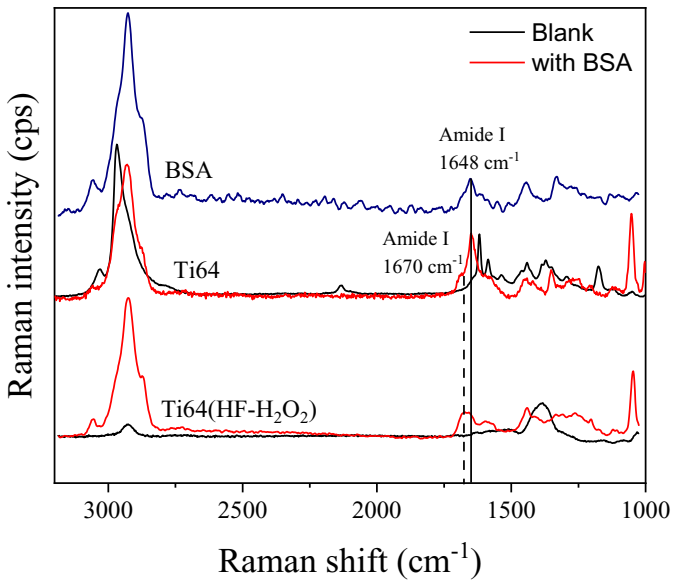

Figure 5.42 SERS spectra of: a) BSA powder; b) Ti64; c) Ti64_BSA; d) Ti64(HF-H_2O_2); e) Ti64(HF-H_2O_2)_BSA. The position of Amide I band after adsorption is shown.

After BSA adsorption, the signal of the proteins can be detected in the SERS spectra (Figure 5.42). In particular, the bands at high wavenumber, between 2700 and 3000 cm^{-1} and in the Amide I region are well visible. Below 1500 cm^{-1}, the signal from the nanoparticles heavily interferes with the BSA spectra. Some interfering signals are present on Ti64 (Figure 5.42) between 1500 and 1700 cm^{-1}, probably due to contaminations, but they do not prevent the precise detection of the Amide I band after adsorption. On pure BSA and Ti64_BSA (Figure 5.42), the Amide I band is in the same position, around 1648 cm^{-1}, indicating that also after adsorption on the titanium substrate albumin is mainly in its native α-helical conformation. Still, the small shoulder appeared at 1670 cm^{-1} suggest a partial denaturation of the proteins. On the other hand, on Ti64(HF-H_2O_2)_BSA, the Amide I band is completely shifted at 1670 cm^{-1} and broadened with respect to pure BSA (Figure 5.42), suggesting a much higher denaturation on the chemically treated alloys with respect to the untreated substrate.

On Ti, the BSA has a complex pattern and the precise band positions can be hardly resolved (Figure 5.43). In the Amide I region, contributes around 1655 cm^{-1} and 1690 cm^{-1} can be found, suggesting a partial denaturation as in case of adsorption on Ti64.

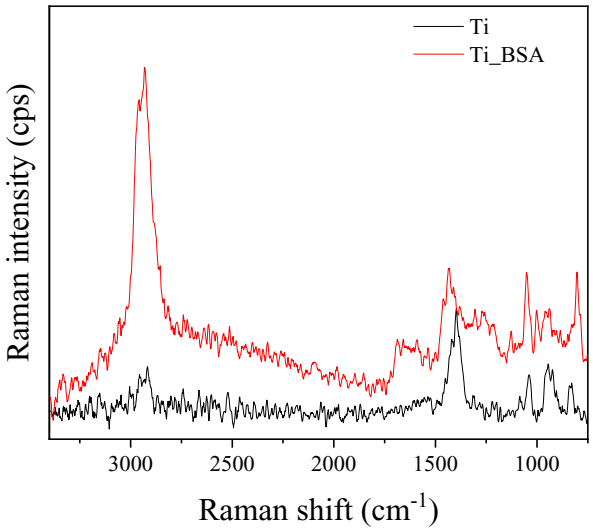

Figure 5.43 SERS spectra of: a) Ti; Ti_BSA

On other samples, such as Ti(A-HC-H), Ti64(SrAg), SBA2 and AgSBA2, the signal of the protein was not detected (Figure 5.44). This may be caused by the absence of a close contact between AgNPs and BSA, related to the particular surface structure of the samples. On the treated titanium surfaces, the high porosity and the elongated shape of the pores themselves, where BSA can adsorbs into, may limit the interactions between the proteins and the nanoparticles. On the other hand, on BGs, the interactions between BSA and AgNPs can be physically limited due to the presence of the silica-gel layer on the adsorbed proteins.

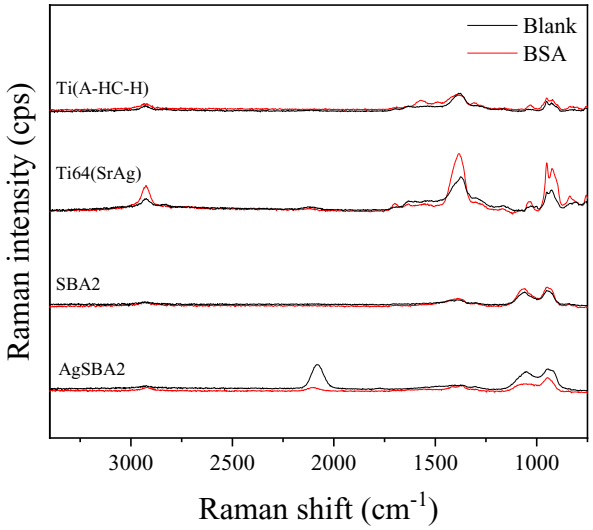

Figure 5.44 SERS spectra, before (black) and after (red) BSA adsorption on: Ti(A-HC-H), Ti64(SrAg), SBA2 and AgSBA2

At last, the intrinsic signal of PS is too high to detect the adsorbed albumin (Figure 5.45).

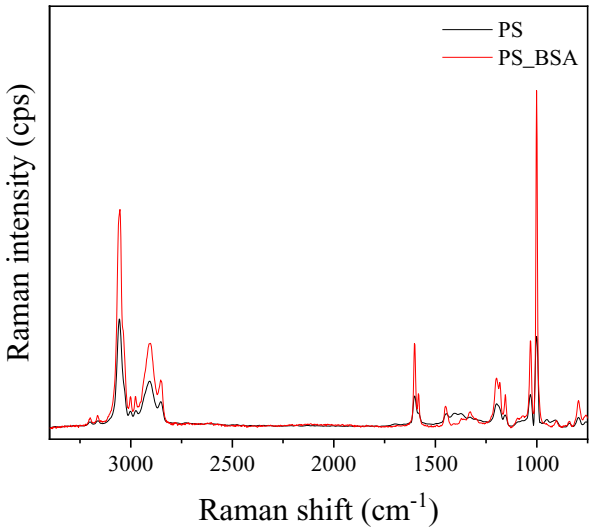

Figure 5.45 SERS spectra, before (black) and after (red) BSA adsorption on PS.

In light of the results obtained for albumin adsorption, fibronectin was investigated by SERS only on Ti, Ti64 and Ti64(HF-H_2O_2). Probably due to the lower amount of adsorbed FN with respect to BSA, the signal of fibronectin is low and barely detected on Ti and Ti64. On Ti64(HF-H_2O_2), the spectrum is dominated by a broad and undefined band between 1000 and 1700 cm^{-1}, possibly due to autofluorescence of the protein layer excited by the laser. Any detection of the adsorbed proteins is therefore impossible and the graphs are not shown for sake of concision

Spotting silver nanoparticles have been found useful to investigate the denaturation of proteins during adsorption, but, up to now, this methodology presents severe limitations. Conformational information was obtained just for one protein type and on substrates with specific properties, such as low porosity and roughness or non-reactive. Anyhow, it is not to be excluded that improvements can be made in the future, for examples by employing different metallic colloids or different laser wavelengths, and that SERS spectroscopy may expand the family of techniques suitable for investigate proteins adsorption on biomaterial surfaces.

ATR-FTIR

Protein secondary structure after adsorption was also investigated by ATR-FTIR, which is widely employed for this kind of characterization [55]. In particular, Amide I bands were deconvoluted to resolve the composition of the secondary structure of albumin and fibronectin, since it is strictly dependent on the protein conformation [56]. For sake of clarity and better discussion of the results, adsorption of both BSA and FN on titanium-based samples and on the bioactive glasses will be presented separately.

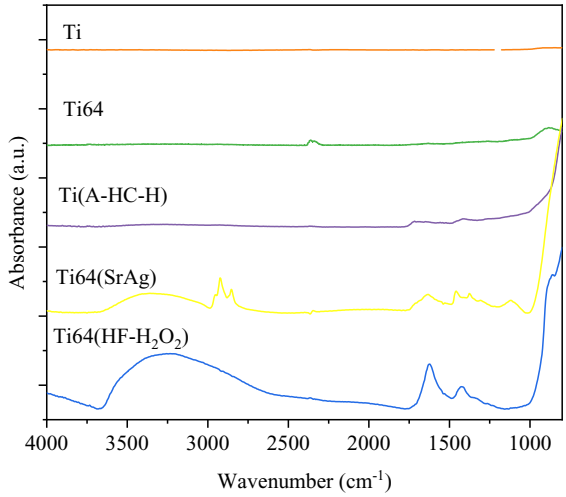

Figure 5.46 ATR-FTIR spectra of titanium surfaces before protein adsorption.

The FTIR spectra of the titanium substrates before adsorption were collected as controls (Figure 5.46). The spectra of Ti and Ti64 are featureless, as expected from pure metallic samples. On all the chemically treated surfaces, a band below 1000 cm^{-1} was found, which can be attributed to the Ti-O stretching in the oxide layer [57]. It was not visible on Ti and Ti64 due to the very low thickness of the native oxide. Apart from the TiO band, also the spectra of Ti(A-HC-H) has not specific signals. On the other hand, several bands were observed on Ti64(SrAg) and Ti64(HF-H_2O_2). On both surfaces, a broad band between 3000 and 3500 cm^{-1} arose due to the OH stretching [58]. This band is more intense on Ti64(HF-H_2O_2) since it has the highest surface hydroxylation. Signal of carbonaceous contaminations were observed in the Ti64(SrAg) spectra, in particular the triplet between 2750 and 3000 cm^{-1} and the bands between 1000 and 1500 cm^{-1}, which arise from stretching or bonding of CH and CO bonds [58].At last, the two intense peaks at about 1427 and 1625 cm^{-1} on Ti64(HF-H_2O_2) can be attributed to adsorbed water and hydroxyls group [59].

After albumin adsorption, the protein signal was found on all the substrates, in particular regarding the Amide I and Amide II bands (Figure 5.47).

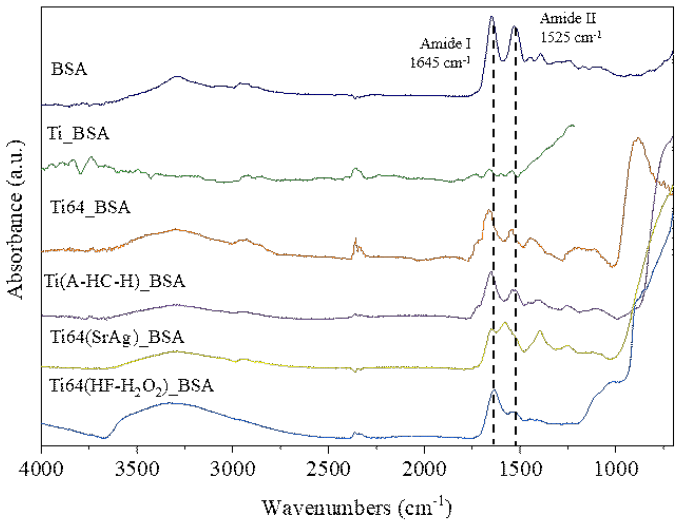

Figure 5.47 ATR-FTIR spectra of titanium surfaces after albumin adsorption. The position of Amide I and Amide II bands for BSA is reported.

After BSA adsorption, the OH halo is visible also on all substrates, while the two OH related peaks found on pristine Ti64(HF-H_2O_2) disappeared, being covered by protein bands. Even after adsorption, some interfering bands were observed in around 1600 cm^{-1} on Ti64(SrAg). The conformation of the adsorbed albumin was evaluated by deconvolution of the Amide I band, and the results are reported in Figure 5.48 and Table 5.18, along with deconvolution on albumin before and after thermal denaturation.

Table 5.18 Secondary structure of albumin, pure, after thermal denaturation and after adsorption on titanium surfaces.

	β-sheets/turns	α-helix	random coils	β-sheets
	1660-1680	1650-1660	1640-1650	1620-1640
BSA	27%	56%	-	17%
BSA_h	24%	48%	-	33%
Ti_BSA	11%	67%	-	22%
Ti64_BSA	39%	38%	-	43%
Ti(A-HC-H)_BSA	26%	55%	-	18%
Ti64(SrAg)_BSA	12%	42%	23%	23%
Ti64(HF-H2O2)_BSA	39%	-	61%	-

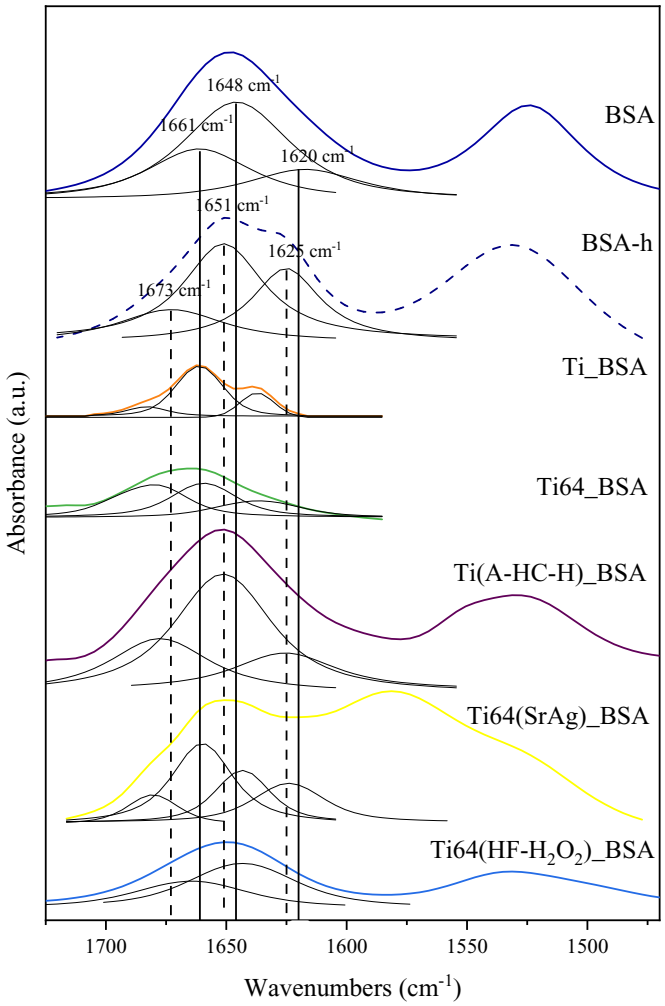

Figure 5.48 Amide I and Amide II bands region of BSA, as native or denatured, and after adsorption on titanium samples, with deconvolution of the Amide I band. The positions of the native (solid lines) and denatured (dashed lines) protein components are also reported.

Amide I band of native albumin has three components, at 1620 cm^{-1}, 1648 cm^{-1}, and 1661 cm^{-1}, corresponding respectively to β-sheets or β-turn, α-helix, and β-sheets, as previously reported in literature [60–63]. After the thermal denaturation, the amount of α-helix was reduced while β-structures increased, as consequence of conformational changes. After adsorption on Ti, Ti64, Ti(A-HC-H), and Ti64(SrAg), the contributes of α-helix and β-structures in different proportions have been found, indicating a partial denaturation with a partial loss of the helical portion, comparable to the one occurring during the thermal denaturation (Table 5.18). On Ti64, the greater loss of α-structures was observed among those samples. Concurrently, there is also the presence of β-sheets on Ti and Ti64. Contrary, no random coils were detected on untreated surfaces. Albumin adsorbed on Ti(A-HC-H) seems to be present almost in a native conformation. On the other hand, on Ti64(SrAg), the proteins underwent strong denaturation, with the appearance of a band which can be attributed to random coils, around 1640 cm^{-1}. A broad band around 1580 cm^{-1} was also detected, but it can be attributed to a signal from the substrate (Figure 5.47). The most intense denaturation was observed on Ti64(HF-H_2O_2), where a shift of the main band was observed to values corresponding to unordered structures (1643 cm^{-1}) [56,62,63], and at the same time, also a contribute

from β-sheets has arisen. A quantitative evaluation of the degree of loss of the α-helices is not completely reliable because some minor contributes could have been lost due to interfering bands of the substrate, but it can be considered on a qualitatively basis.

The same analysis was performed in the case of fibronectin adsorption. The signals of the proteins are not visible on Ti and Ti64, probably due to the very low amount of protein adsorbed. On the other hand, Amide I and II bands and the OH halo appeared on all the chemically treated surfaces (Figure 5.49). The intensities of these bands are lower compared to the one of adsorbed BSA possibly since the overall amount of FN is lower.

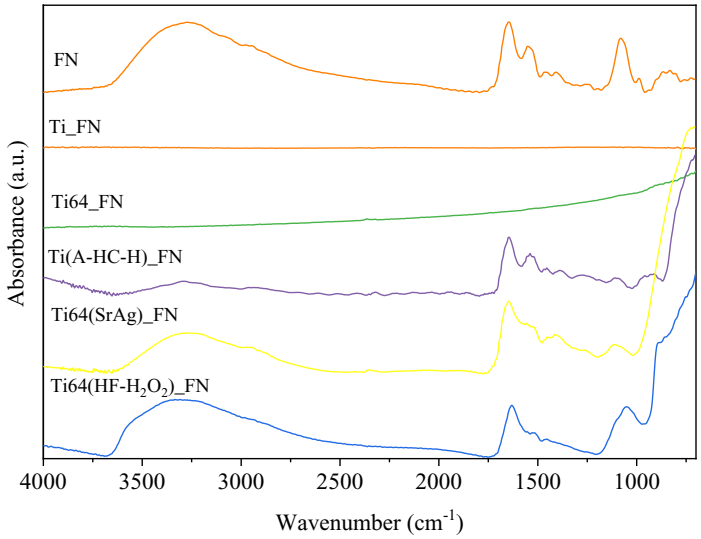

Figure 5.49 ATR-FTIR spectra of titanium surfaces after fibronectin adsorption. The position of Amide I and Amide II bands for FN is reported.

The secondary structure of fibronectin was obtained by Amide I band deconvolution (Table 5.19 and Figure 5.50). Deconvolution was not possible on untreated Ti and Ti64 since the fibronectin signal was not detected at all. The native and denatured protein show contributions corresponding to random coils between 1644-1641 cm^{-1}, β-sheets at 1619 and 1623 cm^{-1} and β-sheets/β-turns around1673 cm^{-1} and 1665 $cm^{-1}$for FN and FN_h, respectively. The denaturation provokes a small band shift and a reduction of the random coils, while the β-sheets or β-turns structures increase (Table 5.19). FN on Ti(A-HC-H) and on Ti64(SrAg) has a similar loss of the β-sheet structure, which was not found any more on both substrates, in favor of the formation of random coils and β-turns, with the former accounting for about the 60-70% of the overall structure. On the other hand, FN shows a very broad contribution at 1639 cm^{-1} on Ti64(HF-H_2O_2), which here was namely attributed to β-sheets, a minor portion of β-turns and the absence of random coil. Still, as stated for BSA adsorption, the bands of the substrate itself may limit the resolution of the fitting process and, as consequence, hinder the possibility of an accurate quantitative evaluation of the contribution of random coils and β-sheets.

Table 5.19 Secondary structure of fibronectin, pure, after thermal denaturation and after adsorption on treated titanium surfaces.

	β-sheets/turns	α-helix	random coils	β-sheets
	1660-1680	1660-1680	1650-1660	1640-1650
FN	30%	-	55%	15%
FN_h	40%	-	47%	13%
Ti(A-HC-H)_FN	30%	-	70%	-
Ti64(SrAg)_FN	39%	-	61%	-
Ti64(HF-H2O2)_FN	18%	-	-	82%

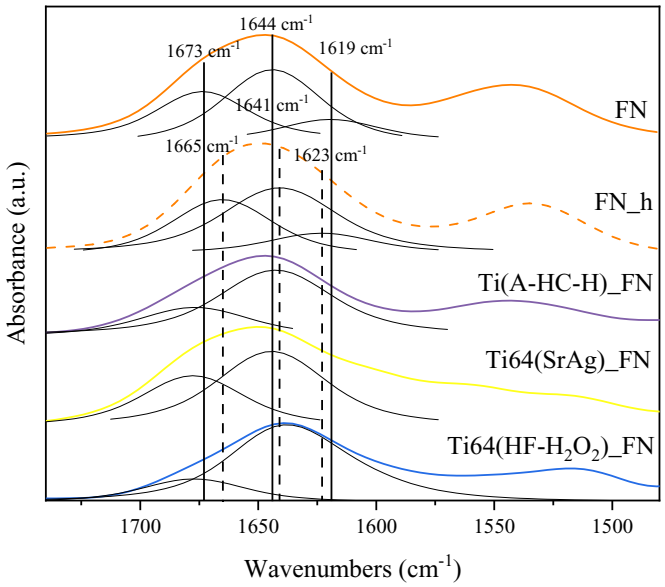

Figure 5.50 Amide I and Amide II bands region of FN, as native or denatured, and after adsorption on titanium samples, with deconvolution of the Amide I band. The component positions of the native (solid lines) and denatured (dashed lines) protein components are also reported.

The secondary structure of albumin and fibronectin is affected when adsorbing on untreated and treated titanium surfaces. The extent of denaturation may be related to the amount of OH groups present on the surfaces. Regarding Ti and Ti64, where it was possible to evaluate only the secondary structure of BSA, it was found that the protein denatures a bit more on alloyed than pure titanium. Ti64 has a lower amount of basic OH groups, which are in their uncharged state at the adsorption pH, than pure Ti (Table 5.3), and it is slightly more hydrophobic (Table 5.7). In case of absence of dehydrogeated hydroxyl groups, the general assumption that protein structures are more disrupted in case of adsorption on a hydrophobic surfaces seems confirmed. On the other hand, things change when acidic OH groups are in play. Concerning BSA, it is almost in the native form on Ti(A-HC-H), slightly denatured on Ti64(SrAg) and heavily changed on Ti64(HF-H_2O_2). Considering FN instead, it has a similar conformation on Ti(A-HC-H) and Ti64(SrAg), which is quite different from the one adopted on Ti64(HF-H_2O_2). It has been reported that the secondary structure of BSA is affected by the hydroxylation degrees of titanium surfaces. In particular, an high surface OH density provokes a loss of α-helices, while negative charged surfaces may increase β-sheet structures [67]. The results reported here support this hypothesis, offering even more insights on the effect of OH groups. Ti64(HF-H_2O_2) has a high amount of strong acidic OH groups, which

are in the $Ti\text{-}O^-$ state at the pH of adsorption, and this can explain the high content of random coils and β-sheets that compose adsorbed albumin and fibronectin, respectively. When the amount of acidic OH is lower, the dimension of the adsorbed proteins seems to play a role. In fact, slight differences in the amount of acidic OH groups, as in case of Ti(A-HC-H) and Ti64(SrAg), results in different protein structures when a small protein, such as albumin, is adsorbed. On the other hand, the structure of a larger protein as fibronectin is not affected by low hydroxylation degrees, being similar on Ti(A-HC-H) and Ti64(SrAg). FN denatures most when adsorbed on Ti64($HF\text{-}H_2O_2$). It can be concluded that the concentration of total and acidic OH needs to overcome a threshold for the protein-surface interactions to be enough to disrupt the protein secondary structures (Figure 5.51).

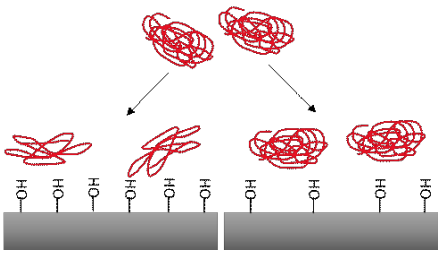

Figure 5.51 Effect of the hydroxylation of titanium surfaces on the conformation of adsorbed proteins

ATR-FTIR was performed also for investigation of protein adsorption on SBA2 and AgSBA2. Before protein adsorption, the spectra of SBA2 and AgSBA2 (Figure 5.52) show only the broad bands related to OH and adsorbed water around 1600 cm^{-1} and CO_3 groups of carobnates, around 1400 cm^{-1} [65]

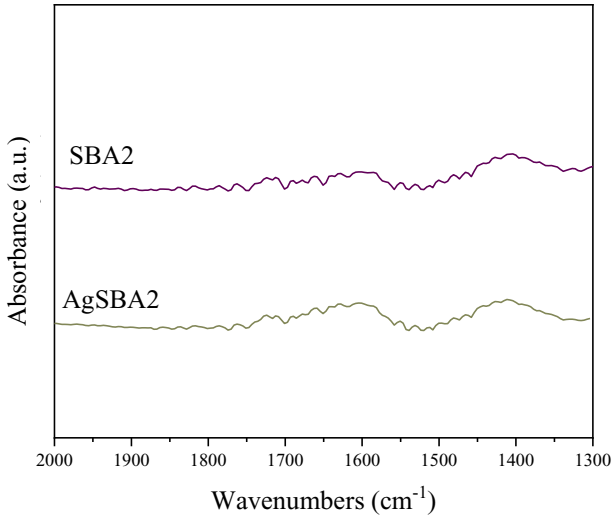

Figure 5.52 ATR-FTIR spectra of BG surfaces before protein adsorption.

After soaking in the BSA solution, small bands that can be ascribed to Amide I, and other organic signals were observed in the 1200-1700 cm^{-1} region. The Amide II band may not be visible due to the complex structuration of the combined layer. Also, the OH band at high wavelength appeared, as consequence of the hydrated silica-gel formation (Figure 5.53).

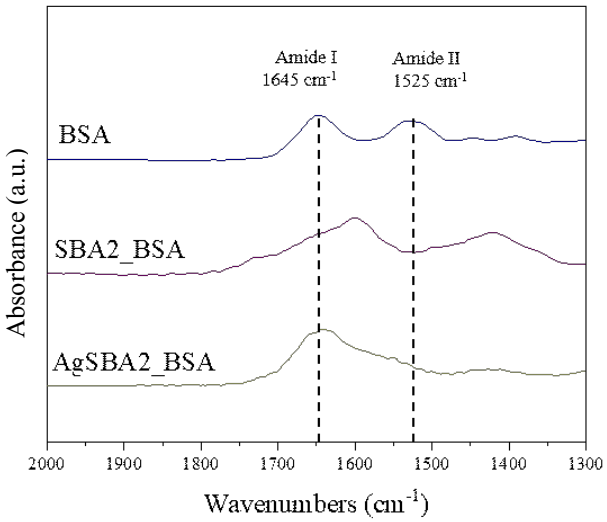

Figure 5.53 ATR-FTIR spectra of BGs after albumin adsorption. The position of Amide I and Amide II bands for BSA is reported.

Even though the FTIR adsorption bands of the proteins are weak, due to the complex conformation of the surface layer, by subtraction of the spectra of the bare BGs it was possible to perform the fitting of the Amide I band and to obtain the structure of the adsorbed BSA (Table 5.20 and Figure 5.54).

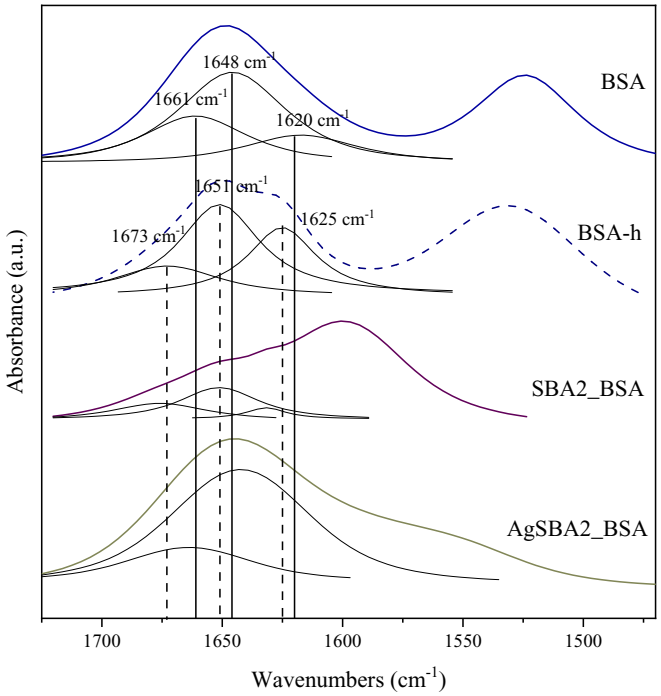

Figure 5.54 Amide I and Amide II bands region of BSA, as native or denatured, and after adsorption on BG samples, with deconvolution of the Amide I band. The component positions of the native (solid lines) and denatured (dashed lines) protein components are also reported.

Table 5.20 Secondary structure of albumin, pure, after thermal denaturation and after adsorption on BG surfaces.

	β-sheets/turns	α-helix	random coils	β-sheets
	1660-1680	1650-1660	1640-1650	1620-1640
BSA	-	100%	-	-
BSA_h	5%	66%	-	29%
SBA2_BSA	9%	54%	-	37%
AgSBA2_BSA	21%	-	79%	-

Albumin has a very different secondary structure when adsorbed onto the two different bioactive glass samples. On SBA2, it seems to more retain its native structure, by showing similar amounts of α-helices and overall β-structures. Doping the glass with silver resulted in a strong denaturation of the adsorbed proteins, which completely loss the helical structure, forming mainly random coils and β-sheets or turns.

In the same way as BSA, fibronectin Amide I band was detected on SBA2 and Ag-SBA2 after adsorption (Figure 5.55). Again, Amide II was not observed, while strong bands related to the reaction of the glass arose, in particular on SBA2.

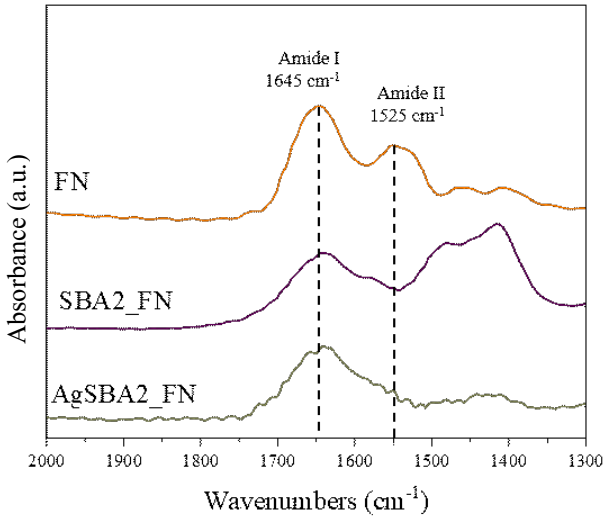

Figure 5.55 ATR-FTIR spectra of BGs after fibronectin adsorption. The position of Amide I and Amide II bands for FN is reported.

By deconvolution of the Amide I band, it was possible to analyze the secondary structure of FN (Table 5.21 and Figure 5.56).

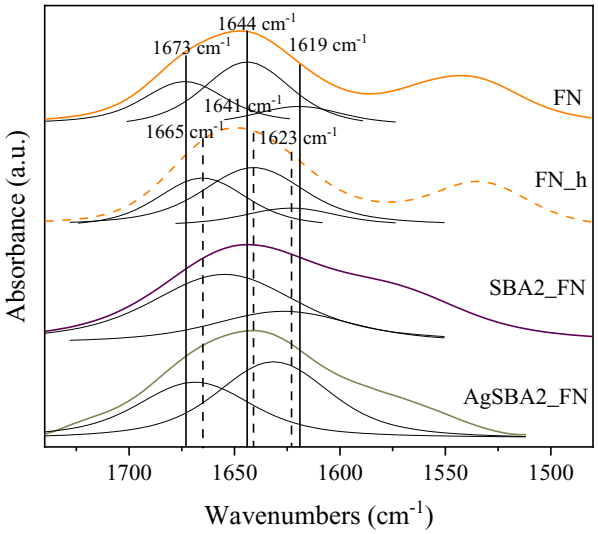

Figure 5.56 Amide I and Amide II bands region of FN, as native or denatured, and after adsorption on BG samples, with deconvolution of the Amide I band. The component positions of the native (solid lines) and denatured (dashed lines) protein components are also reported.

Table 5.21 Secondary structure of fibronectin, pure, after thermal denaturation and after adsorption on BG surfaces.

	β-sheets/turns	α-helix	random coils	β-sheets
	1660-1680	1650-1660	1640-1650	1620-1640
FN	30%	-	55%	15%
FN_h	40%	-	47%	13%
SBA2_FN	-	-	69%	31%
AgSBA2_FN	42%	-	-	58%

Fibronectin underwent denaturation during the adsorption on both SBA2 and AgSBA2. On the former, β-turns disappears, while random coils and β-sheets increased. On the doped glass, β-structures were found increased at the expense of random coils, which were no more detected.

The low amount of proteins adsorbed and the complex chemistry of the glass surface after protein adsorption may have hindered to some extent the exact determination of secondary structure of BSA and FN, still some differences between the two BGs are clear. BSA is not denatured during adsorption on SBA2, while the presence of silver in the glass surface resulted in a great loss of its native structure. As already discussed, thiol groups have a great affinity for silver, that may cause also the cleavage of disulphide bonds inside the proteins. Furthermore, positive surfaces can reduce the α-helix in the proteins through electrostatic interactions [66] and this effect can be related to the presence of positive silver ions in AgSBA2.

FN is denatured after adsorption on both the surfaces. Due to the very low amount of cysteine in fibronectin, the differences in the conformation of the adsorbed fibronectin are not to ascribe to thiol-silver interactions. SBA2 seems to produce more disordered structure in the fibronectin. On the other hand, silver may increase the presence of β-sheets through electrostatic interatctions between COO^- FN groups and Ag^+ ions in the glass, as in the case of BSA.

On PS substrates it was not possible to investigate the secondary structure of adsorbed proteins since the vibrational bands of the polymers dominate the spectra after adsorption (Figure 5.57), not allowing to detect the protein signals.

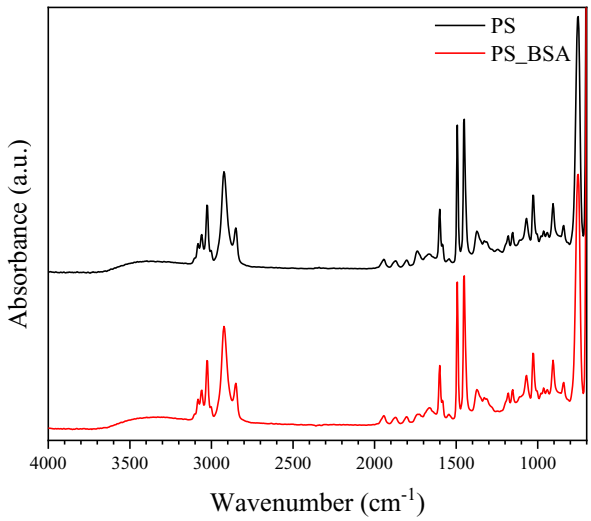

Figure 5.57 ATR-FTIR spectra of PS before and after BSA adsorption.

In this work, ATR-FTIR was useful to investigate the denaturation of proteins during adsorption on different substrates, despite some limitations of this technique were observed. Surface of biomedical interest are often highly hydroxylated [67], so it is necessary to overcame the interference due to vibrational bands of OH. The determination of proteins conformation with FTIR is not trivial also on reactive surfaces such as bioactive glasses, since the reactions at the surface and the structure of the mixed protein-silica gel layer results in interfering bands. At last, this technique was found not suitable for study adsorption on polymeric materials.

ζ potential after protein adsorption

Surface zeta potential measurements were performed also after protein adsorption on the different substrates. The titration curves are sensible to the exposed chemical groups, so they were analyzed to obtain information on the orientation and 3D conformation (ternary structure) of albumin and fibronectin. Similarity between curves indicate that similar functional groups are exposed, and as consequence, the protein orientation on the surface is analogous.

To validate the measurement meaning, it was assessed if the protein layer is eventually detached during the analysis. In order to do so, the amount of nitrogen was evaluated by XPS after the acidic titration curves. The detachment at low pH was chosen due to its biological interest, since it means that protein-surface interactions may remain strong and stable even in inflammatory conditions (pH 4.0-4.5). Since adsorption is performed at physiological pH 7.4, proteins are expected to be adsorbed around that pH value.

The zeta potential titration curves of albumin and fibronectin in solution have been measured as reference (Figure 5.58). The standard deviations were always low

(< 5 mV) in all the measured pH range for both BSA and FN. The IEP of BSA and FN are respectively 4.5 and 4.9, in the range found in literature [68,69]. They have a similar behavior, which can be dictated by a similar strength of the acid carboxyl groups and basic amine groups of the amino acid residues. In the considered pH range, the amino groups are always in the protonated NH_3^+ state, due to their high pK_a, which is over 9, while the carboxyl switches from the COO^- to the COOH state in few pH points around their pK_a, which is about 4 [70]. Thus, three different situations of the charge can be found on proteins according to the pH, which correspond to different portion of the potential titration curves:

- pH < 3.5, acidic plateau: only NH_3^+ groups contribute to the surface charge, carboxyl groups are fully protonated:
- 4 < pH < 6, linear segment: carboxyl groups began to deprotonate and the overall charge of the protein decreases;
- pH > 6, basic plateau: all the carboxyl groups are in the COO^- state and both positive and negative charges are exposed on the surface.

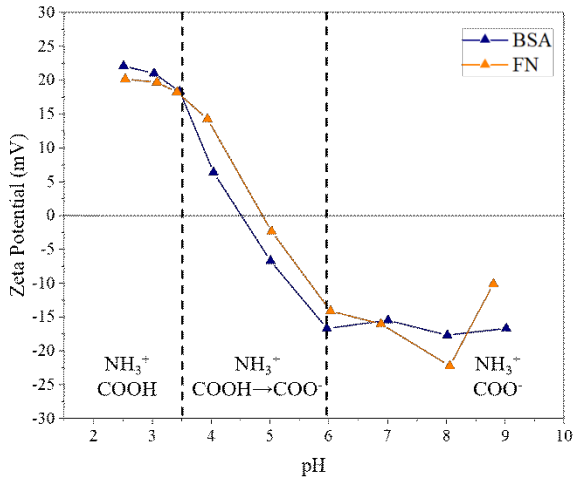

Figure 5.58 ζ potential titration curves of albumin and fibronectin in solution. The state of basic and acidic resides is also represented.

It was also tested if denaturation has an effect on the zeta potential of a protein, by measuring the zeta potential titration curves of heated albumin (Figure 5.59). Also for BSA_h, the standard deviations are lower than 5 mV for all the measured points. The thermal denaturation mainly affects both the IEP and the onset of the acidic plateau: both the changes are explainable with a lower acidic strength of the carboxyl groups. The kind of changes in the ζ potential of a denatured protein in solution may not be representative of the ones that can occur when a protein is denatured as consequence of adsorption on a surface, but they assess that the ζ potential of a protein is conformational sensitive. Therefore, it is reasonable to discuss the following results in term of protein denaturation and orientation on the surface.

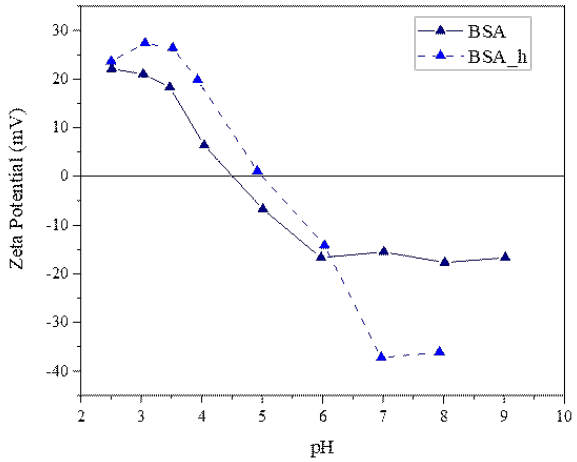

Figure 5.59 ζ potential titration curves of albumin in solution before (BSA) and after thermal denaturation (BSA_h).

As it has been done for the other results, the zeta potential results will be discussed first focusing on titanium-based substrates, then on bioactive glasses, and, at last, on PS.

The residual nitrogen on untreated and treated titanium samples with albumin is reported in Table 5.22.

Table 5.22 Residual nitrogen after the zeta potential measure in the acidic range (atomic %) and IEP of titanium surfaces with adsorbed BSA (-: not measured).

	N%	IEP
BSA	-	4.5
Ti_BSA	8.43	5.0
Ti64_BSA	8.23	4.8
Ti(A-HC-H)_BSA	11.09	5.0
Ti64(SrAg)_BSA	10.67	4.6
Ti64(HF-H_2O_2)_BSA	12.93	4.5

Comparing these results with the nitrogen concentration measured right after protein adsorption (Table 5.9 and Table 5.14), it is possible to observe where the protein layer is still adsorbed on the surface, after the titration, and where it is not. The amount of nitrogen on Ti and Ti64 after the titration measures is sensibly reduced, indicating protein detachment. On the other hand, the treated surfaces show similar N% before and after the acidic titration range almost in all cases, meaning that the proteins are not detached and that the potential titration curves are significative of the adsorbed protein orientation. Surface modifications that occur during the potential measurement determine an increase of the standard deviations, so the pH at which protein detachment happens can be obtained. In the case of Ti and Ti64, the standard deviation increased abruptly below pH 4, spiking up from values lower than 5 mV, in the pH range from 4 to 9, to 10-25 mV, indicating that albumin is removed in quite acidic condition. On Ti64_BSA, high standard deviations, between 10 an 20 mV, were observed also at pH higher than 9, suggesting a degradation of the surface at alkaline pH. Among other factors, the instability of protein-surface bonds in the case of polished surfaces may be caused by unfavorable electrostatic charges. In fact, both Ti and Ti64 have the IEP at pH

4.1, and below that point, both titanium and BSA expose only positive charges on the surface. A similar thing, from the surface charge point of view, may happen also on Ti(A-HC-H), which have an IEP of 5.6, but the surface porosity can help to retain more the adsorbed proteins. On the other hand, Ti64(SrAg) and Ti64(HF-H_2O_2) always exposes negative charges that can bind the amino groups on the protein. The titration curve of all the treated surfaces after adsorption shows very small standard deviations, which were always lower than 3 mV.

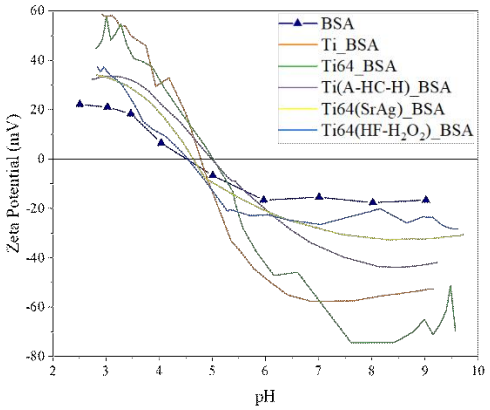

Figure 5.60 ζ potential titration curves of albumin adsorbed on titanium surfaces. The titration curve of BSA in solution is also reported.

After BSA adsorption, the zeta potential of the surfaces (Figure 5.10 and Figure 5.11) greatly changed (Figure 5.60). The IEPs are all shifted close to the one of albumin (Table 5.22), confirming the presence of the protein layer on all the substrates, also on Ti and Ti64, where BSA detaches at lower pH. As consequence, also the shape of the potential curves is affected. The titration curves of Ti_BSA and Ti64_BSA are similar, regarding the IEP, the slope around the IEP, and the eventual plateaus. The curves became quite irregular at the extreme of the pH range as consequence of detachment of the proteins. With respect to BSA in solution, albumin on these surfaces exposes more hydrophobic moieties outwards to the solution, as consequence of changes in the tertiary structure, as suggested by the increased slope of the curve around the IEP. On the other hand, the three dimensional conformation of albumin is more retained in the transient layer formed on Ti64(SrAg) and Ti64(HF-H_2O_2). The ζ potential of those substrates after adsorption is similar to the one of BSA and it is similar between each other. On these surfaces, albumin exposes the hydrophilic domains towards the solution, as in the case of the native protein. At last, Ti(A-HC-H)_BSA shows an intermediate behavior between the polished and the other two treated surfaces. It is reported that albumin spread more when adsorbs on hydrophobic surfaces while it retains its spatial organization on the hydrophilic ones [71]. This fact is in agreement with the results reported here: Ti and Ti64 are much more hydrophobic than Ti64(SrAg) and Ti64(HF-H_2O_2). Ti(A-HC-H) has a similar contact angle to untreated titanium, still the surface porosity and the high amount of BSA adsorbed avoid high spreading of the proteins.

Concerning fibronectin adsorption, the results were similar to the one obtained for BSA (Table 5.23). Looking at the residual nitrogen, it was fund that again Ti and Ti64 are not able to maintain the protein layer through the measuring process. According to the standard deviations, this may happen again at pH around 4, during the acidic titrations. The standard deviations are between 0 and 3 mV from pH 4 to 9 for Ti, increasing up to 10 mV below pH 4. In case of Ti64, the behavior is analogous between pH 3 and 8.5, while at higher pH the standard deviations increase between 5 and 8. The causes of this detachment may be related to changes in the surface charge of both the substrate and the protein, as in the case of albumin. The protein layer was found mainly intact on Ti64(SrAg) and Ti64(HF-H_2O_2), in accordance with the standard deviations, which are always lower than 1 mV on the former surface and lower than 5 mV, apart for one point at pH 4.5 where the error was 6 mV, on the latter. Unexpectedly, the residual N% was found very low on Ti(A-HC-H). The standard deviation of Ti(A-HC-H) are low (<3 mV) along all the measured pH range, so the detachment may take place even during the preparation step of the titration measurement. The weakness of bonding with FN can be related to the high IEP of the substrates, at 5.5, and the net positive charge of that surfaces basically in all the acidic range. Being the fibronectin quite bigger than BSA, the pores may be less capable to physically hold the proteins on the surface. As consequence, the titration curve of Ti(A-HC-H)_FN cannot be considered reliable for the characterization of fibronectin adsorption on this surface.

Table 5.23 Residual nitrogen after the zeta potential measure in the acidic range (atomic %) and IEP of titanium surfaces with adsorbed FN (-: not measured).

	N%	IEP
FN	-	4.9
Ti_FN	8.11	4.6
Ti64_FN	6.92	4.6
Ti(A-HC-H) _FN	3.01	(5.0)
Ti64(SrAg) _FN	13.12	4.4
Ti64(HF-H_2O_2) _FN	11.68	4.3

IEP of Ti(A_HC-H)_FN is not significative and reported in brackets.

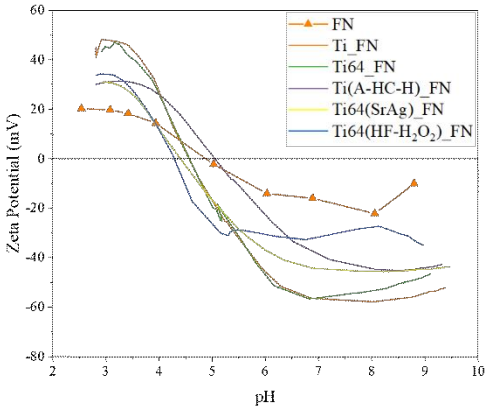

Figure 5.61 ζ potential titration curves of fibronectin adsorbed on titanium surfaces. The titration curve of FN in solution is also reported.

After fibronectin adsorption, the significative IEPs of the surfaces are shifted near the one of FN in solution (Table 5.23 and Figure 5.61), confirming the presence

of the protein layer. As was observed for BSA, the zeta potential curves of Ti_FN and Ti64_FN are practically identical, showing a more hydrophobic conformation of the protein after adsorption, in particular at pH higher than 4, before the protein detachment. Also Ti64(SrAg)_FN and Ti64(HF-H_2O_2)_FN have a similar titration curves, in analogy to BSA adsorption. Here, the two curves are very similar at pH values under pH 5.5, while at basic pH, Ti64(SrAg)_FN has a little more negative surface. Anyhow, the difference is close to 10 mV, which is the resolution limit of the instrument. With respect to the protein in solution, FN adopts a more hydrophobic tertiary structure or orientation after adsorption on the treated surfaces. Generically, the spatial orientation of fibronectin may be less dependent on the surface than the one of BSA, possibly due to the larger dimension.

It was noticed that both Ti64(HF-H_2O_2)_BSA and Ti64(HF-H_2O_2)_FN have a shift in the basic plateau onset to lower pH with respect to the other protein covered specimens. This may be related to two different factors. The first one is more related to the denaturation of proteins occurring on this surface. It is known that a change in the chemical environment of carboxyl groups, for example as consequence of modifications in the secondary structure, lead to a change of the pK_a of these groups [72], as experimentally previously shown. The stronger are the acidic groups on a surface, the more shifted at low pH is the basic plateau and viceversa. The titanium surface treated with hydrogen peroxide causes a greater denaturation of the adsorbed proteins, possibly causing the shift observed in the potential measures. The second factor is an influence of the substrate potential, that has an effect on the one of the protein layer due to its low thickness. At the moment, it is not possible to further hypothesize which effect is actually responsible for the behavior observed. Further studies need to be addressed to this point.

Regarding protein adsorption on titanium surfaces the hydrophilicity of the surfaces plays a role in determining the overall structure of adsorbed proteins: albumin retains its native structure, with hydrophilic moieties outwards, on hydrophilic surfaces, spreading more on hydrophobic ones (Figure 5.62). At last, it is possible that bigger proteins, such as fibronectin, are less affected by the surface properties than the smaller ones, such albumin.

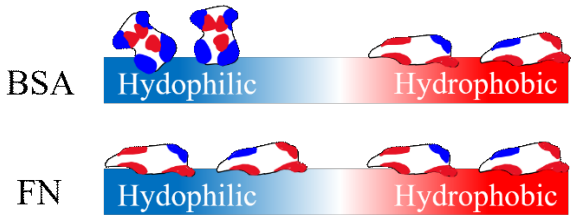

Figure 5.62 Effect of surface hydrophilicity and hydrophobicity on the albumin and fibronectin spreading and exposition of hydrophilic (blu) and hydrophobic (red) moieties.

Concerning bioactive glasses, the residual nitrogen is not enough to understand what occurs during the potential measurements. The full compositions by XPS of SBA2_BSA and AgSBA2_BSA after the acidic titration curve are reported in Table 5.24.

Table 5.24 Composition of SBA2_BSA and AgSBA2_BSA after zeta potential acidic titration range

	ATOMIC COMPOSITION (%)							
	Si	O	C	Ca	Ag	P	Na	N
SBA2_BSA	34.03	51.74	10.88	1.21	-	-	0.35	1.30
AgSBA2_BSA	17.58	40.83	31.87	1.34	0.07	0.64	0.39	7.27

The residual nitrogen is decreased with respect to the as adsorbed glasses (Table 0.9), as well as Ca, P, Na and Ag, for the AgSBA2 sample. Contemporaneously, the Si content is much increased. These results suggest that the silica-gel layer, containing the adsorbed albumin and the precipitated calcium and phosphate ions, is removed during the potential measurement. On AgSBA2 also the silver present before protein adsorption seems to be removed. The detachment of the layer may be caused by chemical reactions induced by low pH and by the shear stress applied on the surface by the flow of the electrolyte solution. These processes may begin soon, just below pH 5, as indicated by the increased standard deviations on AgSBA2. On these samples, the deviations are below 1 mV between pH 5 and 9, they increase between 3 and 9 mV down to pH 3.5, and further grew between 10 and 12 mv at more acidic pH. In the case of the undoped glass, the surface may be stable in the pH range between 4 and 0, where the deviations are lower than 3 mV. Below pH 4, they increase between 4 and 7 mV. As consequence, the titration curves (Figure 5.63) cannot be considered representative of the protein adsorbed on bioactive glasses.

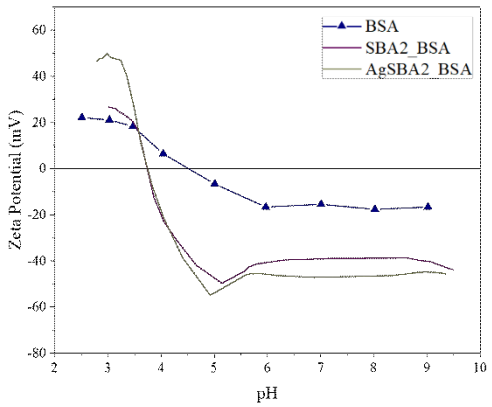

Figure 5.63 ζ potential titration curves of albumin adsorbed on BG surfaces. The titration curve of BSA in solution is also reported.

The titration curves of SBA2_BSA and AgSBA2_BSA are similar, indicating that, despite the silver incorporation and the adsorption of different amounts of proteins, the surface chemistry and reactivity of the glass remained the same. The fact that some proteins are still present on the surface, or that not all have been removed before the end of the measurement, can be deduced by the shift of the BG IEPs, which were undetected prior protein adsorption and after appeared at 3.7.

The compositions of SBA2_FN and AgSBA2_FN after the zeta potential measurement are reported in Table 5.25. Surprisingly, in this case, the residual amount of nitrogen increased on both samples.

Table 5.25 Composition of SBA2_FN and AgSBA2_FN after zeta potential acidic titration range

	ATOMIC COMPOSITION (%)							
	Si	O	C	Ca	Ag	P	Na	N
SBA2_FN	24.45	47.56	23.06	0.60	-	-	0.14	4.18
AgSBA2_FN	11.40	33.16	46.85	1.02	0.30	1.04	-	6.22

Si increased, but less than what was observed with the BSA adsorbed samples, while the amount of other elements is again low. In the case of fibronectin, the protein containing silica-gel layer is just partially removed during the potential measurement, exposing the proteins that diffused and were embedded inside the gel during the adsorption step. The extreme complexity of protein-bioactive glass interactions is further unveiled by these results. According to the fact that fibronectin N% increased after partial removal of the reaction layer, it is possible that the proteins contained inside the silica-gel layer are even more than the ones exposed on the glass surface after the soaking in the protein solution. Anyhow, the stability of the gel layer seems to be affected by the type of protein adsorbed, with fibronectin that increases it with respect to BSA, at least in case of AgBSA2. The standard deviations for the silver doped BG are about 1 mV between pH 4 and pH 9, and increase up to 6-8 mV below pH 3.5. On AgSBA2_BSA the reactions were found to take place from pH 5. SBA2_FN has an analogous behavior: the standard deviations are lower than 1 mV at pH higher than 4, in the range 4 to 10 mV at pH between 3 and 4 and about 11 mV at lower pH. These data are also a confirmation of the presence of protein inside the reaction layer on bioactive glasses, which was reported only once [73], according to what has been found in literature. Unfortunately, as in the case of BSA, the resulting titration curves (Figure 5.64) are not representative of the conformational state of adsorbed fibronectin.

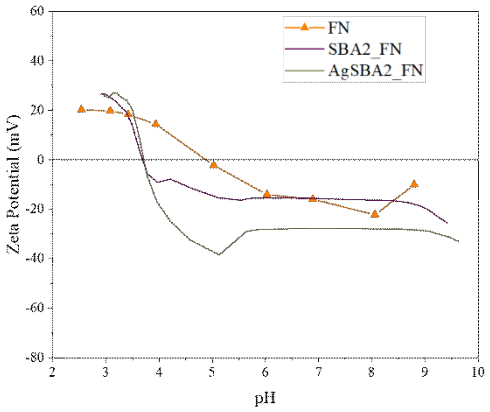

Figure 5.64 ζ potential titration curves of fibronectin adsorbed on BG surfaces. The titration curve of FN in solution is also reported.

As in the case of BSA, the IEP of SAB2_FN and AgSBA2_FN was observed at 3.7 for both glasses. The proteins that remain on the surfaces can cause the increase of the IEP with respect to the pristine surfaces. After FN adsorption, the two glasses present some differences in the zeta potential, in particular, SBA2_FN has a higher potential above the IEP. The difference may be caused by the concomitance of a different interactions between FN and the two glasses and a

different chemistry of the surface, as also possible to notice in the XPS results (Table 5.25). Unfortunately, it is not possible to specifically determine the causes of these differences, due to the complexity of the system.

Contrary to adsorption on titanium surfaces, the ζ potential measurement was not helpful to investigate the orientation of proteins adsorbed on bioactive glasses. Still, it allows to better understand the intricate events that occur on the surface of reactive materials during the contact with protein containing solutions.

After the potential measure in the acidic range, the nitrogen on PS_BSA (Table 5.26) was reduced with respect to the samples before the measures (Table 5.9). It is possible to hypothesize a partial detachment of the proteins from the surface, that can occur during the preliminary step of the measures, since all the standard deviations are quite low (<3 mV) on all pH range.

Table 5.26 Residual nitrogen after the zeta potential measure in the acidic range (atomic %) and IEP of PS with adsorbed BSA

	N%	IEP
BSA	-	4.5
PS_BSA	5.69	5.3

Despite the protein layer may be damaged, the potential titration curve clearly shows the presence of remaining albumin on PS surface (Figure 5.65). In fact, it is completely different from the one of the bare substrates (Figure 5.14), with the presence of a basic and acidic plateau, even if the last one is not stable, and the IEP is shifted from around 4 to 5.3. These differences cannot be ascribed totally to the protein conformation, but albumin may assume a much different conformation on PS than in solution exposing more hydrophobic groups, in accordance to the fact that hydrophobic surfaces enhance protein spreading during adsorption.

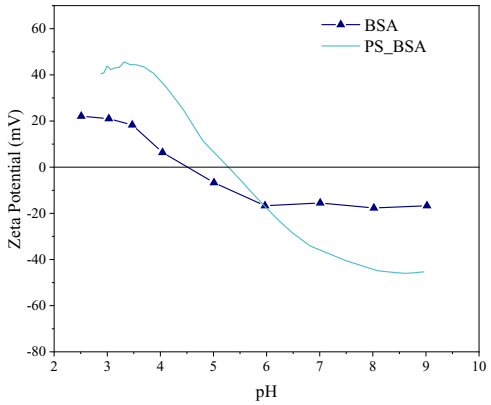

Figure 5.65 ζ potential titration curves of albumin adsorbed on PS. The titration curve of BSA in solution is also reported.

In the case of PS_FN, the amount of nitrogen after the ζ potential was slightly increased (Table 5.27). Since on PS there is no reactive layer that can embed proteins, contrary to what happen with glasses, it is possible that the small changes are due to a variability of the adsorption, that can result in different amount of adsorbed fibronectin. On the other hand, it may be reasonable to conclude that FN is not detached from the polymer during the measure, which is also corroborated by the very small standard deviations, always lower than 3 mV. Therefore, the

potential titration curve may be quite indicative of the conformation of adsorbed fibronectin.

Table 5.27 Residual nitrogen after the zeta potential measure in the acidic range (atomic %) and IEP of PS with adsorbed FN

	N%	IEP
FN	-	4.9
PS_FN	8.1	5.0

The IEP of PS_FN is very closed to the one of FN in solution (Table 5.27), but the potential curve after adsortpion is steeper than the one of pure FN (Figure 5.66). As in the case of albumin, a change in the tertiary structure of adsorbed fibronectin is observed and it can be related to adsorption on a highly hydrophobic surface.

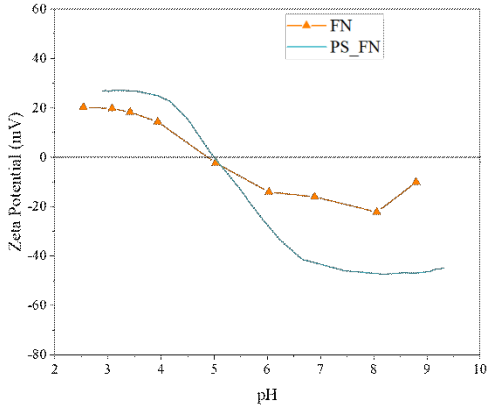

Figure 5.66 ζ potential titration curves of fibronectin adsorbed on PS. The titration curve of FN in solution is also reported.

Solid surface ζ potential is capable of providing information on the tertiary structure and orientation of adsorbed proteins, with the limitation that the adsorbed needs to be stable and not detach during the measurement. This can happen when there is enough protein adsorbed on the surface and when the surface-protein bonds are strong enough, as in the case of adsorption on Ti64(SrAg) and Ti64(HF-H_2O2). It was confirmed the general belief that proteins change more their overall 3D conformation and tertiary structure when they are smaller in dimension and adsorbed on hydrophobic materials, than on the hydrophilic ones.

5.3. Competition for the surface: sequential and co-adsorption

Using single protein solutions for adsorption it is useful to isolate and investigate the effect of each surface property on the adsorption mechanisms, but it is a completely different situation with respect to the biological environment. In order to better mimic the contact with physiological fluids, sequential adsorptions and co-adsorption of albumin and fibronectin were performed. The firsts aimed to investigate if proteins that reach early the surface can be replaced by proteins that came later or if they can prevent adsorption of the other ones. Co-adsorption have the goal to mimic a complex environment, where the fluid contains more proteins.

Due to the high similarities between albumin and fibronectin, many of the techniques employed in the first part of this thesis are not capable of distinguish between BSA and FN. Therefore, XPS, SERS, FTIR and KPFM are not applicable in this context. Albumin and fibronectin can be observed by labeling with different colors, green and red respectively, and the ζ potential was employed, since BSA and FN showed different titration curves even after adsorption on the samples. Measurements of water ater contact angle were also performed.

5.3.1. Sequential adsorption by fluorescent quantification and imaging

Sequential adsorption can be a simple simulation of the Vroman effect, and it can allow to evaluate the extent of a protein replace on a surface. At first, the amount of albumin or fibronectin that adsorbs on a preformed protein layer, of fibronectin and albumin respectively, was investigated on a limited set of surfaces, namely Ti, Ti64 and Ti64(HF-H_2O_2). The preliminary reduction of the number of the tested substrates allowed to contemporaneously acquire the fluorescent signal from both the adsorption conditions: FN adsorbed on a BSA layer and vice versa. In this manner, it was possible to compare the amount of the first protein adsorbed on the surface after the second adsorption event. The results are reported in Figure 5.67.

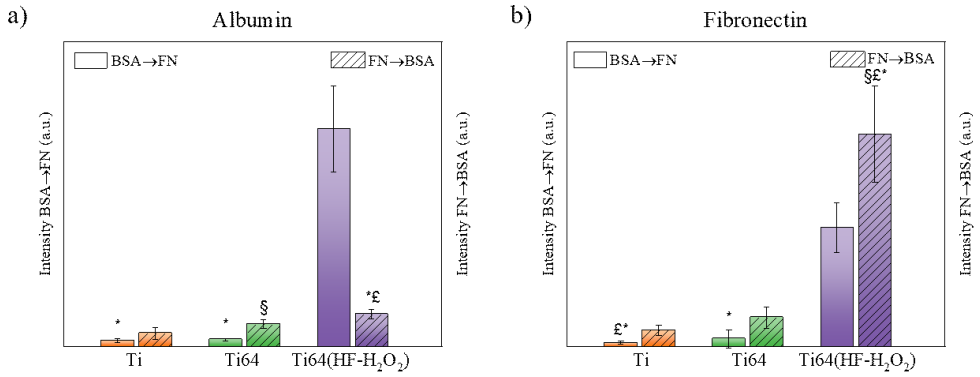

Figure 5.67 Fluorescent quantification of (a) albumin and (b) fibronectin in sequential adsorption: FN on a BSA layer (BSA→FN) and BSA on a FN layer (FN→BSA). Significance, $p < 0.05$: * vs Ti64(HF-H_2O_2)_BSA-FN; § vs Ti64_FN-BSA; £ vs Ti_FN-BSA.

The treated surface confirms its higher adsorption capability with respect to the mirror polished ones, in any circumstances. The first important information is that both proteins are contemporaneously present on the surfaces in all the cases, neither albumin nor fibronectin are capable of completely remove the pre-adsorbed protein, while they still can bound on a preexistent protein layer. Even though it is not possible to quantified how much proteins are substituted and removed during a second adsorption process, it is evident in most of the cases that the amount of protein adsorbed during the first adsorption is higher than the one bonded during the second adsorption, for instance fibronectin directly adsorbed on the surfaces it is more than the one adsorbed on the albumin layer. This reduction is statistically significant on all surfaces but for albumin on Ti and Ti64 (Figure 5.68 a). In this

case, BSA adsorbed as the second protein has a greater adsorption than when adsorbed on the clean surfaces, even though the difference is statistically significant only on Ti64. The adsorption on mirror polished surfaces was found quite low and weak, as discussed in the previous paragraphs, thus it is possible that the affinity of albumin for fibronectin is slightly higher than for Ti and Ti64. Furthermore, the much reduced amount of BSA adsorbed on Ti64(HF-H_2O_2)_FN, with respect to the one found on Ti64(HF-H_2O_2)_BSA-FN, might be significative of a very limited displacement power of albumin towards fibronectin, with the latter remaining more adhered on the surface. In the case of fibronectin, the difference between FN-BSA and BSA-FN are more limited, which can indicate that the larger protein can replace more the smaller BSA from the surface.

After these preliminary experiments, the sequential adsorption has been studied on all the surfaces investigated in this work (Figure 5.68).

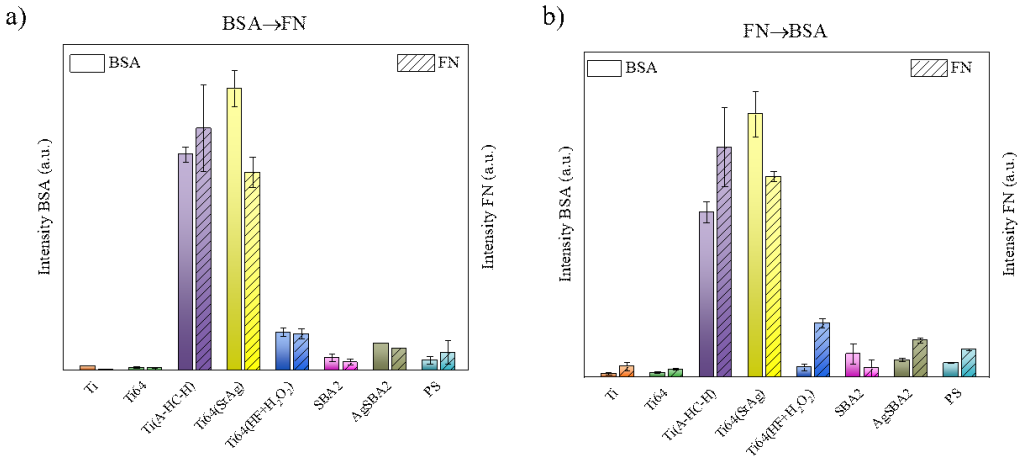

Figure 5.68 Fluorescent quantification of albumin and fibronectin sequential adsorption on all the investigated surfaces: FN on a BSA layer (BSA→FN)(a) and BSA on a FN layer (FN→BSA)(b).

These experiments were designed to compare the behavior of different surfaces in the same conditions, mimicking the subsequent arrive of different proteins on the biomaterial surfaces. As consequence, quantitative comparison can be performed between the different surfaces focusing on one protein in the same conditions, for instance albumin on BSA→FN experiment, but is not possible to compare the amount of adsorbed albumin in both conditions or BSA and FN on the same surface. The adsorption trend observed for the pure protein solution (Figure 5.19 and Figure 5.22), with the titanium treated surfaces adsorbing the most proteins, followed by silver doped bioactive glasses, polystyrene and mirror polished titanium, was here confirmed even in the case of secondary adsorption. The most relevant information that can be drawn from these results are that, in the end, the transient matrix is composed by both albumin and fibronectin, confirming that none of the two proteins is able to completely remove a pre-adsorbed protein nor entirely avoid the sequential adsorption of another one. It is possible to hypothesize that the final protein layer may be composed by the first protein adsorbed to the surface directly adhered on the substrate, while the second protein distributed both in contact with

the surface, in the regions where it was able to replace the first protein, and adsorbed in a multilayer on the top of the other protein layer in the other regions.

The compresence of albumin and fibronectin inside the transient matrix on a biomaterial surface is of biological interest. In fact, there is an open debate on a possible synergistic effect of a albumin-fibronectin mixed protein layer, that can enhance cell attachment despite the adverse anti-adhesive effect of albumin [74].

The compresence of both proteins on the surface was also determined by fluorescent imaging.

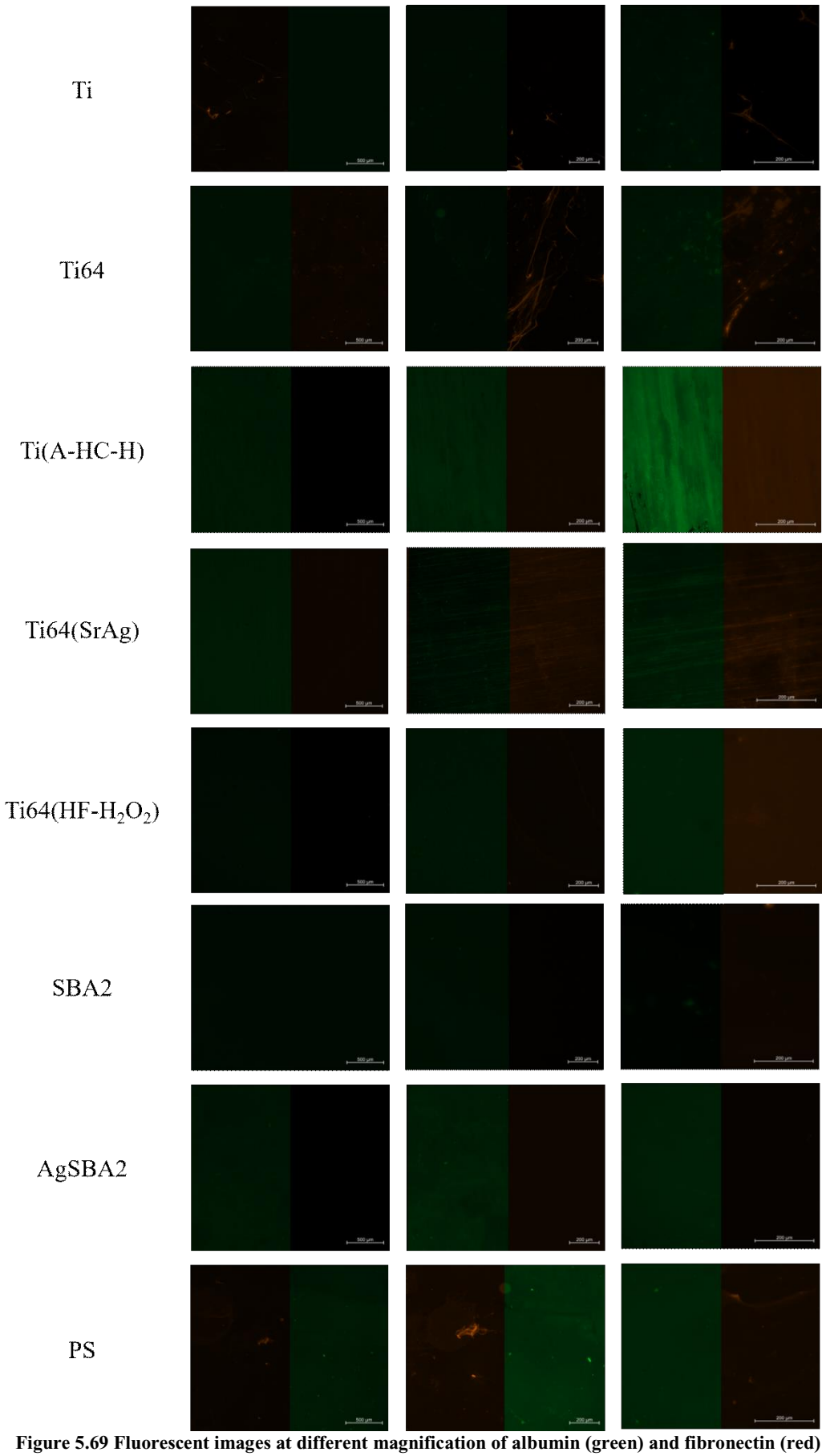

Figure 5.69 Fluorescent images at different magnification of albumin (green) and fibronectin (red) on all surfaces after sequential adsorption BSA→FN

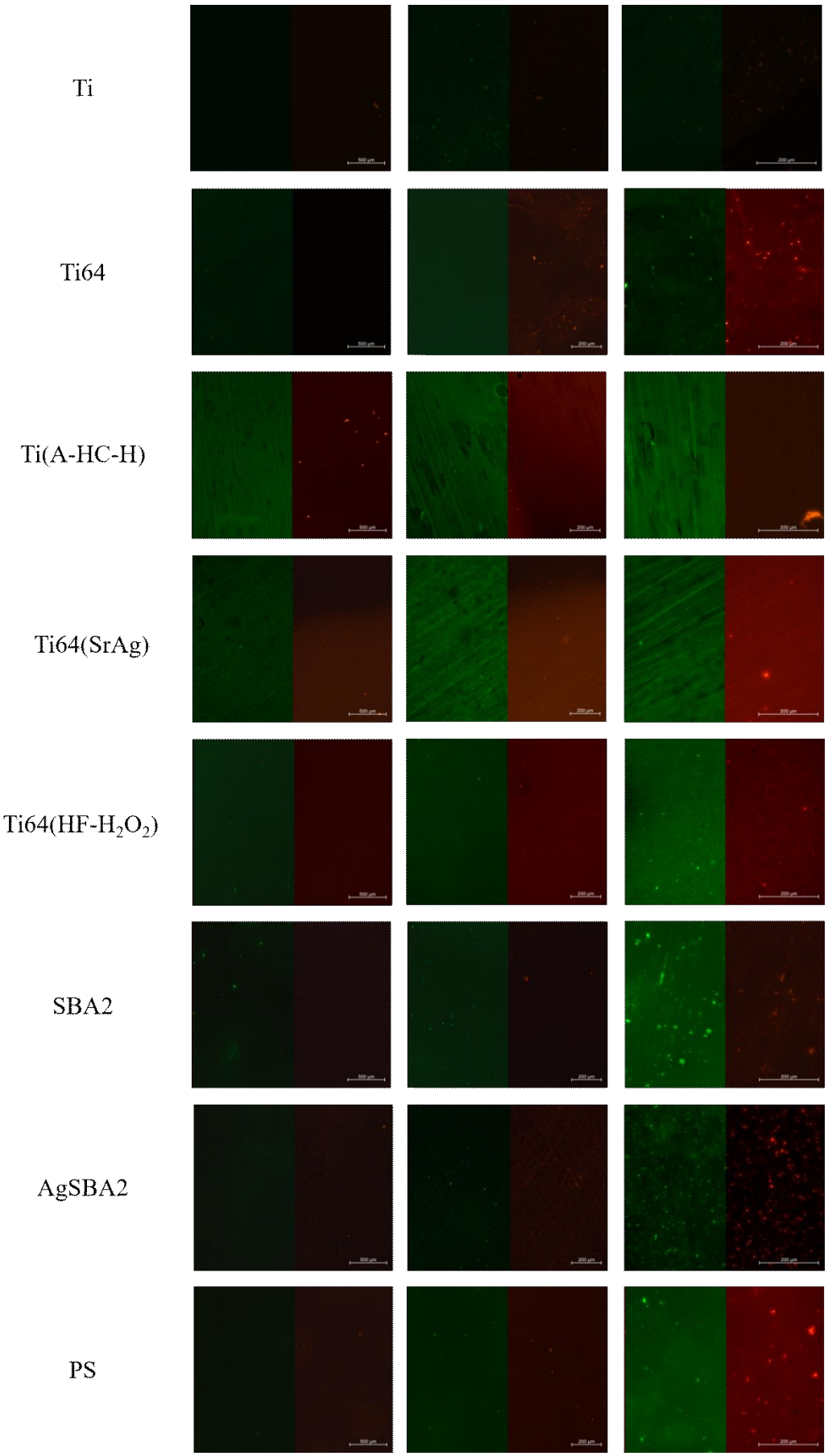

Figure 5.70 Fluorescent images at different magnification of albumin (green) and fibronectin (red) on all surfaces after sequential adsorption FN→BSA

When fibronectin is adsorbed on albumin (Figure 5.69), the underlying BSA layer can be seen on all the surfaces at any magnification, while FN was not observed at low magnification on surfaces such as Ti, BGs and PS probably due to a low amount of protein adsorbed. On treated titanium, Ti(A-HC-H) and Ti64(SrAg), the effect of the topography on adsorption is preserved in case of the frist adsorbed proteins and it is active also in case of adsorption of the second protein. Interestingly, as in the case of adsorption from a single protein solution (Figure 5.31), on flat surfaces such as Ti, Ti64, and PS, fibronectin forms filamentous network even when adsorbing on the albumin layer, limiting its spreading on the surface. In the case of sequential adsorption of albumin on fibronectin (Figure 5.70), BSA was observed on all the surfaces. The structured surface of treated titanium samples affects the adsorption also in this case. Again, fibronectin was not observed, if not at high magnification, on surfaces that are known to bind a low amount of proteins such as polished titanium samples and bioactive glasses. Interestingly, in this case, fibronectin is more evenly distributed on the surface, without the presence of the filamentous structure observed before. The exposition of the adsorbed protein layer to the aqueous environment of the albumin solution promotes a rearrangement of fibronectin. A conformational modification of the adsorbed protein as consequence of the interaction with other molecules in the fluids may increase or reduce its biological activity, and this aspect shall be further clarified. At the present time, it is not possible to tell if the rearrangement is simply due to the fact that fibronectin molecules had more time to rearrange and colonize the surfaces or if albumin has an active role on it.

5.3.2. Sequential and co-adsorption by solid surface ζ potential

Solid surface zeta potential proven to be sensitive to the type of protein adsorbed on the surface, as discussed previously in this work. The titration curves of sequential adsorption and co-adsorption on the different surfaces where compared to provide information on the composition of the protein transient matrix.

The evolution of the surface zeta potential with respect to the pH on titanium surfaces in the different adsorption conditions is reported in Figure 5.71. In general, the curves are not much different from one another, but it is still possible to get some interesting information.

Regarding Ti and Ti64 samples, the standard deviations of curves after sequential and co-adsorption rise up to high values (from values lower than 3 mV to values higher than10 mV) when the pH is lowered around 4 and below, as in the case of adsorption from single protein solution. The only exceptions are Ti_BSA-FN and Ti_BSA+FN, where the standard deviations are always below 5 mV. In analogy to what has been already discussed (paragraph 5.2.5), a detachment of the adsorbed proteins might happen around inflammatory pH despite the kind of adsorption that occurred, as consequence of changes in the charges of both substrates and proteins. Focusing on the IEP of Ti and Ti64 in the different adsorption situations (Table 5.28), it can be noticed that in sequential adsorption

the IEP is more shifted towards the IEP of the first protein adsorbed, while in case of co-adsorption the IEP is in the middle. This may relate to the fact that the first protein adsorbed is always the most abundant on the surface, limiting sequential adsorption and thus dictating the behavior of the zeta potential. In case of co-adsorption, the layer composition is more homogeneous and the ζ potential is determined by both albumin and fibronectin. Since proteins seem to severely detach from these surfaces, the extremes of the curves cannot be considered representative of the protein layer potential.

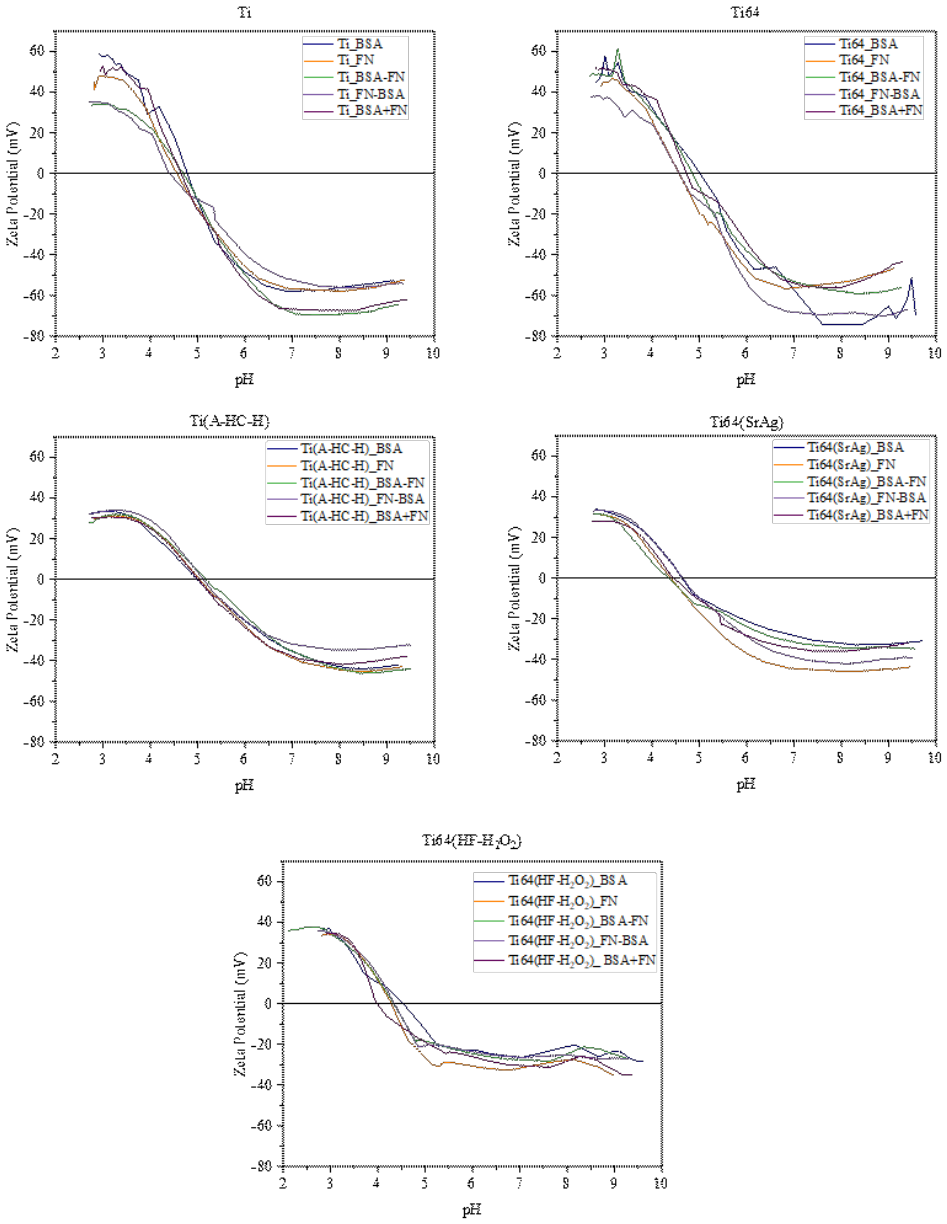

Figure 5.71 ζ potential titration curve for titanium surfaces after protein adsorption in various conditions: single protein solution (BSA and FN); sequential adsorption (BSA-FN and FN-BSA); co-adsorption (BSA+FN).

Table 5.28 IEP of titanium surfaces after protein adsorption in various conditions: single protein solution (BSA and FN); sequential adsorption (BSA-FN and FN-BSA); co-adsorption (BSA+FN).

	IEP				
	BSA	FN	BSA-FN	FN-FBSA	BSA+FN
Ti	5.0	4.6	4.7	4.4	4.6
Ti64	4.8	4.6	4.9	4.6	4.7
Ti(A-HC-H)	5.0	(5.0)	5.2	5.1	5.0
Ti64(SrAg)	4.6	4.4	4.3	4.7	4.5
Ti64(HF-H_2O_2)	4.5	4.3	4.3	4.4	4.0

IEP of Ti(A_HC-H)_FN is not significative and reported in brackets.

Ti(A-HC-H) showed very low standard deviation (<3 mV) in every kind of adsorption. Nevertheless, as already discussed, on this surface protein detachment, in particular of fibronectin, can take place even during the preliminary step of the measurement preparation. This, plus the fact that all the curves overlap almost perfectly hinder further consideration about the composition of the protein layer in the different cases.

The standard deviations were small also considering the different adsorptions on Ti64(SrAg), always below 3 mV at each pH. Contrary to Ti(A-HC-H), on this surface it has been established that albumin and fibronectin are not removed while performing the titration measurement. As consequence, those curves may be considered representative of the double protein layer. Interestingly, in the case of sequential adsorption, the IEP is closer to the second protein adsorbed, opposed to the case of Ti and Ti64 samples. In the case of the surface modified alloys the great adsorption capability, which in this case may be dominated by the surface topography since the first protein layer masks the chemical properties of the biomaterial, allows more adsorption of the protein that is adsorbed in a second time (Table 5.28). As consequence, the layer of this protein can be more continuous and influence more the final IEP. In the case of co-adsorption, the resulting IEP is well between the one of Ti64(SrAg)_BSA and the one of Ti64(SrAg)_FN. The layer formed in this case is homogeneous, exposing to the electrolyte both albumin and fibronectin, without a clear predominance of one or the other protein.

As well as Ti64(SrAg), also Ti64(HF-H_2O_2) can maintain the albumin and fibronectin layer during the zeta potential measurement. The standard deviations obtained for the sequential adsorptions are comparable with the one resulting from single adsorption, not exceeding 5 mV in any case, so it may be concluded that also in these cases the titration curve is representative of the multiprotein layer. Contrary, in the case of Ti64(HF-H_2O_2)_BSA+FN, the standard deviations rose around pH 4.5, between 5 and 10 mV. The co-adsorbed layer may preset some sort of instability, which can also explain the very low IEP and the different shape of the curve (Figure 5.71). Unfortunately, during this work it was not possible to further investigate this aspect, which will request more attention in the future. In the sequential adsorption, the IEPs have the same trend observed for Ti64(SrAg): they are closer to the one of the protein that is adsorbed on a preexistent layer (Table 5.28). The reason can be similar as before: the nanospongeous oxide layer may physically increase the adsorption of albumin on a fibronectin layer and vice versa.

It has been reported that albumin is capable of displacing larger molecules such as fibronectin or fibrinogen on TiO_2 surfaces, while fibronectin mainly form a bi-layer on top of the pre-adsorbed albumin [75]. These findings agree with the results reported here for highly adsorbing surfaces such as treated titanium. On mirror polished surfaces, the zeta potential seems to suggest the contrary, but it is also possible that the results on Ti and Ti64 are affected by an early detachment of the second adsorbed protein, which may be somehow undetectable considering the standard deviations. The fact that IEP of the protein layer formed after sequential adsorption may not be determined by the most abundant protein can be of biological interest: exposed functional groups may belong also to proteins in lower concentration in the adsorbed layer. The structure of the transient protein matrix that it is formed in the case of multistep adsorption or mixed protein solution needs to be investigated more in the future, to elucidate surface-protein and protein-protein interactions and to correlate with surface properties.

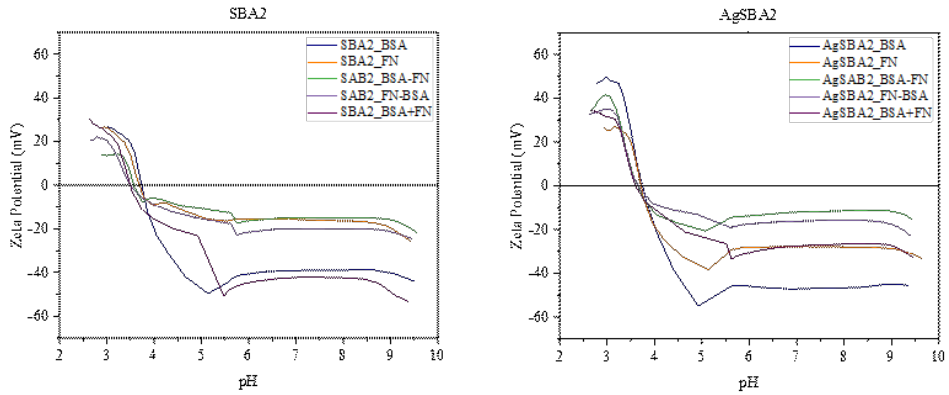

Figure 5.72 ζ potential titration curve for BG surfaces after protein adsorption in various conditions: single protein solution (BSA and FN); sequential adsorption (BSA-FN and FN-BSA); co-adsorption (BSA+FN).

Table 5.29 IEP of BG surfaces after protein adsorption in various conditions: single protein solution (BSA and FN); sequential adsorption (BSA-FN and FN-BSA); co-adsorption (BSA+FN).

	IEP				
	BSA	FN	BSA-FN	FN-FBSA	BSA+FN
SBA2	3.7	3.7	3.6	3.5	3.5
AgSBA2	3.7	3.7	3.6	3.6	3.6

The results obtained for sequential and co-adsorption for bioactive glass surfaces are shown in Figure 5.72 and Table 5.29. As extensively discussed, the resulting surface layer on BGs after adsorption is formed by a mixture of hydrated silica-gel and the adsorbed proteins. In case of sequential adsorption this complexity may even increase, since the glass can further react during the second adsorption step and proteins can be embedded at different depth inside the new reaction layer. Furthermore, all the samples tend to react at pH around 4, as indicated by the standard deviations, which are lower than 5 mV for each point measured at pH higher than 4, and they increase between 5 and 10 mV at pH lower than 3.5. Consequently, it is hardly possible to correlate the potential curves with the composition of the protein layer.

In the end, ζ potential titration curves after sequential and co-adsorption were preformed also on PS (Figure 5.73 and Table 5.30). As in the case of a single protein

adsorption, the standard deviations remained low along all the measurements (always lower than 2 mV), as consequence, it is possible to hypothesize a stability of the protein layers and that the curves can be representative of them. Considering the IEP, the isoelectric points are closer to the one of PS_BSA than the one of PS_FN in both cases of sequential adsorption (Table 5.30). On the other hand, the IEP of PS_BSA+FN is similar to the one of PS_FN. These similarities can be observed also in the shape of the titration curves, in particular in the central region of the pH range (Figure 5.73). The samples after sequential adsorptions behave more like the substrate with an albumin layer, while the one after co-adsorption is closer to the surface with fibronectin.

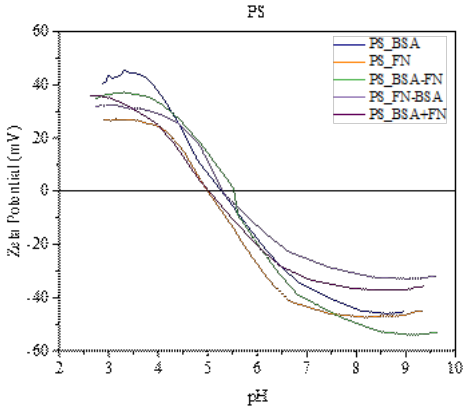

Figure 5.73 ζ potential titration curve for PS after protein adsorption in various conditions: single protein solution (BSA and FN); sequential adsorption (BSA-FN and FN-BSA); co-adsorption (BSA+FN).

Table 5.30 IEP of PS after protein adsorption in various conditions: single protein solution (BSA and FN); sequential adsorption (BSA-FN and FN-BSA); co-adsorption (BSA+FN).

	IEP				
	BSA	FN	BSA-FN	FN-FBSA	BSA+FN
PS	5.3	5.0	5.5	5.3	5.0

Based on the potential data, it seems that albumin can strongly adhere on PS, avoiding an extensive subsequent coverage by fibronectin. When FN is already present on the polymeric surface, albumin can still attach on it. On the other hand, where albumin and fibronectin compete at the same time for the surface, the latter may prevail on the former. The case of PS is different from all the other surfaces and it may be related to the fact that it is the most hydrophobic surface of all and it has no functional groups. These can extensively change surface-protein interactions.

5.4. Protein effect on *in vitro* bioactivity

In vitro bioactivity of biomaterial is usually tested by assessing the precipitation of hydroxyapatite on the surface during soaking in Kokubo's SBF solution [76]. Contrary to what occurs *in vivo*, there are no organic molecules in the SBF solution, such proteins, that can adsorb on the surface and affect the surface properties that are responsible for bioactivity. It has been reported that the presence of proteins may hinder the precipitation of hydroxyapatite on the surface of titanium substrates. When albumin and fibronectin are dissolved in the simulated solution, even at lower

concentration with respect to biological fluids, 4 and 0.05 mg/ml, the precipitation of calcium phosphates is inhibited. The same occurs when proteins are pre-adsorbed on the surface and a protein-free solution is used [77–79]. Here, the influence of albumin on the hydroxyapatite precipitation on the bioactive Ti64(HF-H_2O_2) was investigated using near physiological protein concentration in SBF (20 mg/ml).

At first, the deposition of calcium phosphate species was monitored by EDS at different time points (Table 5.31).

Table 5.31 Evolution of P and Ca composition by EDS (% atomic) of Ti64(HF-H_2O_2) soaked in SBF and SBF with albumin (SBF+BSA) at different time points.

SBF			
Days	P	Ca	Ca/P
1	0.14	0.35	2.5
3	0.19	0.38	2.00
7	0.23	0.37	1.61
14	0.14	0.2	1.43
SBF+BSA			
Days	P	Ca	Ca/P
1	-	0.24	/
3	0.14	0.21	1.5
7	0.22	0.34	1.54
14	0.26	0.31	1.19

Deposition of calcium and phosphate ions was observed since the first time point on the samples immersed on pure SBF, while on the samples soaked with BSA, P and Ca were contemporaneously present on the surface after 3 days. At 1 day only Ca was found. The presence of albumin seems to limit the early precipitation of ions, while after 7 days the quantity was comparable in the two conditions. Ti64(HF-H_2O_2) bioactivity is based on the adsorption of Ca^{2+} ions, which are bounded by the acidic OH groups, that can subsequently trigger the adsorption of HPO_4^{2-} and the consequent precipitation of hydroxyapatite [2]. As consequence, the initial Ca/P ratio in the absence of BSA it is higher than the value for mature hydroxyapatite, which is of 1.67 [80], and it is decreased at longer time, when phosphate ions precipitates more. This ratio is reduced in the presence of albumin, which may limit the availability of hydroxyl groups that can attract calcium ions.

The deposition and growth of hydroxyapatite was confirmed also by FESEM images. After 1 day, no hydroxyapatite precipitates were observed, independently form the presence of BSA in the SBF solution. After 3 d, HA particles were observed on the samples soaked without albumin, as EDS confirmed (Figure 5.74).

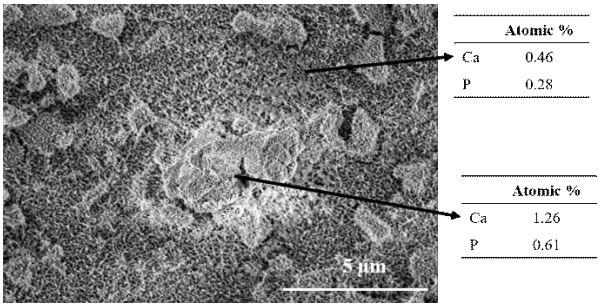

Figure 5.74 HA precipitate on Ti64(HF-H_2O_2) after 3 d soaking in SBF. Ca and P quantified by EDS are reported.

At the same time point, no aggregates were found when the samples are immersed in the presence of proteins (Figure 5.75), confirming the hypothesis of a bioactivity delay effect of albumin.

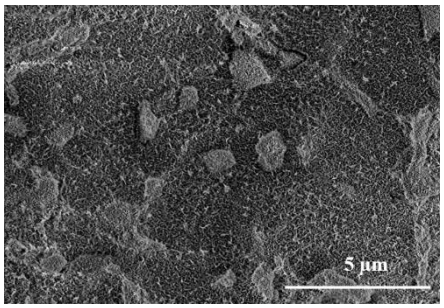

Figure 5.75 Ti64(HF-H_2O_2) after 3 d soaking in SBF+BSA: no HA precipitates were observed.

After 7 days, the situation was not much changed for both samples soaked in SBF (Figure 5.76) or SBF+BSA (Figure 5.77), with small and no precipitates respectively. This is in accordance with the low precipitation kinetic of hydroxyapatite on this kind of surface [2].

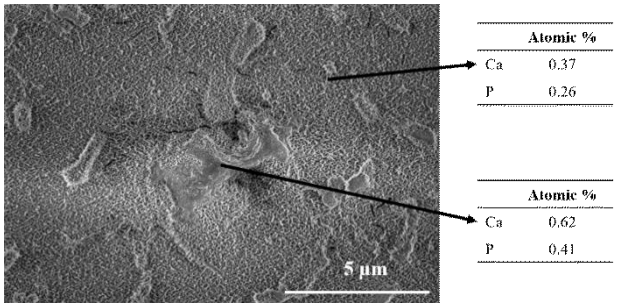

Figure 5.76 HA precipitate on Ti64(HF-H_2O_2) after 7 d soaking in SBF. Ca and P quantified by EDS are reported.

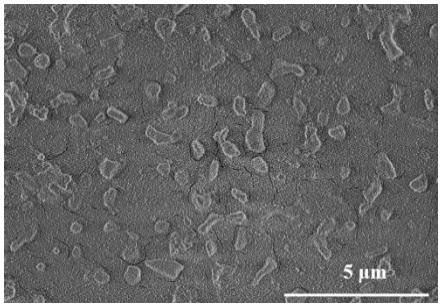

Figure 5.77 Ti64(HF-H_2O_2) after 7 d soaking in SBF+BSA: no HA precipitates were observed.

Hydroxyapatite precipitation occurred mainly between the 7th and the 14th day for samples soaked in both kind of solutions. After two weeks, big precipitates were found on all the samples. When precipitation take place in the absence of albumin, it can be so intense to form thick coating in some areas, while in others it maintains the typical cauliflowers structures (Figure 5.78). In presence of the protein, only cauliflowers like hydroxyapatite aggregates were observed (Figure 5.79).

The capability of biomaterials to retain their bioactive properties, even when proteins can adsorb on the samples and interfere with the surface chemistry responsible for hydroxyapatite precipitation, is a remarkable fact in light of clinical applications. In a biological environment the biomaterial will not interact only with

the mineral portion of the biological fluids, as in the case of Kokubo's SBF solution, still it shall be able to promote hydroxyapatite formation in order to ensure proper osteointegration.

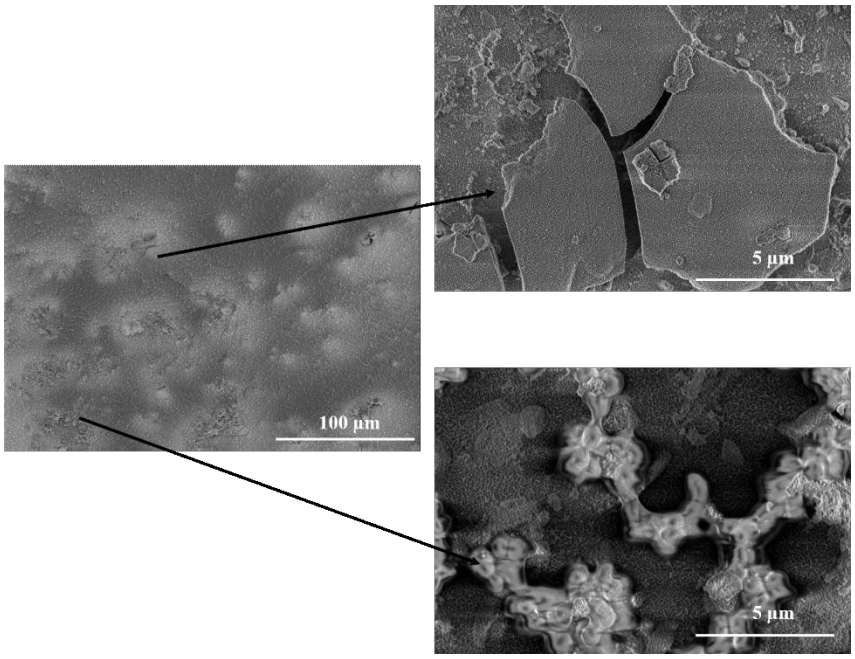

Figure 5.78 HA precipitate on Ti64(HF-H_2O_2) after 14 d soaking in SBF. Details of the precipitate conformation are shown at high magnification.

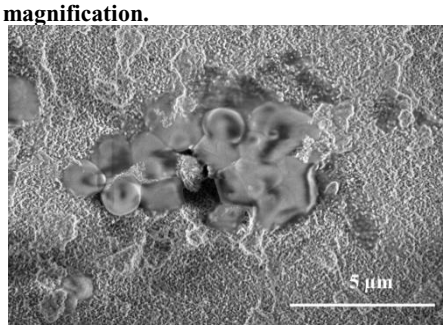

Figure 5.79 HA precipitate on Ti64(HF-H_2O_2) after 7 d soaking in SBF+BSA.

5.5. Osteoimmunomodulation of titanium biomaterials

As described and discussed in Chapter 4, a complete characterization of a biomaterial intended for osseointegration must include the evaluation of the immune response and its implications on the subsequent bone cells behavior. Good implant osseointegration requires a preliminary pro-inflammatory response, which is able to activate osteogenesis, and a subsequent switch to an anti-inflammatory response to avoid chronic inflammation and the development of scar tissue or, in case of implants, a fibrous capsule.

In this work, the osteoimmunomodulation properties of three surfaces selected among the samples investigated, namely Ti64, Ti64(SrAg), and Ti64(HF-H_2O_2), were assessed. These substrates were chosen since they are all based on the Ti6Al4V alloy and have very different surface properties and protein adsorption characteristics. The hope was to correlate the cellular response to the formation of the transient protein matrix.

Here, the first step of the osteoimmunomodulation was tested. The macrophages response to the different surfaces was investigated in terms of viability, cell morphology and spreading, and released molecules such as cytokines, chemokines, and growth factors.

5.5.1. Viability assay

Cellular viability on Ti64, Ti64(SrAg) and Ti64(HF-H_2O_2), was tested with the metabolic MTT assay. This assay is capable to quantify the metabolic activity of cells, through the cytosolic enzymatic reduction of MTT to formazan salts, which are then dissolved and the optical density of the colored solution measured by UV-vis absorbance. The metabolic activity is related both to the number and viability of cells on the samples.

MTT assay results for macrophages cultured for 3 and 7 days on the titanium substrates are shown in Figure 5.80.

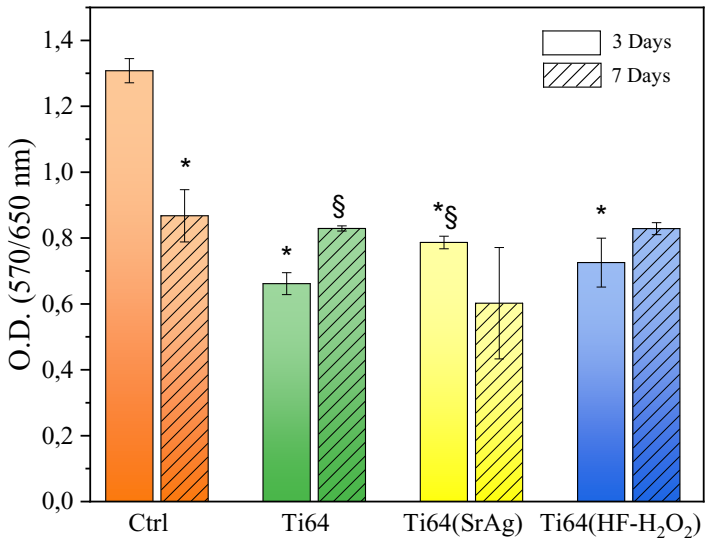

Figure 5.80 MTT optical density (O.D.) for macrophages cultured on titanium surfaces for 3 (unpatterned bars) and 7 (patterned bars) days. p values < 0.05: * vs Ctrl 3d; § vs Ti64 3d.

After 3 days of culture, the metabolic activity of the macrophages was found significantly higher on the plastic control than on the other surfaces. This is quite expected, since the bottom of the well is the standard culture substrate and it was treated to promote cell adhesion. Among the titanium substrates, the only notable difference at 3 days was found between Ti64 and Ti64(SrAg). The hydrogen peroxide treated Ti64(HF-H_2O_2) showed an intermediate behavior. After 7 days, the macrophage activity on the control was greatly reduced with respect to the one observed after 3 days. Contrary, on polished Ti64 the measured optical density was significantly higher, indicating an increased metabolic activity of the macrophages over time. On the two treated surfaces the differences between 3 and 7 days of culture were not significative, even though the observed trend suggest a reduction of the viability of cells on Ti64(SrAg) and an increase on Ti64(HF-H_2O_2).

A reduced MTT signal can be the results of a lower number of viable cells on the surface, but also of a lower metabolic activity of the macrophages themselves.

In both cases, it may be significant of a reduction of the inflammation state caused by the macrophage response to the materials. In fact, a reduced activity of the immune cells is needed to achieve the resolution of the inflammatory response and an effective wound healing [81]. With respect to the polished surface, Ti64(SrAg) seems to elicit an augmented early response by macrophages, which may decrease after one week, even though not in a significant manner due to the high error bar. On the other hand, Ti64(HF-H_2O_2) stimulates a cells response that is analogous to the one of Ti64.

5.5.2. Macrophages spreading and morphology

The response of macrophages to the different surfaces was further characterized by investigating the spreading on the samples and the apect of the cells. In fact, it was reported that differently polarized macrophages show different morphologies: M1 macrophages have a globular conformation, while M2 cells are more elongated [82].

Thanks to cytoplasm and nuclear staining and the large field reconstruction tool of the fluorescent confocal microscope, it was possible to investigate the structure and the distribution of macrophages on a very large portion of the different surfaces, after 3 and 7 days of culture (Figure 5.81).

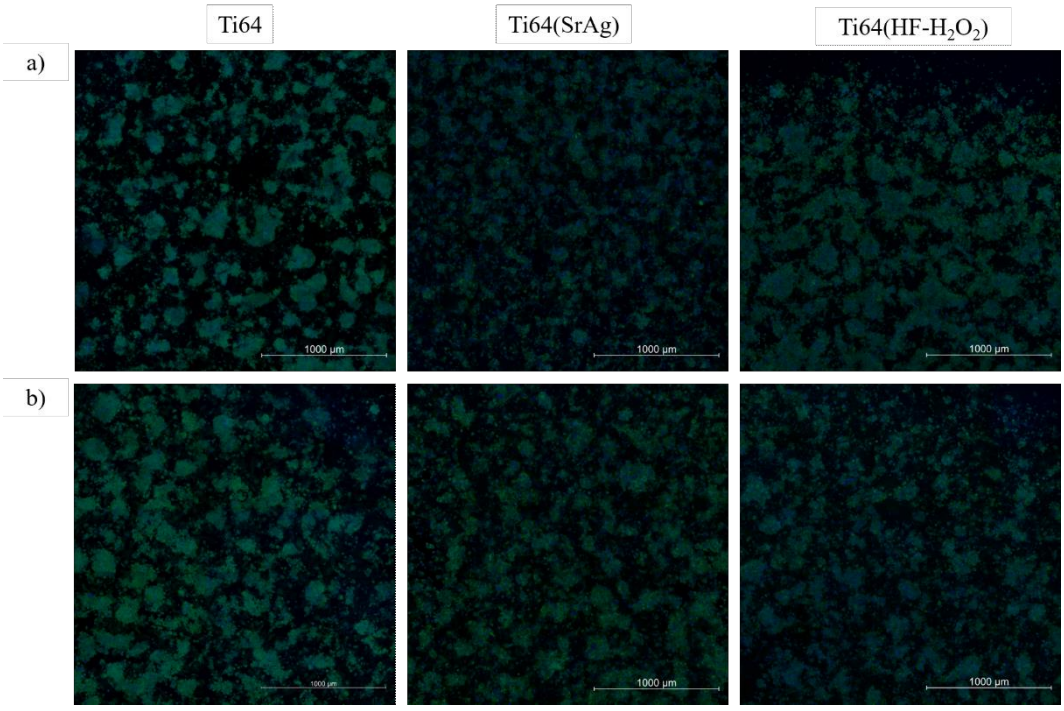

Figure 5.81 Large field fluorescent images of stained THP-1 (nuclei blue; cytoskeleton green) cultured for 3 days (a) and 7 days (b) on Ti64, Ti6(SrAg) and Ti64(HF-H_2O_2).

In all cases, the cells appear to form clusters which are homogeneously distributed on all the titanium surfaces, Ti64, Ti64(SrAg) and Ti64(HF-H_2O_2), both after 3 days (Figure 5.81 b) and 7 days (Figure 5.81 c). The formation of macrophages cluster on biomaterial surfaces seems a common behavior of those cells and it has been reported as a preliminary step towards cell fusion and formation of FBGCs [83].

The clusters on Ti64 and Ti64(HF-H_2O_2) appear bigger than on Ti64(SrAg) after 3 days, as possible to qualitatively observe in Figure 5.81. On the untreated titanium, they became lager after 7 days, while on Ti64(HF-H_2O_2), the cluster dimensions decreased passing from 3 to 7 days of culture. Instead, clusters on Ti64(SrAg) are not much changed. Those observation are confirmed by measuring the percentage of area covered by macrophage cytoskeletons, thanks to the Zeiss imaging analysis software. The results are reported in Figure 5.82. These results confirm that the spreading of macrophages on Ti64(SrAg) is reduced with respect to the other two surfaces, in particular at 3 days of culture, while Ti64 and Ti64(HF-H_2O_2) have a similar behavior, with about the 50% of the surface covered by macrophages. At longer culturing time, the polished Ti64 surface is the only one showing an increasing in the extension of macrophages clusters, while Ti64(HF-H_2O_2) has a reduced coverage and Ti64(SrAg) does not change much. At 7 days, the coverage on the treated titanium samples is statistically significantly lower than the one observed on Ti64.

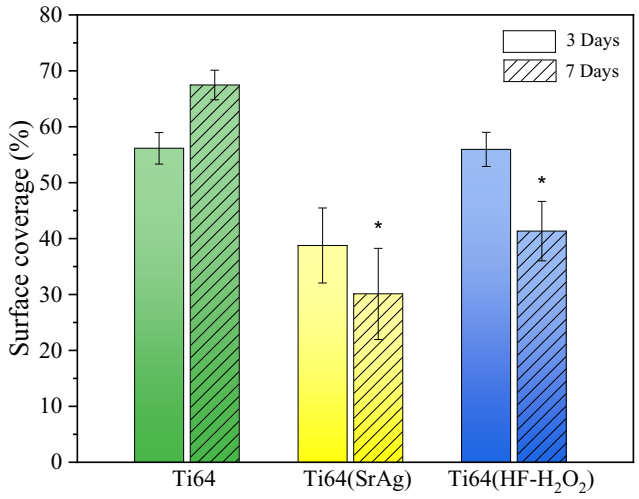

Figure 5.82 Samples area covered (percentage) by macrophage cytoskeleton after culture for 3 (unpatterned bars) and 7 days (patterned bars). p values < 0.05: * vs Ti64 7 days

The results obtained with fluorescent microscopy can be compared with the results obtained by MTT assay. According to the MTT, the viability after 3 days is higher on Ti64(SrAg) than the other two surfaces (Figure 5.80), while it is the contrary for the surface coverage (Figure 5.82). In this case, it is possible that the higher MTT signal is more related to an increased metabolic activity of the macrophages at early stages on Ti64(SrAg), than to the actual number of cells on the surface. After 7 days, the results between the two techniques are more concurrent on all the surfaces. At longer culture time, it seems that the untreated Ti64 surface sustains the macrophages activity and growth, while the chemical treated surfaces may hinder in a more effective way the immune response.

Fluorescent microscopy was also used to evaluate the morphology of macrophages. As possible to see in Figure 5.83 and Figure 5.84 the shape of cells are not much different, regardless the surface they were cultured on and for how much time. The macrophages mainly show a spheroidal shape of the cytoskeleton, typical of M1 polarization, while no elongated M2 cells were detected [82]. Several

large polynucleated FBGCs, with dimension up to 50-60 µm, were observed on all the surfaces (Figure 5.83 b and Figure 5.84 b). The presence of FBGCs is indicative of the ongoing of the FBR processes and that the presence of the titanium surfaces stimulate an inflammatory state, which is quite common in the case of biomaterials [84]. The results obtained by MTT viability assay and microscopy investigation do not allow to obtain clear information about the different osteoimmunomodulation properties of the untreated and treated titanium surfaces.

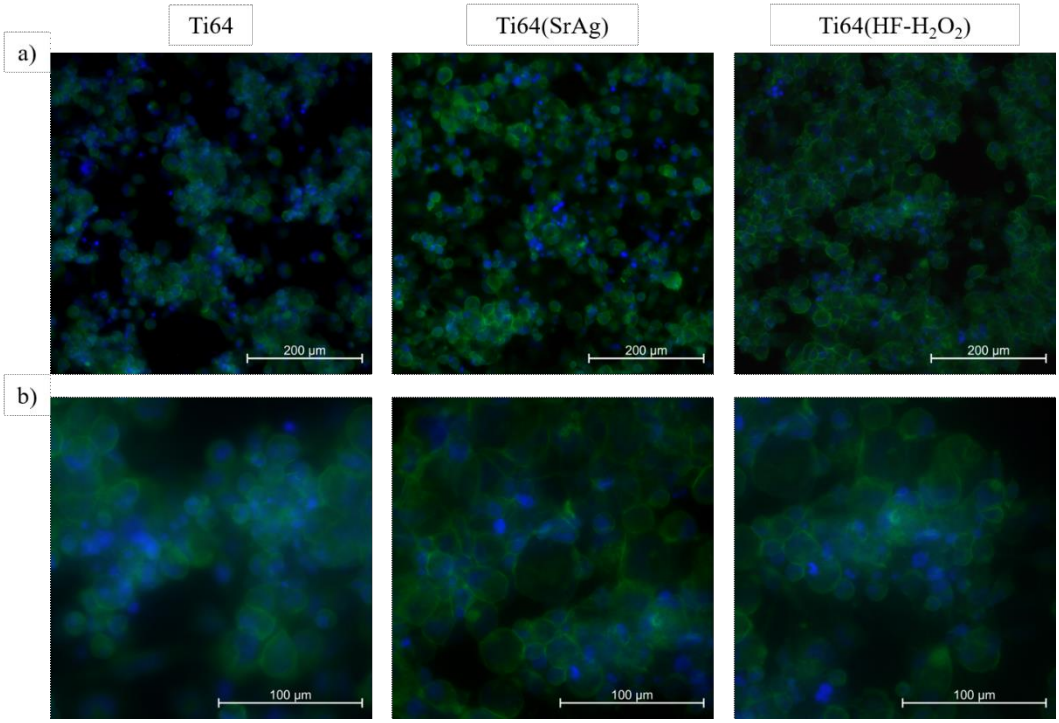

Figure 5.83 Fluorescent staining of the nuclei (blue) and cytoskeleton (green) of macrophages cultured for 3 days on the different titanium substrates. a) 200x magnification; b) 500x magnification.

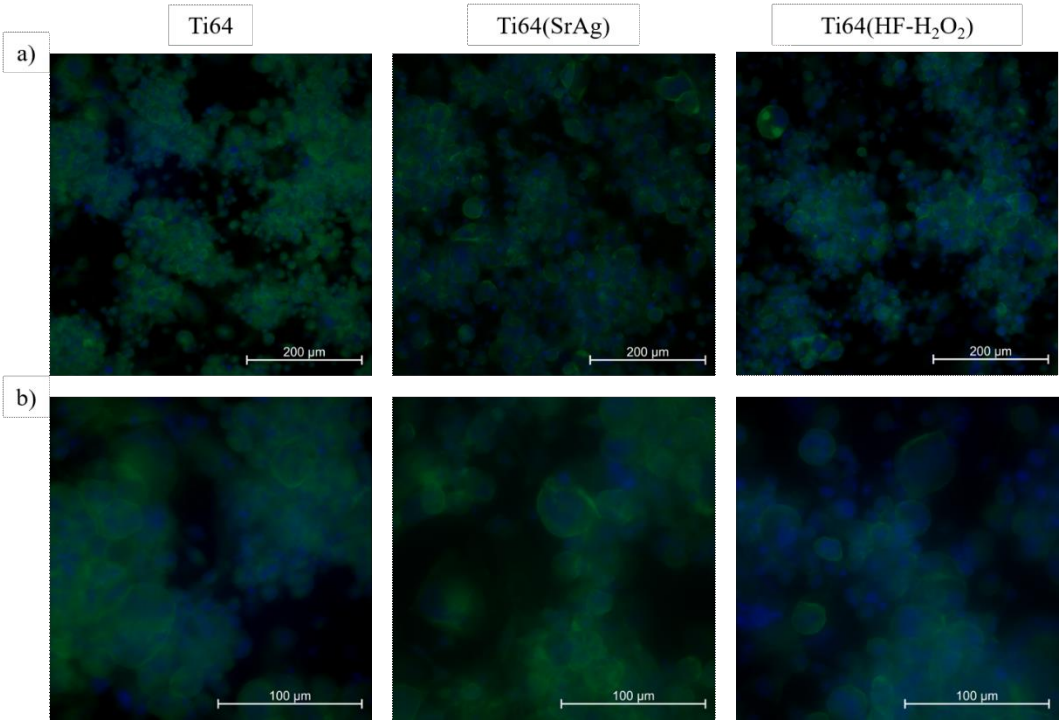

Figure 5.84 Fluorescent staining of the nuclei (blue) and cytoskeleton (green) of macrophages cultured for 7 days on the different titanium substrates. a) 200x magnification; b) 500x magnification.

5.5.3. Cytokines and factors release by macrophages during interaction with titanium surfaces

As widely discussed in Chapter 4, the factors and cytokines released by macrophages at the implant site during the foreign body reaction process are fundamental in determining the development of the events at the implant-tissue interface and its eventual osseointegration. M1 macrophages can sustain a more inflammatory response by the release of TNF-α, IL-1β, IL-6 or IL-7, while M2 polarization can induce osteogenesis by the release of INF-γ, IL-4, IL-10 and VEGF [85,86]. Therefore, the measurement of the release of these factors in the culture medium allows the evaluation of the macrophages response to the untreated Ti64 and treated Ti64(SrAg) and Ti64(HF-H_2O_2). Two different experiments were performed, and within each one every surface was in triplicate. The trend in the measured concentration of each of all the molecules investigated was consistent between the two rounds. Here the results are related to the second one, since some factor and cytokines were to abundant to be quantified in the firs experiment. All the 27 factors analyzed are reported in details in Appendix B, here the main and more interesting findings will be discussed.

Each of the investigated factor has been released by cells cultured on the three different typologies of titanium surfaces (Appendix B). All the investigated factors have been detected by the assay. Therefore, the differences in the induced immune response between Ti64, Ti64(SrAg), and Ti64(HF-H_2O_2) cannot be by the presence or absence of released factors among the 27 one investigated. As expected, factors related to both M1 polarization, such TNF-α and IL-1β, and M2 polarization, as IL-1Ra, IL-10 and VEGF were observed in all cases. At first, it seems that the population of macrophages evolving on the surfaces is heterogeneous, composed by differently M1 or M2 polarized macrophages, or cells with intermediate polarization, as in the normal course of a FBR.

The main factors deputed to the upregulation and downregulation of the inflammatory response are shown in Figure 5.85. Regarding the pro-inflammatory cytokines, IL-1β, IL-4, IL-6 and the TNF-α, the general tendency is of an increased release over time, from 3 to 7 days. In particular, the difference is significative for all surfaces regarding IL-6, while TNF-α is augmented on Ti64 and Ti64(HF-H_2O_2) and IL-4 and IL-1β only on Ti64(HF-H_2O_2). Differences between surfaces at the same time were recorded only between Ti64(SrAg) and the other two substrates in case of IL-4 at 3 days, where the concertation of the interleukin was higher for the Sr and Ag containing surface, and for IL-1β, which was higher on Ti64(HF-H_2O_2) than Ti64 after 7 days. On the other hand, looking at the anti-inflammatory cytokines, a very interesting findings was that macrophages cultured on Ti64(SrAg) expressed a higher amount of IL-10, which is the main anti-inflammatory factor, after 3 days of culture than the other two surfaces. At 7 days, IL-10 was stable on Ti64(SrAg) while it increased on Ti64 and Ti64(HF-H_2O_2). The same evolution from 3 to 7 days was observed also for INF-γ, while IL-1Ra increased only on Ti64(HF-H_2O_2).

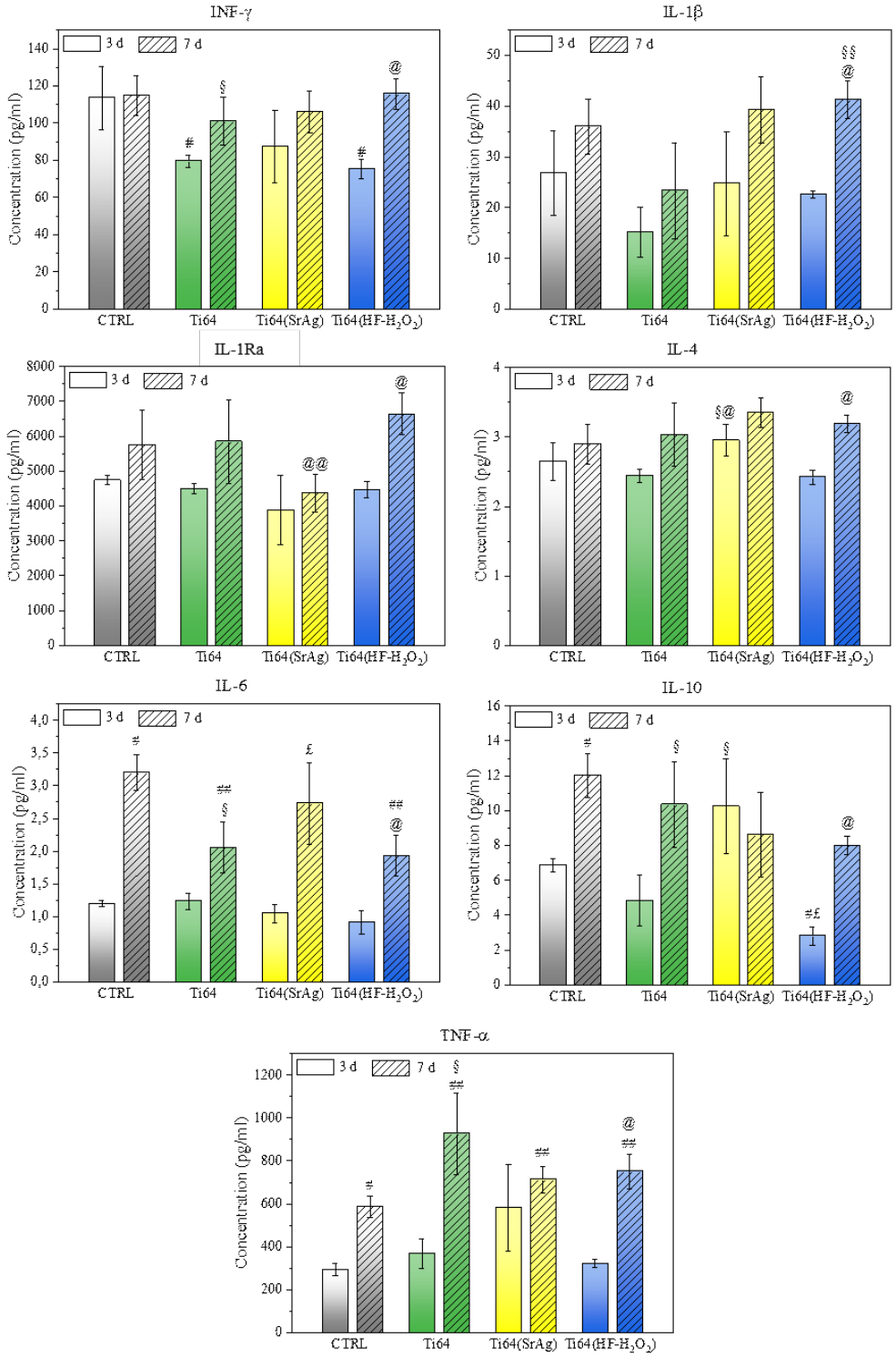

Figure 5.85 Concentration of INF-γ, IL-1β, IL-1Ra, IL-4, IL-6, IL-10, TNF-α released by macrophages in the culture medium after 3 (unpatterned bars) and 7 days (patterned bars) of culture on plastic well (CTRL)(white), Ti64 (green), Ti64(SrAg)(yellow) and Ti64(HF-H_2O_2)(light blue): p values < 0.05: # vs CTRL 3d, § vs Ti64 3d; £ vs Ti64(SrAg) 3d; @ vs Ti64(HF-H_2O_2) 3d; ## vs CTRL 7d, §§ vs Ti64 7d; ££ vs Ti64(SrAg) 7d; @@ vs Ti64(HF-H_2O_2) 7d.

From those results, it seems evident that an inflammatory state is present on all the titanium samples, both after 3 and 7 days, with a possible worsening of the immune response on all the surface, as suggested by the increase of IL-6. A more acute inflammation may be present on Ti64(HF-H_2O_2), since on this surface the release of the other pro-inflammatory factors by macrophages is increased. As

previously reported [87], surface -OH groups of Ti64(HF-H_2O_2) may be responsible for the more inflammation state. Interestingly, it was observed also the evolution of an anti-inflammatory response on all the surfaces. This effect may happen early on Ti64(SrAg), as suggested by the high presence of IL-10 after 3 days, while it can be delayed on Ti64 and Ti64(HF-H_2O_2). A late activation of anti-inflammatory pathways of macrophages on Ti64 and Ti64(HF-H_2O_2) is consistent with the higher concentration of anti-inflammatory factors at 7 days, while it was observed earlier on Ti64(SrAg). Silver and strontium have a well-known anti-inflammatory effect [88,89], in particular, Sr was found to reduce titanium particle induced osteoclastogenesis by interfering with TNF-α pathways [90] and upregulate anti-inflammatory cytokines, such as IL-10 [89]. The presence of such ions can therefore explain the early anti-inflammatory response of macrophages cultured on Ti64(SrAg). The overall picture is that of active macrophages populations on all the surfaces, which are eliciting an FBR towards the titanium samples, but the response may be developing in a favorable way towards implant integration.

It is of concern also to evaluate the effect of surface modification on the immune response, by confronting the treated surface with the polished Ti64. As possible to see from Figure 5.86, the trend of the molecules released by macrophages cultured on Ti64 is confirmed to be different from the one on the treated surfaces. Ti64(SrAg) has a clear early anti-inflammatory response, related to the higher value of IL-10 at 3 days, while the situation evolves towards a more similar situation with respect to Ti64 after 7 days. Still, a more sustained inflammatory state may persist, since IL-1β remains highly expressed and IL-6 release is increased. Contrary, on Ti64(HF-H_2O_2) the response of macrophages seems more delayed, still increasing with time, compared to Ti64 samples (Figure 5.86 b). The release of anti-inflammatory factors, such as IL-1Ra, IL-4 and IL-10, is augmented on the treated surface after 7 days with respect to Ti64, contemporaneously, also the pro-inflammatory IL-1β and IL-6 are increased, while TNF-α is decreased.

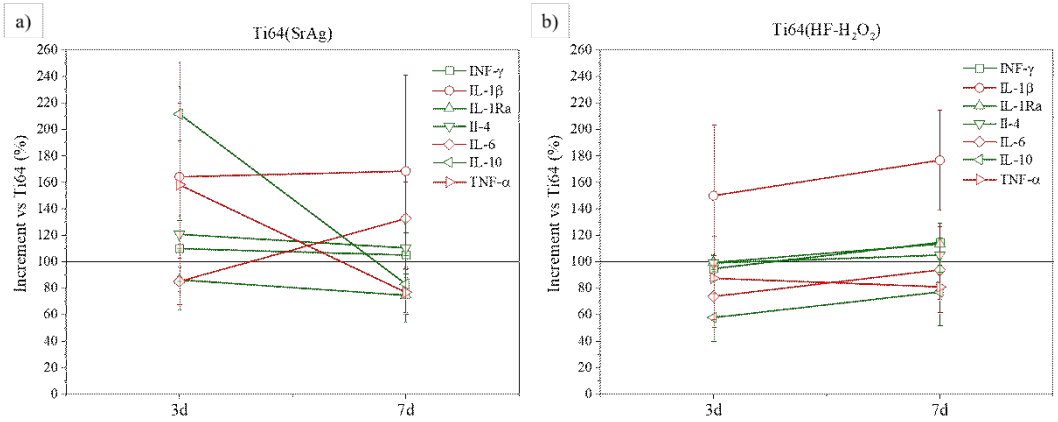

Figure 5.86 Evluotion of pro (red) and anti-inflammatory (green) factors on Ti64(SrAg) and Ti64(HF-H_2O_2) during time, expressed as the normalization over the release on Ti64 (100 % is the value relative to Ti64).

An interesting correlation was also found by comparing factors which are related to angiogenesis and vascularization: IL-9, IP-10, RANTES and VEGF. As

shown in Figure 5.87, all those factors are downregulated by Ti64(SrAg) both at 3 and 7 days of culture, with respect to Ti64 and Ti64(HF-H_2O_2). The surfaces treated with hydrogen peroxide, Ti64(HF-H_2O_2), is also the only one where an increase in those factors was observed after 7 days, while on Ti64 and Ti64(SrAg) they mainly remain constant, apart VEGF on Ti64.

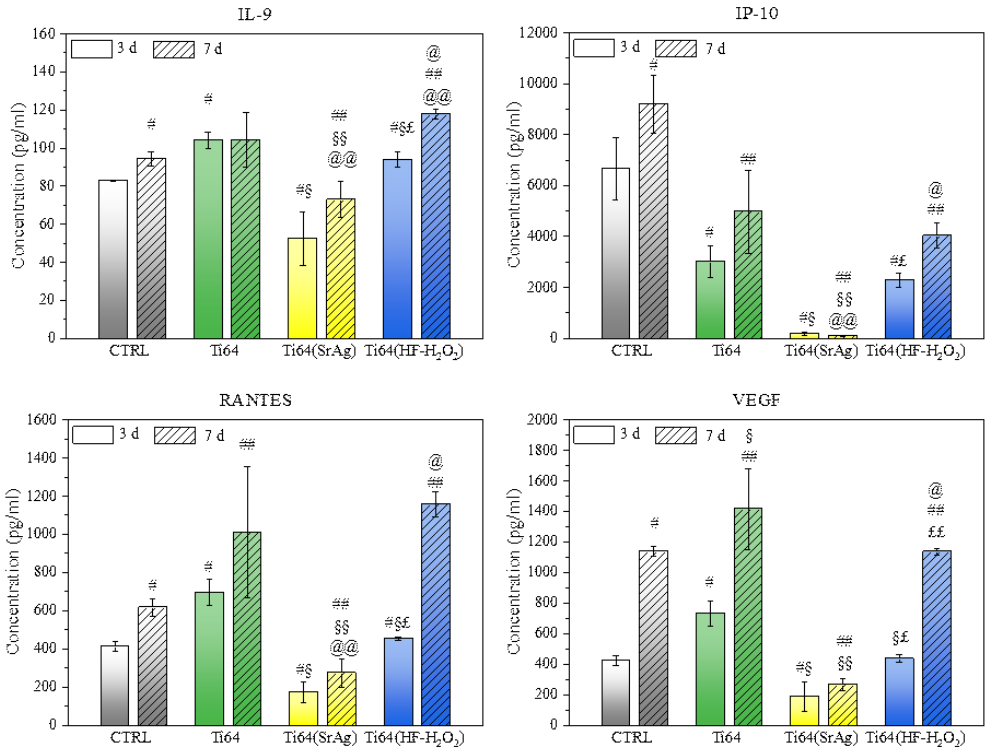

Figure 5.87 Concentration of IL-9, IP-10, RANTES and VEGF released by macrophages in the culture medium after 3 (unpatterned bars) and 7 days (patterned bars) of culture on plastic well (CTRL)(white), Ti64 (green), Ti64(SrAg)(yellow) and Ti64(HF-H_2O_2)(light blue): p values < 0.05: # vs CTRL 3d, § vs Ti64 3d; £ vs Ti64(SrAg) 3d; @ vs Ti64(HF-H_2O_2) 3d; ## vs CTRL 7d, §§ vs Ti64 7d; ££ vs Ti64(SrAg) 7d; @@ vs Ti64(HF-H_2O_2) 7d.

In order to obtain the growth of healthy bone around an implant, angiogenesis and osteogenesis must be balanced. Blood vessels are required for nutrient intake and structural template, but an uncontrolled vascularization may compromise bone tissue. On the other side, osteogenesis mudt be promoted, but a too fast grown of new bone can result in a chronic inflammation state and strong FBR. One of the main factors controlling angiogenesis is VEGF, which promotes endothelial cells migration. VEGF has also a crucial role in the activity of bone cells, in a dose dependent manner [91]: an overexpression of VEFG can induce recruitment of osteoclast and consequent osteoclastogenesis, while a physiological concentration result in bone homeostasis. Further complexity is added by a direct effect of VEGF in promoting osteoblast activity. Even though the action mechanism of VEGF in bone remodeling is not fully clear, a balance in its expression around an implant close to the physiological situation is of uttermost importance. The release of VEGF is strictly related to the presence of IL-9, RANTES, and IP-10. IL-9 and RANTES are known to induce the secretion of VEGF [92,93], while IP-10 has a potent angiostatic activity [94] and it can be released to stabilize vascularization. Production of IP-10 can be induced by VEGF, forming a control loop for the growth

of new blood vessels [95,96]. In light of these considerations, the correlations between the different factors observed on the investigated titanium surfaces are consistent, in particular regarding the low expression of IL-9, IP-10, RANTES and VEGF induced by Ti64(SrAg) on macrophages and the increase of the same factors over time generated by Ti64(HF-H_2O_2).

As well as pro and anti-inflammatory factors, it is possible to compare the release of angiogenetic molecules between unmodified and treated titanium samples (Figure 5.88). With respect to Ti64, Ti64(SrAg) elicits the same release trend by macrophages, despite the absolute amount of factors release is extremely lower (Figure 5.88 a). On the other hand, Ti64(HF-H_2O_2) may excite the angiogenetic activity better than the polished surface after 7 days. In fact, the release of IL-9, RANTES, and VEGF increases more on the treated surface than on Ti64 from 3 to 7 days, while the angiostatic IP-10 has a similar trend.

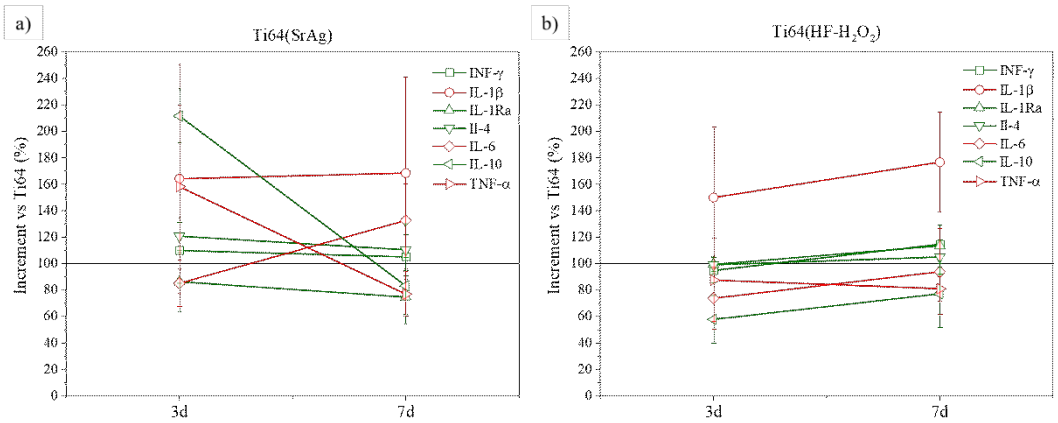

Figure 5.88 Evolution of angiogenetic (green) and agiostatic (red) factors on Ti64(SrAg) and Ti64(HF-H_2O_2) during time, expressed as the normalization over the release on Ti64 (100 % is the value relative to Ti64).

It is possible to hypothesize that the different surfaces may induce different angiogenesis and that titanium surface treatments can have a different macrophage-mediated response of osteoprogenitor cells. Due to the complexity of osteoimmunomodulation processes, the data collected in this work are not sufficient to draw conclusions on which surface can elicit the better immune response with the aim of a subsequent osseointegration, still those results are the necessary foundations on which further investigations involving bone cells can be built.

The different macrophage response may be related to the presence of metallic ions or -OH groups on the material surface through the different protein adsorption properties that have been investigated in this thesis. In fact, Ti64(SrAg) has proven a much higher adsorption capability than both Ti64 and Ti64(HF-H_2O_2), binding more albumin and fibronectin from the FBS in the culture medium. Different studies have reported that the macrophage response to biomaterials is mediated by adsorbed proteins, which can affect cell polarization and cytokine release [97]. For instance, fibronectin seems to promote macrophage adhesion and to increase their anti-inflammatory activity [98,99], which can explain the early release of anti-inflammatory factors by macrophages cultured on Ti64(SrAg). Also, increased adsorption of albumin by hydrophilic surface have been found to dampen the pro-

inflammatory effect of biomaterials [100], further explaining the results obtaining on the silver-strontium doped material.

5.6. Bibliography

[1] M. Rabe, D. Verdes, S. Seeger, Understanding protein adsorption phenomena at solid surfaces, Adv. Colloid Interface Sci. 162 (2011) 87–106. https://doi.org/10.1016/j.cis.2010.12.007.

[2] S. Ferraris, S. Yamaguchi, N. Barbani, M. Cazzola, C. Cristallini, M. Miola, E. Vernè, S. Spriano, Bioactive materials: In vitro investigation of different mechanisms of hydroxyapatite precipitation, Acta Biomater. 102 (2019) 468–480. https://doi.org/10.1016/j.actbio.2019.11.024.

[3] A. Cochis, J. Barberi, S. Ferraris, M. Miola, L. Rimondini, E. Vernè, S. Yamaguchi, S. Spriano, Competitive Surface Colonization of Antibacterial and Bioactive Materials Doped with Strontium and/or Silver Ions, Nanomaterials. 10 (2020) 120. https://doi.org/10.3390/nano10010120.

[4] P. Pawlus, R. Reizer, W. Zelasko, Prediction of parameters of equivalent sum rough surfaces, Materials (Basel). 13 (2020) 1–20. https://doi.org/10.3390/ma13214898.

[5] S. Ferraris, S. Yamaguchi, N. Barbani, C. Cristallini, G. Gautier di Confiengo, J. Barberi, M. Cazzola, M. Miola, E. Vernè, S. Spriano, The mechanical and chemical stability of the interfaces in bioactive materials: The substrate-bioactive surface layer and hydroxyapatite-bioactive surface layer interfaces, Mater. Sci. Eng. C. 116 (2020) 111238. https://doi.org/10.1016/j.msec.2020.111238.

[6] M.M. Shalabi, A. Gortemaker, M.A. Van't Hof, J.A. Jansen, N.H.J. Creugers, Implant surface roughness and bone healing: A systematic review, J. Dent. Res. 85 (2006) 496–500. https://doi.org/10.1177/154405910608500603.

[7] J.R. Jones, Review of bioactive glass: From Hench to hybrids, Acta Biomater. 9 (2013) 4457–4486. https://doi.org/10.1016/j.actbio.2012.08.023.

[8] S.-H. Choi, J.-H. Ryu, J.-S. Kwon, J.-E. Kim, J.-Y. Cha, K.-J. Lee, H.-S. Yu, E.-H. Choi, K.-M. Kim, C.-J. Hwang, Effect of wet storage on the bioactivity of ultraviolet light- and non-thermal atmospheric pressure plasma-treated titanium and zirconia implant surfaces, Mater. Sci. Eng. C. 105 (2019) 110049. https://doi.org/10.1016/j.msec.2019.110049.

[9] I. Frateur, L. Lartundo-Rojas, C. Méthivier, A. Galtayries, P. Marcus, Influence of bovine serum albumin in sulphuric acid aqueous solution on the corrosion and the passivation of an iron-chromium alloy, Electrochim. Acta. 51 (2006) 1550–1557. https://doi.org/10.1016/j.electacta.2005.02.116.

[10] L. Burgos-Asperilla, M.C. García-Alonso, M.L. Escudero, C. Alonso, Study of the interaction of inorganic and organic compounds of cell culture medium with a Ti surface, Acta Biomater. 6 (2010) 652–661. https://doi.org/10.1016/j.actbio.2009.06.019.

[11] Z. Yuan, J. Bi, W. Wang, X. Sun, L. Wang, J. Mao, F. Yang, Synthesis and properties of Sr 2+ doping α-tricalcium phosphate at low temperature, J. Appl. Biomater. Funct. Mater. 19 (2021) 228080002199699. https://doi.org/10.1177/2280800021996999.

[12] M.C. Biesinger, L.W.M. Lau, A.R. Gerson, R.S.C. Smart, Resolving surface chemical states in XPS analysis of first row transition metals, oxides and hydroxides: Sc, Ti, V, Cu and Zn, Appl. Surf. Sci. 257 (2010) 887–898.

https://doi.org/10.1016/j.apsusc.2010.07.086.
[13] A. Shchukarev, B.Ö. Malekzadeh, M. Ransjö, P. Tengvall, A. Westerlund, Surface characterization of insulin-coated Ti6Al4V medical implants conditioned in cell culture medium: An XPS study, J. Electron Spectros. Relat. Phenomena. 216 (2017) 33–38. https://doi.org/10.1016/j.elspec.2017.03.001.
[14] G. Riccucci, M. Cazzola, S. Ferraris, V.A. Gobbo, M. Guaita, S. Spriano, Surface functionalization of Ti6Al4V with an extract of polyphenols from red grape pomace, Mater. Des. 206 (2021) 109776. https://doi.org/10.1016/j.matdes.2021.109776.
[15] A. V. Shchukarev, D. V. Korolkov, XPS study of group IA carbonates, Cent. Eur. J. Chem. 2 (2004) 347–362. https://doi.org/10.2478/BF02475578.
[16] J.W. Ma, W.J. Lee, J.M. Bae, K.S. Jeong, S.H. Oh, J.H. Kim, S.H. Kim, J.H. Seo, J.P. Ahn, H. Kim, M.H. Cho, Carrier Mobility Enhancement of Tensile Strained Si and SiGe Nanowires via Surface Defect Engineering, Nano Lett. 15 (2015) 7204–7210. https://doi.org/10.1021/acs.nanolett.5b01634.
[17] P.W. Wang, L. Zhang, Structural role of lead in lead silicate glasses derived from XPS spectra, J. Non. Cryst. Solids. 194 (1996) 129–134. https://doi.org/10.1016/0022-3093(95)00471-8.
[18] L.H. Tjeng, M.B.J. Meinders, J. van Elp, J. Ghijsen, G.A. Sawatzky, R.L. Johnson, Electronic structure of Ag2O, Phys. Rev. B. 41 (1990) 3190–3199. https://doi.org/10.1103/PhysRevB.41.3190.
[19] G. Schön, J. Tummavuori, B. Lindström, C.R. Enzell, C.R. Enzell, C.-G. Swahn, ESCA Studies of Ag, Ag2O and AgO., Acta Chem. Scand. 27 (1973) 2623–2633. https://doi.org/10.3891/acta.chem.scand.27-2623.
[20] R.A. Gittens, L. Scheideler, F. Rupp, S.L. Hyzy, J. Geis-Gerstorfer, Z. Schwartz, B.D. Boyan, A review on the wettability of dental implant surfaces II: Biological and clinical aspects, Acta Biomater. 10 (2014) 2907–2918. https://doi.org/10.1016/j.actbio.2014.03.032.
[21] E.A. Vogler, Protein adsorption in three dimensions, Biomaterials. 33 (2012) 1201–1237. https://doi.org/10.1016/j.biomaterials.2011.10.059.
[22] K. Song, J. Lee, S.O. Choi, J. Kim, Interaction of surface energy components between solid and liquid on wettabilit, Polymers (Basel). 11 (2019). https://doi.org/10.3390/polym11030498.
[23] S. Yamaguchi, P.T. Minh Le, M. Ito, S.A. Shintani, H. Takadama, Tri-functional calcium-deficient calcium titanate coating on titanium metal by chemical and heat treatment, Coatings. 9 (2019). https://doi.org/10.3390/coatings9090561.
[24] M. Mozammel, E.F.T. Aghaj, N.N. Ilkhechi, A.R. Aghjehkohal, Structural and wettability investigation of titanium dioxide coating: influence of dopant concentration (Si and Sr), J. Mater. Sci. Mater. Electron. 28 (2017) 12467–12474. https://doi.org/10.1007/s10854-017-7068-2.
[25] A.A. Mosquera, J.M. Albella, V. Navarro, D. Bhattacharyya, J.L. Endrino, Effect of silver on the phase transition and wettability of titanium oxide films, Sci. Rep. 6 (2016). https://doi.org/10.1038/SREP32171.
[26] D. Guldiren, I. Erdem, S. Aydin, Influence of silver and potassium ion exchange on physical and mechanical properties of soda lime glass, J. Non. Cryst. Solids. 441 (2016) 1–9. https://doi.org/10.1016/j.jnoncrysol.2016.03.007.
[27] M. Miola, G. Fucale, G. Maina, E. Verné, Antibacterial and bioactive composite bone cements containing surface silver-doped glass particles,

Biomed. Mater. 10 (2015). https://doi.org/10.1088/1748-6041/10/5/055014.
[28] G.M. Harbers, D.W. Grainger, Cell–Material Interactions: Fundamental Design Issues for Tissue Engineering and Clinical Considerations, in: J.O. Hollinger (Ed.), An Introd. to Biomater., CRC Press, 2012: pp. 77–110. https://doi.org/10.1201/b11561-9.
[29] S. Ferraris, M. Cazzola, V. Peretti, B. Stella, S. Spriano, Zeta potential measurements on solid surfaces for in Vitro biomaterials testing: Surface charge, reactivity upon contact with fluids and protein absorption, Front. Bioeng. Biotechnol. 6 (2018) 1–7. https://doi.org/10.3389/fbioe.2018.00060.
[30] B.S. Bal, M.N. Rahaman, Orthopedic applications of silicon nitride ceramics, Acta Biomater. 8 (2012) 2889–2898. https://doi.org/10.1016/j.actbio.2012.04.031.
[31] F. Baino, E. Fiume, M. Miola, E. Verné, Bioactive sol-gel glasses: processing, properties and applications, Int. J. Appl. Ceram. Technol. 15 (2018) 841–860.
[32] D. Breite, M. Went, A. Prager, A. Schulze, Tailoring membrane surface charges: A novel study on electrostatic interactions during membrane fouling, Polymers (Basel). 7 (2015) 2017–2030. https://doi.org/10.3390/polym7101497.
[33] Y.S. Hedberg, M.S. Killian, E. Blomberg, S. Virtanen, P. Schmuki, I. Odnevall Wallinder, Interaction of Bovine Serum Albumin and Lysozyme with Stainless Steel Studied by Time-of-Flight Secondary Ion Mass Spectrometry and X-ray Photoelectron Spectroscopy, Langmuir. 28 (2012) 16306–16317. https://doi.org/10.1021/la3039279.
[34] K. Magyari, C. Gruian, B. Varga, R. Ciceo-Lucacel, T. Radu, H.J. Steinhoff, G. Váró, V. Simon, L. Baia, Addressing the optimal silver content in bioactive glass systems in terms of BSA adsorption, J. Mater. Chem. B. 2 (2014) 5799–5808. https://doi.org/10.1039/c4tb00733f.
[35] K. Zheng, M. Kapp, A.R. Boccaccini, Protein interactions with bioactive glass surfaces: A review, Appl. Mater. Today. 15 (2019) 350–371. https://doi.org/10.1016/j.apmt.2019.02.003.
[36] C. Gruian, E. Vanea, S. Simon, V. Simon, FTIR and XPS studies of protein adsorption onto functionalized bioactive glass, Biochim. Biophys. Acta - Proteins Proteomics. 1824 (2012) 873–881. https://doi.org/10.1016/j.bbapap.2012.04.008.
[37] T.A. Scot, I.E. Mercer, Concise encyclopedia biochemistry and molecular biology, 3rd ed., Spektrum Akademischer Verlag GmbH, 1997. https://doi.org/10.1016/S0031-9422(97)89024-3.
[38] R.N. Foster, E.T. Harrison, D.G. Castner, ToF-SIMS and XPS Characterization of Protein Films Adsorbed onto Bare and Sodium Styrenesulfonate-Grafted Gold Substrates, Langmuir. 32 (2016) 3207–3216. https://doi.org/10.1021/acs.langmuir.5b04743.
[39] Z. Tan, Y. Xia, M. Zhao, X. Liu, Electron stopping power and inelastic mean free path in amino acids and protein over the energy range of 20-20,000 eV, Radiat. Environ. Biophys. 45 (2006) 135–143. https://doi.org/10.1007/s00411-006-0049-0.
[40] V.I. Garmash, N.A. Djuzhev, E.P. Kirilenko, M.A. Makhiboroda, D.M. Migunov, Experimental determination of the energy dependence of electron inelastic mean free path in silicon oxide and silicon nitride, J. Surf. Investig. 10 (2016) 767–770. https://doi.org/10.1134/S1027451016040066.
[41] J.S. Stevens, A.C. De Luca, M. Pelendritis, G. Terenghi, S. Downes, S.L.M.

Schroeder, Quantitative analysis of complex amino acids and RGD peptides by X-ray photoelectron spectroscopy (XPS), Surf. Interface Anal. 45 (2013) 1238–1246. https://doi.org/10.1002/sia.5261.

[42] M. Kulkarni, A. Mazare, J. Park, E. Gongadze, M.S. Killian, S. Kralj, K. von der Mark, A. Iglič, P. Schmuki, Protein interactions with layers of TiO2 nanotube and nanopore arrays: Morphology and surface charge influence, Acta Biomater. 45 (2016) 357–366. https://doi.org/10.1016/j.actbio.2016.08.050.

[43] K. Skorstengaard, M.S. Jensen, P. Sahl, T.E. Petersen, S. Magnusson, Complete primary structure of bovine plasma fibronectin, Eur. J. Biochem. 161 (1986) 441–453. https://doi.org/10.1111/j.1432-1033.1986.tb10464.x.

[44] S. Jia, Y. Zhang, T. Ma, H. Chen, Y. Lin, Enhanced hydrophilicity and protein adsorption of titanium surface by sodium bicarbonate solution, J. Nanomater. 2015 (2015). https://doi.org/10.1155/2015/536801.

[45] Y. Yan, H. Yang, Y. Su, L. Qiao, Albumin adsorption on CoCrMo alloy surfaces, Sci. Rep. 5 (2015) 1–10. https://doi.org/10.1038/srep18403.

[46] E. Rahimi, R. Offoiach, K. Baert, H. Terryn, M. Lekka, L. Fedrizzi, Role of phosphate, calcium species and hydrogen peroxide on albumin protein adsorption on surface oxide of Ti6Al4V alloy, Materialia. 15 (2021). https://doi.org/10.1016/j.mtla.2020.100988.

[47] J. Park, J. Yang, C.Y. Lee, S. Na, S.W. Lee, S. Haam, Y.-M. Huh, D.S. Yoon, K. Eom, T. Kwon, Single-molecule recognition of biomolecular interaction via KPFM.pdf, ACS Nano. 5 (2011) 6981–6990.

[48] H. Lee, S.W. Lee, G. Lee, W. Lee, K. Nam, J.H. Lee, K.S. Hwang, J. Yang, H. Lee, S. Kim, S.W. Lee, D.S. Yoon, Identifying DNA mismatches at single-nucleotide resolution by probing individual surface potentials of DNA-capped nanoparticles, Nanoscale. 10 (2018) 538–547. https://doi.org/10.1039/C7NR05250B.

[49] S. Kashiwaya, J. Morasch, V. Streibel, T. Toupance, W. Jaegermann, A. Klein, The Work Function of TiO2, Surfaces. 1 (2018) 73–89. https://doi.org/10.3390/surfaces1010007.

[50] A.E. Ledesma, D.M. Chemes, M. de los A. Frías, M. del P. Guauque Torres, Spectroscopic characterization and docking studies of ZnO nanoparticle modified with BSA, Appl. Surf. Sci. 412 (2017) 177–188. https://doi.org/10.1016/j.apsusc.2017.03.202.

[51] X.J. Shi, D. Li, J. Xie, S. Wang, Z.Q. Wu, H. Chen, Spectroscopic investigation of the interactions between gold nanoparticles and bovine serum albumin, Chinese Sci. Bull. 57 (2012) 1109–1115. https://doi.org/10.1007/s11434-011-4741-3.

[52] N. Schwenk, B. Mizaikoff, S. Cárdenas, Á.I. López-Lorente, Gold-nanostar-based SERS substrates for studying protein aggregation processes, Analyst. 143 (2018) 5103–5111. https://doi.org/10.1039/C8AN00804C.

[53] A. Rygula, K. Majzner, K.M. Marzec, A. Kaczor, M. Pilarczyk, M. Baranska, Raman spectroscopy of proteins: A review, J. Raman Spectrosc. 44 (2013) 1061–1076. https://doi.org/10.1002/jrs.4335.

[54] J.L. Lippert, D. Tyminski, P.J. Desmeules, Determination of the Secondary Structure of Proteins by Laser Raman Spectroscopy, 13 (2021) 3. https://pubs.acs.org/sharingguidelines (accessed July 22, 2021).

[55] E. Migliorini, M. Weidenhaupt, C. Picart, Practical guide to characterize biomolecule adsorption on solid surfaces (Review), Biointerphases. 13 (2018) 06D303. https://doi.org/10.1116/1.5045122.

[56] A. Barth, Infrared spectroscopy of proteins, Biochim. Biophys. Acta - Bioenerg. 1767 (2007) 1073–1101. https://doi.org/10.1016/j.bbabio.2007.06.004.

[57] M.M. Ba-Abbad, A.A.H. Kadhum, A.B. Mohamad, M.S. Takriff, K. Sopian, Synthesis and catalytic activity of TiO 2 nanoparticles for photochemical oxidation of concentrated chlorophenols under direct solar radiation, Int. J. Electrochem. Sci. 7 (2012) 4871–4888.

[58] A.H. Kuptsov, G.N. Zhizhin, Handbook of fourier transform raman and infrared spectra of polymers, Elsevier Science Publisher B.V., Amsterdam, n.d.

[59] Y. Li, Y. Bian, H. Qin, Y. Zhang, Z. Bian, Photocatalytic reduction behavior of hexavalent chromium on hydroxyl modified titanium dioxide, Appl. Catal. B Environ. 206 (2017) 293–299. https://doi.org/10.1016/j.apcatb.2017.01.044.

[60] M. Xiao, M. Biao, Y. Chen, M. Xie, B. Yang, Regulating the osteogenic function of rhBMP 2 by different titanium surface properties, J. Biomed. Mater. Res. Part A. 104 (2016) 1882–1893. https://doi.org/10.1002/jbm.a.35719.

[61] Z. Xu, V.H. Grassian, Bovine serum albumin adsorption on TiO2 nanoparticle surfaces: Effects of ph and coadsorption of phosphate on protein-surface interactions and protein structure, J. Phys. Chem. C. 121 (2017) 21763–21771. https://doi.org/10.1021/acs.jpcc.7b07525.

[62] M. Jackson, H.H. Mantsch, The use and misuse of FTIR spectroscopy in the determination of protein structure, Crit. Rev. Biochem. Mol. Biol. 30 (1995) 95–120. https://doi.org/10.3109/10409239509085140.

[63] A. Gand, M. Tabuteau, C. Chat, G. Ladam, H. Atmani, P.R. Van Tassel, E. Pauthe, Fibronectin-based multilayer thin films, Colloids Surfaces B Biointerfaces. 156 (2017) 313–319. https://doi.org/10.1016/j.colsurfb.2017.05.023.

[64] X.N. Hu, B.C. Yang, Conformation change of bovine serum albumin induced by bioactive titanium metals and its effects on cell behaviors, J. Biomed. Mater. Res. - Part A. 102 (2014) 1053–1062. https://doi.org/10.1002/jbm.a.34768.

[65] B.R. Barrioni, A.C. Oliveira, M. de Fátima Leite, M. de Magalhães Pereira, Sol–gel-derived manganese-releasing bioactive glass as a therapeutic approach for bone tissue engineering, J. Mater. Sci. 52 (2017) 8904–8927. https://doi.org/10.1007/s10853-017-0944-6.

[66] A.J. Raghavendra, N. Alsaleh, J.M. Brown, R. Podila, Charge-transfer interactions induce surface dependent conformational changes in apolipoprotein biocorona, Biointerphases. 12 (2017) 02D402. https://doi.org/10.1116/1.4977064.

[67] T. Hanawa, Titanium-tissue interface reaction and its control with surface treatment, Front. Bioeng. Biotechnol. 7 (2019). https://doi.org/10.3389/fbioe.2019.00170.

[68] R. Li, Z. Wu, Y. Wangb, L. Ding, Y. Wang, Role of pH-induced structural change in protein aggregation in foam fractionation of bovine serum albumin, Biotechnol. Reports. 9 (2016) 46–52. https://doi.org/10.1016/j.btre.2016.01.002.

[69] B. Fernández-Montes Moraleda, J.S. Román, L.M. Rodríguez-Lorenzo, Influence of surface features of hydroxyapatite on the adsorption of proteins relevant to bone regeneration, J. Biomed. Mater. Res. - Part A. 101 A (2013)

2332–2339. https://doi.org/10.1002/jbm.a.34528.
[70] T. Peters, All About Albumin, Elsevier, 1995. https://doi.org/10.1016/B978-0-12-552110-9.X5000-4.
[71] C.F. Wertz, M.M. Santore, Effect of Surface Hydrophobicity on Adsorption and Relaxation Kinetics of Albumin and Fibrinogen: Single-Species and Competitive Behavior, Langmuir. 17 (2001) 3006–3016. https://doi.org/10.1021/la0017781.
[72] M. Oliveberg, V.L. Arcus, A.R. Fersht, pKA Values of Carboxyl Groups in the Native and Denatured States of Barnase: The pKA Values of the Denatured State Are on Average 0.4 Units Lower Than Those of Model Compounds, Biochemistry. 34 (1995) 9424–9433. https://doi.org/10.1021/bi00029a018.
[73] E.A.B. Effah Kaufmann, P. Ducheyne, S. Radin, D.A. Bonnell, R. Composto, Initial events at the bioactive glass surface in contact with protein-containing solutions, J. Biomed. Mater. Res. 52 (2000) 825–830. https://doi.org/10.1002/1097-4636(20001215)52:4<825::AID-JBM28>3.0.CO;2-M.
[74] M. Hindié, E. Camand, R. Agniel, F. Carreiras, E. Pauthe, P. Van Tassel, Effects of human fibronectin and human serum albumin sequential adsorption on preosteoblastic cell adhesion, Biointerphases. 9 (2014) 029008. https://doi.org/10.1116/1.4867598.
[75] M. Pegueroles, C. Tonda-Turo, J.A. Planell, F.-J. Gil, C. Aparicio, Adsorption of Fibronectin, Fibrinogen, and Albumin on TiO 2 : Time-Resolved Kinetics, Structural Changes, and Competition Study, Biointerphases. 7 (2012) 48. https://doi.org/10.1007/s13758-012-0048-4.
[76] T. Kokubo, S. Yamaguchi, Simulated body fluid and the novel bioactive materials derived from it, J. Biomed. Mater. Res. - Part A. 107 (2019) 968–977. https://doi.org/10.1002/jbm.a.36620.
[77] A.P. Serro, A.C. Fernandes, B. Saramago, J. Lima, M.A. Barbosa, Apatite deposition on titanium surfaces - The role of albumin adsorption, Biomaterials. 18 (1997) 963–968. https://doi.org/10.1016/S0142-9612(97)00031-8.
[78] A.P. Valagão Amadeu do Serro, A.C. Fernandes, B. De Jesus, V. Saramago, The influence of proteins on calcium phosphate deposition over titanium implants studied by dynamic contact angle analysis and XPS, Colloids Surfaces B Biointerfaces. 10 (1997) 95–104. https://doi.org/10.1016/S0927-7765(97)00060-X.
[79] L. Gao, B. Feng, J. Wang, X. Lu, D. Liu, S. Qu, J. Weng, Micro/nanostructural porous surface on titanium and bioactivity, J. Biomed. Mater. Res. - Part B Appl. Biomater. 89 (2009) 335–341. https://doi.org/10.1002/jbm.b.31221.
[80] F. Baino, M. Marshall, N. Kirk, C. Vitale-Brovarone, Design, selection and characterization of novel glasses and glass-ceramics for use in prosthetic applications, Ceram. Int. 42 (2016) 1482–1491. https://doi.org/10.1016/j.ceramint.2015.09.094.
[81] A. Ortega-Gómez, M. Perretti, O. Soehnlein, Resolution of inflammation: An integrated view, EMBO Mol. Med. 5 (2013) 661–674. https://doi.org/10.1002/emmm.201202382.
[82] Z. Tang, X. Wei, T. Li, H. Wu, X. Xiao, Y. Hao, S. Li, W. Hou, L. Shi, X. Li, Z. Guo, Three-Dimensionally Printed Ti2448 With Low Stiffness Enhanced Angiogenesis and Osteogenesis by Regulating Macrophage

Polarization via Piezo1/YAP Signaling Axis, Front. Cell Dev. Biol. 9 (2021) 1–20. https://doi.org/10.3389/fcell.2021.750948.

[83] J.Y. Fang, Z. Yang, B. Han, Switch of macrophage fusion competency by 3D matrices, Sci. Rep. 10 (2020) 1–12. https://doi.org/10.1038/s41598-020-67056-9.

[84] J.M. Anderson, A. Rodriguez, D.T. Chang, Foreign body reaction to biomaterials, Semin. Immunol. 20 (2008) 86–100. https://doi.org/10.1016/j.smim.2007.11.004.

[85] M. Rauner, W. Sipos, P. Pietschmann, Osteoimmunology, Int. Arch. Allergy Immunol. 143 (2007) 31–48. https://doi.org/10.1159/000098223.

[86] M.B. Greenblatt, J.-H. Shim, Osteoimmunology: A Brief Introduction, Immune Netw. 13 (2013) 111. https://doi.org/10.4110/in.2013.13.4.111.

[87] R. Klopfleisch, F. Jung, The pathology of the foreign body reaction against biomaterials, J. Biomed. Mater. Res. - Part A. 105 (2017) 927–940. https://doi.org/10.1002/jbm.a.35958.

[88] K.K.Y. Wong, S.O.F. Cheung, L. Huang, J. Niu, C. Tao, C.M. Ho, C.M. Che, P.K.H. Tam, Further evidence of the anti-inflammatory effects of silver nanoparticles, ChemMedChem. 4 (2009) 1129–1135. https://doi.org/10.1002/cmdc.200900049.

[89] Z. Cai, Y. Li, W. Song, Y. He, H. Li, X. Liu, Anti-Inflammatory and Prochondrogenic in Situ-Formed Injectable Hydrogel Crosslinked by Strontium-Doped Bioglass for Cartilage Regeneration, ACS Appl. Mater. Interfaces. 13 (2021) 59772–59786. https://doi.org/10.1021/acsami.1c20565.

[90] S. Zhu, X. Hu, Y. Tao, Z. Ping, L. Wang, J. Shi, X. Wu, W. Zhang, H. Yang, Z. Nie, Y. Xu, Z. Wang, D. Geng, Strontium inhibits titanium particle-induced osteoclast activation and chronic inflammation via suppression of NF-κB pathway, Sci. Rep. 6 (2016) 1–11. https://doi.org/10.1038/srep36251.

[91] A. Grosso, M.G. Burger, A. Lunger, D.J. Schaefer, A. Banfi, N. Di Maggio, It takes two to tango: Coupling of angiogenesis and osteogenesis for bone regeneration, Front. Bioeng. Biotechnol. 5 (2017) 1–7. https://doi.org/10.3389/fbioe.2017.00068.

[92] N. Sismanopoulos, D.A. Delivanis, K.D. Alysandratos, A. Angelidou, M. Vasiadi, A. Therianou, T.C. Theoharides, IL-9 Induces VEGF Secretion from Human Mast Cells and IL-9/IL-9 Receptor Genes Are Overexpressed in Atopic Dermatitis, PLoS One. 7 (2012) e33271. https://doi.org/10.1371/journal.pone.0033271.

[93] G.T. Liu, Y.L. Huang, H.E. Tzeng, C.H. Tsai, S.W. Wang, C.H. Tang, CCL5 promotes vascular endothelial growth factor expression and induces angiogenesis by down-regulating miR-199a in human chondrosarcoma cells, Cancer Lett. 357 (2015) 476–487. https://doi.org/10.1016/j.canlet.2014.11.015.

[94] J. Yang, A. Richmond, The angiostatic activity of interferon-inducible protein-10/CXCL10 in human melanoma depends on binding to CXCR3 but not to glycosaminoglycan, Mol. Ther. 9 (2004) 846–855. https://doi.org/10.1016/j.ymthe.2004.01.010.

[95] R.J. Bodnar, C.C. Yates, A. Wells, IP-10 blocks vascular endothelial growth factor-induced endothelial cell motility and tube formation via inhibition of calpain, Circ. Res. 98 (2006) 617–625. https://doi.org/10.1161/01.RES.0000209968.66606.10.

[96] C.-S. Lin, G. Lin, K.-C. Chen, H.-C. Ho, T.F. Lue, Vascular Endothelial

Growth Factor Induces IP-10 Chemokine Expression, Biochem. Biophys. Res. Commun. 292 (2002) 79–82. https://doi.org/10.1006/bbrc.2002.6611.

[97] F. Billing, B. Walter, S. Fink, E. Arefaine, L. Pickarski, S. Maier, R. Kretz, M. Jakobi, N. Feuerer, N. Schneiderhan-Marra, C. Burkhardt, M. Templin, A. Zeck, R. Krastev, H. Hartmann, C. Shipp, Altered Proinflammatory Responses to Polyelectrolyte Multilayer Coatings Are Associated with Differences in Protein Adsorption and Wettability, ACS Appl. Mater. Interfaces. 13 (2021) 55534–55549. https://doi.org/10.1021/acsami.1c16175.

[98] G. Li, P. Yang, X. Guo, N. Huang, R. Shen, An in vitro evaluation of inflammation response of titanium functionalized with heparin/fibronectin complex, Cytokine. 56 (2011) 208–217. https://doi.org/10.1016/j.cyto.2011.06.020.

[99] J. Maciel, M.I. Oliveira, R.M. Gonçalves, M.A. Barbosa, The effect of adsorbed fibronectin and osteopontin on macrophage adhesion and morphology on hydrophilic and hydrophobic model surfaces, Acta Biomater. 8 (2012) 3669–3677. https://doi.org/10.1016/j.actbio.2012.06.010.

[100] R.M. Visalakshan, M.N. Macgregor, S. Sasidharan, A. Ghazaryan, A.M. Mierczynska-Vasilev, S. Morsbach, V. Mailänder, K. Landfester, J.D. Hayball, K. Vasilev, Biomaterial Surface Hydrophobicity-Mediated Serum Protein Adsorption and Immune Responses, ACS Appl. Mater. Interfaces. 11 (2019) 27615–27623. https://doi.org/10.1021/acsami.9b09900.

Chapter 6

Conclusions and future perspectives

In this work, adsorption of albumin and fibronectin has been characterized and investigated on eight different biomaterials that are applied for bone contact application, namely pure titanium and titanium alloy, pristine and after three different chemical treatments, a bioactive glass composition, possibly doped with silver, and polystyrene (as a control).

The first step was to characterize the surface properties, with special attention to morphology, surface chemistry, wettability, surface energy and charge and exposed functional groups, -OH in particular.

The chemical treatments on Ti and Ti64 heavily impact on their surface properties. Thicker oxide layers with micro and nanostructures are grown, increasing both porosity and surface roughness, resulting in the following roughness increasing order: Ti, Ti64 < Ti64(HF-H_2O_2) < Ti64(SrAg) < Ti(A-HC-H). The surface chemical composition is changed with the presence of Ca, Sr, and Ag on Ti64(SrAg). Interestingly, a strong difference is obtained regarding the density and nature of -OH groups. Acidic hydroxyls, absent on the untreated samples, appear after the treatments in a different amount. Also, the total hydroxylation degree is widely affected by the different treatments, with the following increasing order: Ti(A-HC-H) < Ti, Ti64 < Ti64(SrAg) < Ti64(HF-H_2O_2). Surface energy, in particular the polar component, and wettability show the same variation trend than hydroxylation degree. These features are correlated in case of all the titanium samples but Ti64(SrAg). This surface results the most wettable and the one with the higher energy thanks because of the contribution of strontium and silver ions, too. At last, the surface potential, and consequently the surface charge, is different between untreated and treated surfaces, confirming the generation of surface hydroxyl groups, absent on the pristine Ti and Ti64 samples. Ti (A-HC-H) has the most positive surface, while Ti64(SrAg) and Ti64(HF-H_2O_2) have a negative potential in the pH range between 3 and 9.

Regarding the two bioactive glass samples considered, the silver ionic exchange has a surprisingly little effect on the physiochemical properties of the BG surface, apart from glass composition. In fact, SBA2 and AgSBA2 have similar wettability and surface energy, which are intermediate between the one of Ti64(SrAg) and the one of Ti64(HF-H_2O_2), and zeta potential vs pH behavior, showing a negative surface. The surface treatment introduces silver in the surface as expected, both as ions or nanoparticles, and slightly increases the surface roughness, due to the surface reaction. The other investigated surface properties, SFE, wettability and surface potential are unchanged by the presence of the silver.

PS is confirmed to be a hydrophobic, non-polar surface without specific functional groups exposed.

The characterization of protein adsorption on the different surfaces investigated is obtained thanks to the combined use of several characterization techniques. To define a set of methods to investigate the various aspect of protein-material interactions on bulk biomaterials was among the aims of this thesis. This goal was achieved thanks to the use of conventional techniques, such as BCA protein assay or FTIR, coupled with more innovative approach to methods seldom used for investigating protein adsorption, such as Kelvin probe force microscopy or solid surface zeta potential. One of the more important take home message observed during the evaluation of different characterization techniques is the necessity to merge more techniques to obtain information about the distinct aspect of protein adsorption, and that the possibility to employ a certain technique is strictly dependent on the substrate considered and adsorption conditions.

Regarding the total amount of protein adsorbed, the general rule of thumb stating that hydrophobic surfaces adsorb more protein than hydrophilic one can be invalidated by other important properties of the surface. In particular, the dominant role is assumed by surface topography, with a special consideration to the porosity, as in case of Ti(A-HC-H) and Ti64(SrAg). This effect is also dependent on the size of the protein adsorbed, since the differences were higher in case of albumin than fibronectin. Hydrophobicity became the main driving forces when surfaces are similarly flat, as in case of Ti, Ti64, and PS, with the latter adsorbing more than the metallic surfaces. When it comes to reactive surfaces, such as bioactive glasses, it is hard to compare them with unreactive ones, due to the intrinsic dynamicity of the surfaces, which changes during the adsorption, and the fact that proteins themselves became part of the reaction layer. Even though the physical surface properties of SBA2 and AgSBA2 are not much different, the presence of silver greatly enhances the adsorption of protein with high cysteine content, such albumin, thanks to metal-thiol affinity.

Regardless of the type of protein-surface interactions, whether they are electrostatic or hydrogen bonds, via protonated and unprotonated -OH groups, hydrophobic or thiol mediated, both albumin and fibronectin are chemically intact after adsorption, without significant changes in their polypeptidic chain. Furthermore, the proteins are able to maintain their charged groups, namely carboxyls and ammines, within the transient protein matrix.

The adsorbed protein layers are able to cover mainly homogeneously all the surfaces, both in case of highly concentrated albumin solution and of one with lower fibronectin content. On textured surfaces, such as Ti(A-HC-H), Ti64(SrAg) or Ti64(HF-H_2O_2), it was noticed that proteins may accumulate within surface depression, confirming the enhancing effect of topography in terms of total proteins adsorbed. On flat surfaces, fibronectin easily forms filamentous structures. The affinity of the proteins towards the surfaces seems to be the driving force for the formation of aggregates on the samples: the higher the affinity, the more homogeneous the protein layer is.

The biological properties of the transient matrix are dictated not only by the adsorbed protein profile, but also by their conformation and secondary structure. Interesting results were obtained by evaluating protein denaturation on the different surfaces. On titanium surfaces, hydroxyl groups are the main responsible for the loss of native structure. Noticeably, the -OH groups shall possess an acidic behavior to exert an effect on the protein structure, so that they assume a deprotonated O^- state at pH 7.4, and, in the case of larger proteins, to overcome a certain density threshold. In fact, Ti64(HF-H_2O_2), which has the highest concentration of acidic -OH, denatures adsorbed proteins to the highest degree, while Ti(A-HC-H) and Ti64(SrAg) change the protein structure to a lower level, depending on the size of the adsorbed proteins: if the protein is small, even low difference in the OH density can change the protein structure, while a larger protein structure is not affected until a certain hydroxylation is reached. In fact, Ti64(HF-H_2O_2), which has the highest concentration of acidic -OH, denatures adsorbed proteins to the highest degree, while Ti(A-HC-H) and Ti64(SrAg) change the protein structure to a lower and similar level, despite having different hydroxylation degrees and acidic -OH percentages. Hydroxyl groups may also increase the binding strength of the protein with the surface. Focusing on the glass samples, again silver heavily affects the interactions with proteins. Its great affinity for disulphide bonds results in a high loss of albumin native structure, which is reduced in case of undoped SAB2. Also, fibronectin structure is altered by the presence of silver in the glass surface, possibly through electrostatic interactions, since it contains cysteine residues in very low amount.

The surface properties, in particular wettability, influence the overall 3D structure and protein orientation on the samples, too. In this case, the results obtained in this work agree with the rule that proteins spread more on the hydrophobic surfaces with respect to the hydrophilic ones. This phenomenon is more emphasized in case of the small proteins, such as albumin, with respect to the bigger ones, as fibronectin.

The characterization of the adsorption from a single protein solution on biomaterials of orthopedic interest performed during this thesis allowed to deepen the knowledge about the effect of distinct surface properties on the features of the adsorbed transient matrix, as summarized in Table 6.1. This information may provide useful indication for the design of novel biomaterials. It was tempted to obtain quantitative correlations between surface properties and different aspects of protein adsorption, such as adsorbed mass or conformation. Unfortunately, the

complex interplay between all the different features of the samples, such as roughness, wettability, SFE or hydroxylation, does not allow to obtain a one-to-one correlation with adsorption features. More complex mathematic correlations are beyond our capability and knowledge, still, they are worthy of future investigations.

Table 6.1 Effect of the surface properties on the characteristic of the adsorbed proteins (/: effect not observed; +: quite significative effect; ++: highly significative effect)

Surface properteis		Adsorbed proteins			
		Adsorbed amount	Binding strength	Secondary structure	Orientation
Roughness and porosity		++	+	/	/
Hydroxylation	Basic OH	+	/	/	/
	Acidic OH	+	++	++	/
Wettability		+	+	/	++
Surface charge		/	/	/	+
Chemistry (Ag doping)		++	+	++	/

Following the characterization of adsorption from a simple single protein solution, the focus of the work shifted to the competition for the surface between proteins, by sequential adsorption and co-adsorption of albumin and fibronectin. Interestingly, none of the two proteins is capable of completely avoid the adsorption of the other one when pre-adsorbed on the surface. *Vice versa*, neither albumin nor fibronectin can totally displace and substitute a pre-adsorbed protein. The data suggest that in the case of competitive adsorption, surface hydrophobicity may have a pivotal effect, since polystyrene seems to have a different behavior with respect to the other surfaces.

In order to test bioactivity, the standard *in vitro* procedure involves the use of a fully inorganic solution, without considering the possible effect of biological molecules such as proteins. Here, albumin shows to delay the bioactivity of Ti64(HF-H_2O_2), resulting in later precipitation of hydroxyapatite crystals with respect to the SBF solution without proteins.

At last, the immune response of three selected samples, Ti64, Ti64(SrAg) and Ti64(HF-H_2O_2), was tested, as first step towards the assessment of the osteoimmunomodulation properties of such materials, with the aim of determining if protein adsorption plays a role with respect to the foreign body reaction. As expected, all three surfaces induce an inflammatory state in the cultured macrophages, with the formation of foreign body gigantic cells and the release of pro-inflammatory cytokines. Interestingly, despite there are no differences in cell viability, morphology and spreading between the different surfaces, Ti64(SrAg) elicits a peculiar response, where the release of factors related to angiogenesis is hindered and with hints of an early anti-inflammatory reaction by macrophages. Those effects may be related to the ion release and the higher protein adsorption capability of this titanium surface enriched with Ca, Sr, and Ag. Further studies will

focus on how the macrophages response affect the osteogenesis by affecting the differentiation of the mesenchymal cells.

In the end, this thesis provides some new insight on the mechanisms of interaction between proteins and biomaterials, and on how the surface features may affect the resulting protein layer. Importantly, these results were obtained in *roughland*, the world of real biomaterials, which is far away from a model flat space, where there are more tools available to investigate protein adsorption. Alongside with that, the new set of optimized characterization techniques used in this work will help to further investigate adsorption on new materials.

Nevertheless, many questions are still open and in need of answers, and a lot of work remains to be done. Even though in high concentration, single protein solutions are a far less complex system than the physiological environment where implants shall operate. Thus, a necessary step is to investigate how the investigated surfaces adsorb proteins from biological fluids such as serum or blood. It is desirable that correlations between the behavior of a certain protein in a simple or complex solution will be found, so that results obtained using single protein systems, easier to investigate, can be scaled up to *in vivo* situations.

Further efforts shall be also spent in the development of new investigation methodologies and the optimization of the already existing characterization techniques: several aspects of the adsorbed transient matrix are not trivial to study on rough and complex biomaterials, for instance the thickness of the adsorbed layer or the exact determination of protein orientation. For this purpose, material engineers and scientists shall join forces with biologists and biotechnologists, since coupling common biological assay with material characterization techniques seems a promising way to gather more information about this topic.

At last, even the most detailed report of the adsorbed protein layer is incomplete if not coupled with the knowledge of the host response to such protein covered biomaterials. Adsorption studies shall be coupled with *in vitro* cellular culture, for instance by growing cells on already formed protein layer or complete transient matrix, such as pre-adsorbed albumin, fibronectin or even whole serum, or complete transient matrix. It is of uttermost importance to correlate the properties of adsorbed proteins, such as amount or conformation, to cellular response. Due to the intimate connection between cells belonging to very different systems, as in the case of the osteoimmunomodulation, where the behavior of bone cells is highly determined by the foreign body reaction of the immune ones, the interplay between cells shall be always considered. But this is a story for another PhD thesis.

Appendix A

Water contact angle after protein adsorption

Wettability measurement after protein adsorption

Static water contact angle was measured by the sessile drop techniques on all the materials involved in this work (DSA 100 Drop Shape Analyser; KRŰSS, Hamburg, Germany). A 5 µl drop of ultrapure water was manually dropped on the surface of the sample and the image was captured after 10 s. Then, the software of the instrument automatically calculated the contact angle. Three measurements were done on each sample and the results averaged.

Water contact angle after single protein adsorption

The water contact angle is highly sensitive to the chemistry of the surface, so it may be changed by protein adsorption. The wettability of a biomaterial is fundamental in determining the cells response and adhesion, consequently, the contact angle of the transient protein matrix is of interest, since it is the interface for cells-implant interactions.

The contact angle has been measured on all surfaces after the adsorption of both BSA and FN (Figure A1). The changes in θ values after adsorption do not follow a clear trend. On Ti and Ti64, θ decreases down to about 20°, which is also lower than the values reported in literature for Ti-based substrates, which is around 50° [1,2]. On the other hand, the contact angle does not vary on Ti(A-HC-H) while it increases on Ti64(SrAg), and values similar to the ones reported in literature were obtained. At last, BSA adsorption on Ti64(HF-H_2O_2) resulted in a super-hydrophilic surface. Regarding these samples, FN has a similar trend, with a decrease in θ for Ti and Ti64, no changes after adsorption on Ti(A-HC-H) and an increase on the treated Ti64 samples. It is possible that on more hydrophobic surfaces, such as the untreated titanium samples, the proteins attach to the surface with the hydrophobic residues, exposing more hydrophilic patches outwards. The opposite happens on more hydrophilic surfaces. Ti(A-HC-H) has an intermediate behavior, probably due to its low hydroxylation degree still having a lower θ than the untreated surfaces, which offers low anchoring points for hydrophilic domains.

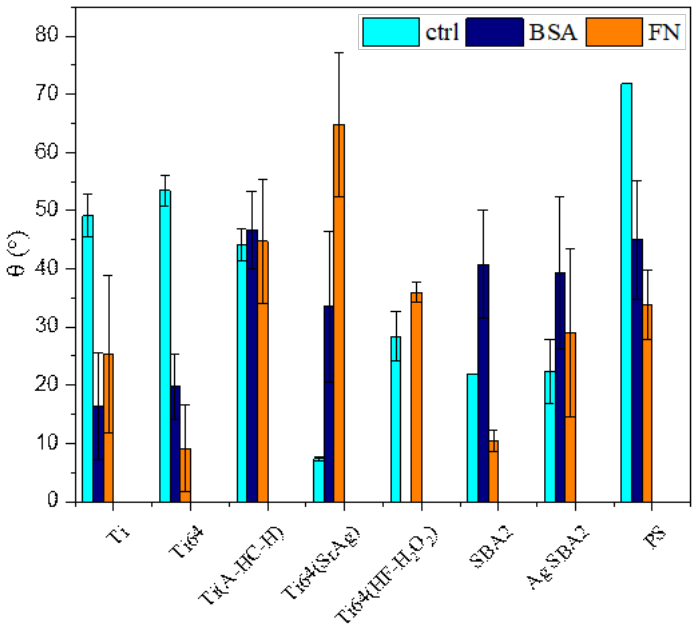

Figure A1 Water contact angle, θ, of the samples investigated after BSA and FN adsorption. The values of the samples before adsorption (ctrl) are also reported.

Due to the reactivity and the mixed composition of the surface layer, the contact angle after adsorption of BSA and FN on BGs samples may not be due only to protein orientation but also to the silica-gel layer. In any case, BSA makes the contact angle increase, up to 40°, which is similar to what is reported in literature [3]. The behavior after FN adsorption seems more random. PS turns more hydrophilic after adsorption of both type of proteins, with θ around 40°, in agreement with previous findings [4,5]. This can happen for a reason similar to the case of Ti and Ti64.

The protein layer that form on an implant surface when it is implanted has a much more complex composition than just albumin or fibronectin, and as consequence, the contact angle may vary a lot with respect to the one reported here. Still, the results reported here are interesting. After protein adsorption, the wettability of a surface can drastically change, and in the same way, how cells interact with the implant. Noticeably, all the surfaces may be considered hydrophilic ($\theta < 60°$) after protein adsorption, having a favorable wettability for cellular interactions. It seems that there is no a clear rule on how that happens and how to predict the results starting from the wettability of the pristine surface. Even there are some exception, as general consideration, it is possible to say that the contact angle is decreased when proteins are adsorbed on hydrophobic surfaces, while it is increased when adsorption takes place on hydrophilic

Water contact angle after sequential and co-adsorption

Water contact angle θ was measured with a double aim: the first was to try to understand the stratification of the protein transient matrix, the second was to investigate the wetting properties of the adsorbed layer.

The values of θ does not show a common trend for the different adsorption conditions (Figure A2). Due to the high standard deviations that characterize some samples, only qualitative comparisons have been made. Considering sequential adsorption, in some sample, it seems that the first protein adsorbed affects more the WCA. This happens in the cases of Ti64 and Ti64(SrAg), and on the treated titanium alloy it agrees with the zeta potential measurements. On Ti, Ti(A-HC-H), Ti(HF-H_2O_2) and PS, the WCA does not changes significantly in the cases of sequential adsorption, also with respect to adsorption of a single protein. Regarding bioactive glasses, the sequential adsorptions result in a very low contact angle. This may be influenced by the presence of a thick and very hydrated silica-gel layer, that has a long time to form during the contact of glasses with protein solution. Interestingly, the highest contact angles were measured in the case of co-adsorption on all surfaces but Ti(A-HC-H) andTi64(SrAg). It is possible that albumin and fibronectin interact in solution, forming aggregates that influences their orientation and conformation on the surfaces. On Ti(A-HC-H) and Ti64(SrAg), the very porous surfaces may have a role in limiting the hydrophobic effect of those aggregates.

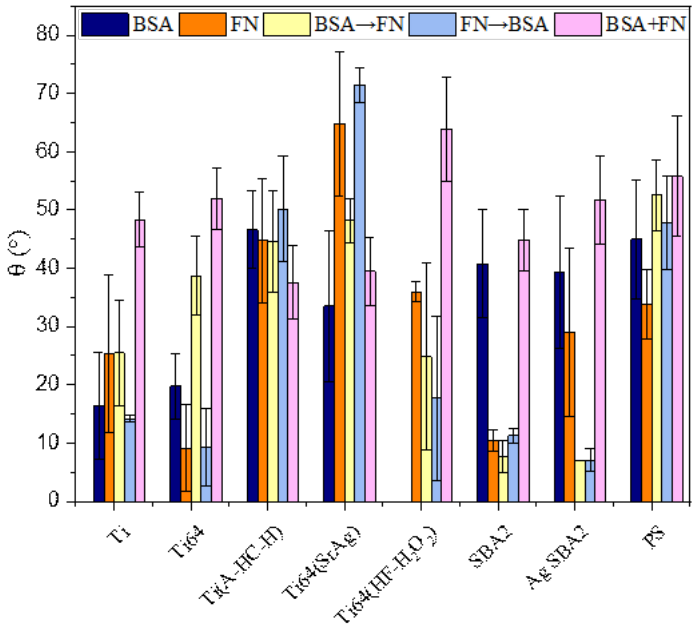

Figure A2 Water contact angle, θ, of the samples investigated after protein adsorption in various conditions: single protein solution (BSA and FN); sequential adsorption (BSA-FN and FN-BSA); co-adsorption (BSA+FN).

As already disclaimed, the very high dispersion of the water contact angle data does not allow to precisely discriminate the wettability differences among different adsorption conditions. What is of biological relevance, it is that almost in all cases, apart Ti64(SrAg)_FN, the resulting θ are always below 60°, which is the threshold values for a surface to have a wettability that is beneficial for cell adhesion and growth.

Bibliography

[1] A.P. Serro, A.C. Fernandes, B. Saramago, J. Lima, M.A. Barbosa, Apatite deposition on titanium surfaces - The role of albumin adsorption, Biomaterials. 18 (1997) 963–968. https://doi.org/10.1016/S0142-9612(97)00031-8.

[2] A.P. Valagão Amadeu Do Serro, A. Catarino Fernandes, B. De Jesus Vieira Saramago, W. Norde, Bovine serum albumin adsorption on titania surfaces and its relation to wettability aspects, J. Biomed. Mater. Res. 46 (1999) 376–381. https://doi.org/10.1002/(SICI)1097-4636(19990905)46:3<376::AID-JBM10>3.0.CO;2-T.

[3] B. Sweryda-Krawiec, H. Devaraj, G. Jacob, J.J. Hickman, A New Interpretation of Serum Albumin Surface Passivation, Langmuir. 20 (2004) 2054–2056. https://doi.org/10.1021/la034870g.

[4] D.E. MacDonald, B. Markovic, M. Allen, P. Somasundaran, A.L. Boskey, Surface analysis of human plasma fibronectin adsorbed to commercially pure titanium materials, J. Biomed. Mater. Res. 41 (1998) 120–130. https://doi.org/10.1002/(SICI)1097-4636(199807)41:1<120::AID-JBM15>3.0.CO;2-R.

[5] J. Ballester-Beltrán, P. Rico, D. Moratal, W. Song, J.F. Mano, M. Salmerón-Sánchez, Role of superhydrophobicity in the biological activity of fibronectin at the cell-material interface, Soft Matter. 7 (2011) 10803–10811. https://doi.org/10.1039/c1sm06102j.

Appendix B

Cytokines and factors released by macrophages: complete report

Table B1 c

	Description	Significative differencies
EOTAXIN	Chemoattractant for eosinophil cells	Increased form 3d to 7d, not for Ti64
FGF basic	Pleiotropic cytokine of ghe FGF superfamily	Increased for Ti64(HF-H_2O_2) from 3 to 7d
G-CSF	Glycoprotein that stimulates production and release form bone marrow of granulocytes and stem cells	Ti64(SrAg) higher than Ti64(HF-H_2O_2) at 3d
GM-CSF	Hematopoietic growth factor involved in the generation of granulocytes, macrophages, and dendritic cells from hematopoietic progenitor cells	Increased for Ti64(HF-H_2O_2) from 3 to 7d
INF-γ	Prymari activator of macrophages and stimulator of natural killer cells and neutrophils	Increased for Ti64 and Ti64(HF-H_2O_2) from 3 to 7d
IL-1β	Pro-inflammatory cytokine	Increased for Ti64(HF-H_2O_2) from 3 to 7d, Ti64 lower than Ti64(HF-H_2O_2) at 7d
IL-1Ra	Anti-inflammatory cytokine	Increased for Ti64(HF-H_2O_2) from 3 to 7 d, Ti64 lower than Ti64(HF-H_2O_2) at 7d
IL-2	Involved in adaptive immunity, proliferation of B cells, activated T cells, NK cell function	Increased form 3d to 7d, at 3d Ti64(SrAg) higher than Ti64(HF-H_2O_2)
IL-4	Involved in adaptive immunity, proliferation of B and cytotoxic T cells, enhances MHC class II expression, stimulates IgG and IgE production	Ti64(SrAg) higher than Ti64(HF-H_2O_2) and Ti64 at 3d, increased for Ti64(HF-H_2O_2) from 3 to 7d
IL-5	Involved in adaptive immunity, proliferation of B and cytotoxic T cells, enhances MHC class II expression, stimulates IgG and IgE production	Increased for Ti64 and Ti64(HF-H_2O_2) from 3 to 7d
IL-6	Pro-inflammatory cytokine, involved in B-cell differentiation	Increased form 3d to 7d
IL-7	Involved in early deveopment of B and T cells and thymic development of T cells	Several point at a too low concentration to be detected, at 7d Ti64(SrAg) lower than Ti64(HF-H_2O_2)
IL-8	Pro-inflammatory cytokine, involved in chemotaxis for neutrophilis and T cells	At 3d Ti64 higher than the others and Ti64(HF-H_2O_2) higher than Ti64(SrAg), increased fro 3 to 7d on treated surfaces
IL-9	Involved in adaptive immunity and proliferation of T cells; maybe involved in osteoclastogenesis and tumorigenesis; may induce gene expression and secretion of VEGF	At 3d Ti64 higher than the others and Ti64(HF-H_2O_2) higher than Ti64(SrAg), Ti64(srAg) 7d is the lowest, increased for Ti64(HF-H_2O_2) from 3 to 7 d

IL-10	Anti-inflammatory cytokine, inhibits cytokine production and mononuclear cell function	Ti64(SrAg) higher than Ti64(HF-H_2O_2) and Ti64 at 3d, increased for Ti64(HF-H_2O_2) from 3 to 7d
IL-12(p70)	Involved in cell-mediated immune response and induces INF-γ production by natural killer and T cells	None
IL-13	Homologous to IL-4	Increased form 3d to 7d
IL-15	Pleiotropic cytokine involved in both the innate and adaptive immune response	Increased for Ti64(HF-H_2O_2) from 3 to 7d
IL-17	Pro-inflammatory cytokines involved in the recruitment of monocyte and neutrophilis and downstreaming of cytokines and chemokines0	Increased for Ti64(HF-H_2O_2) from 3 to 7d, Ti64(HF-H_2O_2) higher than Ti64 at 7d
IP-10	a chemokine secreted by several cell types including T lymphocytes, neutrophils, endothelial cells, monocytes, and fibroblasts; can elicit diverse effects in different cell types by binding to a common chemokine receptor, CXCR3; these effects include attraction of T cells and monocytes, regulation of angiogenesis (angiostatic activity), and differentiation of naive T cells to pro-inflammatory T helper 1 cells.	Ti64(SrAg) the lowest at 3 and 7d, increased for Ti64(HF-H_2O_2) from 3 to 7d
MCP1(MCAF)	One of the key chemokines in the regulation of migration and infiltration of monocytes/macrophages	At 3d Ti64 higher than the others and Ti64(HF-H_2O_2) higher than Ti64(SrAg)
MIP-1α	Chemokine with effects in chemotaxis and transendothelial migration	Ti64(HF-H_2O_2) the lowest at 3d, increased for Ti64(HF-H_2O_2) from 3 to 7d
MIP-1β	Chemokine with effects in chemotaxis and transendothelial migration	Ti64(HF-H_2O_2) the lowest at 3d and lower than Ti64(SrAg) at 7d, increased for Ti64(HF-H_2O_2) from 3 to 7d
PDGF-BB	Chemotactic and mitogenic agent that stimulates bone cell replication	Increased for Ti64(HF-H_2O_2) from 3 to 7d
RANTES	Chemokine regulated upon activation of normal T-cell, expressed and secreted, initially recognized as a chemo-attractant for immune cells and may induce the production of VEGF	Ti64(SrAg) the lowest at 3 and 7d, increased for Ti64(HF-H_2O_2) from 3 to 7d
TNF-α	Pro-inflammatory factor, main regulators of inflammatory cytokine production	Increased for Ti64 and Ti64(HF-H_2O_2) from 3 to 7d
VEGF	Key regulator of angiogenesis, may induce IP-10 expession	Ti64(SrAg) the lowest at 3 and 7d, increased for TI64 and Ti64(HF-H_2O_2) from 3 to 7d

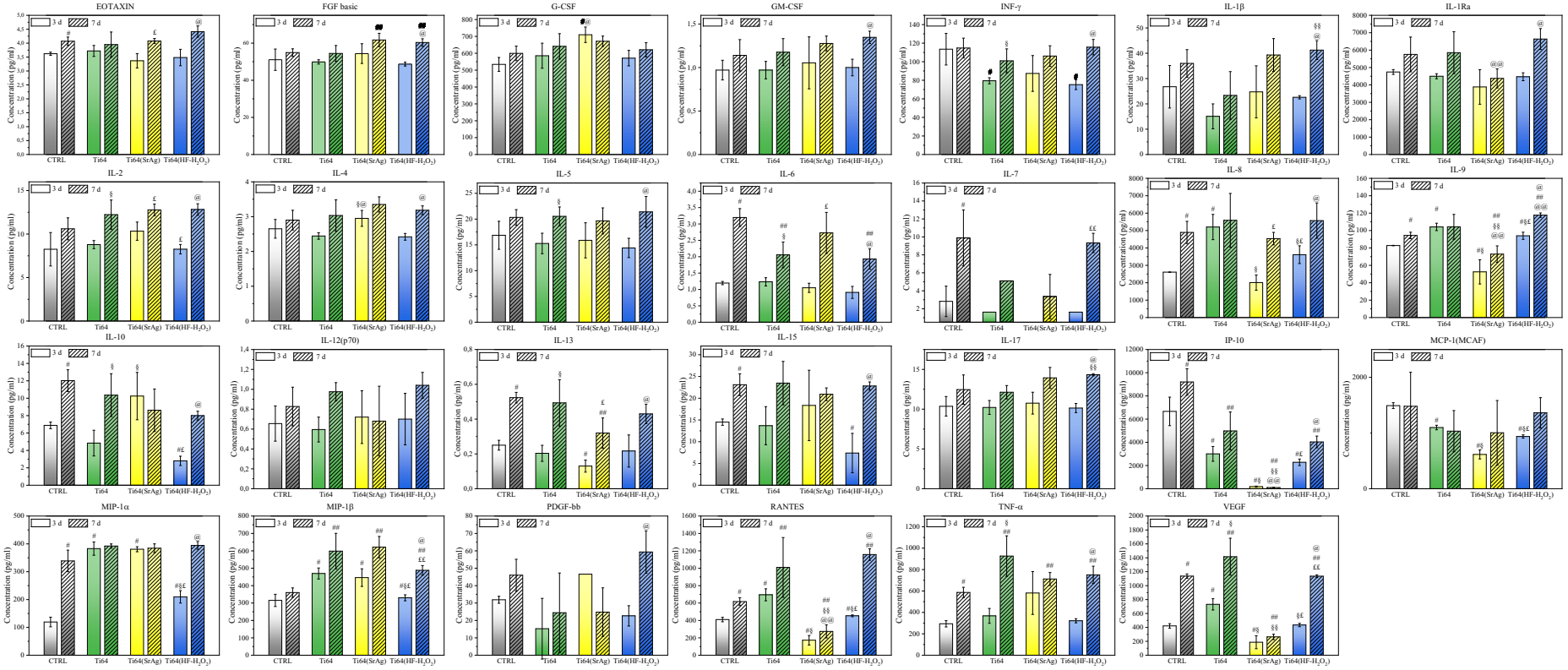

Figure B1 Concentration of the analyzed 27 factors and cytokines released by macrophages in the culture medium after 3 (unpatterned bars) and 7 days (patterned bars) of culture on plastic well (CTRL)(white), Ti64 (green), Ti64(SrAg)(yellow) and Ti64(HF-H_2O_2)(light blue): p values < 0.05: # vs CTRL 3d, § vs Ti64 3d; £ vs Ti64(SrAg) 3d; @ vs Ti64(HF-H_2O_2) 3d; ## vs CTRL 7d, §§ vs Ti64 7d; ££ vs Ti64(SrAg) 7d; @@ vs Ti64(HF-H_2O_2) 7d.

Bibliography

[1] G.A. Duque, A. Descoteaux, Macrophage cytokines: Involvement in immunity and infectious diseases, Front. Immunol. 5 (2014) 1–12. https://doi.org/10.3389/fimmu.2014.00491.